Exploring the dual role of fumarate as an intracellular and extracellular hypoxia-induced signalling molecule

Marcos Felipe Castro Guarda

Oriel College

University of Oxford

A thesis submitted for the degree of Doctor of Philosophy

January 2025

Acknowledgements

The work presented in this thesis was made possible by an unquantifiable amount of support, encouragement and inspiration from my colleagues, friends and family.

A special thanks goes to Professor Lisa Heather, who provided me with the incredible opportunity to move from the other end of the world and join the Heather group, one of the best decisions I have ever made. I would like to thank Professor Lisa Heather for being an extraordinary supervisor and mentor, always caring for every member of her group. Her enthusiasm for research and exceptional expertise, combined with her incredible personal qualities and remarkable dedication as a supervisor, make her a true role model whose influence will continue to guide me throughout my career.

I would like to thank my friends Kaitlyn and Claudia, who taught me that two incredible people I never imagined I would meet could become friends and family. Kaitlyn, thank you for always looking out for me and supporting every decision I made. Claudia, thank you for being there for me and offering advice whenever I needed it.

I would also like to thank the Cardiac Metabolism Research Group (CMRG) for always being a collaborative team. Special mentions go to my co-supervisor, Dr Kerstin Timm, for her constant enthusiasm about my research and her help and feedback whenever I needed it, and to Professor Carolyn Carr for her invaluable help and guidance in the cell lab. I would like to thank the people I met during this journey: Thomas for his generosity and charisma, Ryan for his boundless energy, Ríona for her vibrant spirit, Aaron for his team spirit, Dona for her positivity, Eline for her humour and Catriona and Javier for their empathy and kindness.

I would like to thank Atenea, Hazal, Lena, and Catherine for their amazing friendship over these years and for always being there for me.

I would like to thank my family, who have made me the person I am today and to whom I dedicate this work. To my extraordinary siblings, Ignacio and Valeria, for their unquantifiable support in my decisions and boundless enthusiasm for everything I do. To my parents, Claudio and Fresia, for their unconditional love, support, invaluable lessons, and constant encouragement in pursuing my dreams, which have been my greatest motivation and inspiration during this journey.

Finally, I would like to thank the Chilean government's Agencia Nacional de Investigación y Desarrolo (ANID) for my studentship and the Department of Physiology, Anatomy, and Genetics at the University of Oxford for their support and for providing laboratories to carry out my thesis. A special mention goes to Sarah Noujaim for her invaluable administrative support from the very beginning of my DPhil.

Abstract

Myocardial ischemia is characterised by a restriction in blood flow to the heart, which limits nutrient and oxygen supply and removal of waste products. In healthy hearts, ischemia triggers a cardiac metabolic shift from oxidative metabolism to anaerobic glycolysis to limit the consumption of low oxygen levels.

Previously, the Heather's group observed that hypoxia causes a significant increase in fumarate intracellular concentrations within the healthy heart. However, the downstream effects of fumarate accumulation during cardiac hypoxia and its role in heart metabolic adaptation remain unclear. Therefore, this thesis used several molecular and omics-based approaches to investigate the biological and metabolic effects of elevated fumarate concentrations on human cardiomyocytes. Additionally, hypoxia is associated with increased reactive oxygen species production, and the fumarate derivatives are FDA-approved molecules for treating autoimmune diseases due to their role in enhancing antioxidant defence mechanisms via promoting the nuclear factor erythroid 2 [NF-E2]-related factor 2 (Nrf2) activation, which also has been reported to modulate metabolic pathways in other tissues. Therefore, the effect of native fumarate and fumarate derivatives in activating Nrf2 pathway and their impact on cardiomyocyte metabolism was evaluated in human cardiomyocytes.

The first results chapter evaluated whether fumarate derivatives activate antioxidant defence pathways in human cardiomyocytes. The results revealed that the fumarate derivatives (dimethyl fumarate (DMF), monomethyl fumarate and diroximel fumarate) promoted Nrf2 activation in human-induced Pluripotent Stem Cell-derived Cardiomyocytes (hiPSC-CM), increasing the expression of several antioxidant enzymes and antioxidant defence pathways, including glutathione metabolism and pentose phosphate pathway.

The second results chapter determined the impact of the fumarate derivatives on hiPSC-CM metabolism. Fumarate derivatives induced a metabolic shift within the cardiomyocytes, decreasing fatty acid β-oxidation while increasing glycolytic metabolism. These changes were accompanied by mitochondrial network fragmentation and reduced mitochondrial activity. Surprisingly, experiments using a genetic mouse cardiac model with constitutive Nrf2 activation showed that Nrf2 may not mediate the metabolic changes.

Subsequent studies revealed that DMF was hydrolysed into native fumarate. The third results chapter studied the impact of elevated fumarate concentrations on cardiomyocyte biology and metabolism. Fumarate transcriptionally regulated circadian rhythm pathways and cardiomyocyte metabolism, reducing oxidative metabolism while increasing glycolytic metabolism. Furthermore, under hypoxic conditions, fumarate was released into the extracellular space via the monocarboxylate transporter 1, modulating Gi-coupled signalling pathways to decrease cAMP levels.

The final results chapter evaluated the therapeutic use of DMF in reversing insulin resistance phenotype. Type 2 diabetes (T2D) rat hearts presented with increased oxidative stress, and insulin-resistant hiPSC-CM showed dysregulation of the Nrf2 pathway. Supplementation of insulin-resistant hiPSC-CM with DMF significantly increased Nrf2-target antioxidant genes and decreased the expression of genes involved in fatty acid β-oxidation.

In conclusion, this work provides a novel role for fumarate under hypoxia, beyond its energetic role in the Krebs cycle, acting as a signalling intracrine molecule modulating cardiomyocyte metabolism and, extracellularly, as a paracrine molecule regulating Gi-coupled signalling molecules in neighbouring cells. Moreover, this thesis shows evidence for repurposing the use of fumarate derivatives in humans to reverse metabolic dysfunctions and protect against the oxidative stress induced by cardiac metabolic disorders like T2D.

Contents

Abbreviations

ACO	Aconitase
Actb	Actin Beta
ACSL	Acyl-CoA synthetase long-chain family member
ADP	Adenosine diphosphate
AMPK	AMP-activated protein kinase
AMP	Adenosine monophosphate
Akt	Serine/threonine kinase
ARE	Antioxidant response element sequence
ATP	Adenosine triphosphate
ATP5B	ATP synthase F1 subunit beta
ATP5F1A	ATP synthase F1 subunit alpha
BAX	BCL2 associated X, apoptosis regulator
BCL2	BCL2 apoptosis regulator
CACT	Carnitine/acylcarnitine translocase
CD36	Cluster of differentiation 36/fatty acid translocase
CPT1	Carnitine palmitoyltransferase 1
CPT2	Carnitine palmitoyltransferase 2
CS	Citrate synthase
COXII	Cytochrome c oxidase subunit 2
COX4-1	Cytochrome c oxidase subunit 4i1
CYPB	Cyclophilin B
CYC1	Cytochrome C1
DEG	Differential gene expression
DMF	Dimethyl fumarate
DMS	Dimethyl succinate
DNP	2,4-dinitrophenylhydrazone
ECAR	Extracellular acidification rate
ECI	Enoyl-CoA delta isomerase

ENO	Enolase
FAD^+	Oxidised flavin adenine dinucleotide
$FADH_2$	Reduced flavin adenine dinucleotide
GAPDH	Glyceraldehyde-3-phosphate dehydrogenase
GLUD1	Glutamate dehydrogenase 1
GLUT	Glucose transporter
GPCR	G-protein coupled receptor
GSEA	Gene set enrichment analysis
GSH	Reduced glutathione
GSSG	Oxidised glutathione
GSVA	Gene set variation analysis
H_2O_2	Hydrogen peroxide
HCA2	Hydroxycarboxylic acid receptor 2
HDAC1	Histone deacetylase 1
HIF	Hypoxia-inducible factor 1
hiPSC-CM	Human-induced Pluripotent Stem Cell-derived Cardiomyocytes
HK	Hexokinase
HMOX1	Heme oxygenase 1
KEAP1	Kelch-like ECH-associated protein 1
KEEG	Kyoto Encyclopaedia of Genes and Genomes
LDH	Lactate dehydrogenase
MCAD	Medium-chain acyl-CoA dehydrogenase
MCT	Monocarboxylate transporter
MDH	Malate dehydrogenase
MMF	Monomethyl fumarate
MTHFD2	Methylene tetrahydrofolate dehydrogenase 2
mTOR	Mechanistic target of rapamycin
NAD^+	Oxidised nicotinamide adenine dinucleotide
NADH	Reduced nicotinamide adenine dinucleotide
NDUFV1	NADH:ubiquinone oxidoreductase core subunit v1

NDUFB8	NADH:ubiquinone oxidoreductase subunit B8
Nrf2	Nuclear factor erythroid 2 [NF-E2]-related factor 2
NQO1	NAD(P)H quinone dehydrogenase 1
OXPHOS	Oxidative phosphorylation
PDH	Pyruvate dehydrogenase
PDK	Pyruvate dehydrogenase kinase
PFKM	Phosphofructokinase muscle isoform
PGK	Phosphoglycerate kinase
PK	Pyruvate kinase
PGC1A	Peroxisome proliferator-activated receptor gamma coactivator 1-alpha
PTM	Post-translational modifications
ROS	Reactive oxygen species
Rpl32	Ribosomal Protein L32
SDH	Succinate dehydrogenase
SFN	Sulforaphane
SLC25A3/PHC	Mitochondrial phosphate carrier protein
SOD1	Superoxide Dismutase 1
SRXN1	Sulfiredoxin 1
Total H3	Total histone 3
TXNRD1	Thioredoxin reductase 1
T2D	Type 2 diabetes
OCR	Oxygen consumption rate
UBC	Ubiquitin C
UQCRC2	Ubiquinol-cytochrome C reductase core protein 2
VM	Vumerity/diroximel fumarate

Chapter 1

General introduction

1.1 Cardiac metabolism in the healthy heart.

The average resting adult heart beats between 60 and 90 times per minute[1]. Cardiomyocytes continuously undergo cycles of contraction and relaxation, which makes the heart a high-energy demanding organ which utilises around 6 kg of ATP per day[2]. Under healthy conditions, this energy is generated predominantly from oxygen-dependent reactions inside the mitochondria, which produce 95% of the total ATP needed by the heart, whereas the remaining 5% is generated from oxygen-independent reactions occurring in the cell cytosol and mitochondria[3]. Long-chain fatty acids (LCFA) are the preferred substrate for cardiomyocyte mitochondrial metabolism, contributing to 60% of cardiac ATP production. To a lesser extent, glucose and lactate oxidation contribute 30% to ATP production, with ketones and amino acids representing a small contribution of approximately 5% each[4] [5] **(Figure 1.1)**.

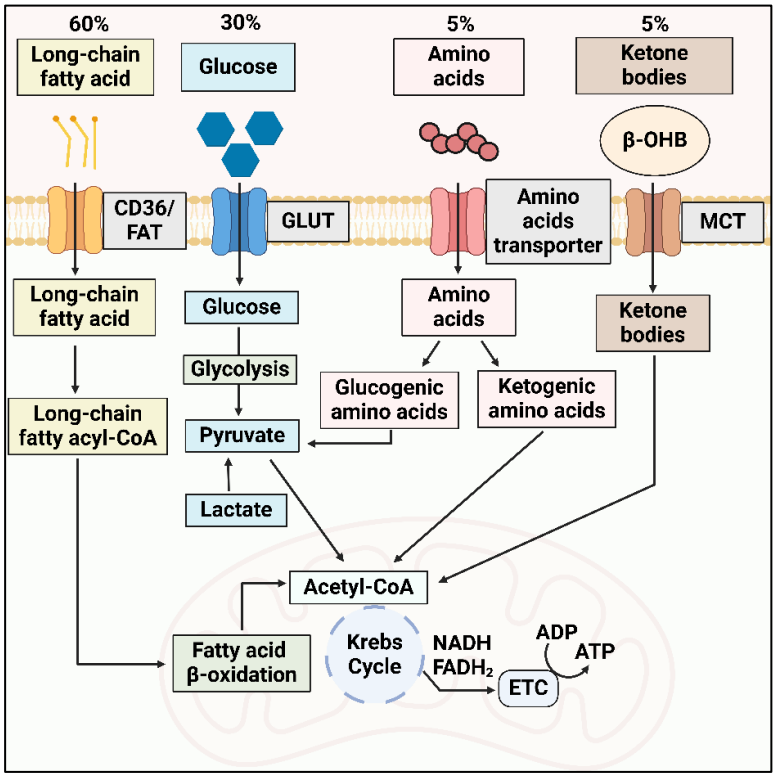

Figure 1.1: Cardiac mitochondrial substrate utilisation for oxidative metabolism. The illustration displays the substrate usage by the heart for mitochondrial oxidative metabolism, indicating substrate preference (expressed as percentages) and the metabolic pathways involved in the incorporation of each substrate into the mitochondria[4-7]. CD36/FAT, cluster of differentiation 36/fatty acid translocase. GLUT, glucose transporter. MCT, monocarboxylate transporter. β-OHB, β-hydroxybutyrate. ETC, electron transport chain.

1.1.1 Fatty acid metabolism within the heart.

To meet its high energy demands, the heart depends on fatty acids present in the bloodstream. These fatty acids are found in different states: as non-esterified fatty acids (free fatty acids) bound to albumin, or esterified as triacylglycerols packaged as lipoprotein chylomicrons, when derived from the diet, or in very-low-density lipoproteins, when synthesised by the liver[8, 9]. Triacylglycerols are hydrolysed to non-esterified fatty acids by the endothelial enzyme lipoprotein lipase, previously synthesised in the cardiomyocyte[10]. LCFA are transported into the cardiomyocyte by two different mechanisms: a slow-rate passive transport diffusing directly across the cell membrane via a flip-flop mechanism, and a rapid facilitated transport mediated by membrane transporters. Three different types of transporters have been identified expressed within the heart, the plasma membrane-associated fatty acid binding protein (FABPpm), the fatty acid transport proteins 1 and 6 (FATP1 and 6), and the fatty acid translocase (FAT/CD36), the latter is considered the primary fatty acid transporter in the cardiomyocyte[11, 12].

LCFA are esterified to long-chain fatty acyl-CoA (LCFAcyl-CoA) in the cytosol of the cardiomyocyte by the enzyme long-chain acyl-CoA synthetase (ACSL). LCFAcyl-CoAs are the substrates for the mitochondrial carnitine shuttle, composed of the outer carnitine palmitoyltransferase 1 (CPT1), the intermembrane carnitine/acylcarnitine translocase (CACT), and inner carnitine palmitoyltransferase 2 (CPT2)[6, 13], as detailed in **Figure 1.2.**

Inside the mitochondria, saturated LCFAcyl-CoA with an even number of carbons enter mitochondrial β-oxidation, a cycling four-step process that generates acetyl-CoA, the primary substrate utilised by the Krebs cycle, and the electron carriers NADH and $FADH_2$, which support ATP production, via the electron transport chain. In contrast, unsaturated fatty acids require an additional enzymatic step in which the cis-double bond in the carbon

skeleton is isomerised to the trans configuration by the enzyme enoyl-CoA isomerase, or reduced by the enzyme 2,4-dienoyl CoA reductase using an NADPH molecule[14].

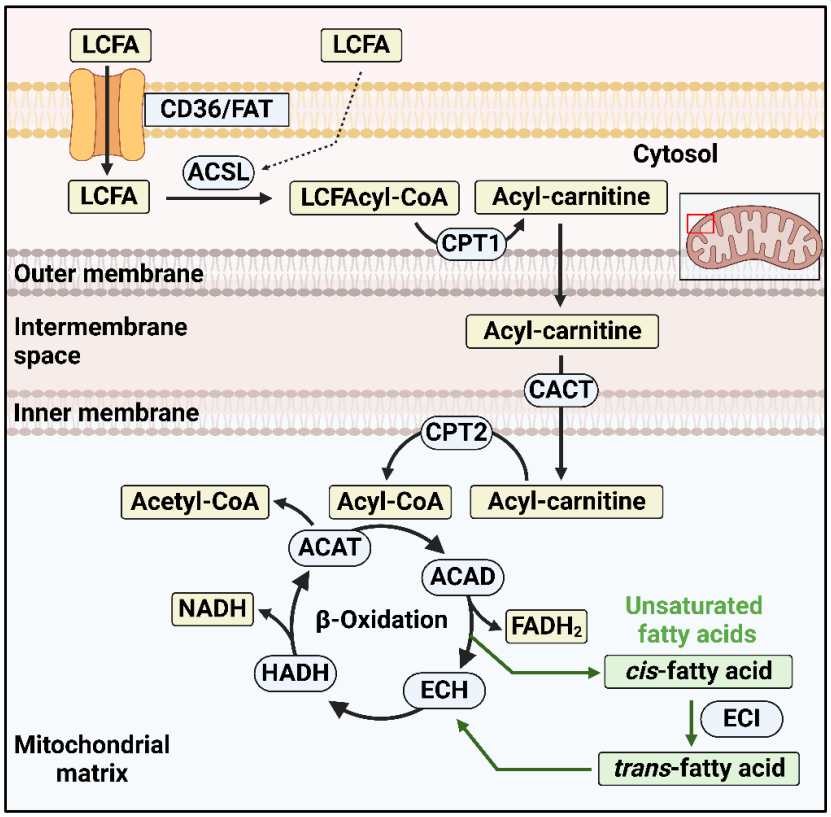

Figure 1.2: Fatty acid oxidation. The picture displays the uptake of non-esterified fatty acid into the cell through fatty acid transporters or diffusion across the membrane. In the cytosol, fatty acid is conjugated to CoA by the enzyme acyl-CoA synthetase long-chain family member (ACSL) and incorporated into mitochondria via the carnitine shuttle, where is utilised to produce acetyl-CoA and electron carriers through the mitochondrial β-oxidation components. CD36/FAT, cluster of differentiation 36/fatty acid translocase. LCFA, long-chain fatty acids. LCFAcyl-CoA, long-chain fatty acyl-CoA. CPT1, carnitine palmitoyltransferase 1. CACT, carnitine/acylcarnitine translocase CPT2, carnitine palmitoyltransferase 2. ACAD, acyl-CoA dehydrogenase. ECH, enoyl-CoA hydratase. HADH, hydroxyacyl-CoA dehydrogenase. ACAT, acetyl-CoA acetyltransferase. ECI, enoyl-CoA delta isomerase.

1.1.2 Glucose metabolism within the heart.

Glucose metabolism has a lower energy production efficiency compared with LCFA oxidation, as one molecule of glucose generates 31 molecules of ATP, whereas one molecule of LCFA, palmitate, produces 129 molecules of ATP[13]. The heart obtains glucose directly from the bloodstream or from its intracellular glycogen stores. Glucose uptake into the

cardiomyocyte is mediated mainly by a family of transmembrane transporters known as glucose transporters (GLUT), with GLUT1 and GLUT4 being the predominant cardiac isoforms[15, 16]. Continuous glucose uptake is achieved through the phosphorylation of glucose by the enzyme hexokinase, producing glucose 6-phosphate, which can subsequently enter three different pathways: glycolysis, glycogen synthesis, and the pentose phosphate pathway[6]. Glycolysis is an oxygen-independent metabolic pathway that occurs in the cytosol through the activity of ten enzymes, producing pyruvate as the final product. Under aerobic conditions, pyruvate is transported into the mitochondria and decarboxylated into acetyl-CoA, which is utilised by Krebs cycle as an energetic molecule. Alternatively, under anaerobic conditions, pyruvate is reduced to lactate in the cytosol, generating 2 molecules of ATP **(Figure 1.3)**.

Glucose oxidation involves the uptake of pyruvate by the mitochondria, and once inside the mitochondrial matrix, pyruvate is decarboxylated by the enzyme pyruvate dehydrogenase (PDH) into acetyl-CoA. PDH is allosterically modulated by [acetyl-CoA]/[CoA] and [NADH]/[NAD^+] ratios, through phosphorylation and dephosphorylation modifications mediated by the PDH inhibitor, pyruvate dehydrogenase kinase (PDK) and the PDH activator, pyruvate dehydrogenase phosphatase (PDP)[17].

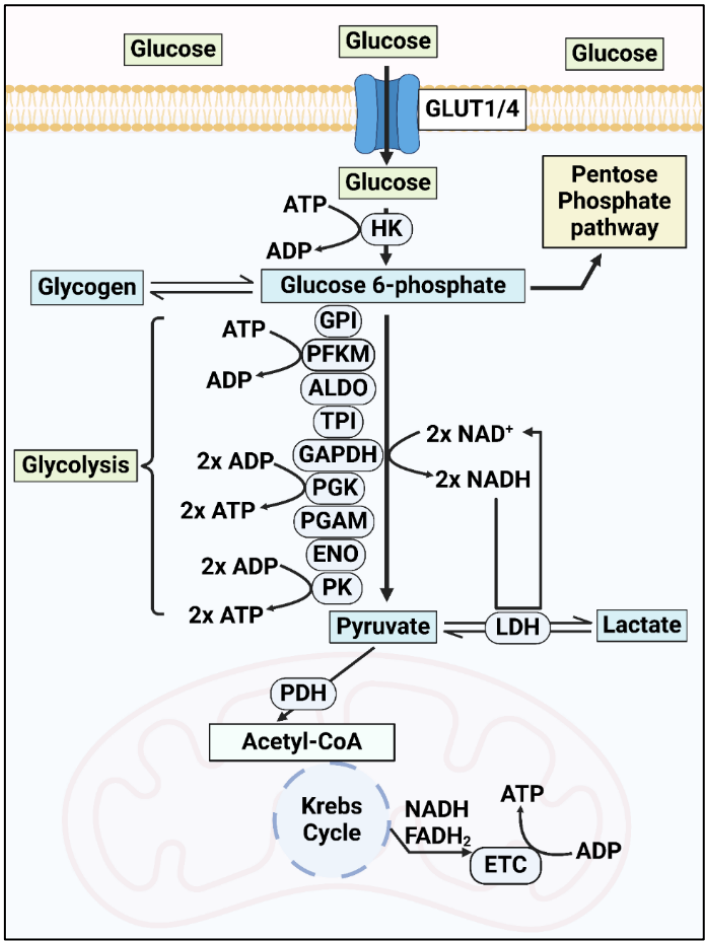

Figure 1.3: Glucose metabolism. The illustration represents glucose metabolism into pyruvate through glycolysis and its subsequent utilisation in oxidative metabolism through mitochondria incorporation and decarboxylation into acetyl-CoA, or its reduction into lactate during anaerobic metabolism in the cytosol. GLUT1/4, glucose transporter 1 and 4. HK, hexokinase. GPI, glucose phosphate isomerase. PFKM, phosphofructokinase muscle isoform. ALDO, aldolase. TPI, triosephosphate isomerase. GAPDH, glyceraldehyde-3-phosphate dehydrogenase. PGK, phosphoglycerate kinase. PGAM, phosphoglycerate mutase. ENO, enolase. PK, pyruvate kinase. LDH, lactate dehydrogenase. PDH, pyruvate dehydrogenase. ETC, electron transport chain.

1.1.3 Regulation of glucose and fatty acid metabolism.

Glucose and fatty acid metabolism are both highly regulated processes where transcription factors play an essential role. The carbohydrate-responsive element-binding protein (ChREB) is the principal transcription factor mediating glucose metabolism[18]. ChREB is activated by high concentration of glucose, inducing post-translational modifications that induce its nuclear translocation resulting in upregulation of several glycolytic genes,

including pyruvate kinase, phosphofructokinase, GLUT2 and GLUT4[19, 20]. Peroxisome-proliferator activated receptors (PPARs) are a family of hormone-nuclear receptors known for their transcriptional activity regulating fatty acid metabolism[21]. PPARα is the main isoform found in the heart tissue[22]. It is activated by binding fatty acids, inducing its heterodimerisation, nuclear translocation and binding to the promoter regions of peroxisome proliferator response elements. PPARα activity is modulated by its coregulators, the retinoid X receptor and the peroxisome proliferator-activated receptor gamma coactivator 1-alpha (PGC1A/PPARGC1A)[23, 24]. PPARα promotes fatty acid β-oxidation gene expression, including *CD36*, *CPT1*, *CPT2*, *ACAD*, and *HADH* upregulation[25, 26].

In 1962, Garland and colleagues observed in rat hearts perfused for just 15 minutes that the uptake of glucose or pyruvate by the heart was significantly reduced when palmitate and bovine plasma albumin were added to the perfusion medium[27]. This observation suggested a directed and rapid mechanism of cross-regulation between glucose and fatty acid metabolism, which was further explored and investigated by Randle and colleagues, who discovered and published a year later the well-known Glucose-Fatty acid cycle or The Randle cycle[28]. Fatty acid metabolism inhibits glucose metabolism, as it significantly raises the [acetyl-CoA]/[CoA] and [NADH]/[NAD^+] ratios in the mitochondria, which inhibits PDH via activation of PDK. This inhibition triggers an accumulation of the metabolite citrate, which inhibits the glycolytic enzyme phosphofructokinase 1 (PFK1), subsequently increasing glucose 6-phosphate that can inhibit hexokinase by end-product inhibition[28-30]. On the other hand, glucose metabolism inhibits fatty acid metabolism when high glucose concentrations are present in the bloodstream. Glucose uptake via GLUT transporters is subsequently metabolised via glycolysis into pyruvate, which is then decarboxylated into acetyl-CoA in the mitochondria. A fraction of the citrate generated from glucose exits the mitochondria into the cytosol, where it is converted back into acetyl-CoA by the enzyme

ATP-citrate lyase (ACL) and then into malonyl-CoA by acetyl-CoA carboxylase (ACC). Malonyl-CoA acts as a potent inhibitor of carnitine palmitoyltransferase 1 (CPT1), hence reducing the incorporation of long-chain acyl-CoA into the mitochondria[28, 29] **(Figure 1.4)**.

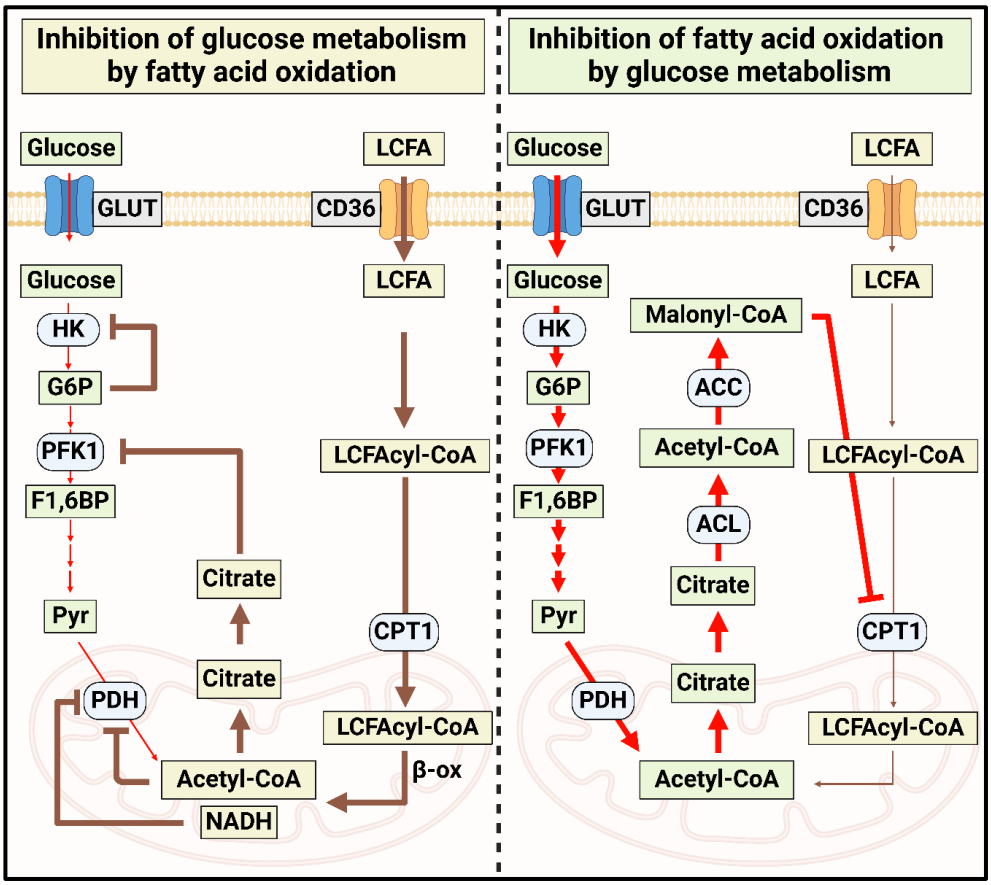

Figure 1.4: Cross-regulation of glucose and fatty acid metabolism via the Randle cycle. High rates of fatty acid oxidation increase the [acetyl-CoA]/[CoA] and [NADH]/[NAD^+] ratios, causing pyruvate dehydrogenase (PDH) inhibition and citrate accumulation, which is released into the cytosol, inhibiting the glycolytic enzyme phosphofructokinase 1 (PFK1). This increases glucose 6-phosphate (G6P) which inhibits hexokinase (HK) activity. Conversely, high rates of glycolysis produce pyruvate (Pyr), which is incorporated into the mitochondria and decarboxylated to acetyl-CoA. Acetyl-CoA is indirectly exported to the cytosol and carboxylated by acetyl-CoA carboxylase (ACC) to malonyl-CoA, which is a potent inhibitor of the carnitine palmitoyltransferase 1 (CPT1), thereby reducing mitochondrial oxidation of long-chain acyl-CoA (LCFA). F1,6BP, fructose 1,6-bisphosphate. β-ox, mitochondrial fatty acid β-oxidation[28, 29].

1.1.4 Krebs cycle and oxidative phosphorylation.

The Krebs cycle, also known as the citric acid cycle, was described in 1937[31], and it represents a series of enzymatic reactions and metabolite oxidation processes within the mitochondria, which are essential for generating the electron carriers necessary for cell energy production. As the principal function of the Krebs cycle is to mediate energy production from fuel molecules[32], it acts as an acceptor of the acetyl-CoA molecules generated through various metabolic pathways. Acetyl-CoA produced during fatty acid β-oxidation directly accesses the Krebs cycle as both processes occur in the mitochondrial matrix, whereas pyruvate, generated as a final product of the glycolytic, must first enter the mitochondria and then be decarboxylated into acetyl-CoA before entering the Krebs cycle. The intermediates involved in the Krebs cycle, as well as the enzymes, and the molecules generated during these reactions, including the electron carriers NADH and $FADH_2$, are detailed in **Figure 1.5.**

The proper functionality of the Krebs cycle is maintained by constant cycling of the carbon flow into and out of the mitochondria, where the replenishment of the Krebs cycle metabolites from other pathways is known as anaplerotic reactions, while the utilisation of the Krebs cycle metabolites by other pathways is known as cataplerotic reactions[33, 34].

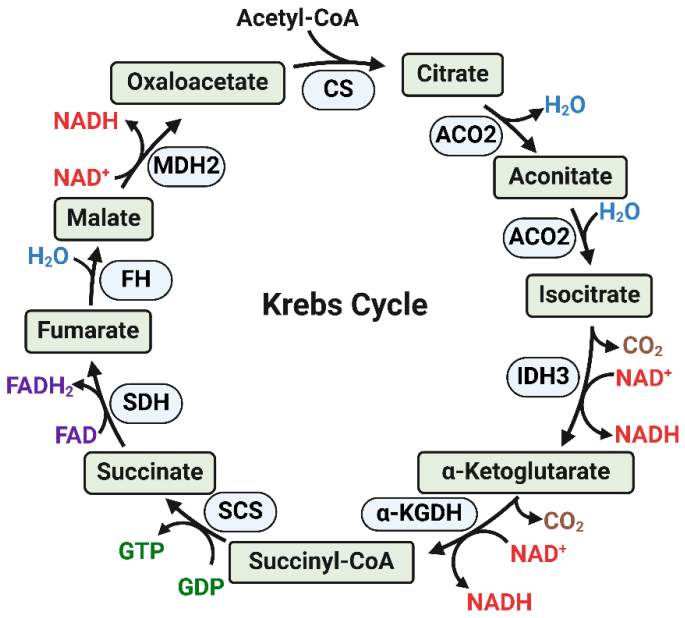

Figure 1.5: The Krebs cycle. The Krebs cycle begins with acetyl-CoA combining with oxaloacetate to form citrate, catalysed by the enzyme citrate synthase (CS). Citrate is subsequently converted into aconitase and then isocitrate by the enzyme aconitase 2 (ACO2). Isocitrate is oxidised to α-ketoglutarate by the enzyme isocitrate dehydrogenase 3 (IDH3), producing NADH and CO_2. α-ketoglutarate is decarboxylated by α-ketoglutarate dehydrogenase (α-KGDH) to form succinyl-CoA, yielding another NADH and CO_2 molecule. Succinyl-CoA is converted into succinate by the enzyme succinyl-CoA synthetases (SCS) generating a GTP molecule. Succinate is oxidised to fumarate by succinate dehydrogenase (SDH) producing the electron carrier $FADH_2$. Fumarate is hydrated to malate by fumarate hydratase and then oxidised to regenerate oxaloacetate by the enzyme malate dehydrogenase 2 (MDH2), producing NADH[31, 32].

The electrons from the carriers NADH and $FADH_2$ generated in the Krebs cycle enter the electron transport chain (ETC) via Complex I or Complex II, respectively. The electrons are transferred to Complex III and Complex IV through their mobile electron carriers ubiquinone and cytochrome C, with molecular oxygen acting as the final electron acceptor. The movement of the electrons through the ETC drives the pumping of protons from the mitochondrial matrix into the intermembrane space, generating a proton gradient essential for the ATP synthase (Complex V) to produce ATP from ADP [35, 36].

1.2 Krebs cycle metabolites as signalling molecules.

Beyond their energetic role, Krebs cycle metabolites can also act as signalling molecules regulating several cellular processes, including epigenetic modifications, immune modulation, regulation of post-translational modifications and the response to hypoxia **(Figure 1.6)**.

Epigenetic modification involves changes in gene expression without inducing a direct alteration in the DNA sequence[37]. Different epigenetic modifications have been identified, and DNA and histone demethylation are mainly facilitated by the 2-oxyglutarate-dependet-dioxygenases (2-OGDO) enzyme family[38]. Notable, the Krebs cycle metabolite α-ketoglutarate is an essential substrate for the 2-OGDO[38, 39] activity, while succinate and fumarate act as inhibitors of their enzymatic activity[40]. Interestingly, a number of Krebs cycle enzymes have also been reported to localise inside the nucleus, modulating DNA and chromatin dynamics by altering the acetylation and methylation levels of histone proteins[41].

The role of the Krebs cycle metabolites regulating the immune system has also been investigated. Citrate plays an important role as an inflammatory signalling molecule in monocytes and macrophages[42, 43]. Succinate has been reported as a novel regulator of the pro-inflammatory response by enhancing immune cell migration and promoting cytokine and interleukin production through its binding and interaction with the membrane receptor succinate receptor 1 (SUCNR1)[44-46]. Similar anti-inflammatory roles, increasing macrophage activation and responsiveness to pathogens, promoting cytokine, interleukin, and type I interferon production have also been identified for fumarate[47, 48]. For example, high blood fumarate concentrations were reported to decrease B-cell population and suppress their ability to produce antibodies[49].

Metabolites can also modulate post-translation modifications (PTM). Acetyl-CoA serves as a substrate for protein acetylation by the acetyltransferases enzyme[50, 51]. Succinate accumulation can drive succinylation [45, 52], while fumarate targets cysteine residues inducing protein succination[53, 54]. Additionally, NAD^+ regulates protein deacetylation levels by controlling sirtuin activity[55].

The Krebs cycle metabolites play an important role in regulating the cellular response to hypoxia, mainly regulating the stabilization of the oxygen-sensitive hypoxia-inducible factor 1-alpha (HIF1-α). α-ketoglutarate acts as a substrate for the HIF prolyl hydroxylase domain (PHD) enzyme, promoting HIF1α hydroxylation and subsequent proteasomal degradation[56]. In contrast, succinate and fumarate promoted HIF1α stabilisation by inhibiting the same PHD enzymes[57-59]. Furthermore, under ischemic conditions, malate derived from the malate-aspartate shuttle is utilised by the mitochondria to produce fumarate and succinate through reverse Krebs cycle activity, further contributing to HIF1α stabilisation[58, 60].

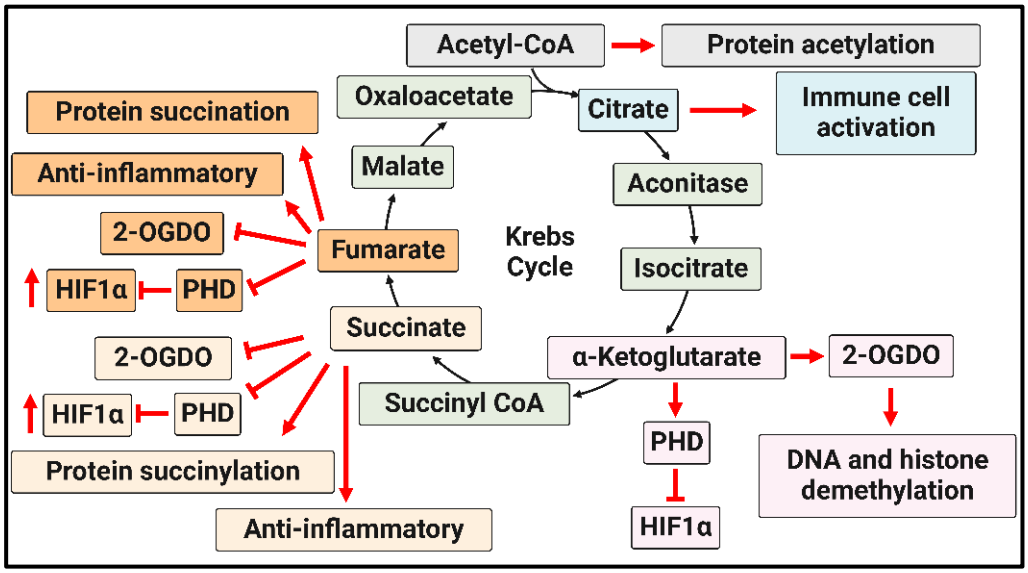

Figure 1.6: Mitochondrial Krebs Cycle metabolites as signalling molecules. Beyond their energy role inside the mitochondria, Kreb cycle metabolites can also participate as signalling molecules in different cell processes, including regulating post-translation modifications, immune regulators, modulating epigenetics changes, and contributing to the cellular response to hypoxia. PHD, prolyl hydroxylase domain protein. OGDO, oxoglutarate-dependent dioxygenases.

1.3 Hypoxia and its dynamic regulation of cardiac metabolism.

The heart responds rapidly to environmental changes, such as variations in oxygen concentration, and it can temporarily adapt its metabolism under stress conditions to favour tissue and cell survival. Myocardial ischemia is a cardiac condition characterised by a restriction in blood flow, limiting the supply not only of oxygen but additionally the supply of nutrients and removal of waste products.

In response to hypoxia and ischemia, the heart attempts to conserve the available oxygen by decreasing its consumption by shifting from oxidative metabolism to anaerobic glycolysis[61, 62]. This adaptation in the cardiomyocyte is mediated by the AMP-activated protein kinase (AMPK) and HIF1. Acute hypoxia impairs oxidative metabolism and decreases the production of ATP by the mitochondria, significantly raising the AMP/ATP ratio[63]. This induces AMPK phosphorylation and activation, which remodels metabolism to acutely increase its glycolysis and glycogenolysis pathways[64, 65] **(Figure 1.7)**.

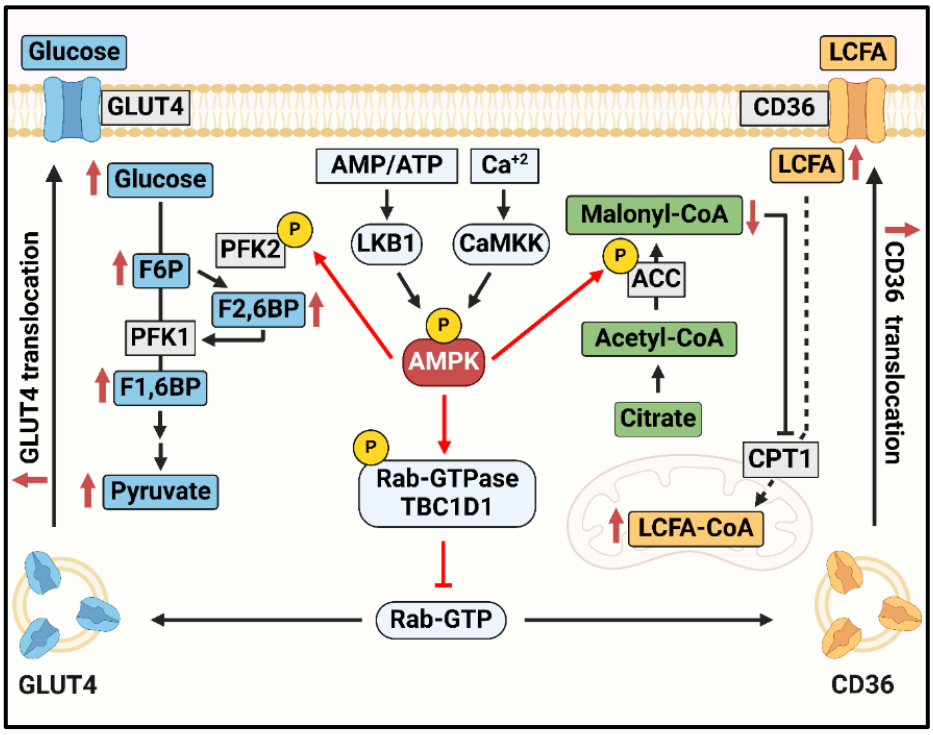

Figure 1.7: Acute hypoxia response mediated by AMPK allosteric phosphorylation. Increasing AMP/ATP ratio under hypoxic conditions or high intracellular Ca^{+2} levels induces AMPK activation through its phosphorylation on threonine 172 by the serine/threonine kinase 11 (LKB1) or the calcium/calmodulin-dependent protein kinase kinase (CaMKK), respectively. Once activated, AMPK promotes glucose transporter 4 (GLUT4) and cluster of differentiation 36/fatty acid translocase (CD36) membrane translocation by phosphorylating and inhibiting the Rab-GTPase activity of the TBC1 domain Family Member 1 (TBC1D1), and then promoting Rab-GTP active form. AMPK enhances glycolysis by phosphorylating and activating the phosphofructokinase 2 (PFK2), increasing the concentration of the allosteric activator of phosphofructokinase 1 (PFK1), fructose-2,6-biphosphate (F2,6BP), and favouring pyruvate production. Furthermore, AMPK phosphorylates and inhibits acetyl-CoA carboxylase (ACC), decreasing malonyl-CoA levels, which facilitates long-chain fatty acid translocation into the mitochondria and subsequent mitochondrial β-oxidation[66, 67].

Chronic hypoxia promotes transcriptional regulation of cardiac metabolism by activating HIF1[68]. HIF1 is a heterodimer composed of an oxygen-sensitive subunit, HIF1α, and a constitutively expressed non-oxygen-sensitive subunit, HIF1β[69]. Under normoxia, HIF1α is hydroxylated by a prolyl hydroxylase domain enzymes (PHD) and recognised by the Von Hippel-Lindau protein (VHL), which is part of the E3 ubiquitin ligase complex, inducing HIF1α polyubiquitination and its proteasomal degradation[70]. HIF1α inactivation is further

guaranteed by an additional hydroxylation at a critical asparagine residue (Asn803) by the factor inhibiting HIF (FIH), which inhibits HIF1 binding to its transcriptional activator (p300/CBP)[71, 72]. PHD and FIH are part of the 2-OGDO family, meaning that their enzymatic activity depends on molecular oxygen, and therefore, under hypoxic conditions PHD enzymes are inhibited. As a consequence, HIF1α protein levels increase, dimerise with HIF1β and translocate to the cell nucleus where HIF1 recognises and binds to a specific promotor sequence the hypoxia response element (HRE)[70, 73]. Metabolically, HIF1 upregulates the glycolytic genes *GLUT1, HK, ALDO, PGK, GAPDH, ENO, and PK*[74-76], as well as LDH that increases pyruvate reduction into lactate[77]. These changes are also accompanied by a reduction in oxidative metabolism, where HIF1 upregulates PDK1, promoting PDH inhibition and decreasing pyruvate decarboxylation to acetyl-CoA[77, 78]. HIF1 also reduces mitochondrial density by increasing the expression of BCL2 Interacting Protein 3 (BNIP3)[79], inducing mitophagy. Additionally, HIF1 suppresses mitochondrial activity by directly affecting the ETC by modifying cytochrome c oxidase (COX) components, specifically, inducing COX4-1 proteasomal degradation and increasing the level of the hypoxic isoform COX4-2[79, 80] **(Figure 1.8)**.

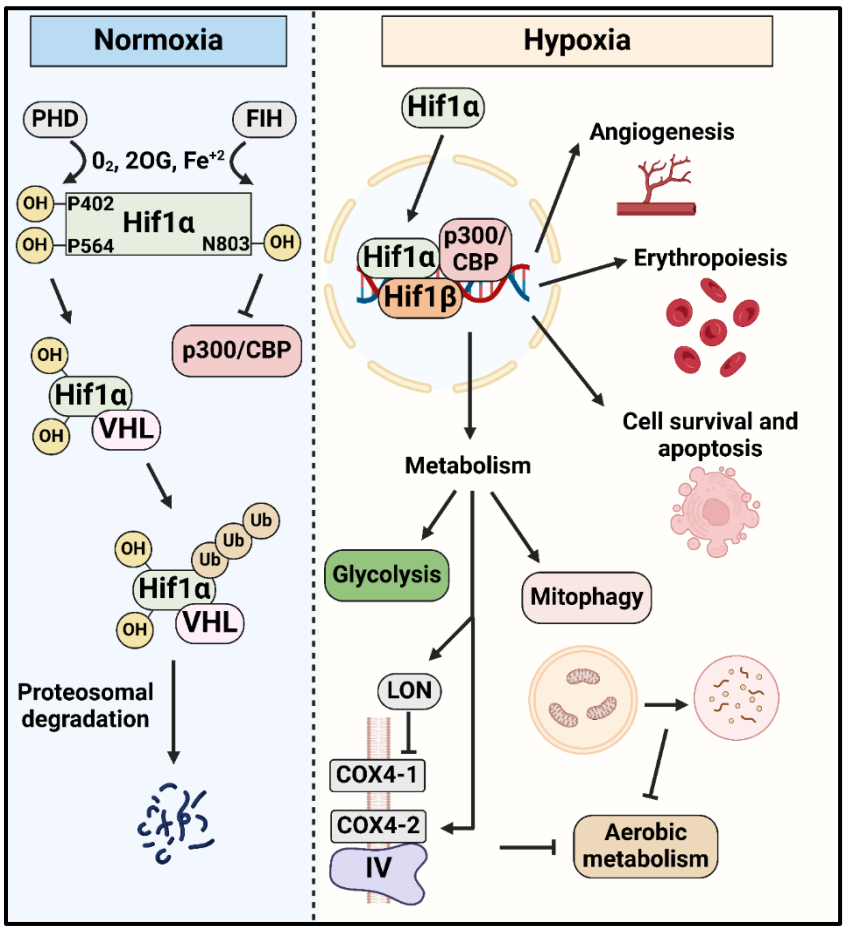

Figure 1.8: Chronic hypoxia and HIF1 transcriptional regulation of cardiac metabolism. Under normoxic conditions, HIF1α is hydroxylated (OH) at proline (P) residues P402 and P564 by prolyl hydroxylase domain (PHD) enzymes. This modification is recognised by the von Hippel-Lindau protein (VHL), inducing HIF1α polyubiquitination (Ub) and proteasomal degradation. HIF1α is also hydroxylated at asparagine (N) 803 by the factor-inhibiting HIF (FIH), preventing HIF1α interaction with its transcriptional activator p300/CBP. Under hypoxic conditions, low oxygen levels impair PHD and FIH activities, allowing HIF1α stabilisation, nuclear translocation, and binding with HIF1β and p300/CBP. Activated HIF1 regulates several cell processes, including metabolism, angiogenesis, erythropoiesis, cell survival and apoptosis. Metabolically, HIF promotes glycolytic metabolism and reduces oxidative metabolism by inducing mitophagy and promoting the degradation of the complex IV cytochrome c oxidase subunit 4 (COX4) isoform 1 (COX4-1) by the mitochondrial ATP-dependent protease Lon (LON), while increasing the levels COX4 isoform 2 (COX4-2)[81-84].

1.4 Nrf2 and antioxidant enzymes: Allies against hypoxia-induced ROS production.

Acute ischemia and hypoxia also lead to alterations in non-metabolic pathways. The lack of sufficient oxygen during hypoxia generates an imbalance between the flow of electrons through the ETC and their final acceptor, resulting in the generation and accumulation of

reactive oxygen species (ROS)[85]. When intracellular concentrations of ROS exceed the antioxidant defence mechanisms, these molecules trigger oxidative stress and oxidative damage, inducing deleterious effects on various cellular compartments and biomolecules, including lipids, proteins and DNA[86, 87]. To protect against oxidative stress, cells rely on multiple enzymes to defend cells against oxidative damage, and interestingly, most of these are regulated by a single transcription factor, the nuclear factor erythroid 2 [NF-E2]-related factor 2 (Nrf2). Nrf2 expression and activity increase in response to oxidative stress, upregulating the expression of genes coding for antioxidant defence enzymes and anti-inflammatory regulators[88, 89]. Nrf2 activation has been described as essential for cell protection against ROS during hypoxia[90, 91] and cardioprotective during ischemia-reperfusion injury through its antioxidant role[92-98].

1.5 Beyond the Krebs cycle: Investigating the role of fumarate in hypoxia.

The metabolic changes induced by hypoxia and ischemia also alter the Krebs cycle metabolite content. Succinate is the most studied metabolite during ischemia. Succinate accumulation has been reported in several models of cardiac ischemia-reperfusion injury[99-102], and it is considered a beneficial metabolite for ischaemic conditions by supporting cardiac energetics, but detrimental during reperfusion due to increased production of reactive oxygen species[99, 103].

In a metabolomics study performed by Prof Lisa Heather's group using healthy and diabetic hearts exposed to normoxia, hypoxia or hypoxia-reoxygenation[104], it was observed that hypoxia significantly increased intracellular levels of succinate and fumarate within the healthy heart. However, in diabetic hearts, the increase in succinate levels under hypoxia was much lower, while the increase in fumarate levels was completely blunted in diabetes **(Figure 1.9)**.

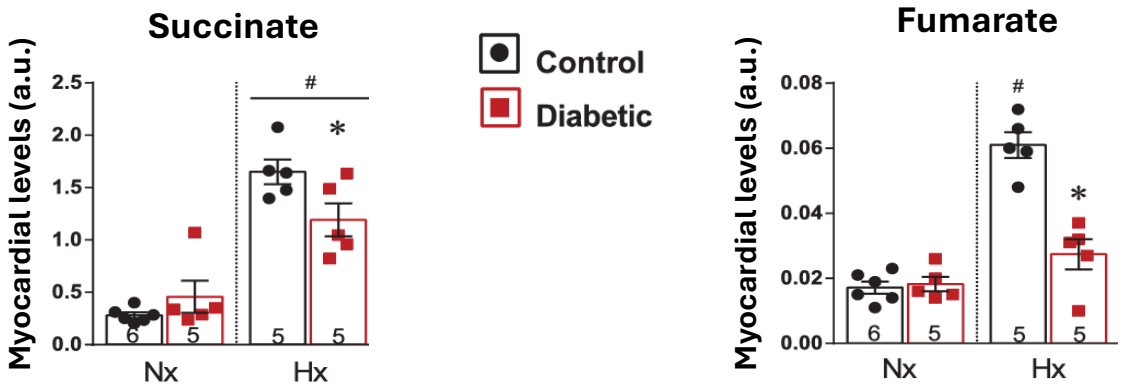

Figure 1.9: Succinate and fumarate levels in response to hypoxia in healthy and diabetic rat hearts. Myocardial levels of succinate and fumarate in healthy (Control) and diabetic rat hearts exposed to normoxia (Nx) or acute hypoxia (Hx). * $p < 0.05$ vs. Control under same oxygen condition, # $p < 0.05$ vs. normoxia within same disease state. Data is expressed as peak area ratio. Figure extracted from a previous publication of the Heather group[104].

Diabetic patients do not respond or recover in the same way following a myocardial infarction, considerably increasing their mortality[105, 106]. However, the mechanism underlying why this metabolic disorder causes this increased mortality after a heart attack is not fully understood. It remains unclear whether changes in metabolite concentrations contribute to this impaired response in diabetes. Interestingly, the observation that among the metabolites within the diabetic heart, fumarate showed a complete blunted elevation in response to hypoxia indicates a potential connection between cardiac metabolic diseases and altered fumarate concentrations. However, this relationship has not been studied, and whether this fumarate increase is critical for the cardiac response to hypoxia is unknown.

Therefore, the key questions are: what is the role of fumarate in cardiac hypoxia/ ischaemia? Does fumarate elevation modulate specific molecular mechanisms and/or signalling pathways that facilitate the heart's response and survival to low oxygen concentrations? Could fumarate be a potential therapeutic tool to amend the impaired response of type 2

diabetes patients to myocardial ischaemia? Or is fumarate elevation just a metabolic stress consequence of hypoxia, which has no effect on the heart?

Understanding the downstream effects of fumarate accumulation on cellular signalling pathways will provide new insight into how the heart adapts to low oxygen levels and determine whether fumarate itself or its signalling targets could be beneficial as a clinical therapeutic tool in myocardial ischaemia and cardiovascular metabolic disorders.

1.6 Thesis aims.

The work described in this thesis aims to understand the molecular mechanisms and signalling pathways modulated by increased intracellular fumarate concentrations within the heart in response to hypoxia. This work will determine whether exogenous administration of fumarate and fumarate derivatives could impact human cardiomyocyte biology and metabolism, as well as investigate the potential therapeutic use of fumarate derivatives in insulin-resistant cardiomyocytes. This will be achieved across four chapters (numbered in this thesis from three to six), focusing on:

Hypothesis: Fumarate is an intracellular metabolite that selectively accumulates during hypoxia and can act as a signalling molecule reprogramming cardiomyocyte biology and metabolism.

Chapter 3: Investigate whether human-induced pluripotent stem cell-derived cardiomyocytes respond to exogenous fumarate derivatives, by evaluating their effect on antioxidant defence pathways.

Chapter 4: Determinate the impact of fumarate derivatives on fatty acid and glucose metabolism, and their effect on mitochondrial dynamics and respiratory capacity in human cardiomyocytes.

Chapter 5: Study the effect of increased fumarate levels on intracellular and extracellular signalling events in human cardiomyocytes.

Chapter 6: Evaluate the role of exogenous fumarate derivatives as a therapeutic tool in insulin-resistant human cardiomyocytes.

Chapter 2

General methods

2.1 Cell culture.

2.1.1 Human-induced Pluripotent Stem Cell-derived Cardiomyocytes.

IMR90, a healthy human-induced pluripotent stem cell (hiPSC) line prepared from fibroblast extracted from lung tissue from a 16-week-old female, was cultured as described previously[107, 108]. Before differentiation, hiPSCs were grown in TeSR-E8 media (StemCell Technologies) on reduced growth factor matrigel-coated plates (Corning). At full confluency, cells were differentiated into hiPSC-derived cardiomyocytes (hiPSC-CM) using a 17-day protocol **(Figure 2.1)**. For days zero and one, differentiation was started with RPMI media (Gibco) supplemented with 1% B27 minus insulin (ThermoFisher) and 6 μM CHIR99201 (Wnt pathway activator) (Tocris). On day 2, the media was changed to fresh RPMI media supplemented with 1% B27 minus insulin. On day 3, cells were cultured in RPMI media supplemented with 1% B27 minus insulin containing 2.5 μM Wnt-C59 (Wnt pathway inhibitor) (Tocris). On days 5, 7, and 9, the media was changed for RPMI media supplemented with 1% B27 minus insulin only. On days 11 and 13, the media was switched to no-glucose RPMI with 1% B27 without insulin. On day 15, the media was changed to RPMI supplemented with 1% B27 complete supplement (ThermoFisher). From day 17, cells were cultured for 1 week in maturation media (DMEM (Sigma Aldrich, 1 g/L glucose) supplemented with 10% heat-inactivated horse serum, 5 μg/mL vitamin B12 (Merck), 0.5 mM ascorbic acid (Merck), 0.84 μM biotin (Merck), 1.7 μM insulin, 80 μM oleic acid: BSA (2:1, Sigma Aldrich), 1x MEM non-essential amino acids, and 0.1X penicillin-streptomycin), replenishing the media every two days. During the cell differentiation and maturation processes, cells were kept at 37°C, 5% CO_2 and atmospheric O_2 (unless otherwise specified).

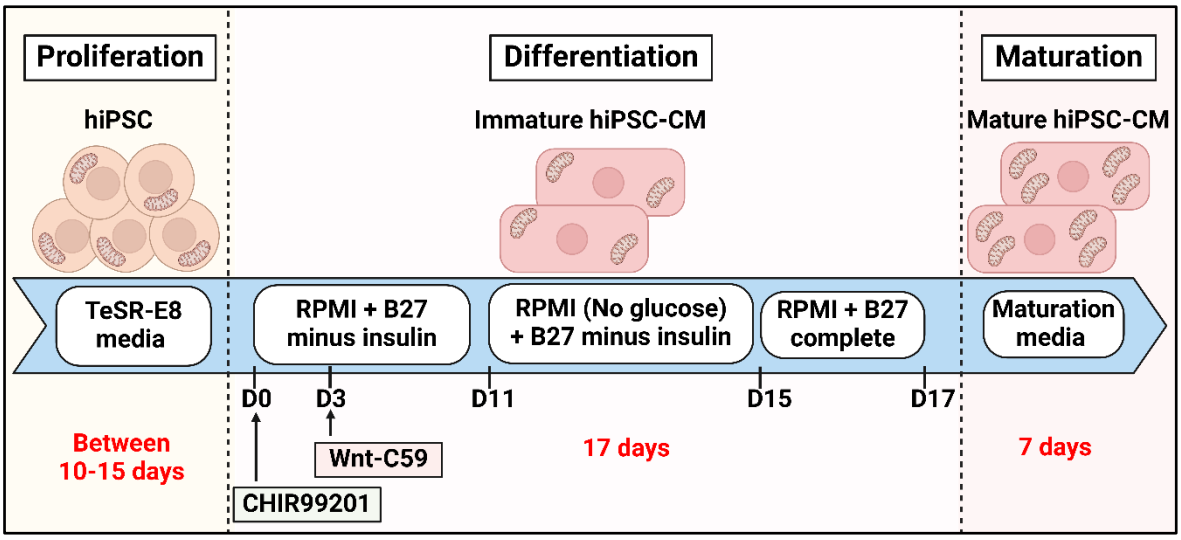

Figure 2.1: Protocol for generating mature human-induced pluripotent stem cell-derived cardiomyocytes. The diagram illustrates the protocol for generating and differentiating hiPSC derived from the IMR90 cell into mature hiPSC-derived cardiomyocytes. The protocol involves the use of the Wnt pathway activator, CHIR99201, to decrease cell pluripotency and initiate mesodermal differentiation[109], and the inhibitor, Wnt-C59, to promote cardiac differentiation[110].

2.1.2 Cardiomyoblasts derived from embryonic rat heart (H9c2) and Human embryonic kidney 293 (HEK293) cell lines.

H9c2 and HEK293 cell lines were purchased from ATCC. Cells were cultured in DMEM (Gibco) high glucose (25 mM) and pyruvate (1 mM), supplemented with 2 mM L-glutamine (Thermo Scientific), 100 U/mL Penicillin-Streptomycin (Gibco) and 10% fetal bovine serum (Gibco).

2.1.3 Molecule administration.

Fumaric acid (Fluka Analytical), dimethyl fumarate (Sigma), monomethyl fumarate (Sigma), Vumerity (Chemistry Department at the University of Oxford), sulforaphane (Sigma), and AZD3965 (MedChemExpress) were prepared in DMSO (Sigma), whereas hydrogen peroxide was dissolved in molecular-grade water. DMSO stocks were diluted in DMEM medium, filtered with a 0.22 µm filter, and added to the same media as the cells. The concentrations tested for fumaric acid were 150 µM, 300 µM, 500 µM and 2 mM. For

dimethyl fumarate, the concentrations were 50 μM, 100 μM, 150 μM, and 200 μM. For monomethyl fumarate and Vumerity, the concentration was 150 μM and 25μM, respectively. For sulforaphane, the tested concentration was 5 μM. For hydrogen peroxide, the concentration was 100μM. For AZD3965, the concentration was 100 nM.

2.2 RNA extraction, cDNA conversion and qPCR.

Cells were lysed using TRIzol reagent (ThermoFisher), and the RNA was purified using RNeasy mini kit (QIAGEN) following the manufacturer's protocol. For frozen tissue, RNA extraction was performed using the RNeasy Fibrous Tissue Mini Kit (QIAGEN). Tissue samples (≤ 30 mg) were weighed into Precellys Lysing kit tubes (Precellys) and homogenised in Buffer RLT (lysis buffer) supplemented with 1% β-mercaptoethanol (Sigma) using a Precellys 24 homogeniser. The manufacturer's protocol was then followed.

RNA concentrations were measured spectrophotometrically using a Nanodrop at 260 nm, where 1 absorbance unit was equal to an RNA concentration of 40 ng/μL. RNA was then reverse-transcribed into cDNA using the High-capacity RNA-to-cDNA kit (Applied Biosystems). For real-time PCR, the StepOnePlus Real-Time PCR System machine and Power SYBR Green PCR Master Mix were used, following the manufacturer's protocol. Each qPCR plate well contained 10 μL Power SYBR Green PCR Master Mix (2X), 0.5 μL of each primer (final concentration of 150 nM), 7 μL molecular-grade water, and 2 μL of cDNA (containing 20 ng of template). Negative control was also carried out without adding a cDNA template into the well. The qPCR thermal cycling condition included an initial holding stage at 95°C for 10 minutes, followed by 40 cycles of 95°C for 15 seconds and the specific annealing temperature of the primers (determined through primer validation) for 1 minute. The final melt curve stage consisted of three steps: 95°C for 15 seconds, 60°C for 1 minute, and 95° for 15 seconds. Gene expression was determined using the $2^{-\Delta\Delta Ct}$ method[98],

and the results were normalised to the housekeeping gene. Primer sequences are listed in **Table 2.1 (Human)**, **Table 2.2 (Mouse)**, and **Table 2.3 (Rat)**.

Primers were designed using the Primer-Blast online tool from the National Center for Biotechnology Information (NCBI), with primer parameters set to a product size between 70 and 200 bp and requiring that primers must span an exon-exon junction to prevent genomic DNA amplification. Primer validation was performed using the previously described qPCR reagent volumes and thermal cycling conditions, with an additional 10-fold serial dilution of the template. Three different annealing temperatures (60°C, 62°C and 64°C) were tested for each pair of primers. The optimal annealing temperature was determined based on the primer efficiency at each temperature, calculated using the slope of a curve plotting the log of the cDNA concentration against Ct values, and according to the equation $Efficiency = -1 + 10^{\left(-\frac{1}{slope}\right)}$. Ideally, the used annealing temperature presented a primer efficiency between 90% and 110%.

Table 2.1: Primer sequences for human genes.

Gene	**5' to 3' Forward sequence**	**5' to 3' Reverse sequence**
Ubiquitin C (*UBC*) (housekeeping gene)	CCTGGTGCTCCGTCTTAGAG	TTTCCCAGCAAAGATCAACC
NAD(P)H quinone dehydrogenase 1 (*NQO1*)	GCTGGTTTGAGCGAGTGTTC	CTGCCTTCTTACTCCGGAAGG
Heme oxygenase 1 (*HMOX1*)	CAGCAACAAAGTGCAAGATTCTG	GCTGAGTGTAAGGACCCATCG
Thioredoxin reductase 1 (*TXNRD1*)	CGATCTGCCCGTTGTGTTTG	CTGCCCTCCTGATAAGCCTTC
Sulfiredoxin 1 (*SRXN1*)	GACACGATCCGGGAGGAC	CAGCCCCCAAAGGAGTAGAAG

Superoxide Dismutase 1 (*SOD1*)	CCTAGCGAGTTATGGC GACG	CTGGTCCATTACTTTC CTTCTGC
Glutamate-Cysteine Ligase Catalytic Subunit (*GCLC*)	GCACCCTCGCTTCAGTA CC	TGGAGATGGTGTATTC TTGTCC
Methylene tetrahydrofolate dehydrogenase 2 (*MTHFD2*)	CCTGGTTGGCGAGAAT CCTG	GTCTCACTGTTGATTC CCACAAC
BCL2 apoptosis regulator (*BCL2*)	TCGCCCTGTGGATGACT GA	CAGAGACAGCCAGGA GAAATCA
BCL2 associated X, apoptosis regulator (*BAX*)	TCATGGGCTGGACATT GGAC	GCGTCCCAAAGTAGG AGAGG
Acyl-CoA synthetase long-chain family member 1 (*ACSL1*)	CTTCTGGTACGCCACGA GAC	GTCGCTGTCAAGTAGT GCG
Cluster of differentiation 36/fatty acid translocase (*CD36*)	TTGCAAAACGGCTGCA GGTC	TCACCAATGGTCCCA GTCTCAT
Carnitine-acylcarnitine translocase (*CACT/SLC25A20*)	CTCGATTCCAGACTGCA CCT	AAGGCTCGGATCATC ACTGC
Carnitine palmitoyltransferase 1B (*CPT1B*)	ACTGCTACAACAGGTG GTT	TCTGCATTGAGACCCA ACTG
Enoyl-CoA delta isomerase 1 (*ECI1*)	TGAGCCTGGAGTTTCTG ACGGA	ACACATCTCCGTCAG GTCCAGG
Peroxisome proliferator-activated receptor gamma coactivator 1-alpha	TCTCAGTAAGGGGCTG GTTG	ACCAGAGCAGCACAC TCGAT

(*PGC1A*)		
Glucose transporter 1 (*GLUT1/SLC2A1*)	AAGCTGACGGGTCGCC TCATG	CTCTCCCCATAGCGGT GGACC
Enolase 1 (*ENO1*)	GCCCTGGTTAGCAAGA AACT	GAATGGCGTTCGCAC CAAAC
Hexokinase 2 (*HK2*)	GACCAAGGGATTCAAG TCCAGT	CGATATCAAAGTCCC CTCTCC
Phosphoglycerate Kinase 1 (*PGK1*)	GAATGGGAAGCTTTTG CCCG	GCAGTGTCTCCACCAC CTATG
NADH:ubiquinone oxidoreductase core subunit v1 (*NDUFV1*)	TGAGACGGTGCTGATG GACTTC	AGGCGGGCGATGGCT TTC
Succinate dehydrogenase complex flavoprotein subunit A (*SDHA*)	TGCCATCCACTACATGA CGG	GCTCTGTCCACCAAAT GCAC
Cytochrome C1 (*CYC1*)	GAGCACGACCATCGAA AACG	CGATATGCCAGCTTCC GACT
Cytochrome c oxidase subunit 4i1 (*COX4-1*)	CTGAGATGAACAGGGG CTCG	AGGGGGCCGTACACA TAGT
ATP synthase F1 subunit beta (*ATP5B*)	TGCTCCCATTCATGCTG AGG	CTCCAGCACCACCAA AAAGC
Citrate synthase (*CS*)	GGGGTGCTGCTCCAGT ATTA	CTAAGGCTCGGCTCC AGATG
Malate dehydrogenase 2 (*MDH2*)	AAGAACAGCCCCTTGG TGAG	GGTCCGAGGTAGCCT TTCAC
Hydroxycarboxylic acid receptor 2 (*HCA2*)	GGCCCAACCTCTCCTTA AAT	GAAACCTTAGGCCGA GTCCA

Table 2.2: Primer sequences for mouse genes.

Gene	5' to 3' Forward sequence	5' to 3' Reverse sequence
Actin Beta (*Actb*) (housekeeping gene)	CTGTCGAGTCGCGTCCACCC	ATGCCGGAGCCGTTGTCGAC
NAD(P)H quinone dehydrogenase 1 (*Nqo1*)	GGTAGCGGCTCCATGTACTC	CGCAGGATGCCACTCTGAAT
Heme oxygenase 1 (*Hmox1*)	GCCCCACCAAGTTCAAACAG	CAGCTCCTCAAACAGCTCAATG
Thioredoxin reductase 1 (*Txnrd1*)	CCCTGGGTCCTATGACTTCG	CGTTCCTCCGAGACCCCATC
Sulfiredoxin 1 (*Srxn1*)	GTGCACAACGTACCAATCG	GCCCCCAAAGGAATAGTAGTAG
Glucose transporter 1 (*Glut1*)	GCAGAGGCTTGCTTGTAGAGT	GGCCCGTCACCTTCTTGCT
Phosphofructokinase muscle isoform (*Pfkm*)	CCTGGTGCTGAGGAATGAGA	TCAAAGGGAGTTGGGCTTCC
Pyruvate kinase muscle isoform (*Pkm*)	CATTTGTACCATTGGGCCTGC	CAGCCGAGCCACATTCATTC
Carnitine palmitoyltransferase 1B (*Cpt1b*)	CACGGGTGGATGTTCGAGAT	GGAGACGGACACAGATAGCC
Acyl-CoA synthetase long-chain family member 1 (*Acsl1*)	GTGGAACTACAGGCAACCCC	ACGGTCTCAAACATATGGGCG
Enoyl-CoA delta isomerase 1 (*Eci1*)	AGCTGGGGACCCTTTTCTCA	CTGCCGAGAATGGTCTGGGATA

Peroxisome proliferator-activated receptor gamma coactivator 1-alpha (*Pgc1a*)	CTGCGGGATGATGGAGACAG	TCGTTCGACCTGCGTAAAGT

Table 2.3: Primer sequences for rat genes.

Gene	5'to3' Forward sequence	5'to3' Reverse sequence
Ribosomal Protein L32 (*Rpl32*) (housekeeping gene)	TCTGGTGAAGCCCAAGATCG	GTTTCCGCCAGTTTCGCTTAAT
NAD(P)H quinone dehydrogenase 1 (*Nqo1*)	AAACGACATCACAGGGGAGC	GGGCACCCCAAACCAATACA
Heme oxygenase 1 (*Hmox1*)	GTCAGGTGTCCAGGGAAGG	CTCTTCCAGGGCCGTATAGA
Thioredoxin reductase 1 (*Txnrd1*)	CTCTCTTTATCCTCAGTGTGCTT	CGCCGCCCTATGAGCAA
Hydroxycarboxylic acid receptor 2 (*Hca2*)	ACAAGATCTCCAACCGGACG	ATCGTGCCACCTGAAAGTGT

2.3 Western blotting.

2.3.1 Protein lysis.

For cell protein lysates, cell media was discarded, and cells were washed with 1x PBS. Then, 150 µL lysis buffer (75 mM Tris-HCl pH 6.8, 3.8% SDS, 4 M Urea, and 20% glycerol) was added directly to each well of a 6-well plate containing approximately 2 million cells. Cells were scraped using a cell scraper, and lysates were homogenised using a 23G needle and collected into Eppendorf tubes.

For tissue protein lysates, 40 mg of tissue was added to an Eppendorf tube containing 400 µL of lysis buffer and homogenised using a Polytron homogeniser at max speed. The homogenate was boiled at 95°C for 5 minutes.

Protein lysates were centrifuged at 13000 rpm for 5 minutes at 4°C, and the supernatant was transferred to a new Eppendorf tube. The protein concentration was determined spectrophotometrically using the Pierce bicinchoninic acid (BCA) protein assay kit (ThermoFisher) and Pierce bovine serum albumin (BSA) standard (ThermoFisher). Samples were prepared using 20 µg of cell protein or 30 µg of tissue protein, 5% β-mercaptoethanol and Laemmli blue loading dye. Finally, samples were denatured by boiling at 95°C for 5 minutes.

2.3.2 Electrophoresis.

Protein samples were loaded onto an SDS-PAGE gel (NuPAGE™ 4-12% Bis-Tris Midi Protein Gels) and separated using electrophoresis at constant voltage in electrophoresis buffer (NuPAGE™ MOPS SDS running buffer (Thermofisher)). The separated proteins were then transferred onto a nitrocellulose membrane at constant voltage (100V) for 1 hour in transfer buffer (25 mM Tris-Base, 192 mM glycine, and 20% methanol). Equal protein loading was confirmed using Ponceau staining. Membranes were blocked with 5% skimmed milk or 5% BSA (prepared in TBS-Tween) for 1 hour at room temperature, and incubated with the primary antibody overnight at 4°C. The next day, membranes were washed for 30 minutes with TBS-Tween and incubated with the secondary antibody for 1 hour at room temperature, using a solution with the same composition as that used for the primary antibody. Then the membranes were washed for 30 minutes with TBS-Tween. Blot images were visualised using the ECL Prime Western Blotting Detection Reagent (Cytiva), detected

with the Chemidoc XRS+ imaging system (Bio-Rad) and quantified using Image Studio Software version 5.2.5. Antibodies are listed in **Table 2.4.**

Table 2.4: Western blot antibodies.

Protein	Antibody details	Dilution
Nuclear factor erythroid 2 [NF-E2]-related factor 2 (Nrf2)	ab62352 (Abcam)	1:1000 5% Milk
Lactate dehydrogenase (LDH)	ab52488 (Abcam)	1:3000 5% Milk
Total Histone 3 (Total H3)	ab10799 (Abcam)	1:1000 5% Milk
Thioredoxin reductase 1 (TXNRD1)	11117-1-AP (Proteintech)	1:6000 5% Milk
Heme oxygenase 1 (HMOX1)	10701-1-AP (Proteintech)	1:3000 5% Milk
NAD(P)H quinone dehydrogenase 1 (NQO1)	ab80588(Abcam)	1:25000 5% Milk
Glyceraldehyde-3-phosphate dehydrogenase (GAPDH)	60004-1-Ig (Proteintech)	1:40000 5% Milk
Total Oxidative phosphorylation (OXPHOS) Human WB Antibody Cocktail	ab110411 (Abcam)	1:1000 5% Milk
S-(2-succinyl)-cysteine	Crb2005017d/6773 (Discovery antibodies)	1:1000 5% BSA
Histone deacetylase 1 (HDAC1)	5356 (Cell Signaling)	1:2000 5% Milk
Beta III Tubulin	ab7751 (Abcam)	1:1000 5% Milk

Mitochondrial phosphate carrier protein (SLC25A3/PHC)	ab67121 (Abcam)	1:1000 5% Milk
Glutamate dehydrogenase 1 (GLUD1)	ab166618 (Abcam)	1:1000 5% Milk
Medium-chain acyl-CoA dehydrogenase (MCAD)	ab92461 (Abcam)	1:10000 5% Milk
Aconitase 2 (ACO2)	ab71440 (Abcam)	1:500 5% Milk
Cyclophilin B (CYPB)	ab178397 (Abcam)	1:1000 5% Milk
Phosphorylated (serine 473) Akt serine/threonine kinase 1 (pAkt)	ab81283 (Abcam)	1:1000 5% Milk
Total Akt serine/threonine kinase 1 (Total Akt)	ab32505 (Abcam)	1:1000 5% Milk
2,4-dinitrophenylhydrazone (DNP)	OxyBlot Protein Oxidation Detection Kit (Millipore S7150)	1:150 (Oxyblot kit Blocking solution)
Goat Anti-Rabbit IgG (horseradish peroxidase (HRP)-conjugated))	ab6721 (Abcam)	1:2000
Goat Anti-mouse IgG (HRP-conjugated)	ab205719 (Abcam)	1:2000
Goat Anti-Rabbit IgG (HRP-conjugated) (Oxyblot kit)	OxyBlot Protein Oxidation Detection Kit (Millipore S7150)	1:300 (Oxyblot kit Blocking solution)

2.4 Subcellular fractionation.

A subcellular fractionation protocol was used to isolate the cell nucleus from the cytosol in hiPSC-CM and frozen heart tissue. The concentrations of reagents used in this protocol were obtained from the previous experimental protocol[111] and are detailed in **Table 2.5**.

Table 2.5: Buffer composition for subcellular fractionation protocol.

Buffer	Composition
Buffer 1	10 mM HEPES pH 7.9 1.5 mM $MgCl_2$ 10 mM KCl
Buffer 2	20 mM HEPES pH 7.9 420 mM KCl 1.5 mM $MgCl_2$ 25% Glycerol 0.2 mM $MgCl_2$

Buffer 1 and Buffer 2 were supplemented with 1 mM DTT, 1X protease inhibitor cocktail tablet (Roche), and phosphatase inhibitors cocktail tablet (Roche). HiPSC-CM, previously grown on matrigel-coated plates, were dissociated by adding TrypLE (Gibco) directly to the plate well and incubated at 37°C for 12-15 minutes. Cells were collected in an Eppendorf tube and centrifuged at 1500 rpm for 5 minutes. After centrifugation, the supernatant was discarded, and the cell pellet was washed twice with 1X DPBS, centrifuging each time at 1500 rpm for 5 minutes.

The pellet was resuspended in 100 µL supplemented Buffer 1, mixed thoroughly, and incubated on ice for 10 min. The homogenate was centrifuged at 6000 rpm for 15 min at 4°C. The supernatant (cytoplasmic fraction) was transferred to a new Eppendorf tube, while the remaining pellet was washed twice with the same supplemented Buffer 1 and centrifuged

under the same conditions. The pellet was resuspended with 50 µL supplemented Buffer 2 and incubated on ice for 1 hour, homogenising every 5 minutes using a vortex mixer. Then, the homogenate was centrifuged at 12000 rpm for 15 minutes at 4°C, and the supernatant (nuclear fraction) was transferred to a new Eppendorf tube. The resulting pellet was resuspended in 50 µL supplemented Buffer 2, obtaining the pellet fraction. To each one of the fractions, 20 µL of protein lysis buffer was added, and further homogenisation was carried out using a 23G needle and syringe. Protein concentration was determined using a nanodrop spectrophotometer, mode 1 ABS = 1 mg/mL (280 nm). Samples were then used for western blotting (**Section 2.3**).

For tissue, 20-30 mg of frozen tissue was homogenised in 200 µL supplemented Buffer 1 using the TissueRuptor 2 (QIAGEN). Then, the same described protocol was followed with the exception that 100 µL was used for supplemented Buffer 2 and 80 µL for protein lysis buffer.

2.5 Metabolic fluxes measurements.

2.5.1 Palmitate oxidation rates.

Fatty acid oxidation was directly quantified by measuring the rate of conversion of [9,10-^{3}H]-palmitate into $^{3}H_2O$[112]. During the last 6 hours of the dimethyl fumarate or fumarate treatment experiments, cells were incubated in radioactive media composed of DMEM 1X supplemented with dimethyl fumarate, fumarate, or control condition, 300 µM palmitate, and 0.0037 mBq/mL [9,10-^{3}H]-palmitate (Revvity). Both non-radioactive and radioactive palmitate were conjugated in the same media to BSA at a ratio 6:1 (palmitate:BSA). When the experiment was finished, the radioactive media was collected, and $^{3}H_2O$ was isolated using the Folch extraction method. Specifically, 0.5 mL of the radioactive media was added to a falcon tube containing 1.88 mL chloroform:methanol (1:2) solution, 0.625 mL

chloroform and 0.625 mL KCl:HCl solution (2M KCl prepared in 0.4M HCl). Samples were mixed on a rotator for 20 min and left to stand on a rack for 1 hour to separate the aqueous from the organic phase. Next, the aqueous phase was transferred to a new falcon tube containing 1 mL chloroform, 1 mL methanol and 0.9 mL KCl:HCl solution. Samples were mixed on a rotator for 20 min and left to stand on a rack for 1 hour. Finally, the upper aqueous phase was transferred to a new falcon tube and 0.5 mL was added to a scintillation vial containing 10 ml of Ecolite scintillation cocktail (BP Medical, USA) and counted for ^{3}H using a scintillation counter.

2.5.2 Glycolytic rates.

For glycolytic measurements, Dowex 1X4-200 chloride form ion exchange resin (Sigma) was prepared in advance. Prior to the experiment, the resin was activated by mixing 250g of Dowex 1-X4 anion exchange resin with 1.25 M NaOH and 1.62 M boric acid prepared in 1 L of distilled water. The resin was carefully rinsed with distilled water until the pH was between 7 and 8.

Radioactive glycolysis was directly quantified by measuring the rate of conversion of [^{3}H]-glucose metabolised into $^{3}H_2O$[112]. During the last 6 hours of the dimethyl fumarate or fumarate treatment experiment, cells were incubated in radioactive media composed of DMEM 1X supplemented with dimethyl fumarate, fumarate, control condition, 300 µM palmitate conjugated to BSA, and 0.0074 mBq/mL [^{3}H]-glucose (Revvity). When the experiment was finished, the radioactive media was collected and $^{3}H_2O$ was isolated by adding 200 µL of the radioactive media into a column (glass Pasteur pipette) containing activated Dowex resin in the top and a small piece of glass wool in the bottom to prevent Dowex from leaking out. After an incubation of 15 minutes, the column was washed twice with distilled water, the eluate was collected in a scintillation vial, and 10 ml of Ecolite

scintillation cocktail was added. The solution was mixed, and the radioactivity was counted for ^{3}H using a scintillation counter.

2.6. Mitochondrial respiration.

Mitochondrial respiration was assessed using a Seahorse analyser under the guidance of Dr Thomas Nicol. HiPSC-CM were seeded onto Seahorse XF96 plates pre-coated with reduced growth factor Matrigel. Cells were seeded at a density of 125,000 cells per well in 100 µL of maturation media. The following day, media was refreshed with 200 µL of maturation media, and cells were incubated for the next 4-5 days until the morphology and beating normalised (media was replaced every two days). The day before the experiment, the sensor cartridge was hydrated in Seahorse XF Calibrant (Agilent) at 37°C in a non-CO_2 incubator overnight.

On the day of the experiment, the culture media (unless otherwise specified) was replaced with 180 µL of Seahorse assay media (Seahorse DMEM, pH 7.4) supplemented with 5.5 mM glucose, 1 mM pyruvate, 4 mM glutamine, 5 µg/mL vitamin B12, 0.5 mM ascorbic acid, 0.84 uM biotin, 1.7 µM insulin, 80 µM oleic acid: BSA (2:1), 1x MEM non-essential amino acids, and 0.1X penicillin-streptomycin. The cells were then incubated for 90 minutes at 37°C in a non-CO_2 incubator.

The oxygen consumption rate was measured using the Mito Stress test (Agilent). The final concentrations used in the assay were 1 µM oligomycin (Oligo), 2 µM FCCP (carbonyl cyanide-4-(trifluoromethoxy) phenylhydrazone), and 0.5 µM rotenone/antimycin A (ROT/AA), all prepared in the same Seahorse media. The running programme utilised for the Seahorse experiments is detailed in **Table 2.6**.

Table 2.6: Seahorse running protocol.

Step	Action	Time (Min)	Details	Step	Action	Time (Min)	Details
1	Calibrate			**31**	Mix	3	Repeat three times
2	Mix	3	Repeat three times	**32**	Wait	0	
3	Wait	0		**33**	Measure	3	
4	Measure	3		**40**	Inject		**ROT/AA**
17	Inject		**Oligo**	**41**	Mix	3	Repeat three times
18	Mix	3	Repeat three times	**42**	Wait	0	
19	Wait	0		**43**	Measure	3	
20	Measure	3		**50**	End		
30	Inject		**FCCP**				

Min: Minutes. **Oligo**: Oligomycin. **FCCP**: carbonyl cyanide-4-(trifluoromethoxy) phenylhydrazone. **ROT/AA**: Rotenone/Antimycin A.

2.7 Transcriptomics Data quantification.

2.7.1 Sequencing and Library Construction.

RNA was extracted from hiPSC-CM, mouse and rat heart following the protocol set out in **Section 2.2**. During the extraction process, RNAse-free DNase (QIAGEN) was added to ensure complete DNA removal. Samples were processed and sequenced by Novogene using an Illumina sequencing PE150. Based on Novogene method section[113], transcripts were purified from total RNA using poly-T oligo, and mRNA was subsequently fragmented. First-strand CDNA synthesis was performed using random hexamer primers, and second-strand cDNA synthesis was carried out using dTTP. The library was made using poly A enrichment. For gene mapping, Hisat2 v2.0.5[114] was used, and the genome references were:

- Homo Sapiens (GRCh38/hg38) for hiPSC-CM.
- Ensembl_rattus_norvegicus_rnor_6_0_gca_000001895_4 for rat heart.

- GRCm39/mm39 for mouse heart.

2.7.2 Differential Expression Analysis.

Differential expression analysis and normalisation of gene counts were carried out using the DESEQ2 pipeline[115]. Genes with fewer than ten counts in half of the samples were classified as lowly expressed genes and removed from the analysis. For visualisation, exploratory analysis, and mean-variance removal, counts were normalised using the variance stabilising transformation (VST)[116]. Each sample and group distribution was observed using principal components via the plotPCA function. Differential gene expression (DEG) between treatments was performed using the raw counts. Accurate differences between treatments were achieved by shrinking the Log_2fold changes using the apeglm method[117]. Significance was defined as a Benjamini-Hochberg corrected alpha of less than 0.05. All the analysis and coding were conducted in R and R Studio v4.3.2. For all the analyses, results with a p-adjusted value < 0.05 or p-value < 0.05 were considered significant.

2.7.3 Enrichment analysis.

The impact of the DEG results on biological pathways and cell processes was determined using different Bioconductor packages. The cluster Profiler package [118-120] was employed to perform the Kyoto Encyclopedia of Genes and Genomes (KEGG) enrichment analysis of a gene set. KEGG pathways were visualised using the Pathview package [121]. Heatmaps and volcano plots were designed using the ggplot2[122], EnhancedVolcano[123], or ComplexHeatmap[124, 125] packages.

Enrichment analyses were also performed using the online tool metascape[126], which in addition facilitates the study of transcription factors, through the transcriptional regulatory relationships unravelled by sentence-based text mining (TRRUST) database[127]. Gene set

enrichment analysis (GSEA) and gene set variation analysis (GSVA) were conducted using FGSEA package[128] and GSVA algorithm[129], respectively.

2.8 Glutathione concentration.

Glutathione levels were measured using the Glutathione Colorimetric Detection Kit (Invitrogen), following the manufacturer's instructions. Cells were dissociated from the cell plate by adding TrypLE and incubating at 37°C for 12-15 minutes. Cells were collected in an Eppendorf tube and centrifuged at 1400 rpm for 10 minutes. After centrifugation, the supernatant was discarded, and the cell pellet was resuspended in DPBS 1X and frozen. On the day of the assay, cells were thawed, centrifuged at 1400 rpm for 10 minutes, and the supernatant was discarded. The pellet was resuspended in 5% aqueous 5-sulfo-salicylic acid dehydrate solution (Sigma), disrupted using a 23G needle and syringe, and centrifuged at 14000 rpm for 10 min at 4°C. The supernatant was split into two equal fractions. One fraction was used directly to measure total glutathione, while the other was treated with 2-vinylpyridine (Sigma) to block free glutathione, allowing for the detection of specifically oxidised glutathione. Samples were diluted in the kit-provided Assay Buffer, transferred to a clear 96-well half-area plate, and mixed with the Colorimetric Detection Reagent and Reaction Mixture. The reaction was incubated for 20 minutes at room temperature, and the absorbance was read at 405 nm using a plate reader. Glutathione concentrations were calculated based on specific standards for total and oxidised glutathione prepared in the same Assay Buffer.

For frozen tissue, 10 mg of tissue was homogenised in 250 µL ice-cold DPBS 1X using the TissueRaptor 2, and centrifuged at 14000 rpm for 10 min at 4°C. The solution was mixed thoroughly with 1 volume of cold 5% aqueous 5 -sulfo-salicylic acid and incubated at 4°C

for 10 minutes. Finally, the samples were centrifuged at 14000 for 10 min at 4°C and the supernatants were used for analysis following the previously described protocol.

2.9 Cardiomyocyte-specific Keap1 knockout mouse model.

Heart tissue from wild-type and cardiomyocyte-specific Keap1 knockout mice was generously provided by Prof Ajay Shah and Dr Anna Zoccarato from King's College London. Based on their publication[130], mice were generated on a C57BL/6 background using the Cre-LoxP system. The gene *Keap1* was flanked by loxP sites, and the cardiomyocyte-specific Cre recombinase expression was driven using the α-myosin heavy chain promoter (αMHC-Cre). During the breeding process, αMHC-Cre positive/Keap1 floxed heterozygous mice (αMHC-Cre^{+}/Keap1$^{fl/+}$) were crossed with αMHC-Cre negative/Keap1 floxed heterozygous mice (αMHC-Cre^{-}/Keap1$^{fl/+}$). From the offspring, wild-type mice (αMHC-Cre^{-}/Keap1$^{+/+}$) were compared to cardiomyocyte-specific Keap1 knockout mice (αMHC-Cre^{+}/Keap1$^{fl/fl}$) **(Figure 2.2)**.

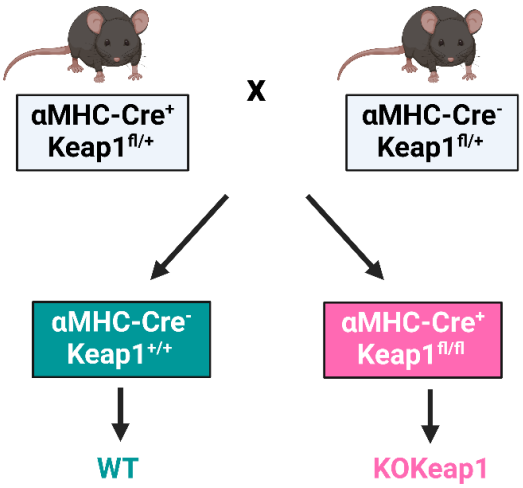

Figure 2.2. Cardiomyocyte-specific Keap1 knockout mouse model generation. The figure illustrates the breeding method used to generate a cardiomyocyte-specific Keap1 knockout. For the purposes of this thesis, αMHC-Cre^{-}/Keap1$^{+/+}$ mice were referred to as wild type (WT) and αMHC-Cre^{+}/Keap1$^{fl/fl}$ mice were identified as KOKeap1.

2.10 Metabolomics.

For metabolite extraction a previously established protocol was followed [104, 131] using tissue from perfused hearts previously exposed to acute hypoxia in Prof Lisa Heather's group generated Dr Latt Mansor[104]. Briefly, 50 mg of tissue was weighed directly into Precellys tubes and homogenised in chloroform:methanol solution (1:2) using the Precellys 24 homogeniser at a speed of 6000 rpm for two cycles of 30 seconds each. HPLC-grade water was added, the solution was thoroughly mixed for 20 seconds and centrifuged at 13200 g for 15 minutes at room temperature. The aqueous and organic fractions were each transferred to separate tubes, and the remaining pellet was re-extracted using half the original volume of chloroform:methanol solution and HPLC-grade water, and the new aqueous and organic fractions combined with the initial corresponding fractions. The aqueous fraction was frozen under liquid nitrogen and freeze-dried using an EC vacuum apparatus (Modulyo). Sample mass spectrometry was subsequently performed for Prof Jules Griffin and Dr Areesha Nazeer at the University of Aberdeen. For fumarate determination, ^{13}C- fumarate was used as an internal standard. Data was normalised to tissue weight, analysed in R and R Studio v4.3.2, and presented as the area ratio of the metabolite peak to the internal standard.

2.11 Statistics.

For statistical analysis, GraphPad Prism version 10 was used. Results, reported as means ± standard error of the mean (SEM), were considered significant at p-value < 0.05. For data sets comparing only two groups, unpaired t-test with Welch's correction was performed. For comparisons involving multiple groups but just one factor, one-way ANOVA was used with Dunnet post hoc adjustment for multiple comparisons and hypothesis testing. For analysis involving two factors, two-way ANOVA was used with the Tukey test for post-hoc comparisons.

Chapter 3

Fumarate derivatives and their cardiac antioxidant role in hiPSC-CM

3.1 Abstract

Fumarate derivatives are FDA-approved pharmacological molecules used for treating autoimmune diseases. These molecules activate the nuclear factor erythroid 2 [NF-E2]-related factor 2 (Nrf2), one of the most important transcription factors regulating antioxidant enzyme expression. While fumarate has low cell permeability, fumarate derivatives showed enhanced permeability, but there is limited information about the effect of fumarate derivatives on human cardiomyocytes. Therefore, this chapter evaluated whether mature human-induced pluripotent stem cells (hiPSC-CM) can respond to exogenous fumarate derivatives by studying their impact on the Nrf2 pathway.

Subcellular fractionation of hiPSC-CM showed that the fumarate derivative, dimethyl fumarate (DMF), significantly increased Nrf2 nuclear translocation. DMF upregulated several antioxidant enzyme genes in a dose- and time-dependent manner, including *NQO1*, *TXNRD1*, *HMOX1* and *SRXN1* evaluated by qPCR. Transcriptomics analysis of DMF-treated hiPSC-CM revealed that the antioxidant genes were among the most significantly upregulated genes and identified Nrf2 as one of the most enriched transcription factors. Nrf2 activation was also observed in hiPSC-CM treated with the fumarate derivatives monomethyl fumarate and diroximel fumarate but not with the succinate derivative, dimethyl succinate, indicating that the upregulation of Nrf2 in hiPSC-CM is specifically induced by fumarate but no other Krebs cycle metabolites. Sulforaphane, a well-known Nrf2 activator, showed similar antioxidant gene regulation to the fumarate derivatives. Furthermore, a genetic mouse cardiac model with constitutive Nrf2 activation confirmed that Nrf2 mediated the fumarate derivative antioxidant effects in hiPSC-CM.

In conclusion, fumarate derivatives upregulated antioxidant defence pathways in human cardiomyocytes primarily by inducing Nrf2 nuclear translocation and increasing its activity.

3.2 Introduction

Fumarate derivatives are synthetic compounds with electrophilic properties derived from fumarate[132]. These molecules have been approved by the FDA for the treatment of autoimmune diseases, specifically multiple sclerosis and psoriasis, and they are in clinical trials for the treatment of different types of cancer, respiratory and digestive pathologies, and neurological disorders[133-136]. Autoimmune diseases are characterised by aberrant immune responses to the host's cellular components, triggering cellular damage and tissue dysfunction, which lead to increased production of reactive oxygen species (ROS) and oxidative stress, exacerbating these negative effects[137-139]. However, fumarate derivatives activate Nrf2 transcription factor[92, 132, 140], upregulating the expression of antioxidant defence enzymes, decreasing ROS deleterious effects, as well as promoting anti-inflammatory regulators[88, 89]. Among the different fumarate derivates, dimethyl fumarate (DMF) has been the most extensively studied[133].

Under control conditions, Nrf2 is located in the cytosol, and its activity is suppressed by the Kelch-like erythroid cell-derived protein with CNC homology [ECH]-associated protein 1 (KEAP1). KEAP1 acts as a protein adaptor composed of three different domains: the BTB domain, which mediates KEAP1 homodimer formation; the intervening region (IVR); and the Kelch domain, required for binding with Nrf2 **(Figure 3.1)**. In contrast, Nrf2 is composed of six different domains, among them, Neh2, critical for KEAP1 binding through the motif DLG and ETGE, and Neh1 domain, which is essential for Nrf2 transcriptional binding to antioxidant response element (ARE) promoter regions[141, 142]. The KEAP1 homodimer binds to DLF and ETGE motifs in Nrf2 and recruits the protein Cullin3 through its BTB domain, which is an E3 ubiquitin ligase complex component which induces the polyubiquitination of Nrf2 and its proteasomal degradation[143]. However, KEAP1 has

critical cysteine residues which react with electrophiles, where the most reactive are Cys151, located in the BTB domain, and Cys273 and Cys288 in the IVR domain. Under stressed conditions, these cysteine residues are oxidised by electrophiles produced by ROS, inducing a conformational change that impairs the ability of the KEAP1 to interact with Nrf2. This allows Nrf2's translocation to the nucleus, accumulation and induction of transcription of antioxidant genes[141-143]. Mechanistically, the fumarate derivatives also modify these cysteine residues to promote Nrf2 activation via the irreversible PTM succination[132].

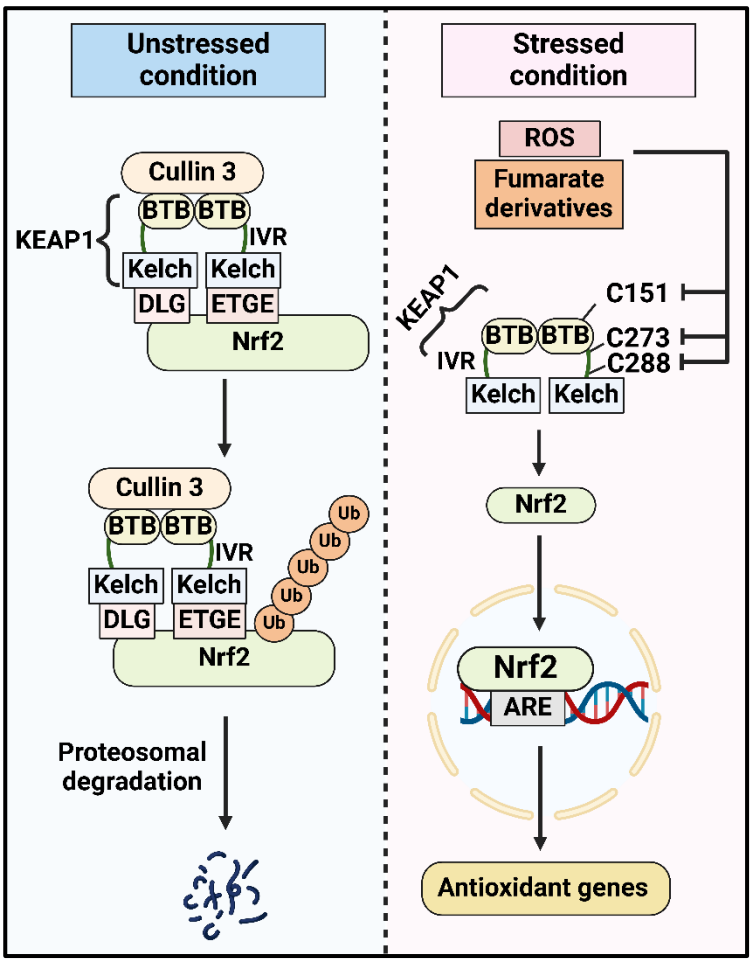

Figure 3.1: Nrf2 pathway activation. Under unstressed conditions, KEAP1 homodimer and Cullin3 induce Nrf2 degradation by the proteasome through the interaction of KEAP1's Kelch domain with Nrf2 motifs DLG and ETGE. However, under stress conditions or in response to fumarate derivatives treatment, cysteine residues (C) in the BTB and IVR domains of KEAP1 are modified, reducing the ability of KEAP1 to interact with Nrf2, allowing its nuclear translocation and the transcription of antioxidant genes. Nrf2, nuclear factor erythroid 2 [NF-E2]-related factor 2. KEAP1, Kelch-like erythroid cell-derived protein with CNC homology [ECH]-associated protein 1

3.3 Chapter aims

During hypoxia, intramyocardial metabolite concentrations are changed, with Krebs cycle intermediates being modified significantly. Fumarate derivatives are well-known molecules that enhance antioxidant defence mechanisms to treat autoimmune diseases. However, whether mature hiPSC-CM can respond to exogenous fumarate derivatives remains unclear. Therefore, this chapter aimed to investigate the response of mature hiPSC-CM to fumarate derivatives, focusing on Nrf2 pathway activation and its antioxidant defence targets. This chapter investigated:

1. Intracellular metabolite concentrations in perfused rat hearts exposed to acute hypoxia compared with normoxia conditions.

2. The effect of fumarate derivatives on Nrf2 pathway activation in hiPSC-CM, including the role of these molecules in inducing Nrf2 nuclear translocation and upregulation of the antioxidant enzyme gene and protein levels.

3. The impact of fumarate derivatives on global gene expression in hiPSC-CM via transcriptomic analysis.

4. The specificity of the fumarate derivatives in regulating the Nrf2 pathway in mature hiPSC-CM using a well-established Nrf2 molecular activator, and a genetic mouse model with constitutive cardiac Nrf2 activation.

3.4 Results

3.4.1 Acute hypoxia increases fumarate intracellular levels within rat hearts.

In order to understand how hypoxia affects intracellular metabolites in the heart, an in-depth metabolomics screening was carried out using heart samples previously perfused in Prof Lisa Heather's group, where isolated rat hearts were exposed to acute hypoxia condition (Po_2 = 90 ± 10 mmHg for 32 minutes) or normoxia conditions (Po_2 = 413 ± 15 mmHg). It was observed that hypoxia significantly modified the intracellular content of 30 of the 77 analysed metabolites (approximately 39% of the total metabolites) **(Figure 3.2)**. Succinate (Suc) and fumarate (Fum) were the most significantly increased metabolites, rising by 5.4 and 3.3-fold, respectively, compared with normoxic hearts. In contrast, the metabolites that decreased most following hypoxia were succinyl-CoA (sucCoA) and cytidine triphosphate (CTP), whose levels were reduced by 70% and 66%, respectively.

The effect of acute hypoxia was specifically evaluated for Krebs cycle metabolites, observing that in response to hypoxia, the metabolites in the first half of Krebs cycle, citrate (Cit), aconitase (Aco) and succinyl CoA (sucCoA) were significantly reduced by 42%, 44%, and 70%, respectively, compared with normoxic hearts. On the other hand, the metabolites from the second half of the Krebs cycle, fumarate (Fum), succinate (Suc), and malate (Mal), were significantly increased by 229%, 440%, and 108%, respectively, compared with normoxic hearts **(Figure 3.3)**.

Overall, these results show that acute hypoxia triggers a significant remodelling in the metabolite content within the heart. For the interest of this thesis, the consequences of elevating fumarate were explored.

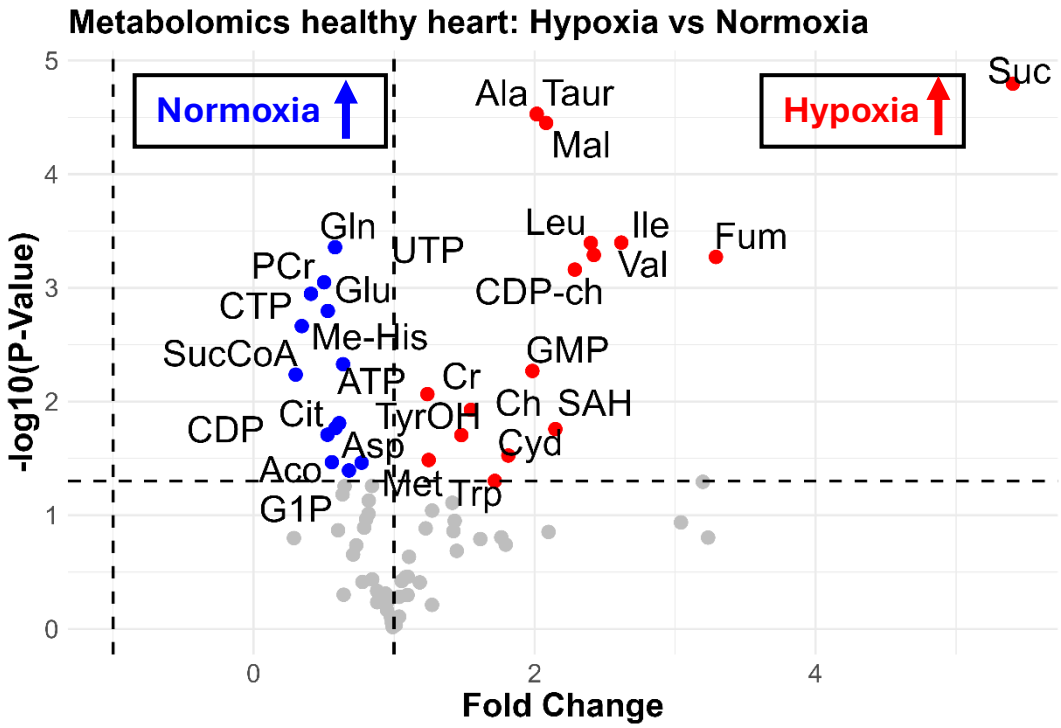

Metabolites decrease in hypoxia	
Metabolite	**Fold Change**
Succinyl-CoA (SucCoA)	0.30
Cytidine triphosphate (CTP)	0.34
Phosphocreatine (PCr)	0.41
Uridine triphosphate (UTP)	0.50
Cytidine diphosphate (CDP)	0.53
Glutamate (Glu)	0.53
Aconitase (Aco)	0.56
Glutamine (Gln)	0.58
Citrate (Cit)	0.58
Adenosine triphosphate (ATP)	0.61
Histidylmethionine (Me-His)	0.64
Glucose-1-phosphate (G1P)	0.68
Aspartate (Asp)	0.77

Metabolites increase in hypoxia	
Metabolite	**Fold Change**
Succinate (Suc)	5.40
Fumarate (Fum)	3.29
Isoleucine (Ile)	2.62
Valine (Val)	2.42
Leucine (Leu)	2.40
Cytidine diphosphate-choline (CDP-ch)	2.29
S-Adenosylhomocysteine (SAH)	2.15
Malate (Mal)	2.08
Taurine (Taur)	2.02
Alanine (Ala)	2.02
Guanosine monophosphate (GMP)	1.98
Cytidine (Cyd)	1.81
Tryptophan (Trp)	1.72
Choline (Ch)	1.55
Tyrosine (TyrOH)	1.48
Methionine (Met)	1.25
Creatine (Cr)	1.24

Figure 3.2: Hypoxia remodels metabolite content within the heart. The volcano plot and tables represent only the significant regulated metabolites under hypoxia in the healthy heart. Fold change is represented as the ratio between mean hypoxia to mean normoxia for each metabolite. Metabolites were considered significant with p-value < 0.05. Decreased metabolites are presented in blue and increased metabolites in red.

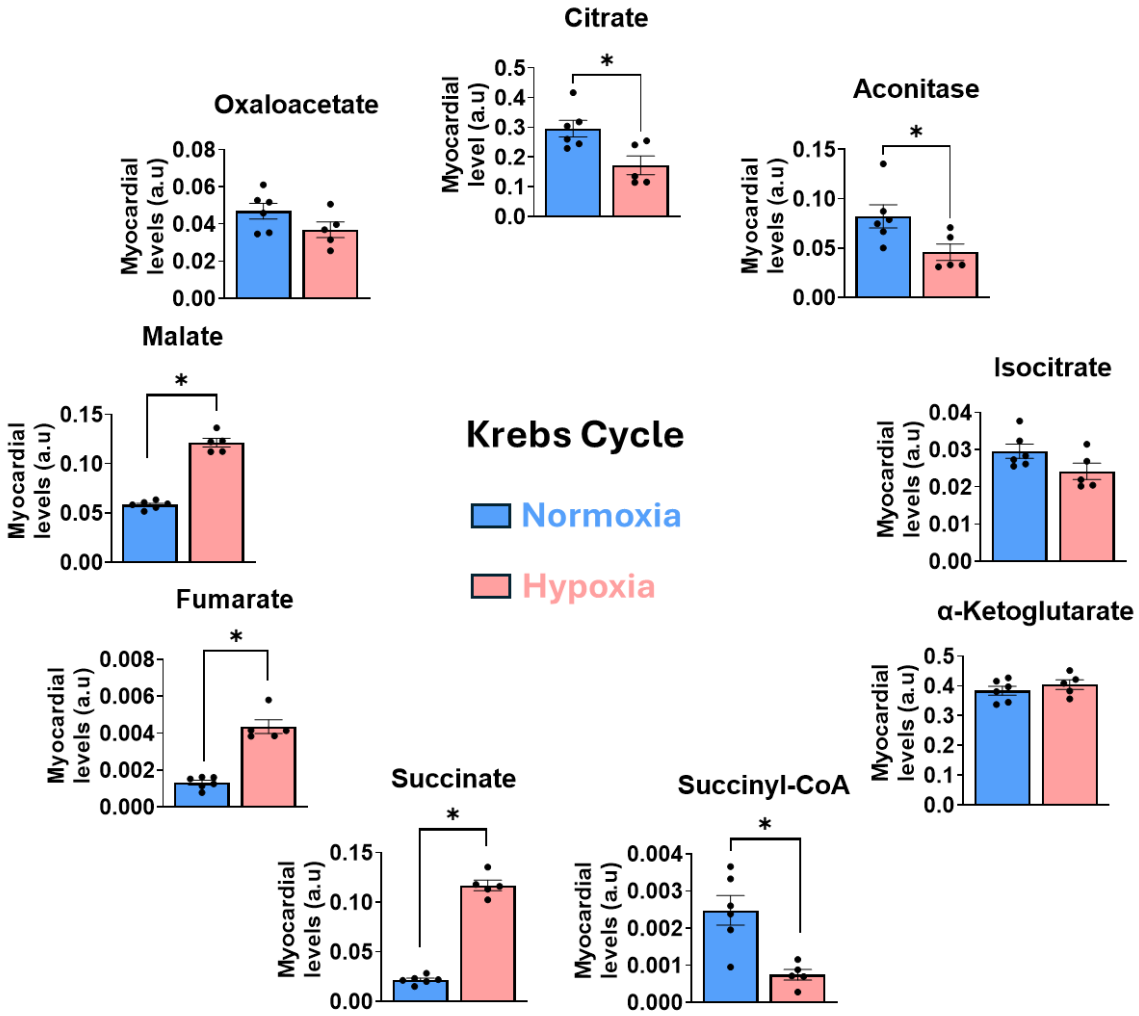

Figure 3.3: Hypoxia differentially modulates Krebs Cycle metabolites within the heart. Krebs cycle metabolite levels following normoxia and acute hypoxia within the rat heart. Data was expressed as peak area ratio. Data was normalised to tissue weight. * $p < 0.05$ vs. normoxia group. a.u., arbitrary units. Each data point represents a biological replicate.

3.4.2 Dimethyl fumarate increases Nrf2 antioxidant target gene expression in hiPSC-CM in a dose-dependent manner.

We were interested in understanding the effects of increased intracellular fumarate on cellular processes. However, as fumarate itself has always been considered a very low or noncell-permeable molecule[144, 145], its effect in human cardiomyocytes was investigated instead using the fumarate derivative, dimethyl fumarate (DMF). DMF has a higher cell membrane permeability than fumarate due to the esterification of the negatively charged

carboxylic groups in the fumarate structure, making this molecule neutrally charged and more lipophilic to cross the cell membrane [144, 146, 147].

To study whether DMF could regulate Nrf2 pathways in hiPSC-CM, the expression of different antioxidant genes that play an essential role in the antioxidant defence within the heart was evaluated by qPCR. HiPSC-CM were cultured with different concentrations of DMF for 24 hours, observing that DMF significantly upregulated the expression of most of the Nrf2 antioxidant targets studied. The expression of the genes NAD(P) dehydrogenase quinone 1 (*NQO1*) **(Figure 3.4A)**, thioredoxin reductase 1 (*TXNRD1*) **(Figure 3.4B)**, heme oxygenase 1 (*HMOX1*) **(Figure 3.4C)**, and sulfiredoxin 1 (*SRXN1*) **(Figure 3.4D)**, showed a dose-dependent increase as the concentration of DMF was increased. The greatest increase in the expression of the antioxidant genes was observed following 150 μM DMF, where the genes *NQO1, TXNRD, HMOX1*, *SRXN1*, and superoxide dismutase 1 (*SOD1*) **(Figure 3.4E)** were upregulated by 16, 4.1, 2.6, 3.7 and 1.4-fold, respectively, compared with control cells. These results show that DMF treatment was able to upregulate the expression of several Nrf2 antioxidant defence target genes in our human cardiomyocytes model.

Glutamate-Cysteine ligase Catalytic Subunit (*GCLC*) **(Figure 3.4F)** showed a significant effect between all the conditions using a one-way ANOVA, but there was not a significant difference between individual groups (did not reach significance at post hoc analyses). Unexpectedly, the expression of the gene methylene tetrahydrofolate dehydrogenase 2 (*MTHFD2*) **(Figure 3.4G)** decreased by 40% following DMF treatment.

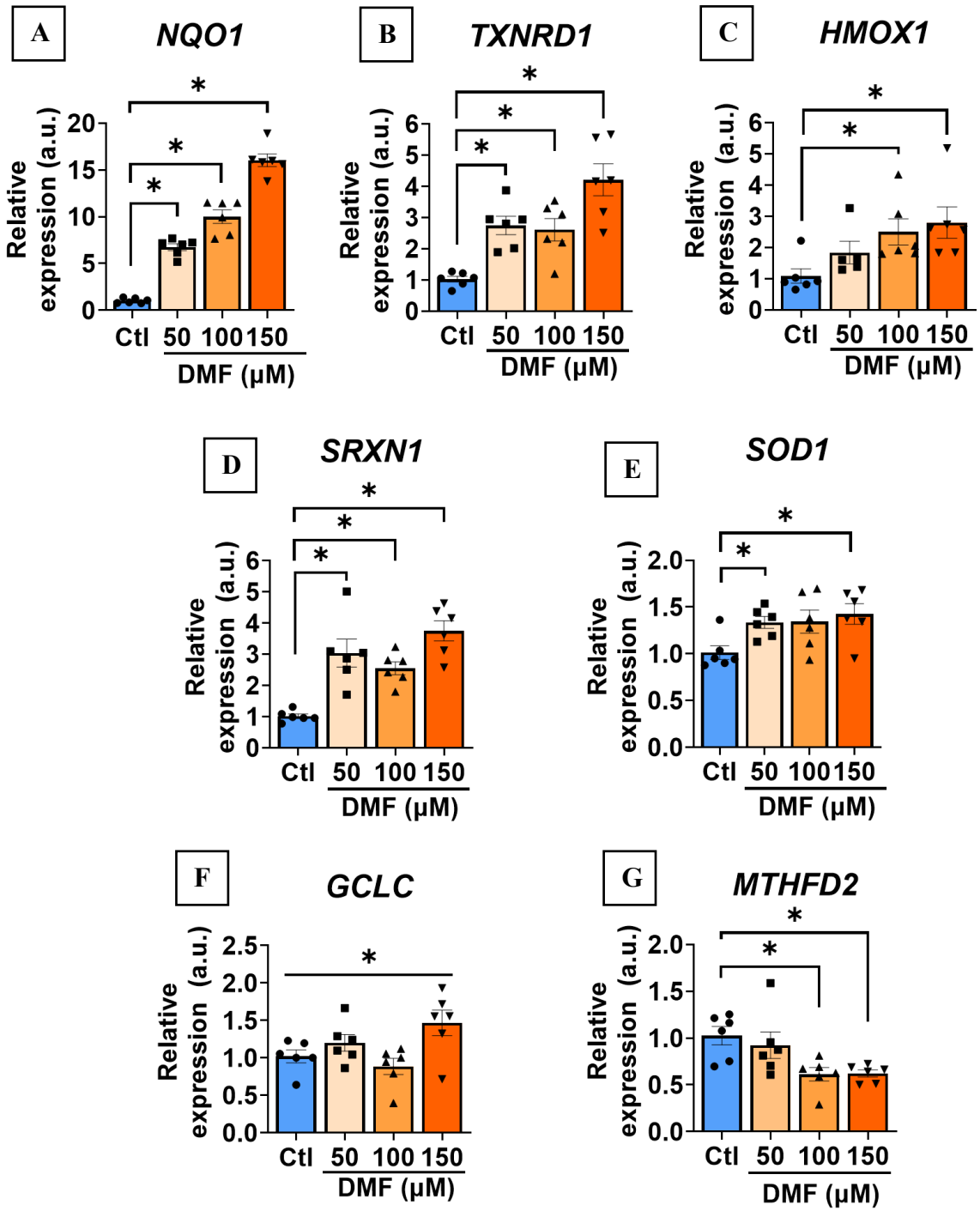

Figure 3.4: Dimethyl fumarate upregulates the expression of most of the Nrf2 antioxidant target genes in hiPSC-CM. Antioxidant gene expression in hiPSC-CM exposed to dimethyl fumarate treatment (50, 100, and 150 μM) (DMF) for 24 hours and compared with untreated cells (Ctl). The evaluated genes were: **(A)** NAD(P) dehydrogenase quinone 1 (*NQO1*), **(B)** Thioredoxin reductase 1 (*TXNRD1*), **(C)** Heme oxygenase 1 (*HMOX1*), **(D)** Sulfiredoxin 1 (*SRXN1*), **(E)** Superoxide dismutase 1 (*SOD1*). **(F)** Glutamate-Cysteine Ligase Catalytic Subunit (*GCLC*) and **(G)** Methylene tetrahydrofolate dehydrogenase 2 (*MTHFD2*). * $p < 0.05$ vs. respective control group. a.u., arbitrary units. Each data point represents a biological replicate.

3.4.3 Dimethyl fumarate induces upregulation of the Nrf2 antioxidant target genes and modulates apoptotic genes after short exposure times in hiPSC-CM.

Given the significant increase in antioxidant gene expression that DMF induced in hiPSC-CM after 24 hours of treatment, the response of these cells to DMF over shorter (3 and 6 hours) and longer intervals (12 and 24 hours) was evaluated **(Figure 3.5)**. Surprisingly, three of the four assessed genes (*NQO1, TXNRD1 AND SRXN1*) were significantly upregulated after just 3 hours of treatment, indicating that the hiPSC-CM presented a rapid response to DMF.

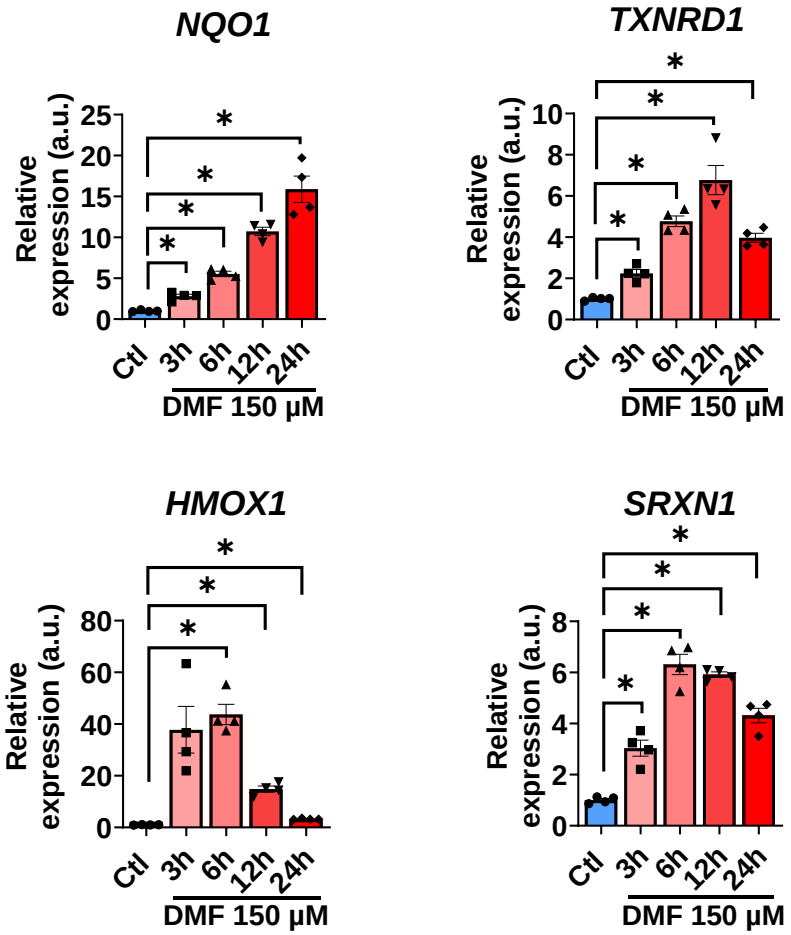

Figure 3.5: Dimethyl fumarate increases Nrf2 antioxidant target gene levels at early time points of treatment in hiPSC-CM. Antioxidant gene expression in hiPSC-CM exposed to dimethyl fumarate treatment (150 µM) (DMF) for 3, 6, 12 or 24 hours and compared with untreated cells (Ctl). The evaluated genes were**:** NAD(P) dehydrogenase quinone 1 (*NQO1*), thioredoxin reductase 1 (*TXNRD1*), heme oxygenase 1 (*HMOX1*), and sulfiredoxin 1 (*SRXN1*). * $p < 0.05$ vs. respective control group. a.u., arbitrary units. Each data point represents a biological replicate.

The increase in antioxidant gene expression was accompanied by a significant and rapid decrease in the expression of the pro-apoptotic gene BCL2 associated X (*BAX*) at 3, 6 and 24 hours following DMF treatment **(Figure 3.6)**, where the most dramatic reduction by 41% compared with the control condition was observed at 6 hours. Even though no significant differences were observed in the anti-apoptotic B-cell leukaemia/lymphoma 2 (*BCL2*) gene expression comparing DMF-treated with untreated cells, the *BAX/BCL2* ratio, a marker of apoptosis propensity showed a significant decrease at 6 and 12 hours, with a 66% significant reduction at 6 hours compared with the control condition. These data demonstrated that DMF promoted the upregulation of antioxidant genes at the early treatment stage, and contributed to anti-apoptotic regulation by decreasing the apoptosis propensity maker *BAX/BCL2* ratio at the gene level in human cardiomyocytes.

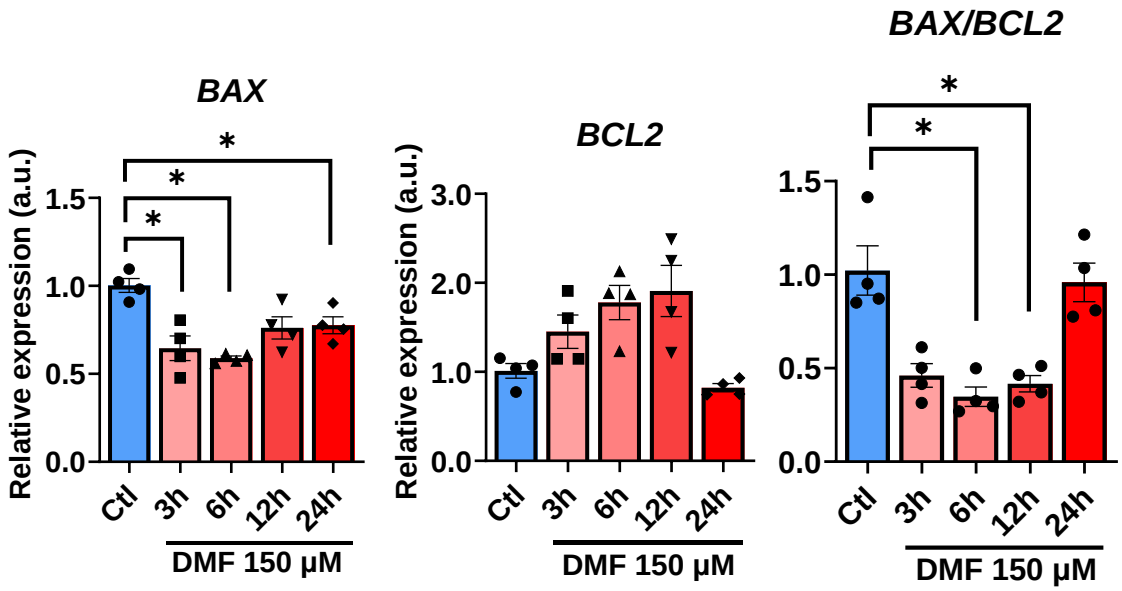

Figure 3.6: Dimethyl fumarate decreases the apoptosis propensity maker *BAX/BCL2* ratio at the gene level in hiPSC-CM. Apoptotic gene expression in hiPSC-CM exposed to dimethyl fumarate treatment (150 µM) (DMF) for 3, 6, 12 or 24 hours and compared with untreated cells (Ctl). The evaluated genes were: B-cell leukaemia/lymphoma 2 associated X (*BAX*) and B-cell leukaemia/lymphoma 2 (*BCL2*) were evaluated. The ratio *BAX/BCL2* was utilised as a marker of apoptosis propensity. * $p < 0.05$ vs. respective control group. a.u., arbitrary units. Each data point represents a biological replicate.

3.4.4 Dimethyl fumarate promotes Nrf2 nuclear translocation in hiPSC-CM.

Given the early response times to DMF treatment and Nrf2's role as the main transcription factor regulating the expression of these genes, we investigated whether DMF was mediating Nrf2 nuclear translocation. For this, we developed a subcellular fractionation protocol to isolate the nucleus from the cytosol, a protocol that was validated using several cytoplasmic, nuclear, mitochondrial and endoplasmic reticulum markers. When the subcellular fractionation protocol was tested in frozen heart tissue **(Figure 3.7)**, it was observed that the nuclear proteins, total histone H3 (Total H3) and histone deacetylase 1 (HDAC1) were detected in the nuclear (Nucl) and pellet (Pellet) fractions, whereas, the cytosolic proteins tubulin (Beta III Tubulin), lactate dehydrogenase (LDH), and glyceraldehyde 3-phosphate dehydrogenase (GAPDH) were identified in the cytosolic (Cyt) fraction. Unexpectedly, the mitochondrial markers, mitochondrial phosphate carrier (SLC25A3/PHC), glutamate dehydrogenase 1 (GLUD1), and the endoplasmic reticulum marker, cyclophilin B (CYPB), were predominantly enriched in the nuclear and pellet fractions, while, the mitochondrial marker, medium-chain acyl-CoA dehydrogenase (MCAD), was detected in the cytosolic fraction. Therefore, using frozen tissue, the subcellular fractionation protocol successfully isolated nuclear from cytosolic proteins, but was sub-optimal for other organelles. Advantageously, Nrf2 translocates exclusively from the cytosol to the nucleus, allowing the use of this protocol for Nrf2 translocation study.

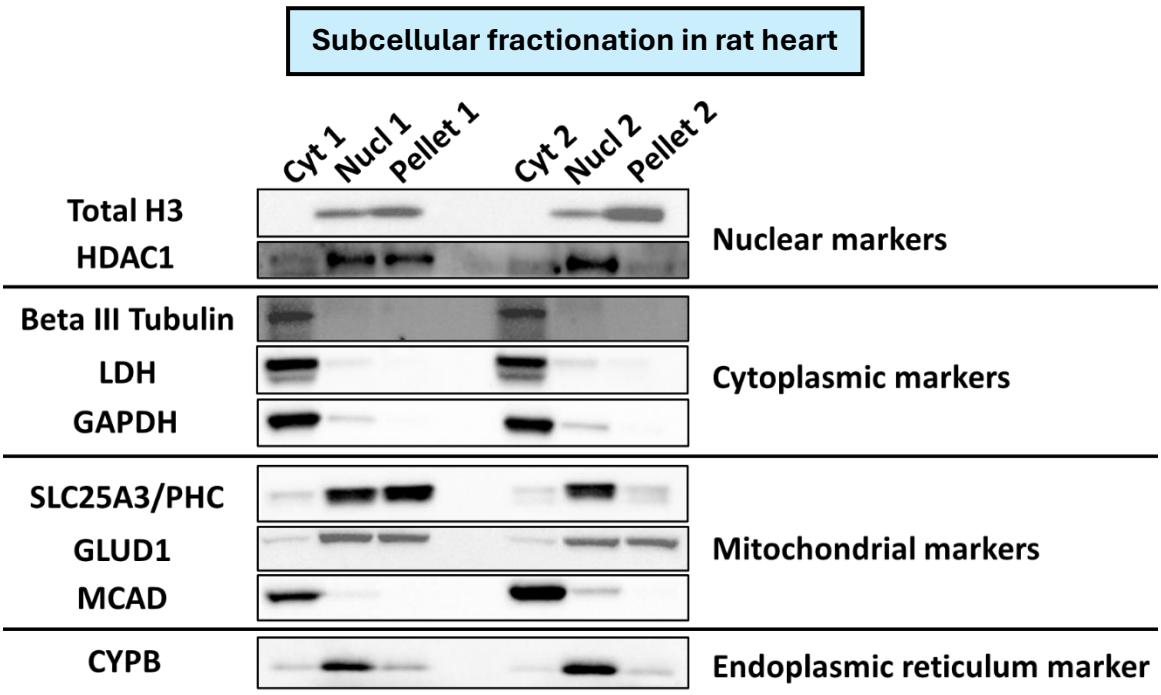

Figure 3.7: Subcellular fractionation protocol validation in rat heart. Subcellular fractionation was performed in frozen rat heart tissue. Total histone H3 (Total H3) and histone deacetylase 1 (HDAC1) were used as nuclear markers for protocol validation. Tubulin (Beta III Tubulin), lactate dehydrogenase (LDH), and glyceraldehyde 3-phosphate dehydrogenase (GAPDH) were employed as cytoplasmic markers. Mitochondrial phosphate carrier (SLC25A3/PHC), glutamate dehydrogenase 1 (GLUD1), and medium-chain acyl-CoA dehydrogenase (MCAD) were used as mitochondrial markers. Cyclophilin B (CYPB) was utilised as an endoplasmic reticulum marker.

Similarly, when the protocol was tested in hiPSC-CM **(Figure 3.8)**, the nuclear markers total H3 and HDAC1 were detected in both nuclear and pellet fractions, whereas, the cytoplasmic markers, LDH and GAPDH, were identified in the cytosolic fraction. These results indicated that a significant amount of the nuclear protein remained in the pellet fraction, therefore, for further experiments, the nuclear and pellet fractions were combined into a single fraction.

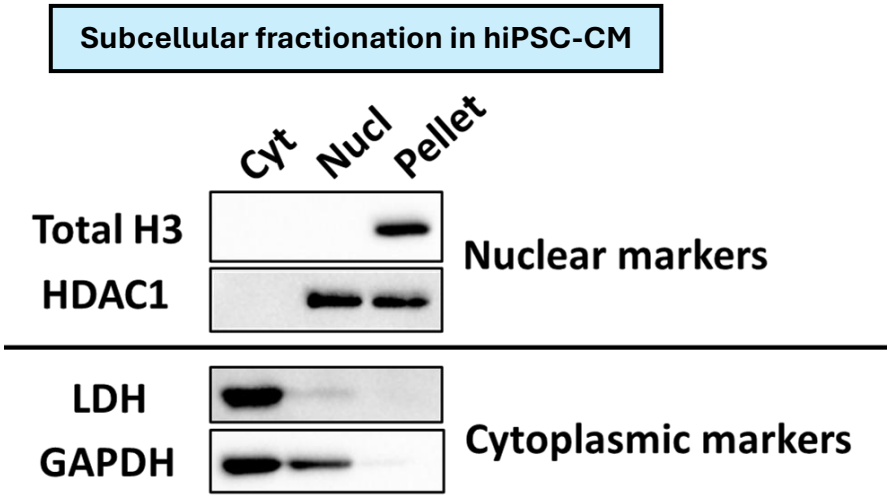

Figure 3.8: Subcellular fractionation protocol validation in hiPSC-CM. Subcellular fractionation protocol tested in hiPSC-CM. Total histone H3 (Total H3) and histone deacetylase 1 (HDAC1) were used as nuclear markers for protocol validation. Lactate dehydrogenase (LDH) and glyceraldehyde 3-phosphate dehydrogenase (GAPDH) were selected as cytoplasmic markers.

To investigate the ability of DMF to induce Nrf2 activation, the previously validated subcellular fractionation protocol was performed in hiPSC-CM treated with 150 µM DMF for 6 hours **(Figure 3.9)**. DMF promoted Nrf2 nuclear translocation in hiPSC-CM by increasing nuclear Nrf2 protein levels by 29%, compared with the control hiPSC-CM. Overall, these data demonstrate that DMF can increase the activity of the Nrf2 pathway by increasing Nrf2 nuclear translocation and upregulating Nrf2 target gene expression at early treatment times in human cardiomyocytes.

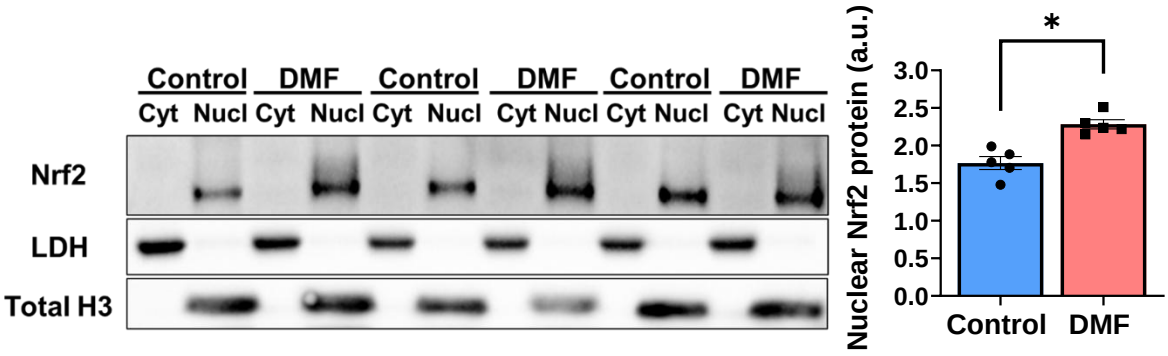

Figure 3.9: Dimethyl fumarate promotes Nrf2 nuclear translocation in hiPSC-CM. Representative subcellular fractionation western blot from hiPSC-CM exposed to dimethyl fumarate treatment (150 µM) (DMF) for 6 hours and compared with untreated cells (Control). For western blotting 20 µg of protein was used and lactate dehydrogenase (LDH) and total histone (Total H3) were used as cytoplasmic and nuclear markers, respectively. * $p < 0.05$ vs. respective control group. a.u., arbitrary units. Each data point represents a biological replicate.

3.4.5 Transcriptomics analyses confirm Nrf2 pathway upregulation under dimethyl fumarate treatment in hiPSC-CM.

Transcriptomics analyses were performed in hiPSC-CM treated with 150 µM DMF for 6 hours to reinforce these findings, and the DMF effect on global gene expression was visualised by comparing DMF and control samples using principal component analysis (PCA). PCA showed a pronounced separation between both conditions, driven by the high variation in the first principal component (PC1), with a 91% variance, occasioned by the distribution of the samples through the x-axis and representing the differences in cell treatments, confirming a strong DMF effect on the cells. On the other hand, the second principal component (PC2) represented variations not associated with the treatment, accounting for a small 6%, suggesting that the main difference between control and DMF treatment is due to the PC1 component (DMF treatment) **(Figure 3.10A)**. Additionally, an inter-sample correlation heatmap using Pearson correlation confirmed similarities between sample members of the same biological group (biological replicates), as the closer the

coefficient is to 1, the higher the similarity between samples, and also showed specific clusters between control and DMF samples **(Figure 3.10B)**.

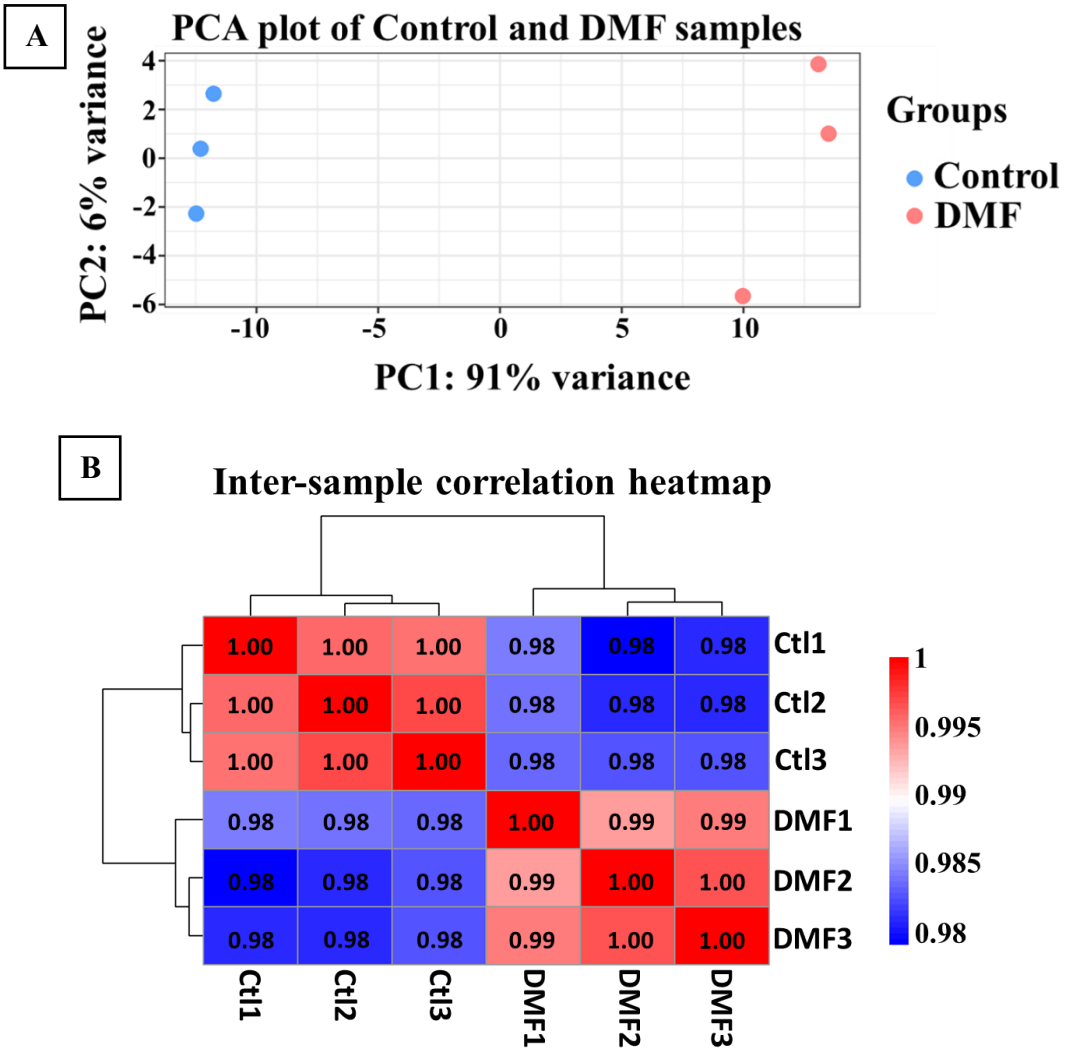

Figure 3.10: Dimethyl fumarate induces a prominent effect on hiPSC-CM transcriptomics. Transcriptomics analyses were performed on hiPSC-CM exposed to dimethyl fumarate treatment (150 µM) (DMF) for 6 hours and compared with untreated cells (Ctl). **(A)** Principal component analyses between control and DMF groups. **(B)** Inter-sample correlation between samples of each condition.

To study which biological pathways were being modulated by DMF, differential gene expression (DEG) analysis using a p-adjusted value < 0.05 and Log_2Fold change equal to 0 was performed in a total of 16069 genes comparing DMF-treated with control hiPSC-CM. DEG identified that 6056 genes were being significantly modulated by DMF (38% of the

total genes), however, to determine which genes were specifically more sensitive to the DMF treatment, the p-adjusted value < 0.05 was kept, but the fold change was set as 1. Under these conditions, the DEG identified 824 significant changes (5%), where 377 genes were significantly upregulated while 447 significantly downregulated, and interestingly, when the DEG was visualised by generating a volcano plot **(Figure 3.11)**, among the top most changed genes the antioxidant genes *NQO1, TXNRD1, HMOX1,* and *SRXN1* were observed in the upregulated genes.

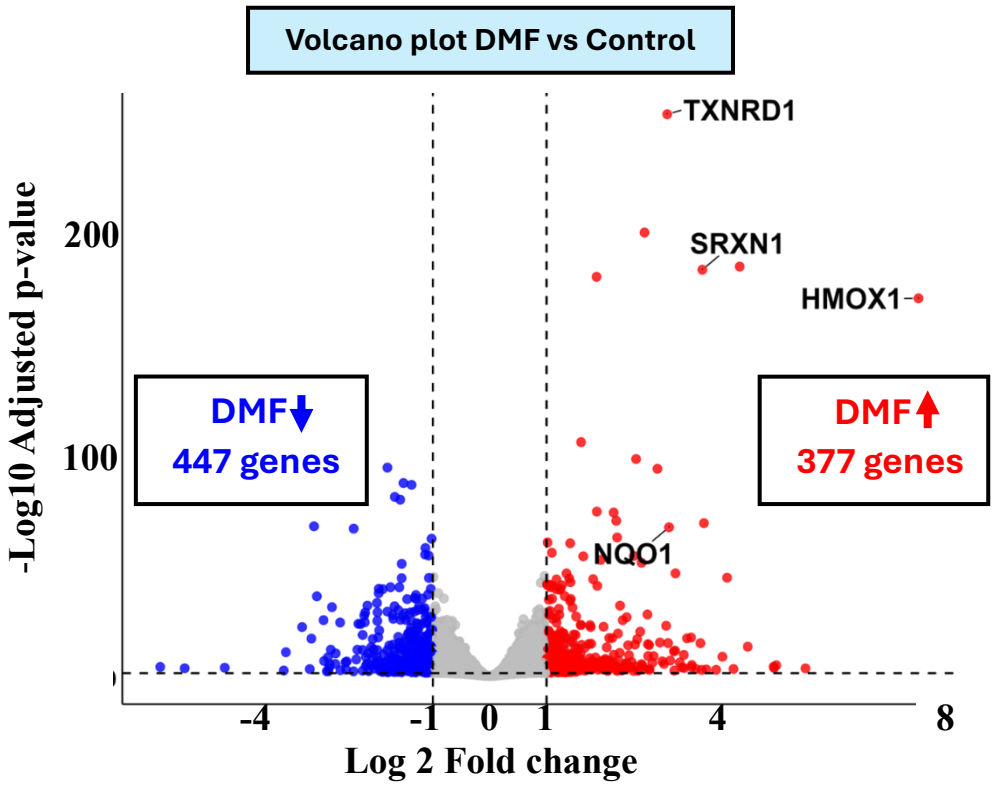

Figure 3.11: Antioxidant genes represent the topmost enriched genes in differential gene expression analysis following DMF treatment in hiPSC-CM. Transcriptomics analyses were performed on hiPSC-CM exposed to dimethyl fumarate treatment (150 µM) (DMF) for 6 hours and compared with untreated cells (Control). DEG was performed using a Log_2Fold change equal to 1 and a p-adjusted value < 0.05. Upregulated and downregulated genes are coloured in red and blue, respectively.

Enrichment analysis was carried out to identify specific pathways for the upregulated genes, and the most enriched pathways were the Nrf2 pathways and ferroptosis **(Figure 3.12A)**. Additionally, another two cell processes regulated by the Nrf2 pathway, glutathione

metabolism, a key molecule required for oxidative stress protection, and the pentose phosphate pathway, an essential metabolic pathway necessary for NADPH production (an important cofactor in antioxidants processes), were also upregulated. Several other processes associated with cellular responses, such as response to hormones, amino acid transport, ABC transporters, small molecules transporter, and the NADPH regeneration pathway itself, were also observed to increase. In contrast, the most downregulated processes were heart, vasculature, and muscle development **(Figure 3.12B)**, and interestingly, DMF, which is clinically used to treat autoimmune diseases, downregulated several pathways linked to the immune system regulation, such as interferon-gamma signalling, cellular response to cytokine stimulus and interaction. Furthermore, DMF also suppresses the regulation of signalling pathways and cell membrane receptors like serine/threonine receptors and class A/1 (GPCRs) receptors.

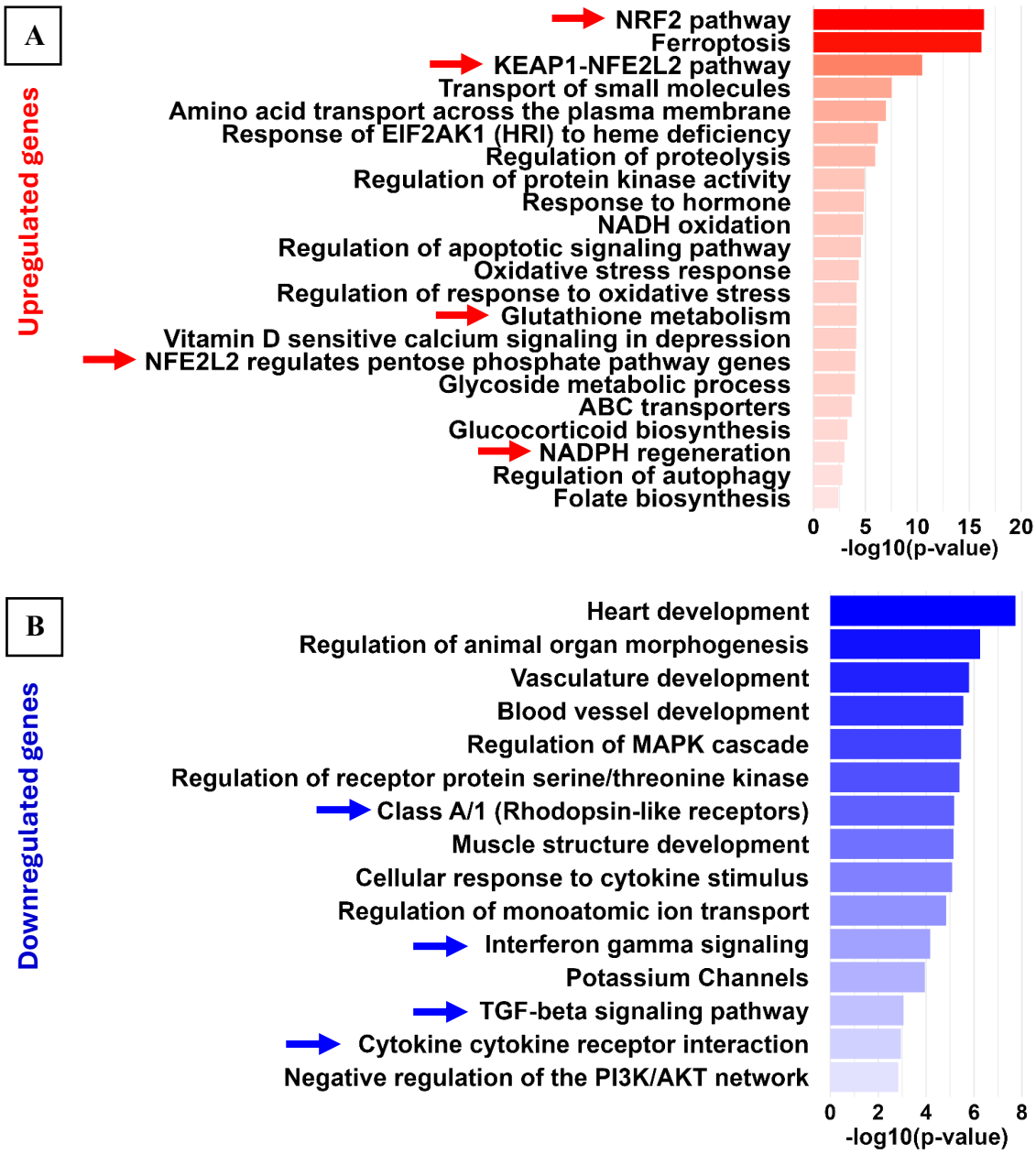

Figure 3.12: Enrichment analysis of differential gene expression comparing dimethyl fumarate-treated hiPSC-CM with untreated cells. Transcriptomics analyses were performed on hiPSC-CM exposed to dimethyl fumarate treatment (150 µM) (DMF) for 6 hours and compared with untreated cells (Control). DEG was performed using a Log_2 Fold change equal to 1 and p-adjusted value < 0.05. Enrichment analysis was conducted using metascape, and the graph of enriched terms represents the 377 upregulated **(A)** or 447 downregulated genes **(B)**.

A direct comparison between the conditions and the cellular pathways was conducted using gene set variation analysis (GSVA), and aligning the resulting gene data with different

biological pathways extracted from the open science platforms Wikipathway, KEGG and Hallmark gene annotation. GSVA analysis showed an increase in the Nrf2 pathway in the DMF-treated group, and moreover, pathways involved in oxidative stress, ferroptosis and mTOC were also upregulated, whereas GPCRs and heart development pathways were downregulated (**Figure 3.13)**.

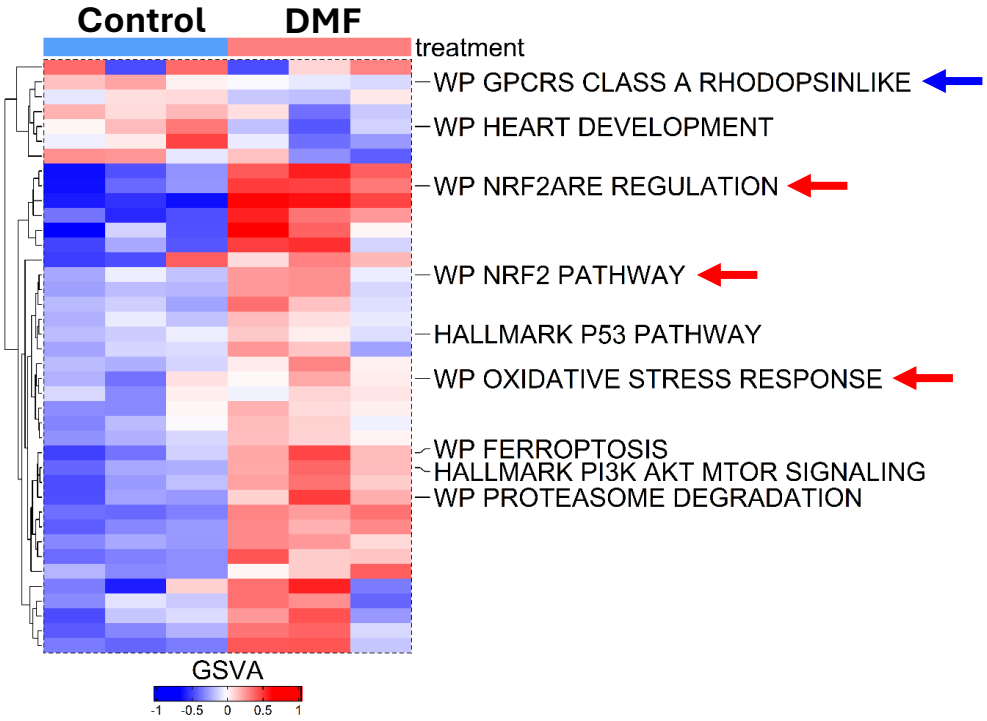

Figure 3.13: Gene set variation analysis comparing dimethyl fumarate-treated hiPSC-CM with untreated cells. Transcriptomics analyses were performed on hiPSC-CM exposed to dimethyl fumarate treatment (150 µM) (DMF) for 6 hours and compared with untreated cells (Control). Each column represents a biological replicate.

Based on the DEG, it was also possible to extrapolate transcription factors involved in each direction of the gene enrichment **(Figure 3.14)**. It was detected that the most enriched transcription factor in the upregulated genes was the DNA damage-inducible transcript 3 (DDIT3), which has been reported to play an essential role in the cell cycle[148] and apoptosis[149] regulation and cellular stress response[150, 151] **(Figure 3.14A)**. Furthermore, among the list of upregulated transcription factors, NFE2L2 (Nrf2) was also observed, confirming that a critical population of the upregulated genes under DMF treatment was, in

fact, regulated by Nrf2. In contrast, among the most enriched transcription factors in the downregulated genes, homeobox A10 (HOXA10) was identified, which plays a role in cardiogenesis and heart development [152, 153] **(Figure 3.14B)**.

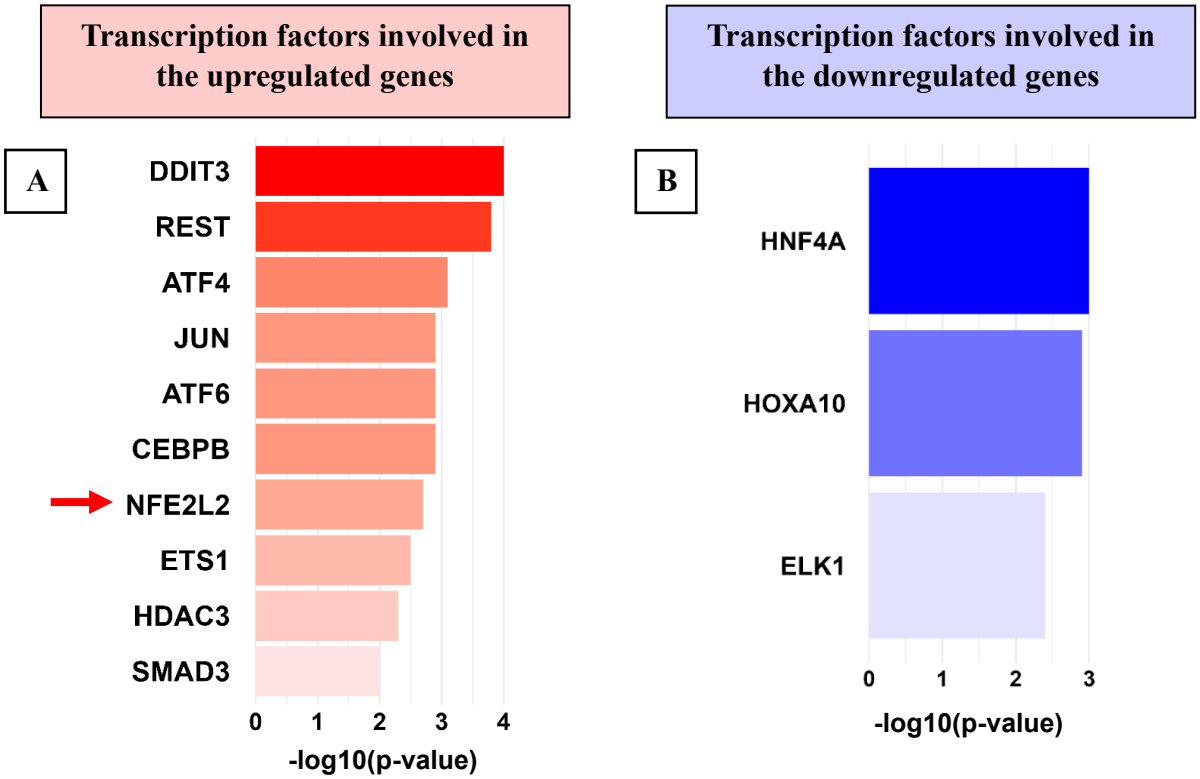

Figure 3.14: Transcription factors involve in the enrichment analysis of differential gene expression comparing dimethyl fumarate-treated hiPSC-CM with untreated cells. Transcriptomics analyses were performed on hiPSC-CM exposed to dimethyl fumarate treatment (150 µM) (DMF) for 6 hours and compared with untreated cells (Control). DEG was performed using a Log_2 Fold change equal to 1 and p-adjusted value < 0.05. Transcription factor enrichment analysis was conducted using metascape, using the transcriptional regulatory relationships unravelled by sentence-based text mining (TRRUST) database.

To evaluate the specific effect of DMF on the antioxidant component of the Nrf2 pathway, a heatmap was created using as a reference the antioxidant genes established in the online tool WikiPathways for Nrf2 pathway in Homo sapiens (WP2884) **(Figure 3.15)**. DMF induced an evident upregulation of the whole pathway when DMF-treated hiPSC-CM were compared with control cells, and surprisingly, the transcripts *BACH1* and *KEAP1*, known as

Nrf2 suppressors, were also upregulated, suggesting a negative feedback loop due to Nrf2 overstimulation with DMF.

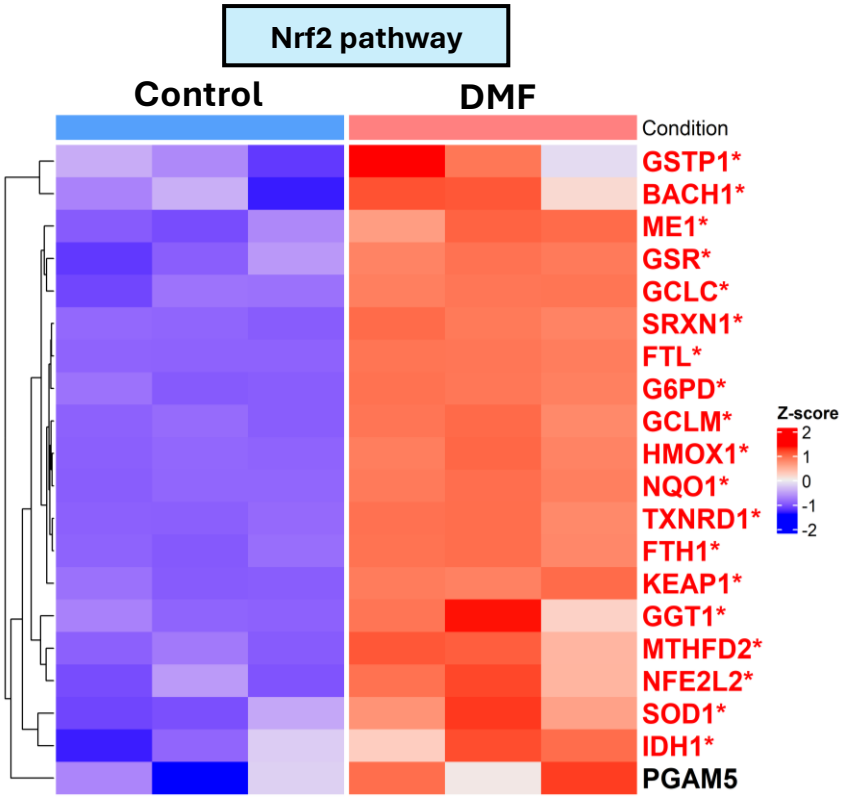

Figure 3.15: Dimethyl fumarate upregulates Nrf2 antioxidant pathway at transcriptomics level in hiPSC-CM. Nrf2 pathway heatmap was generated using normalised counts from the transcriptomics analyses on hiPSC-CM exposed to dimethyl fumarate treatment (150 µM) (DMF) for 6 hours and compared with untreated cells (Control)**.** Significantly upregulated genes are shown in red. * Fold change set as 0 and adjusted p-value < 0.05 vs. respective control group adjusted p-value < 0.05 vs. respective control group. Each column represents a biological replicate.

Overall, these transcriptomics results confirm that DMF can modulate the Nrf2 pathway in human cardiomyocytes at the genetic level, showing that 6 hours of treatment was enough to induce a large transcript change, with the antioxidant genes ranking among the top modulated genes. These findings were further confirmed by identifying the Nrf2 pathway in both the enriched terms and the GSVA analysis, as well as the discovery of Nrf2 as one of the main transcription factors involved in DEG.

3.4.6 Dimethyl fumarate increases Nrf2 antioxidant protein levels in hiPSC-CM.

The next step was to evaluate by western blotting if the observed upregulation of Nrf2 antioxidant genes at both qPCR and transcriptomic levels was also translated into an increase in the protein content of the same antioxidant enzymes. Human cardiomyocytes treated with DMF for 24 hours showed a significant increase in NQO1, TXNRD1 and HMOX1 protein levels by approximately 23-, 1.2-, and 11-fold, respectively, compared with the control condition **(Figure 3.16)**. These results indicated that the genetic effect of DMF on the Nrf2 pathway was also associated with an increase in the translation of the same antioxidant enzymes, suggesting a modulation at a more functional and cellular level.

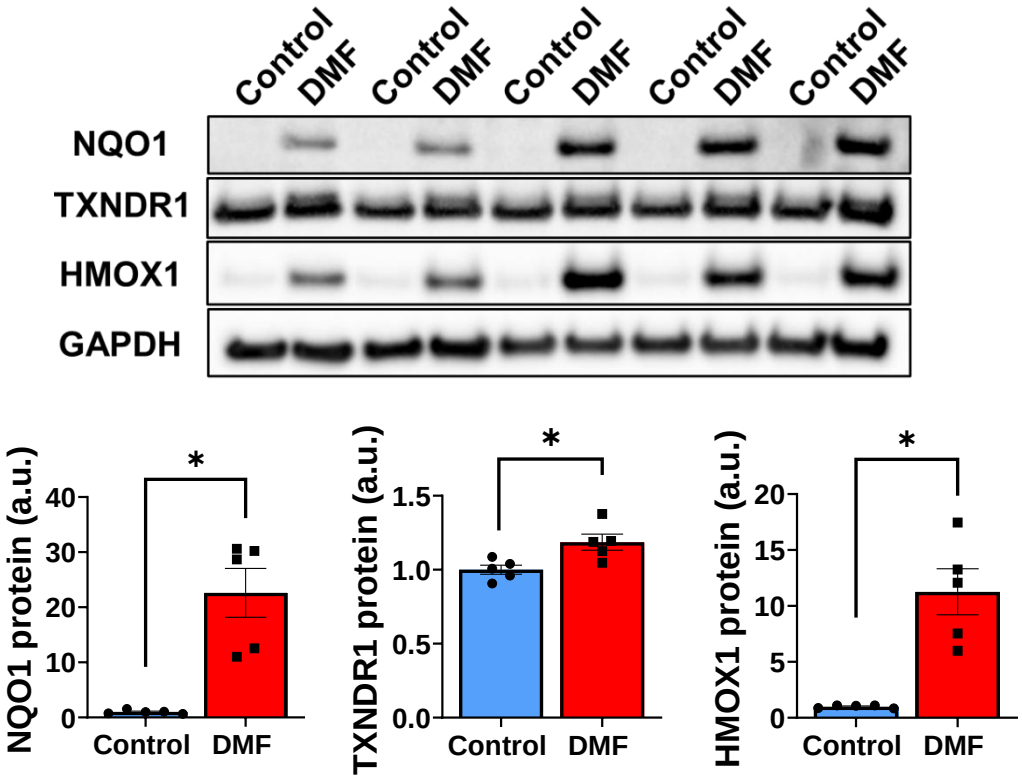

Figure 3.16: Dimethyl fumarate increases the antioxidant protein content in hiPSC-CM. Nrf2 antioxidant targets in hiPSC-CM exposed to dimethyl fumarate treatment (150 µM) (DMF) for 24 hours and compared with untreated cells (Control). The targets evaluated were NAD(P) dehydrogenase quinone 1 (NQO1), thioredoxin reductase 1 (TXNRD1), and heme oxygenase 1 (HMOX1). Glyceraldehyde 3-phosphate dehydrogenase (GAPDH) was used as loading control. * $p < 0.05$ vs. respective control group. a.u., arbitrary units. Each data point represents a biological replicate.

3.4.7 Monomethyl fumarate and Vumerity upregulate Nrf2 antioxidant gene expression similar to dimethyl fumarate in hiPSC-CM.

To further investigate whether other fumarate derivatives could also modulate the Nrf2 pathway, the effect of monomethyl fumarate (MMF) (proposed to be the active form of DMF) on the antioxidant gene expression was studied in hiPSC-CM. MMF, at the same dose used previously for DMF, induced an upregulation of the genes *NQO1*, *TXNRD1*, *HMOX1*, and *SRXN1* by 9-, 3-, 3-, and 4-fold, respectively, and no significant differences were observed between DMF and MMF treatment, suggesting that MMF produced a similar effect to DMF on Nrf2 targets at the same concentration **(Figure 3.17)**.

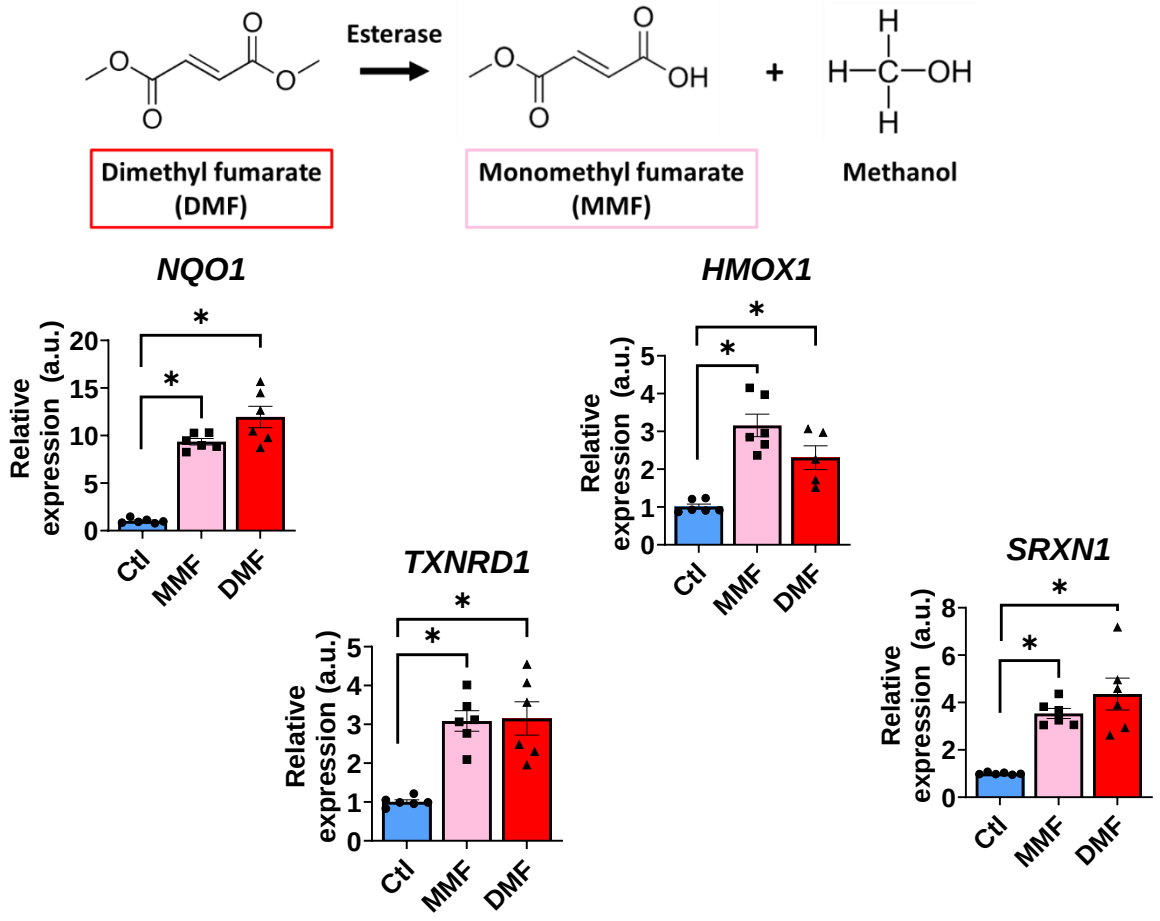

Figure 3.17: Monomethyl fumarate increases Nrf2 antioxidant target gene expression similar to dimethyl fumarate in hiPSC-CM. Expression of Nrf2 antioxidant target genes in hiPSC-CM exposed to dimethyl fumarate (150 µM) (DMF) or monomethyl fumarate (150 µM) (MMF) treatment for 24 hours and compared with untreated cells (Ctl). The targets evaluated were NAD(P) dehydrogenase quinone 1 (*NQO1*), thioredoxin reductase 1 (*TXNRD1*), heme oxygenase 1 (*HMOX1*), sulfiredoxin 1 (*SRXN1*).* $p < 0.05$ vs. respective control group. a.u., arbitrary units. Each data point represents a biological replicate.

Diroximel fumarate, also known commercially as Vumerity (VM), is another fumarate derivative currently used to treat multiple sclerosis, and similar to DMF, VM's active pharmacological molecule is MMF. Therefore, the effect of VM on the antioxidant gene expression in hiPSC-CM was also studied. Cell death and detachment from the plate were caused when human cardiomyocytes were treated with VM at the same concentration used previously for DMF (150 μM) (data not shown). Therefore, a lower dose (25 μM) was used, observing that VM at this concentration significantly increased *NQO1* and *SRXN1* by 16- and 2-fold, respectively, compared with control cells **(Figure 3.18)**.

To evaluate fumarate's specificity on Nrf2 pathway regulation, dimethyl succinate (DMS), a non-fumarate derivative that increases succinate concentration, was used. No significant Nrf2 target gene expression changes were observed for DMS compared with the control condition. These data suggest that the upregulation of Nrf2 targets in human cardiomyocytes is a specific effect of the fumarate derivatives and not for other Krebs cycle metabolites. Additionally, hiPSC-CM treated with MMF at the same concentration as DMF and VM at a lower concentration presented a similar effect on Nrf2 antioxidant target regulation.

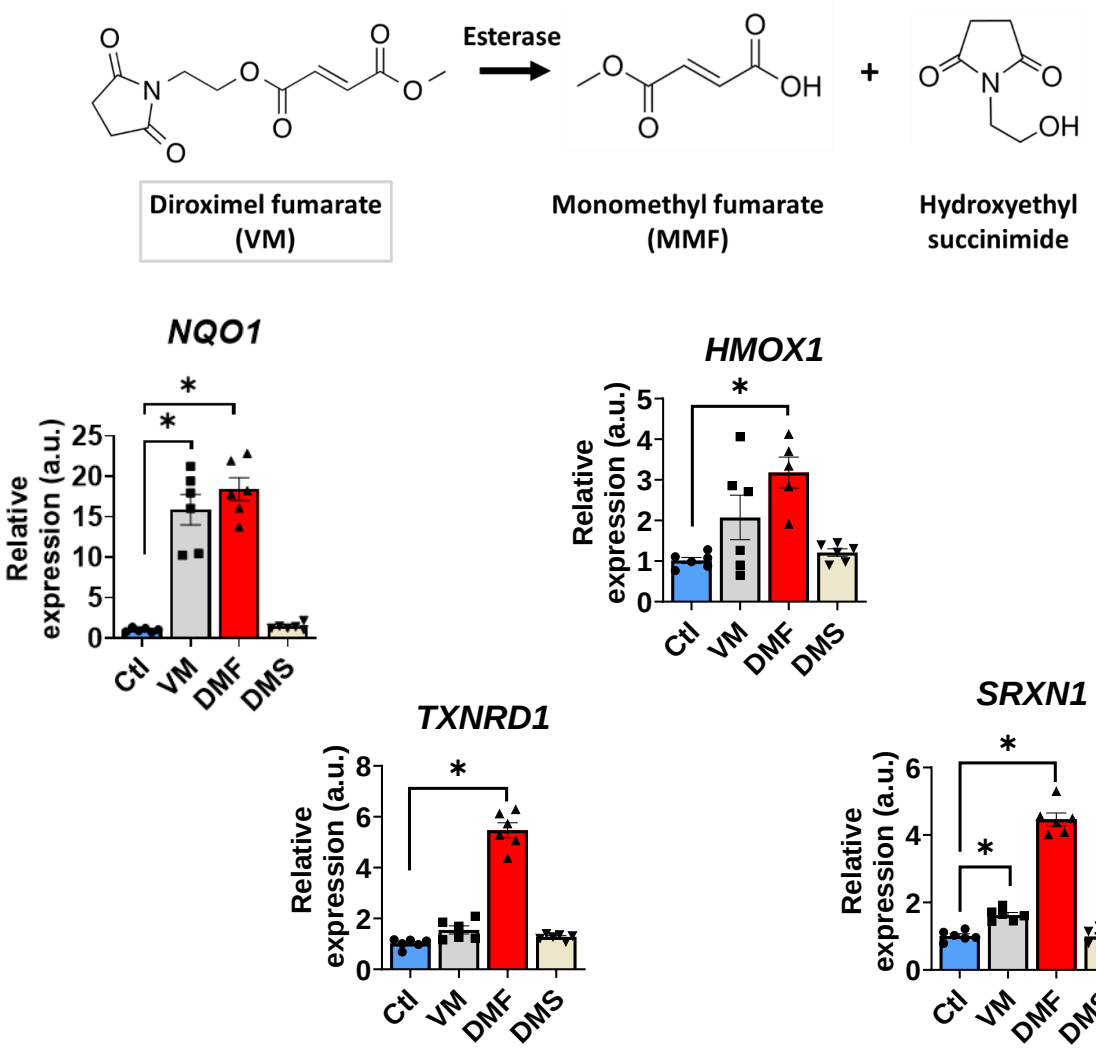

Figure 3.18: Vumerity, at a lower concentration, upregulates Nrf2 antioxidant target gene expression similar to dimethyl fumarate in hiPSC-CM. Expression of Nrf2 antioxidant target genes in hiPSC-CM exposed to vumerity (25 µM) (VM), dimethyl fumarate (150 µM) (DMF), or dimethyl succinate (150 µM) (DMS) for 24 hours and compared with untreated cells (Ctl). The targets evaluated were NAD(P) dehydrogenase quinone 1 (*NQO1*), thioredoxin reductase 1 (*TXNRD1*), heme oxygenase 1 (*HMOX1*), sulfiredoxin 1 (*SRXN1*). * $p < 0.05$ vs. respective control group. Each data point represents a biological replicate.

3.4.8 Sulforaphane and cardiomyocyte-specific *Keap1* mouse models show similar antioxidant regulation to dimethyl fumarate.

Two different additional approaches were carried out to confirm that the antioxidant gene upregulation was driven by Nrf2 activation and not because the fumarate derivatives were targeting other related pathways. Firstly, a molecular approach was carried out using

sulforaphane (SFN), a natural plant compound found mainly in broccoli and broccoli sprouts, which has been historically used as an Nrf2 activator. HiPSC-CM under SFN treatment showed a significant increase in the expression of the antioxidant genes *TXNRD1* and *SRXN1* by 4- and 5-fold compared with the control cells **(Figure 3.19)**. Similarly, an increase in *HMOX1* gene expression bordering significance with a p-value equal to 0.0501 was observed, meanwhile, *NQO1* expression was trending upwards but did not reach significance.

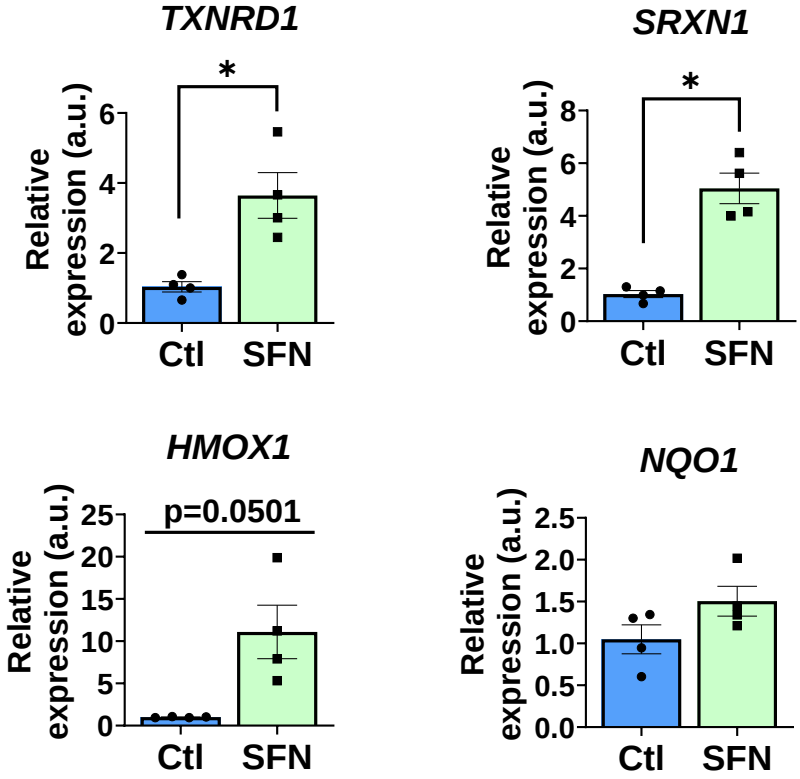

Figure 3.19: Sulforaphane increases Nrf2 antioxidant target gene expression in hiPSC-CM. Expression of Nrf2 antioxidant target genes in hiPSC-CM exposed to sulforaphane (5 µM) (SFN) for 6 hours and compared with untreated cells (Ctl). The targets evaluated were thioredoxin reductase 1 (*TXNRD1*), sulfiredoxin 1 (*SRXN1*), heme oxygenase 1 (*HMOX1*), and NAD(P) dehydrogenase quinone 1 (*NQO1*). * $p < 0.05$ vs. respective control group. a.u., arbitrary units. Each data point represents a biological replicate.

Secondly, tissue from mouse hearts with a cardiomyocyte-specific knockout for the Nrf2 suppressor *Keap1* (KOKeap1), which leads to increased Nrf2 activity, was utilised, and the expression of the different antioxidant genes was measured by qPCR **(Figure 3.20)**. KOKeap1 hearts had significantly upregulated gene expression of *Nqo1, Txnrd1*, and *Srxn1*

by 9-, 6-, and 11-fold, respectively, compared with the wild-type hearts (WT), while no significant differences were observed for *Hmox1*.

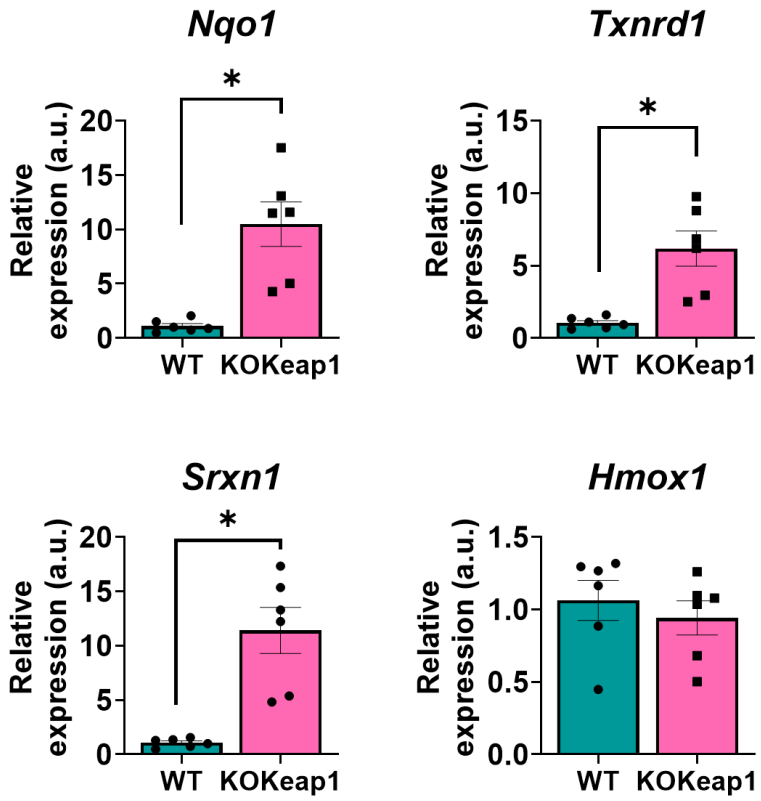

Figure 3.20: Cardiomyocyte-specific *Keap1* knockout upregulated Nrf2 antioxidant target gene expression in mouse heart. Expression of Nrf2 antioxidant target genes in cardiomyocyte-specific *Keap1* knockout (KOKeap1) compared with wild-type (WT) mouse hearts. The targets evaluated were NAD(P) dehydrogenase quinone 1 (*Nqo1*), thioredoxin reductase 1 (*Txnrd1*), sulfiredoxin 1 (*Srxn1*), and heme oxygenase 1 (*Hmox1*). * $p < 0.05$ vs. respective WT group. a.u., arbitrary units. Each data point represents a biological replicate.

These findings were studied in-depth by performing RNA-Seq transcriptomics analysis on KOKeap1 hearts and by comparing with wild-type mouse hearts using a principal component analysis test (PCA) **(Figure 3.21A)**. PC1 presented a 64% variance, occasioned by the distribution of the samples through the x-axis, where, on one of the graph ends (between x = -20 and x = 0), two of the WT samples were close to two samples of the KOKeap1 group, whereas, on the other end (between x = 10 and x = 30), one sample of the KOKeap1 group was clustered with two samples of the WT group. This arrangement was further confirmed by observing a similar sample distribution when an inter-sample

correlation heatmap was generated **(Figure 3.21B)**. This may be due to incomplete penetrance of the knockout allele, individual biological variation, or rescue of the knockout phenotype by alternative transcripts or genes in some samples of the KOKeap1 group. However, when the PC2 was studied, it was identified a 22% variance, and on the y-axis, a clear separation between both groups was observed, therefore, to understand the impact of KOKeap1 on cardiomyocyte biological pathways, a DEG analysis was performed.

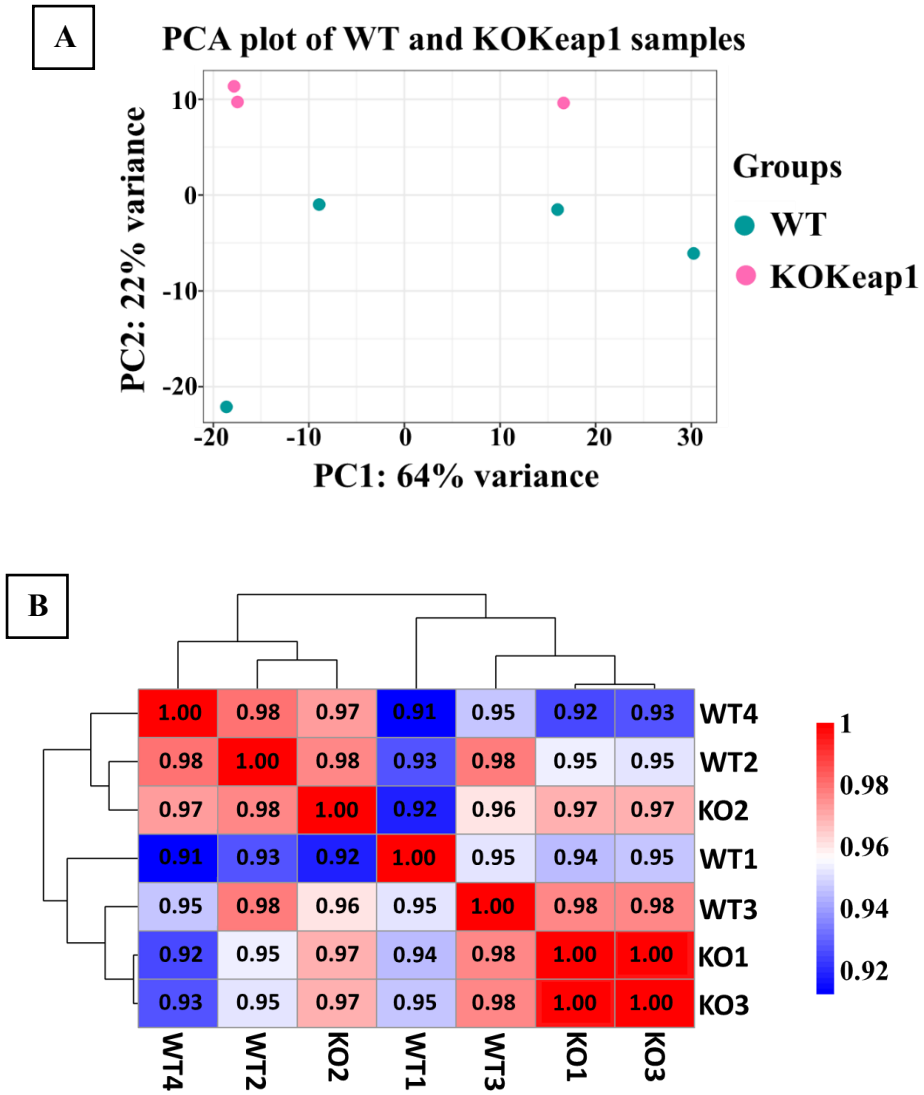

Figure 3.21: *Keap1* cardiac-specific knockout and wild-type mouse heart samples are not clustering separately for each group under principal component PC1, but a clear distribution is observed under PC2. Transcriptomics analyses were performed in cardiomyocyte-specific *Keap1* knockout (KOKeap1/KO) compared with wild-type (WT) mouse hearts. **(A)** Principal component analyses between WT and KOKeap1. **(B)** Inter-sample correlation between samples of each condition.

To determine the magnitude of *Keap1* knockout on the mouse cardiomyocyte global gene profile, differential gene expression (DEG) was performed in a total of 14901 genes comparing KOKeap1 with WT samples using the strict parameters p-adjusted value < 0.05, and Log_2Fold change > 1. DEG identified that 498 genes were significantly modulated by *Keap1* cardiac-specific knockout (approximately 3.4% of the total genes), where 126 genes were significantly upregulated while 372 were significantly downregulated. Interestingly, when the DEG was visualised by generating a volcano plot **(Figure 3.22)**, among the upregulated genes *Nqo1, Txnrd1, and Srxn1* were observed.

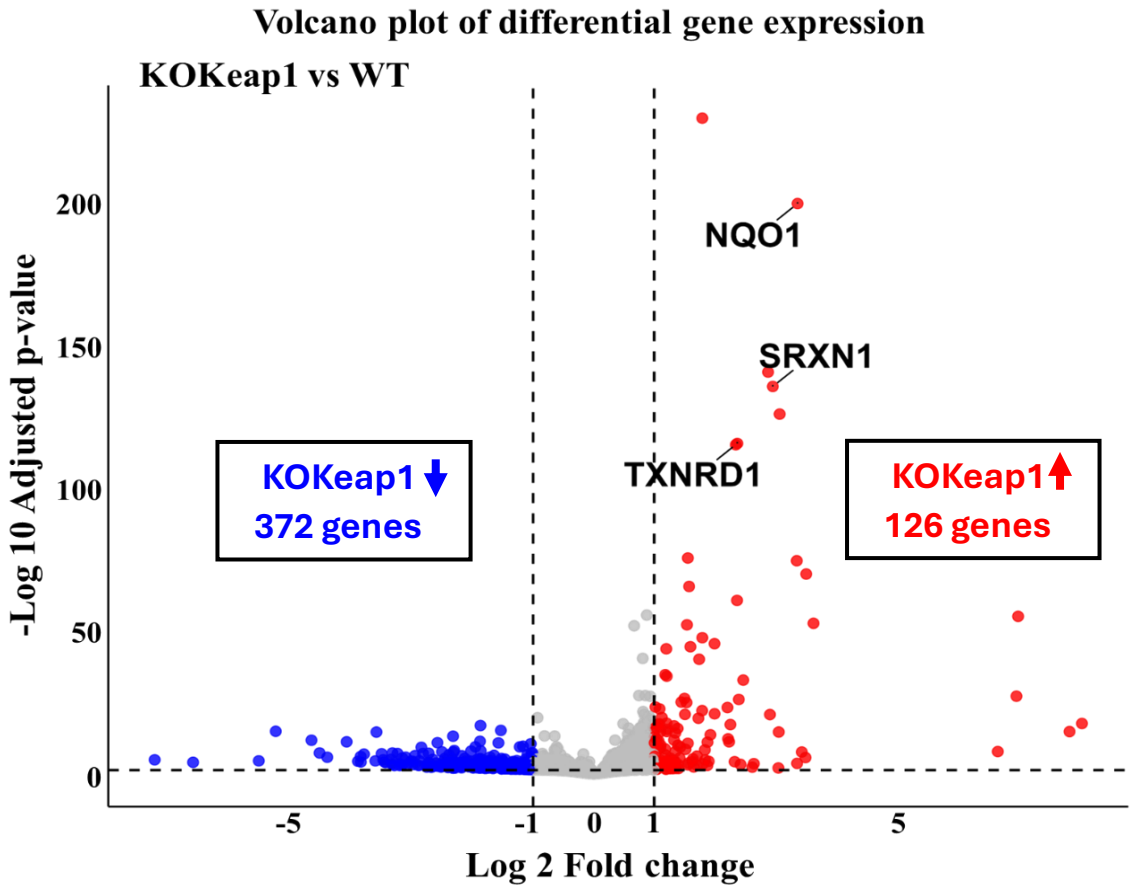

Figure 3.22: Antioxidant genes represent the top most enriched genes in the volcano plot of differential gene expression comparing *Keap1* cardiac-specific knockout and wild-type mouse heart. Transcriptomics analyses were performed in cardiomyocyte-specific *Keap1* knockout (KOKeap1/KO) compared with wild-type (WT) mouse hearts. DEG was performed using a Log_2 Fold change equal to 1 and p-adjusted value < 0.05. Upregulated and downregulated genes are coloured in red and blue, respectively.

To identify the specific biological pathways that were modulated by *Keap1* knockout in mouse cardiomyocytes, enrichment analysis was carried out using the previous significant gene set data from DEG. Among the upregulated genes, the most enriched pathways were glutathione conjugation, oxidative stress and redox pathway, and the NADP metabolic process **(Figure 3.23A)**. These processes play a critical role in the antioxidant defence mechanism and are similar to the pathways observed for DMF enrichment analysis. Surprisingly, practically all the enrichment terms observed for the downregulated genes were associated with the immune system **(Figure 3.23B)**, highlighting the role of the Nrf2 pathway in regulating autoimmune processes. Additionally, three cell processes, GPCR signalling pathways, elongation of very long fatty acids, and cell interactions were also observed to be reduced.

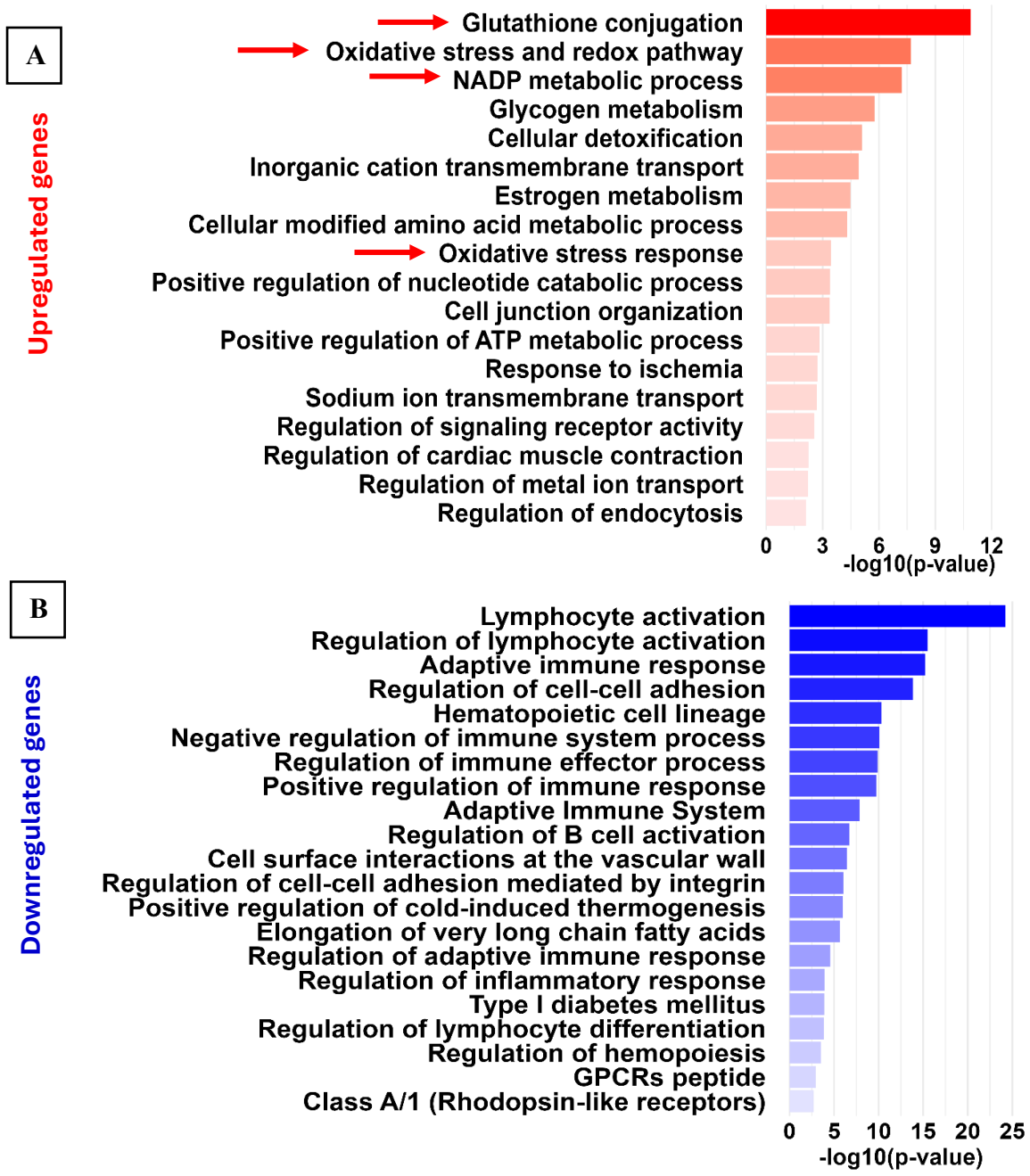

Figure 3.23: Enrichment analysis of differential gene expression comparing *Keap1* cardiac-specific knockout and wild-type mouse heart. Transcriptomics analyses were performed in cardiomyocyte-specific *Keap1* knockout (KOKeap1/KO) compared with wild-type (WT) mouse hearts. DEG was performed using a Log_2 Fold change equal to 1 and p-adjusted value < 0.05. Enrichment analysis was conducted using metascape, and the graph of enriched terms represents the 126 upregulated **(A)** or 372 downregulated genes **(B)**.

Based on the significantly regulated genes detected by the DEG and using the TRRUST database, we identified the transcription factors involved with this genetic modulation, observing that Nfe2l2 (Nrf2) was the most enriched transcription factor for the upregulated

genes **(Figure 3.24A)**. Along with Nrf2, the tumour suppressor p53 (Trp53), which regulated essential genes to maintain cardiac physiological structure and bioenergetics[154, 155], and the peroxisome proliferator-activated receptor gamma (Pparg), a member of the PPAR family well known as metabolic master regulators[156] were also detected. In contrast, the most enriched transcription factor for the downregulated genes was the sterol regulatory element binding transcription factor 1 (Srebf1), a master regulator of cholesterol and lipid synthesis and homeostasis[157, 158], and surprisingly, the Pparg transcription factor, showing that the same transcription factor can enhance or repress specific genes **(Figure 3.24B)**.

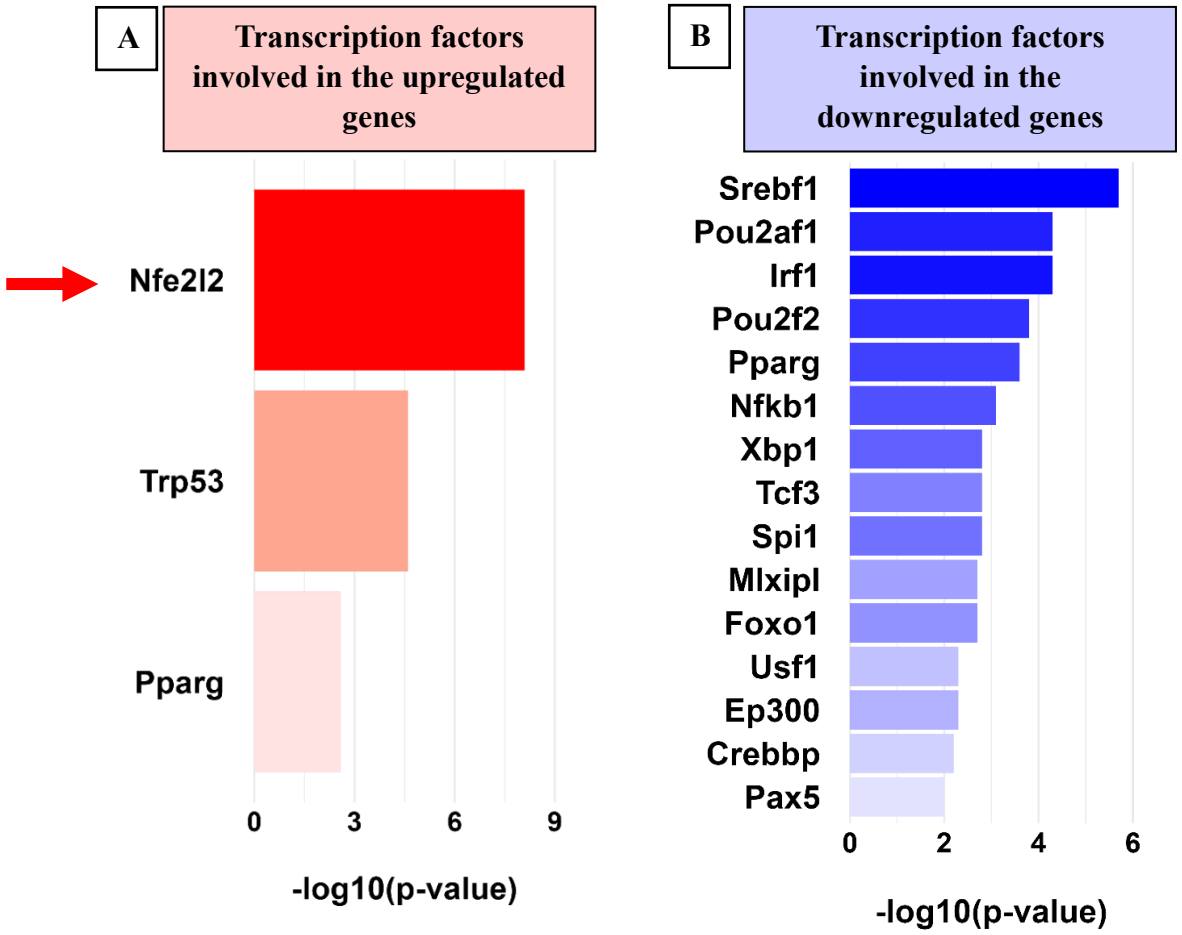

Figure 3.24: Transcription factor enrichment analysis of differential gene expression comparing *Keap1* cardiac-specific knockout and wild-type mouse heart. Transcriptomics analyses were performed in cardiomyocyte-specific *Keap1* knockout (KOKeap1/KO) compared with wild-type (WT) mouse hearts. DEG was performed using a Log_2 Fold change equal to 1 and p-adjusted value < 0.05. Transcription factor enrichment analysis was conducted using metascape, using the transcriptional regulatory relationships unravelled by sentence-based text mining (TRRUST) database.

Lastly, the effect of the cardiomyocyte-specific *Keap1* knockout on the Nrf2 pathways was studied by generating a heatmap of the antioxidant genes regulated by Nrf2 **(Figure 3.25)**, which revealed that KOKeap1 upregulated only specific antioxidant genes, contrasting our previous findings where DMF treatment upregulated nearly all the genes of this pathway in hiPSC-CM. Additionally, to visualise the magnitude of expression change, boxplots were created using mRNA levels, observing that KOKeap1 significantly increased the expression of the genes *Nqo1, Txnrd1, and Srxn1* compared with the WT condition, while no changes were observed for *Hmox1* gene expression.

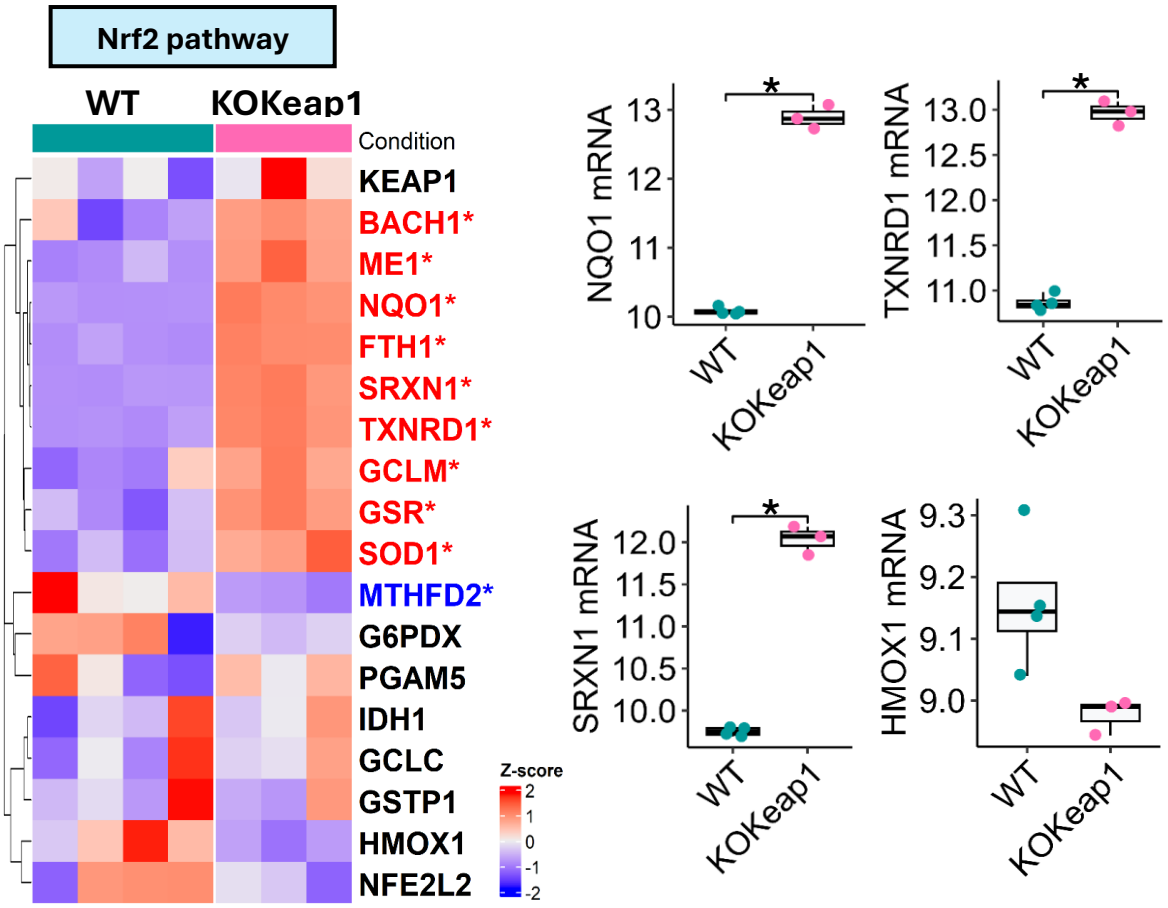

Figure 3.25: *Keap1* cardiac-specific knockout upregulates Nrf2 antioxidant genes in mouse hearts. Nrf2 pathway heatmap and boxplots were generated using normalised counts from the transcriptomics analyses performed in cardiomyocyte-specific *Keap1* knockout (KOKeap1/KO) compared with wild-type (WT) mouse hearts**.** Significantly upregulated genes are shown in red, whereas significantly downregulated genes are shown in blue. * Fold change set as 0 and adjusted p-value < 0.05 vs. respective control group. Each column in the heatmap represents a biological replicate. Each data point in the graphs represents a biological replicate.

In summary, these results show that both SFN, as a pharmacological approach, and the KOKeap1 model, as a genetic model, regulate the Nrf2 antioxidant pathway similarly to the fumarate derivatives, confirming that the effects observed for the fumarate derivates were driven by Nrf2 activation.

3.5 Discussion

3.5.1 Fumarate derivatives enhance the Nrf2 antioxidant pathway in human cardiomyocytes.

Our results show that when the heart is exposed to acute hypoxia, the intracellular concentration of metabolites dramatically changes. We observed a dual regulation of Krebs cycle metabolites, where hypoxia has both, a cataplerotic effect on the first half of the cycle and an anaplerotic effect on the second half (including fumarate levels). Similar increases in fumarate concentrations have also been reported before in a cardiac ischemia model[159], however, the consequences or cellular processes affected by this fumarate elevation are unknown within the human cardiomyocyte.

Overall, the results of this chapter demonstrate that supplementation of exogenous fumarate derivatives activates the Nrf2 antioxidant pathway in hiPSC-CM. Interestingly, although the role of fumarate derivates on Nrf2 activation to improve antioxidant defences has not been shown before in human cardiomyocytes, a similar antioxidant effect has been observed in various models, including both cellular models, such as nervous system cells [132, 160-162], immune system cell[163, 164], hepatocytes[165, 166], non-human cardiomyocytes[167, 168], as well as animal models[169-173], where fumarate derivatives have been described as cardiac protector agents[92, 168, 174]. Here, we also demonstrated that the very rapid increase of the antioxidant defences following fumarate derivatives treatment in human cardiomyocytes was associated with decreasing the apoptosis propensity maker *BAX/BCL2* ratio at the gene

level. These results suggest that these compounds emerge not only as possible molecules to improve defence against reactive oxygen species but also may have a role in preventing apoptosis susceptibility in cardiomyocytes.

Sulforaphane (SFN) and the cardiac-specific *Keap1* knockout (KOKeap1) mouse model confirmed that Nrf2 drove the effects observed for the fumarate derivatives. Sulforaphane, as the molecular approach, presents a similar mechanism of action to fumarate derivatives by decreasing Nrf2-Keap1 interaction[175], and it has been reported to reverse the ageing-induced cardiac muscle dysfunction in old mice by improving Nrf2 activity[176]. However, we observed a distinct antioxidant gene regulation between DMF-treated hiPSC-CM and mouse cardiomyocytes from the KOKeap1 model. This discrepancy is likely due to differences between the acute treatments with fumarate derivatives and SFN compared with the chronic effects of the KOKeap model, which constitutively upregulated Nrf2 pathway within the mouse cardiomyocyte. Hence, potentially a greater negative feedback regulation may be occurring in response to this overactivation. As the elevated fumarate concentration under hypoxia may represent a transient effect induced by this condition, the expected molecular mechanism more closely resembles the acute response of fumarate derivatives and SFN treatments rather than the chronically stable Nrf2 activation seen in the KOKeap1 model.

3.5.2 Fumarate derivatives promoted Nrf2 nuclear translocation and upregulation of complementary antioxidant pathways in human cardiomyocytes.

Using subcellular fractionation, we observed that fumarate derivatives drive Nrf2 nuclear translocation, a process which is triggered by Nrf2 dissociation from its cytosolic repressor KEAP1 and allows Nrf2 nuclear binding to the antioxidant response element sequence present in the antioxidant genes[143]. Interestingly, different molecular mechanisms have

been associated with Nrf2 activation, including post-translation modification (PTM) of Nrf2 protein, such as phosphorylation[177], acetylation[178] and SUMOylation[179], or PTM on KEAP1 that decreases its ability to interact with Nrf2, including glycosylation[180] alkylation[181] and succinylation[182], among several other[183]. However, when we focus on fumarate derivatives, they act by modifying cysteine residues in KEAP1 through a PTM known as succination[54, 135] (which was further studied in **Chapter 5**). In a comparative study investigating the effect of dimethyl fumarate (DMF) and monoethyl fumarate (MEF) on Nrf2 activation, it was detected that succination of cysteine 151, 257, 288 and 273 in KEAP1 were critical to decrease KEAP1-Nrf2 binding[132]. Furthermore, the same study showed that while MEF induced specific succination of cysteine 151, DMF modified all the critical cysteines in KEAP1, inducing a higher translocation and activation of the Nrf2 pathway. Additionally, *in vitro* experiments have shown that fumarate and its derivatives DMF and MEF can interact directly with the Nrf2-binding site at the KEAP1 domain and displace Nrf2 from this site[184]. These results suggest that fumarate derivatives can modulate Nrf2 nuclear translocation and activation indirectly by modifying KEAP1 cysteine residues, decreasing its Nrf2 suppression, and directly by competing with the Nrf2 binding site in KEAP1.

Our transcriptomics analyses confirmed that fumarate derivatives not only enhanced the Nrf2 antioxidant pathway but also regulated other antioxidant pathways and metabolic processes, including glutathione metabolism and the pentose phosphate pathway. The pentose phosphate pathway rate-limiting step is mediated by glucose-6-phosphate dehydrogenase (G6PD), which has been previously reported to be modulated by Nrf2 in other studies[185, 186], including a recent heart model study[130]. This pathway, in addition to redirecting glucose utilisation, generates NADPH, a cofactor that is required for the activity of multiple antioxidant enzymes, including Nqo1[187], Txnrd1[188], and glutathione

reductase[189], which is part of glutathione metabolism. Furthermore, among the enriched transcription factors, DDIT3 was the most upregulated in DMF treatment differential gene expression, DDIT3 has been reported to be able to promote glycolysis and inhibit oxidative phosphorylation, decreasing oxidative stress under specific cell stress conditions[148]. Similarly, oxidative stress suppression has also been described as an effect of Trp53[190], a transcription factor observed to be enriched in the KOKeap1 data, suggesting that Nrf2 activation can boost different redox systems within human cardiomyocytes, which position fumarate as a key protective metabolite.

In this chapter, the role of three different fumarate derivatives, DMF, monomethyl fumarate (MMF) and diroximel fumarate (VM) in Nrf2 activation was evaluated, observing that all of them increase antioxidant gene expression in human cardiomyocytes. Notably, all three molecules have been approved by the FDA for multiple sclerosis treatment[2, 67] and have been reported to modulate the Nrf2 pathway[191, 192]. Clinically, DMF and VM hydrolysis by esterase generates MMF, which is the active molecule of these prodrugs and explains why both molecules have similar effects on the cardiomyocyte. However, in addition to MMF, DMF hydrolysis generates methanol in a 1:1 ratio with MMF, contributing to the adverse gastrointestinal events commonly reported with DMF treatment[193, 194]. This adversity has been prevented with VM, in which the ratio MMF to methanol is 9:1, significantly reducing the gastrointestinal side effects in patients[194]. Curiously, in patients, nearly twice the dose of VM is required to produce an equivalent amount of MMF compared with DMF[191]. However, in our data, we observed that a lower dose of VM was required because when we tested the same concentration as DMF, cell cytotoxicity was observed. This result suggests that despite DMF's hydrolysis producing methanol as a secondary product, human cardiomyocytes can tolerate DMF better than VM.

We used SFN as a pharmacological molecule to activate the Nrf2 pathway, which, despite disrupting KEAP1-Nrf2 interaction similarly to the fumarate derivatives, modifies cysteine residues differently. Fumarate derivatives induce KEAP1 succination, which is an irreversible PTM[195], whereas SFN structure contains an isothiocyanate electrophilic carbon, which interacts with KEAP1's cysteine residues in a more dynamic (reversible) reaction[196]. Curiously, our data showed that a much lower dose of SFN (5 μM) was required to induce similar changes in the antioxidant genes compared with DMF (150 μM), similar results have been observed in other studies[197, 198]. However, it is important to note that SFN is a highly reactive molecule[199] that is metabolised into various sub-products[200], which play a role in several other pathways, including the cell cycle[201] and epigenetic modifications[202]. Suggesting that SFN may activate additional pathways or cell processes that contribute to the upregulation of Nrf2 antioxidant genes.

3.6 Conclusion

Our data demonstrated that fumarate derivatives robustly upregulated critical antioxidant defence pathways in human cardiomyocytes, including the Nrf2 pathway, pentose phosphate pathway and glutathione metabolism. Notably, our findings confirmed that this enhanced antioxidant defence is primarily mediated by promoting Nrf2 nuclear translocation and increasing antioxidant gene expression even at early time points of treatment, which was also accompanied by increased protein levels of the same antioxidant enzymes. This reveals a potential use for fumarate derivatives as a therapeutic tool to improve the antioxidant defence mechanisms within the heart.

Chapter 4

Fumarate derivatives as cardiac metabolic regulators in hiPSC-CM

4.1 Abstract

One of the greatest challenges in studying cardiomyocyte metabolism *in vitro* is that commercially available cell lines are immature, and unlike the adult human heart, their metabolism is primarily glycolytic rather than oxidative. Therefore, this chapter evaluated the mitochondrial oxidative profile and substrate preferences of mature hiPSC-CM. Mitochondrial oxygen consumption rate, showed that mitochondria from our hiPSC-CM preferentially oxidase long-chain fatty acid. They also present metabolic flexibility by activating alternative oxidative pathways when specific substrate pathways were inhibited or shifting to glycolytic metabolism when mitochondria oxidation was impaired, reassembling the metabolic profile of the adult heart.

Previously, fumarate derivatives were shown to influence cardiomyocyte biology, however, their role in hiPSC-CM metabolism is unknown. Hence, this chapter investigated the effect of fumarate derivatives on fatty acid and glucose metabolism. Dimethyl fumarate (DMF) decreased fatty acid oxidation gene expression and fatty acid oxidation rates while increasing glycolytic genes, lactate release, and glycolytic rates. These changes were accompanied by a transient mitochondrial network fragmentation and reduced mitochondrial oxygen consumption. Similar effects were observed with other fumarate derivatives or the well-known Nrf2 activators sulforaphane and hydrogen peroxide. However, cardiomyocyte-specific *Keap1* mouse knockout revealed that Nrf2 may not induce these changes. Interestingly, DMF was hydrolysed to fumarate when the metabolic changes occurred, suggesting that fumarate itself could be mediating these changes.

In conclusion, our hiPSC-CM model resembled the metabolic profile of the adult heart. Furthermore, fumarate derivatives induced a metabolic shift from fatty acid oxidation to glycolytic metabolism in hiPSC-CM, which may not be mediated by the Nrf2 pathway.

4.2 Introduction

4.2.1 Commercial cardiomyocyte models do not mimic adult heart metabolism.

Currently, it remains challenging to find physiologically relevant cardiomyocyte models that resemble the adult heart metabolic profile, which has consequently led to the use of metabolically immature cardiac models, where most commercially available models are fetal and animal-derived cardiomyocytes. However, fetal cardiomyocytes have been reported to present an immature metabolic profile because they generate most of their energy from glycolysis and have underdeveloped mitochondrial morphology and limited oxidative capacity[203]. Cardiomyocytes isolated from rats and mice have been described to be very fragile and tend to shift from oxidative to glycolytic metabolism[204], and in addition, it has been reported that their long-term culture is impossible as they lose their contractility[205]. Furthermore, the use of animal models in research is declining due to ethical concerns about animal welfare, however, *in vitro* and *in silico* models are emerging as promising alternatives[206]. Therefore, part of this chapter focused on evaluating the metabolic profile of our mature hiPSC-CM model, specifically at the mitochondrial oxidative level, to study mitochondrial substrate flexibility and preference.

4.2.2 Exploring the role of fumarate derivatives in cardiomyocyte metabolism.

In response to hypoxia and ischemia, cardiomyocytes limit the use of the available oxygen by shifting from oxidative metabolism to anaerobic glycolysis[61, 62]. Notably, fumarate intracellular accumulation occurred rapidly in response to hypoxia (as observed in Chapter 3) and under ischemia conditions[159] prior to cardiomyocyte metabolic reprogramming. However, there is no evidence about whether fumarate accumulation is involved in this metabolic reprogramming.

Interestingly, findings from the previous chapter revealed that fumarate derivatives can regulate biological processes within the cardiomyocyte. Additionally, the primary molecular target of fumarate derivatives, Nrf2, has been reported to interact with different transcription factors involved in metabolic processes, including glycolysis and fatty acid oxidation[207-209]. Therefore, a major portion of this chapter focused on investigating whether fumarate derivatives could modulate hiPSC-CM metabolism, especially fatty acid oxidation and glycolytic metabolism.

4.3 Chapter aims

Commercially available cardiomyocytes present an immature metabolic profile, meaning these models do not resemble the adult heart metabolic profile. In contrast, our hiPSC-CM are exposed to a maturation process in which they are incubated in media containing fatty acid and low glucose concentration. Hence, part of this chapter focused on evaluating our cell model's mitochondrial oxidative capacity. Furthermore, there is limited information about the effect of fumarate derivatives on human cardiomyocyte metabolism. Therefore, this chapter explored the role of the fumarate derivatives in hiPSC-CM metabolism. This chapter investigated:

1. The metabolic flexibility, mitochondrial substrate preference, and mitochondrial oxidative capacity and dependency in hiPSC-CM.
2. The effect of fumarate derivatives on fatty acid oxidation and glycolytic metabolism in hiPSC-CM and their impact on mitochondrial network morphology, mitochondrial components, and mitochondrial oxygen consumption rate.
3. The specific role of Nrf2 in hiPSC-CM metabolism using a well-established Nrf2 activator and transcriptomics analysis of a genetic mouse cardiac model with constitutive Nrf2 activation.

4. Alternative mechanisms modulated by fumarate derivates involved in hiPSC-CM metabolic regulation.

4.4 Methods

4.4.1 Metabolic fluxes and mitochondrial respiration.

Mitochondrial respiration was carried out following the protocol in **Section 2.6**. Additionally, mitochondrial fuel oxidation rates were measured using the Seahorse Mito Fuel Flex Test Kit (Agilent) in collaboration with Dr Thomas Nicol to determine mitochondrial fuel dependency and capacity for using glutamine, long-chain fatty acid, and glucose. This analysis involved the use of 3 μM BPTES to inhibit the glutamine oxidation pathway, 4 μM Etomoxir to inhibit the long-chain fatty acid oxidation pathway, and 2 μM UK5099 to inhibit the glucose oxidation pathway.

Dependency and capacity were calculated based on the kit protocol.

Dependency % = $(\frac{Baseline\ OCR - Target\ inhibitor\ OCR}{Baseline\ OCR - All\ inhibitors\ OCR})\ x\ 100$

Capacity % = $(1-(\frac{Baseline\ OCR - Other\ two\ inhibitors\ OCR}{Baseline\ OCR - All\ inhibitors\ OCR}))\ x\ 100$

4.4.4 Extracellular lactate.

Cell media was diluted in distilled water in a ratio of 1 to 4, and 5 μL of the dilution was transferred into a 96-well plate, where 100 μL of the reaction mix (prepared by combining 3.5 mL glycine buffer (0.6 M glycine (Sigma), 0.42 M hydrazine hydrate 50-60% purity (Sigma), and 0.06 M KOH (Fisher chemical), adjusted to pH 7.2), 10 mg β-Nicotinamide adenine dinucleotide hydrate (NAD^+) (Sigma), 427 units of L-Lactic Dehydrogenase from bovine heart (Sigma), and 6.5 mL in distilled water) was added and mixed well using a multichannel pipette. The reaction was incubated for 15 minutes at 37°C, and the absorbance was measured at 340 nm using a microplate reader, with the lactate concentration determined by comparing with an L-lactate (Sigma) standard curve.

4.4.6 Mitotracker and Mitochondrial Network Morphology.

After maturation, hiPSC-CM were dissociated from a 6-well plate using TrypleE Express, and 50,000 cells were seeded onto coverslips and placed in a 24-well plate pre-coated with reduced grown factor Matrigel. The cells were incubated for 3-4 days until they recovered their morphology and resumed beating. Subsequently, the cell media was replaced with DMEM 1X media containing 150 μM dimethyl fumarate. After 12 or 24 hours of treatment, the cell media was removed, and the cells were washed twice with DPBS 1x. Mitotracker Red CMXRos (ThermoFisher Scientific), previously diluted in pre-warmed DMEM 1X media (37°C) to a final concentration of 100 nM, was added to the cells and incubated for 25 minutes at 37°C. The cells were washed three times with DPBS 1X (37°C) and fixed using 4% paraformaldehyde (PFA) for 15 minutes at room temperature. Following fixation, PFA was removed, and the cells were rinsed several times with DPBS 1X. The cells were then permeabilised using 0.5% Triton X-100 for 10 minutes at room temperature, followed by three washes with DPBS 1X.

DAPI (4′,6-diamidino-2-phenylindole) was added to stain the cell DNA and incubated for 10 minutes at room temperature. The cells were washed with DPBS 1X, and the coverslips were removed from the plate and mounted onto glass slides using a solution of 50% glycerol and 50% DPBS 1X. Imaging was performed using a Leica TCS SP5 II microscope with a Leica CTR6500 controller. DAPI was excited at 405 nm using a UV laser at 21% intensity, with maximum emission detected at 460 nm. Mitotracker Red CMXRos was excited by a visible laser at 543 nm at 27% intensity, with maximum emission detected at 617 nm. Images were analysed, processed and quantified using ImageJ's Fiji image processing package[210, 211], and the plugins Mitochondrial Network Analysis (MiNA)[212] and Mitochondria Analyzer[213], where mitochondrial network morphology was studied following plugins description **(Figure 4.1)**.

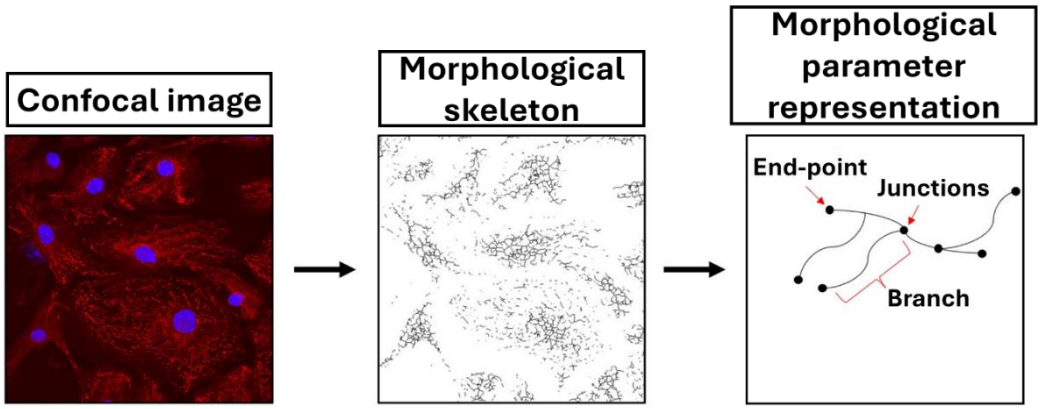

Figure 4.1: Mitochondrial network morphology parameters quantification. This figure was created based on the MiNA[212] publication and illustrates how the mitochondrial network was analysed using the MiNA[212] and Mitochondria Analyzer[213] plugins. The mitochondrial network is skeletonised and quantified, determining different morphological parameters, including mitochondrial density, abundance and length of mitochondrial branches and junctions. Additionally, mitochondrial interconnectivity was calculated by diving the mitochondria area by the mitochondria perimeter[214].

4.4.9 Dimethyl fumarate hydrolysis.

Dimethyl fumarate was prepared in DMSO and directly diluted in DMEM 1X. Samples were then incubated at room temperature for 1, 3, 6, and 24 hours and transferred to glass mass spectrometry vials. Dr John Walsby-Tickle at Oxford University processed and analysed the samples using ion chromatography-mass spectrometry. The results were compared with a fumarate standard, and DMEM 1X was used as a blank.

4.5 Results

4.5.6 hiPSC-CM show metabolic flexibility and preferential use of long-chain fatty acids as energy substrate.

The mitochondrial metabolic profile of the hiPSC-CM was studied by using a Seahorse Analyser. For this, mature hiPSC-CM were incubated in Seahorse media containing either 1 g/L (5.56 mM) glucose or in media mimicking maturation media, containing all the substrates described in **Section 2.1.1**, including 5.56 mM glucose, 100 μM non-essential amino acids and 80 μM oleic acid: BSA. A significant increase in mitochondrial oxygen consumption rate (OCR) was observed in the cells incubated in the maturation media compared with the cells incubated in just glucose, with basal respiration in the OCR measurement 1.7-fold higher in maturation media. This result was accompanied by a 57% decrease in basal levels of extracellular acidification rate (ECAR), measured as a marker of anaerobic glycolytic activity in cells incubated in maturation media compared with cells incubated in glucose alone **(Figure 4.2)**.

Interestingly, when the mitochondrial ATP synthase inhibitor oligomycin (Oligo) was added, cells incubated in maturation media showed increased extracellular pH, reaching values similar to those incubated in just glucose. The maximal respiratory capacity was measured using the uncoupler cyanide-4-(trifluoromethoxy) phenylhydrazone (FCCP), which induced a 2.4-fold increase in the OCR in hiPSC-CM incubated in maturation media compared with cells incubated in just glucose. Additionally, the non-mitochondria respiration, determined using the Complex I and Complex III inhibitors rotenone and antimycin A (ROT/AA), was 3.1-fold higher in maturation media than in glucose-only media cells. No differences between the media conditions were detected in the ECAR following FCCP or ROT/AA addition.

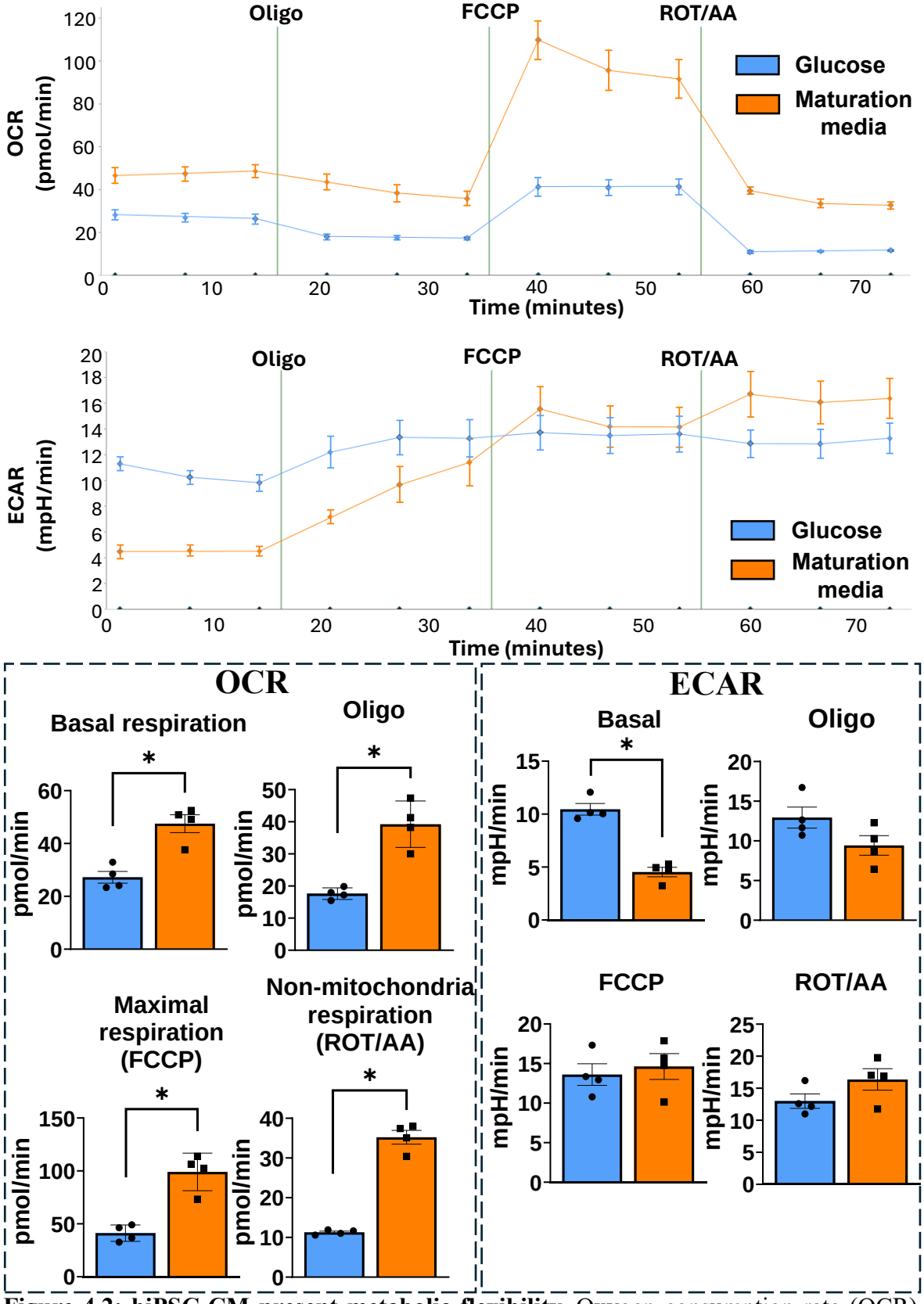

Figure 4.2: hiPSC-CM present metabolic flexibility. Oxygen consumption rate (OCR) and extracellular acidification rate (ECAR) in hiPSC-CM incubated in glucose or maturation media. OCR and ECAR data are represented as the mean ± SEM of the biological replicates. Each data point in the graphs represents a biological replicate.

These results confirm that the hiPSC-CM are metabolically flexible, showing that when fatty acids are available in the cell media, they show an oxidative metabolic profile. However, if glucose is the predominant substrate in the cell media or if oxidative phosphorylation is inhibited, they become more glycolytic.

The capacity of the hiPSC-CM to oxidise different substrates was evaluated by replacing the maturation media in hiPSC-CM with Seahorse media containing a single specific metabolic substrate for 1.5 hours. The hiPSC-CM showed robust mitochondrial oxidative activity with glutamine **(Figure 4.3A)**, palmitate **(Figure 4.3B)** and pyruvate **(Figure 4.3C)**, responding additionally to all the Mito stress test kit compounds. These observations led us to hypothesise that our model of human cardiomyocytes has the ability to oxidise different metabolic substrates to produce energy, which complemented the previous results showing that hiPSC-CM were able to shift between oxidative and glycolytic metabolism, but also raised the question of whether our human cardiomyocyte model preferentially uses one specific substrate over others.

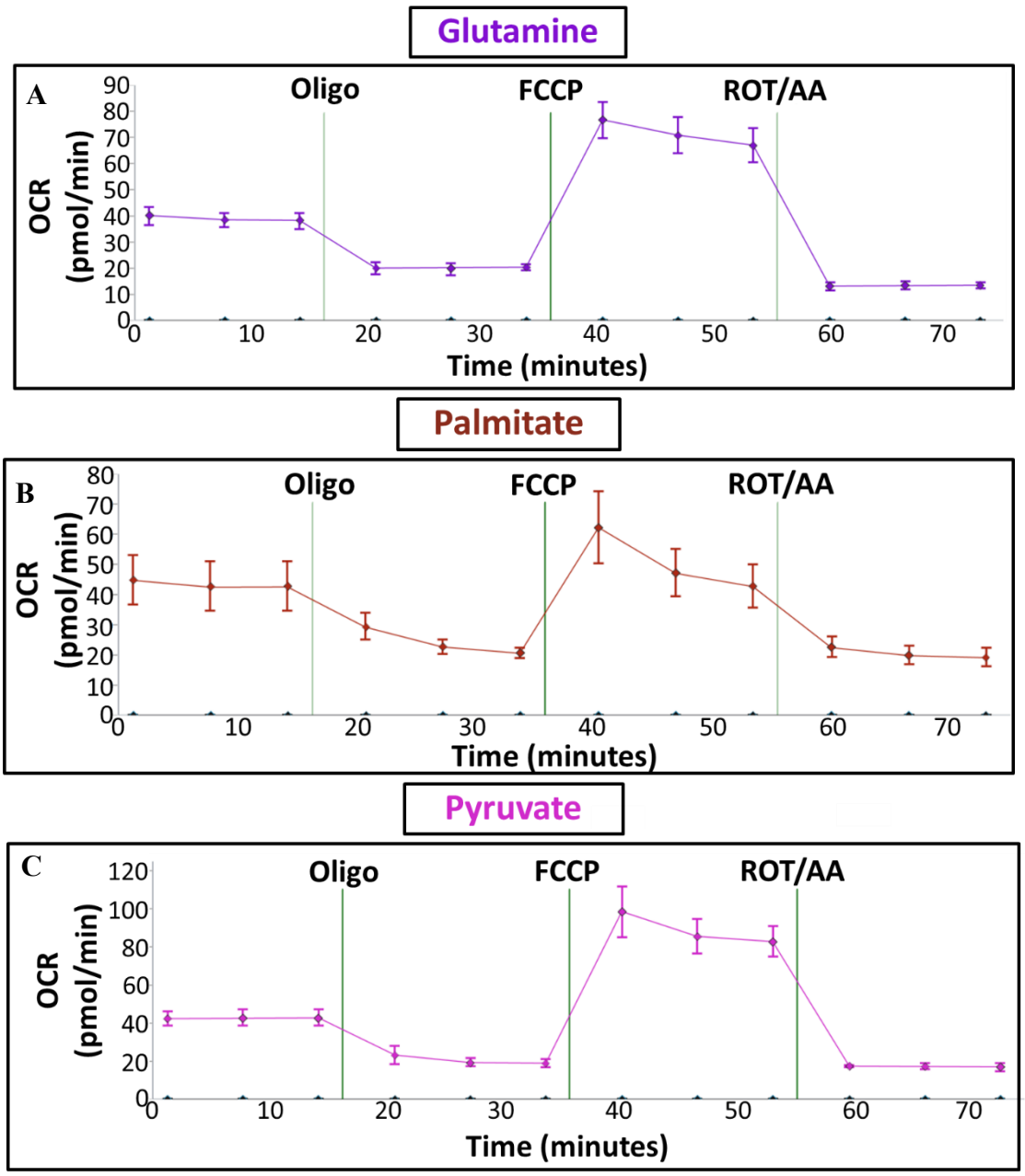

Figure 4.3: hiPSC-CM oxygen consumption rates under different substrates exposition. Oxygen consumption rate (OCR) in hiPSC-CM incubated in Seahorse media containing just one specific substrate. **(A)** 4 mM L-glutamine. **(B)** 300 µM palmitate:BSA. **(C)** 5mM pyruvate. Data represent the mean ± SEM of 4 biological replicates.

To test this hypothesis and determine which substrates were mainly oxidised by hiPSC-CM, a Mito Fuel Flex test was carried out to measure mitochondrial usage of glutamine, long-chain fatty acids, and glucose. The cells were treated with three different inhibitors. BPTES was used to inhibit glutamine metabolism to glutamate through the enzyme glutaminase, as

under physiological conditions, glutamate is incorporated into the Krebs cycle as α-ketoglutarate. Etomoxir was used to inhibit CPT1B, and therefore, long-chain fatty acid uptake into the mitochondria. Finally, UK5099 was used to block the mitochondrial pyruvate carrier and measure glucose oxidation.

Mitochondria substrate utilisation was determined by measuring two parameters: fuel dependency and fuel capacity. Fuel dependency represented mitochondrial reliance on a specific substrate to maintain minimal baseline respiration. Fuel capacity indicates mitochondria's reliance on a specific substrate under high energy demand and, hence, represents the maximum amount of a particular fuel that the mitochondria could oxidise to meet energy demand and compensate for inhibiting other metabolic pathways.

In our hiPSC-CM model, glutamine oxidation showed no significant differences between dependency and capacity, with both parameters reaching a mean percentage of approximately 20% **(Figure 4.4)**. This indicates a low reliance on glutamine metabolism to support respiration. Long-chain fatty acid oxidation dependency was approximately 40%, significantly increasing under energy demand conditions to a capacity of 91%. These results indicated that hiPSC-CM were highly dependent on long-chain fatty acid oxidation to maintain baseline mitochondrial respiration levels, and when other pathways were inhibited hiPSC-CM mitochondria had the capacity to increase the use of long-chain fatty acid further. Glucose oxidation dependency was approximately 8%, and its capacity significantly increased to 54% under energy demand conditions. This indicated a minimal contribution of glucose and pyruvate to maintain baseline mitochondrial respiration levels but a high reliance on these substrates under high energy.

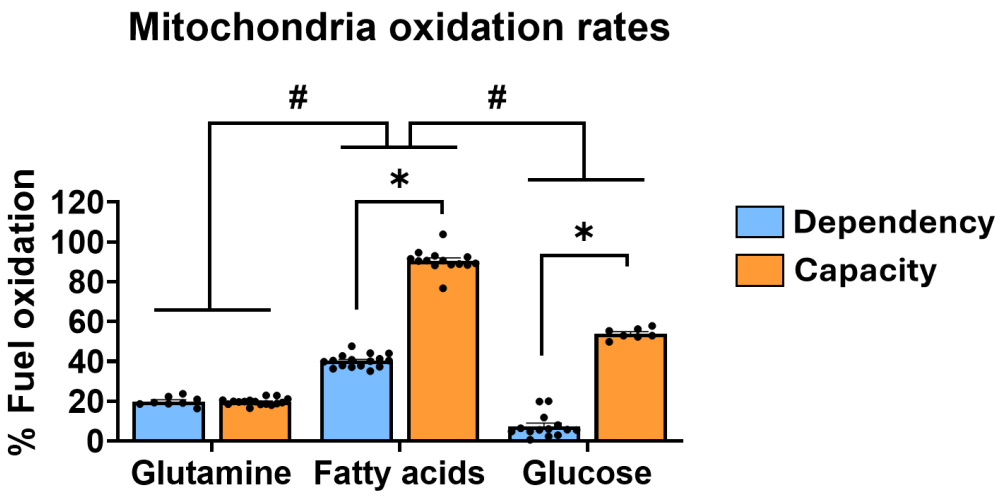

Figure 4.4: Glutamine, long-chain fatty acid and glucose oxidation dependency and capacity in hiPSC-CM. Percentage (%) of fuel oxidation for glutamine, long-chain fatty acid, and glucose in hiPSC-CM. * $p < 0.05$ vs. respective dependency group. # $p < 0.05$ vs. between groups. Each data point represents a biological replicate.

4.5.2 Dimethyl fumarate decreases fatty acid oxidation gene expression and fatty acid oxidation rates.

Having demonstrated that our hiPSC-CM model recapitulated the preference for fatty acids as the main source of energy within the adult heart, we returned to the fumarate derivatives to ask if they modulated cardiac fatty acid metabolism. The expression of genes involved in fatty acid β-oxidation was first investigated. Cells were incubated with dimethyl fumarate (DMF) treatment over shorter (3 and 6 hours) and longer intervals (12 and 24 hours), and the changes in gene expression were determined by qPCR. The results showed that genes involved in fatty acid β-oxidation decreased rapidly following DMF treatment **(Figure 4.5)**, with the expression of acyl-CoA synthetase long-chain family member 1 (*ACSL1*) significantly decreased at 3 and 6 hours by approximately 47% and 34%, respectively, compared with control cells **(Figure 4.5A)**. Similarly, the expression of mitochondrial carnitine palmitoyltransferase 1B (CPT1B) was significantly reduced by 61%, 47%, and 37% at 3, 6 and 12 hours, respectively **(Figure 4.5B)**. The expression of enoyl-CoA delta

isomerase 1 (*ECI1*) was decreased by 29%, 25%, and 30% at 3, 6, and 24 hours, respectively, following DMF treatment **(Figure 4.5C)**. Additionally, a similar effect was reported when the gene levels of the transcriptional regulator of fatty acid β-oxidation genes, the peroxisome proliferator-activated receptor gamma coactivator-1 alpha (*PGC1A*), was evaluated, observing that *PGC1A* gene expression decreased significantly by 46%, 57%, 43%, and 35% at 3, 6, 12, and 24 hours, respectively, compared with control hiPSC-CM **(Figure 4.5D)**.

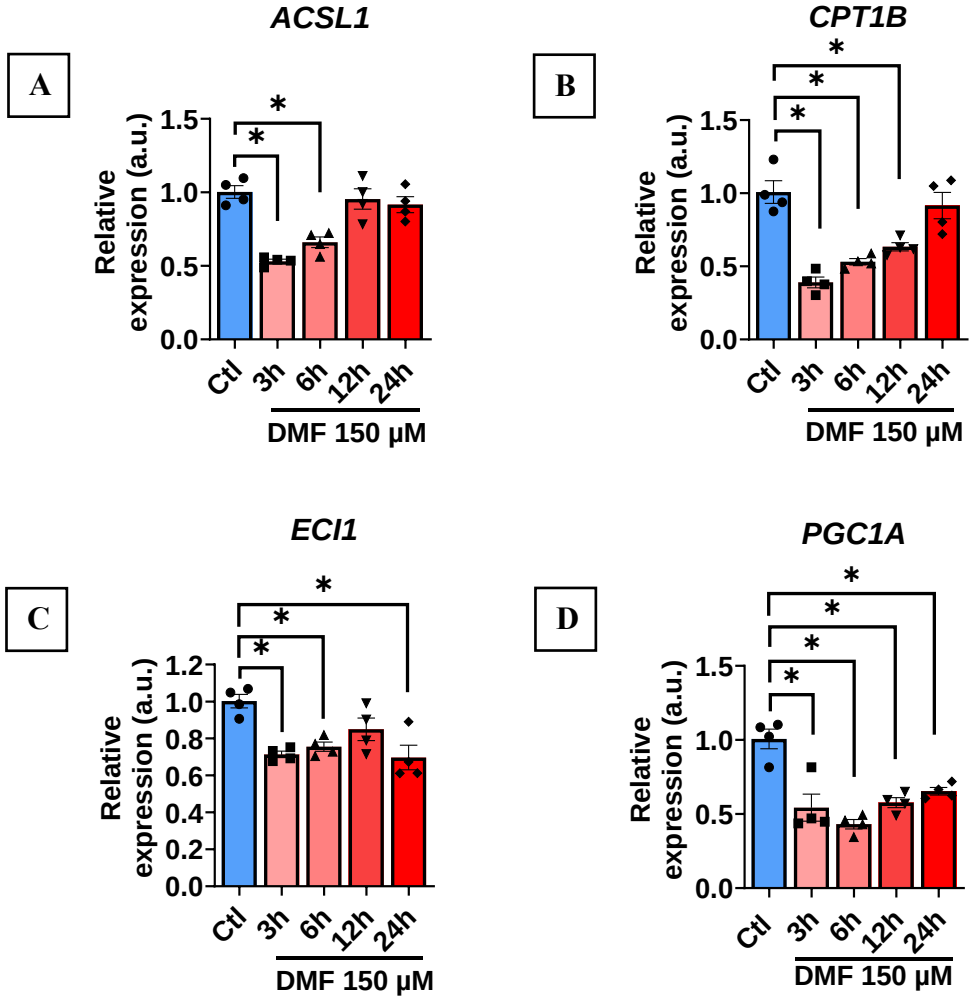

Figure 4.5: Dimethyl fumarate decreases genes involved in fatty acid β-oxidation at early times. Fatty acid β-oxidation gene expression in hiPSC-CM exposed to dimethyl fumarate treatment (150 µM) (DMF) for 3, 6, 12, and 24 hours and compared with untreated cells (Ctl). The targets evaluated were: **(A)** Acyl-CoA synthetase long-chain family member 1 (*ACSL1*) **(B)** Carnitine palmitoyltransferase 1B (*CPT1B*) **(C)** Enoyl-CoA delta isomerase 1 (*ECI1*) **(D)** Peroxisome proliferator-activated receptor gamma coactivator-1 alpha (*PGC1A*). * $p < 0.05$ vs. respective control group. a.u., arbitrary units. Each data point represents a biological replicate.

To further investigate whether the changes at the gene level were also associated with a reduction in the use of fatty acid within the cardiomyocyte, fatty acid oxidation rates were measured by supplementing the cell media with radioactive palmitate. HiPSC-CM exposed to DMF presented a significant decrease in the fatty acid oxidation rates by 47% following 24 hours of treatment **(Figure 4.6)**. These findings indicated that DMF rapidly reduced fatty acid oxidation gene expression and fatty acid oxidation rates in human cardiomyocytes.

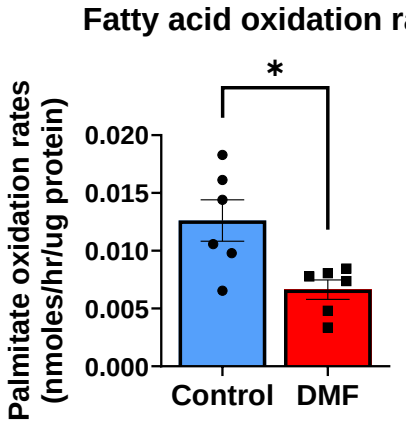

Figure 4.6: Dimethyl fumarate decreases fatty acid oxidation rates. Fatty acid oxidation of [9,10-^{3}H]-palmitate in hiPSC-CM exposed to dimethyl fumarate treatment (150 µM) (DMF) for 24 hours and compared with untreated cells (Control). * $p < 0.05$ vs. respective control group. Each data point represents a biological replicate.

4.5.2 Dimethyl fumarate increases glycolytic gene expression, lactate production, and glycolytic rates.

Glucose metabolism represents the second most used pathway by the heart to supply cell energy, therefore, whether DMF also modified glucose metabolism was subsequently investigated. We identified that DMF increased the expression of glycolytic genes at the latest time points of DMF treatment **(Figure 4.7)**. Glucose transporter 1 (*GLUT1*) expression was significantly increased by 3-fold following 24 hours of DMF treatment compared with control cells **(Figure 4.7A)**. Phosphoglycerate kinase 1 (PGK1) expression also rose 2-fold **(Figure 4.7B)**, and the enolase 1 (*ENO1*) gene was upregulated 1.5- and 2-fold at 12 and 24 hours, respectively **(Figure 4.7C)**. Additionally, the final product of the

glycolytic metabolism, lactate, was measured in the cell media, observing that lactate release was significantly increased following DMF treatment by 2-, 2.3-, and 1.7-fold at 3, 6, and 24 hours, respectively, compared with control cell media **(Figure 4.7D)**.

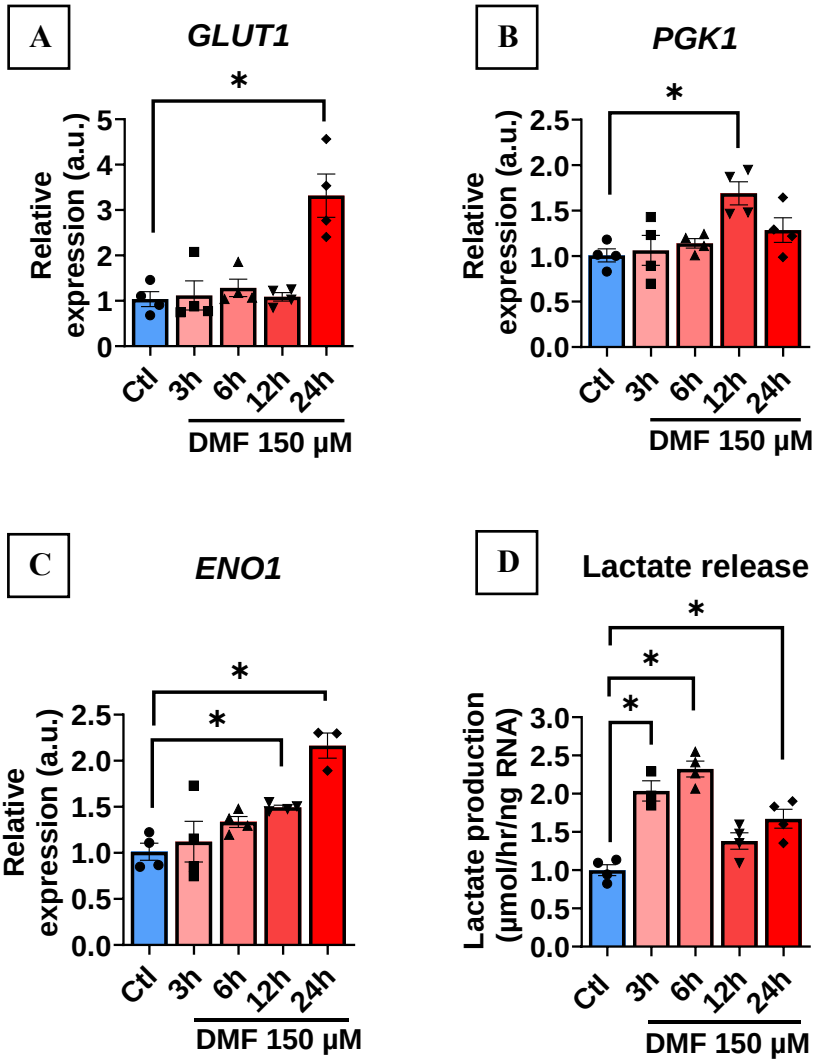

Figure 4.7: Dimethyl fumarate upregulates glycolytic genes and increases lactate release into the cell media. Glucose metabolism gene expression in hiPSC-CM exposed to dimethyl fumarate treatment (150 µM) (DMF) for 3, 6, 12, and 24 hours and compared with untreated cells (Ctl). The targets evaluated were **(A)** Glucose transporter 1 (*GLUT1*), **(B)** Phosphoglycerate kinase 1 (*PGK1*), and **(C)** Enolase 1 (*ENO1*). **(D)** Lactate release into the cell media at 3, 6, 12, and 24 hours following DMF treatment. * $p < 0.05$ vs. respective control group. a.u. Each data point represents a biological replicate.

Moreover, to evaluate whether the changes in gene expression and lactate release were also associated with an increase in glycolytic rates within the cardiomyocytes, the effect of DMF

on glycolytic rates was measured using radioactive glucose. DMF treatment significantly increased the glycolytic rates by 70% compared with control hiPSC-CM following 24 hours of treatment. Furthermore, a time-dependent effect was observed as the glycolytic rates significantly increased by 121% compared with control cells following 48 hours of treatment **(Figure 4.8)**. Overall, these findings indicate that DMF can regulate human cardiomyocyte metabolism, inducing a metabolic shift from fatty acid to glucose metabolism, reducing fatty acid oxidation genes and oxidation rates followed by upregulating glucose metabolism genes and increasing lactate production and glycolytic rates.

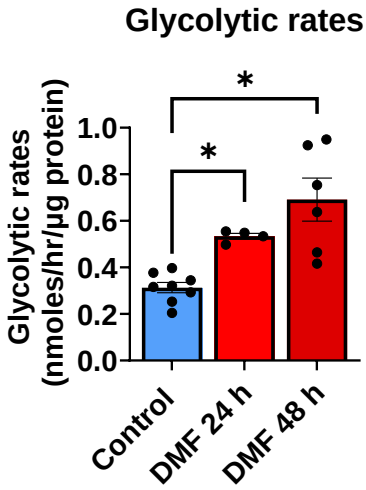

Figure 4.8: Dimethyl fumarate increases glycolytic rates. Glycolysis of [^{3}H]-glucose in hiPSC-CM exposed to dimethyl fumarate treatment (150 µM) (DMF) for 24 hours or 48 hours and compared with untreated cells (Ctl). * $p < 0.05$ vs. respective control group. Each data point represents a biological replicate.

4.5.3 Monomethyl fumarate and Vumerity decrease fatty acid gene expression similarly to dimethyl fumarate in hiPSC-CM.

To further identify whether other fumarate derivatives could also modulate fatty acid oxidation gene expression, the effect of the active form of DMF, monomethyl fumarate (MMF) on the expression of these genes was studied in hiPSC-CM using qPCR. MMF significantly decreased *CPT1B, ECI,* and *PGC1A* gene expression at the same DMF

concentration by 25%, 21%, and 48% following 24 hours of treatment, compared with control cells **(Figure 4.9)**.

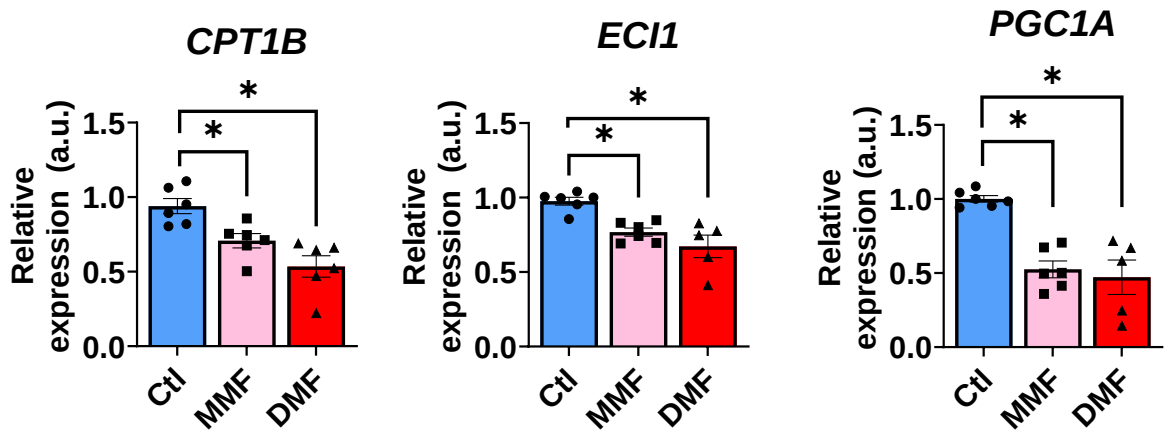

Figure 4.9: Monomethyl fumarate decreases fatty acid β-oxidation gene expression similar to dimethyl fumarate in hiPSC-CM. Expression of fatty acid β-oxidation genes in hiPSC-CM exposed to dimethyl fumarate (150 µM) (DMF) or monomethyl fumarate (150 µM) (MMF) treatment for 24 hours and compared with untreated cells (Ctl). The targets evaluated were carnitine palmitoyltransferase 1B (*CPT1B*), enoyl-CoA delta isomerase 1 (*ECI1*), and peroxisome proliferator-activated receptor gamma coactivator-1 alpha (*PGC1A*). * $p < 0.05$ vs. respective control group. a.u. Each data point represents a biological replicate.

Similarly, Vumerity (VM), at a lower concentration (25 µM), significantly reduced the expression of the same genes *CPT1B, ECI*, and *PGC1A* by 52%, 45%, and 34%, respectively, following 24 hours of treatment compared with untreated cells **(Figure 4.10)**. Interestingly, the non-fumarate derivate, dimethyl succinate (DMS), which increases succinate concentrations, did not show any regulatory effect on these genes compared with the control condition. Overall, these results indicated that both MMF (at the same concentration as DMF) and VM (at a lower concentration) presented a similar effect on the fatty acid β-oxidation genes. As no changes in the fatty acid gene expression were observed following DMS treatment, these results indicate that these metabolic changes were a specific effect of the fumarate derivatives and not for other Krebs cycle metabolites.

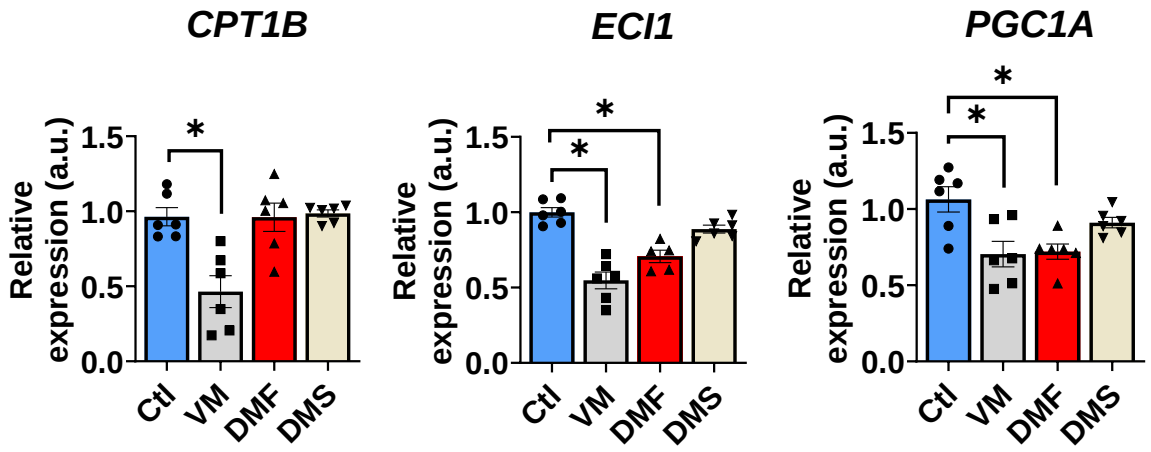

Figure 4.10: Vumerity, at a lower concentration, decreases fatty acid β-oxidation gene expression similar to dimethyl fumarate in hiPSC-CM. Expression of fatty acid β-oxidation genes in hiPSC-CM exposed to Vumerity (25 µM) (VM) , dimethyl fumarate (150 µM) (DMF) or dimethyl succinate (150 µM) (DMS) treatment for 24 hours and compared with untreated cells (Ctl). The targets evaluated were carnitine palmitoyltransferase 1B (*CPT1B*), enoyl-CoA delta isomerase 1 (*ECI1*), and peroxisome proliferator-activated receptor gamma coactivator-1 alpha (*PGC1A*). * $p < 0.05$ vs. respective control group. a.u., arbitrary units. Each data point represents a biological replicate.

4.5.4 Dimethyl fumarate does not affect gene or protein levels of the Krebs cycle or oxidative phosphorylation enzymes.

Given the role of DMF in modulating fatty acid and glucose metabolism, its effect on the gene expression of different Krebs cycle and oxidative phosphorylation components was evaluated by qPCR. The results revealed that DMF did not significantly change the expression of the Krebs cycle enzymes genes citrate synthase (*CS*) or malate dehydrogenase 2 (*MDH2*) **(Figure 4.11)**. Similarly, no changes were observed in the expression of the genes related to oxidative phosphorylation, NADH:ubiquinone oxidoreductase core subunit v1 (*NDUFV1*), succinate dehydrogenase complex flavoprotein subunit A (*SDHA*), cytochrome C1 (*CYC1*), and ATP Synthase F1 Subunit Beta (*ATP5B*). Although one gene coding for a component of the cytochrome c oxidase in the complex IV (*COX4-1*) showed a significant ANOVA effect between all the conditions, there was not a significant difference between individual groups (it did not reach significance at post hoc analyses) (**Figure 4.12**).

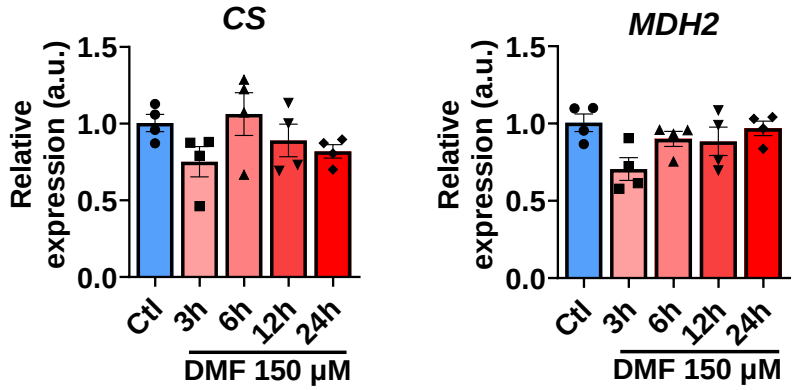

Figure 4.11: Dimethyl fumarate does not affect Krebs cycle gene expression in hiPSC-CM. Krebs Cycle gene expression in hiPSC-CM exposed to dimethyl fumarate (150 µM) (DMF) treatment for 3, 6, 12, and 24 hours and compared with untreated cells (Ctl). The genes evaluated were citrate synthase (CS) and malate dehydrogenase 2 (*MDH2*). Each data point represents a biological replicate.

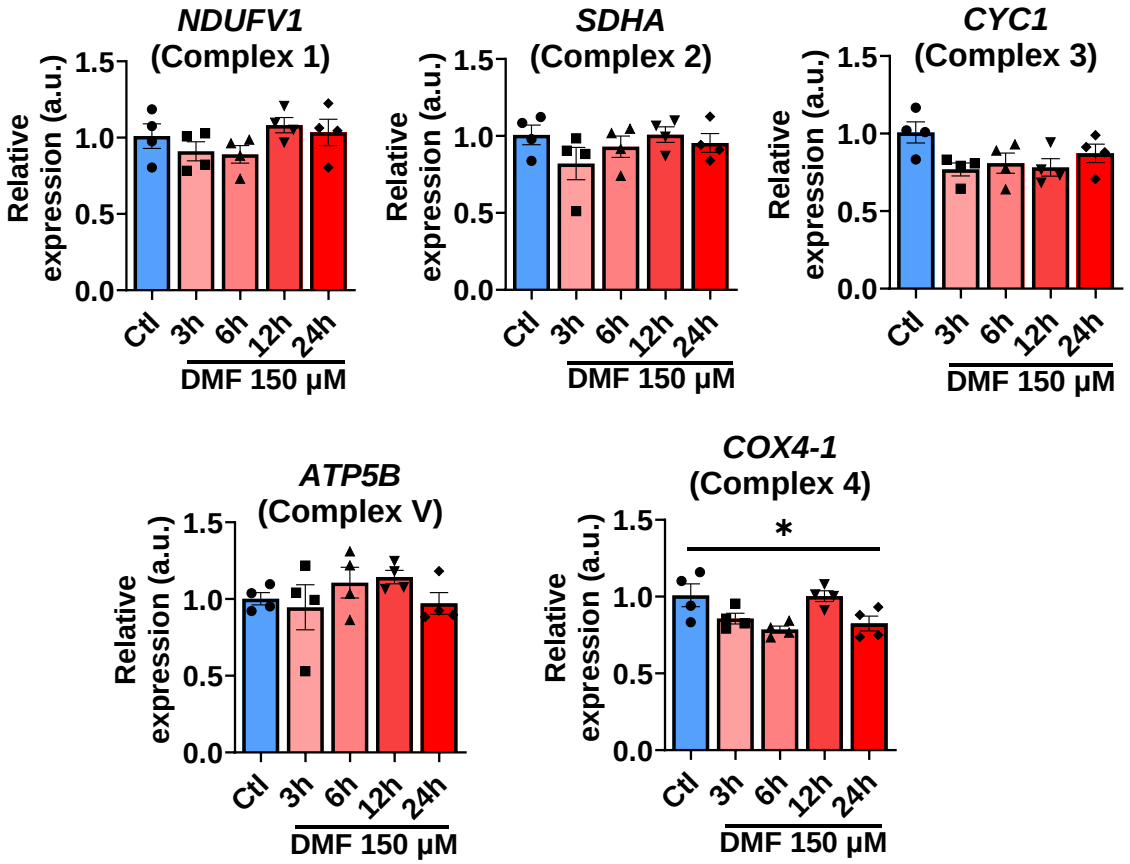

Figure 4.12: Dimethyl fumarate does not affect oxidative phosphorylation enzymes gene expression in hiPSC-CM. Oxidative phosphorylation enzymes gene expression in hiPSC-CM exposed to dimethyl fumarate (150 µM) (DMF) treatment for 3, 6, 12, and 24 hours and compared with untreated cells (Ctl). The genes evaluated were NADH:ubiquinone oxidoreductase core subunit v1 (*NDUFV1*), succinate dehydrogenase complex flavoprotein subunit A (*SDHA*), Cytochrome C1 (*CYC1*), cytochrome c oxidase subunit 4i1(*COX4-1*) and ATP Synthase F1 Subunit Beta (*ATP5B*). * $p < 0.05$ vs. respective control group. a.u. Each data point represents a biological replicate.

Similar results were observed for DMF when studied at protein level. No significant differences were detected in protein levels of the Krebs cycle enzyme aconitase 2 (ACO2) or the oxidative phosphorylation proteins, ATP synthase subunit alpha (ATP5A), Complex III subunit Core 2 (UQCRC2), Complex II subunit 30kDa (SDHB), Complex IV subunit II (COXII), and Complex I subunit NDUFB8 (NDUFB8) when comparing DMF-treated and untreated hiPSC-CM using the unpaired t-test with Welch's correction **(Figure 4.13)**. These results indicate that the metabolic changes induced by DMF are not associated with changes in the Krebs cycle or oxidative phosphorylation components. Interestingly, a double band was unexpectedly observed after DMF treatment for the protein succinate dehydrogenase B (SDHB), which may suggest a posttranslational modification of that protein induced by DMF.

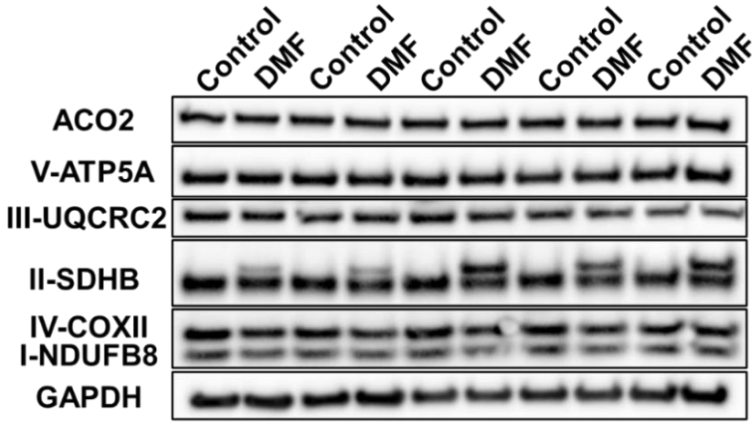

Figure 4.13: Dimethyl fumarate does not affect protein levels of the Krebs cycle or oxidative phosphorylation enzymes. Krebs cycle and oxidative phosphorylation protein levels in hiPSC-CM exposed to dimethyl fumarate (150 μM) (DMF) treatment for 24 hours compared with untreated cells (Control). The target evaluated were aconitase 2 (ACO2), NADH:ubiquinone oxidoreductase subunit B8 (NDUFB8), succinate dehydrogenase complex iron sulfur subunit B (SDHB), ubiquinol-cytochrome C reductase core protein 2 (UQCRC2), cytochrome c oxidase subunit 2 (COXII), and ATP synthase F1 subunit alpha (ATP5F1A). Glyceraldehyde 3-phosphate dehydrogenase (GAPDH) was used as loading control.

4.5.5 Dimethyl fumarate modulates mitochondrial network morphology.

The impact of DMF on the mitochondrial network was studied using mitotracker assay to visualise mitochondria network morphology. DMF induced alterations in the mitochondrial

network morphology without affecting mitochondrial density, specifically promoting the fragmentation of the mitochondria network. This fragmentation was due to a significant reduction of the abundance and length of mitochondrial branches and junctions, and diminished mitochondrial interconnectivity following 12 hours of DMF treatment. However, all the morphological parameters returned to control values following 24 hours of DMF treatment, demonstrating that DMF transiently reshaped mitochondria network morphology towards a fragmented phenotype, which may transiently impair mitochondrial activity **(Figure 4.14)**.

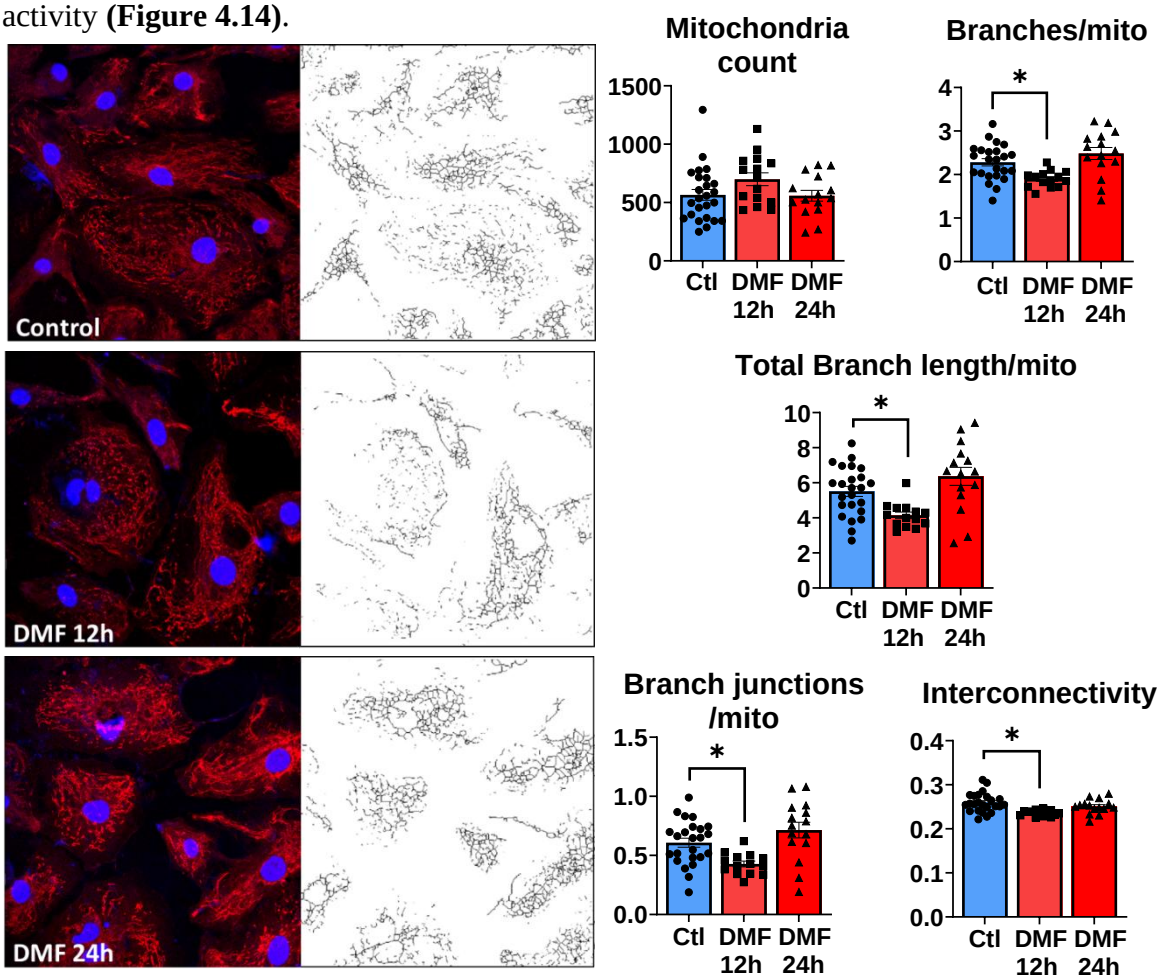

Figure 4.14: Dimethyl fumarate induces a transient disruption of the mitochondrial network morphology. Mitochondrial network in hiPSC-CM exposed to dimethyl fumarate (150 µM) (DMF) for 12 or 24 hours and compared with untreated cells (Ctl). Mitochondria, on red, were stained with Mitotracker Red CMXRos. Cell nuclei, on blue, were stained with DAPI. Mitochondrial network images were obtained by *in silico* modelling using the plugins MiNA[212] and Mitochondria Analyzer[213] for Fiji (ImageJ) [210, 211]. * $p < 0.05$ vs. respective control group. Each data point represents the average of an image containing 7–8 cells. Three biological replicates were used for each condition, with five images acquired per biological replicate. Additional images were acquired for the control condition

4.5.6 Dimethyl fumarate decreases mitochondria respiration.

To study whether DMF affected mitochondrial activity, a Seahorse assay was performed to measure mitochondrial oxygen consumption in hiPSC-CM exposed to DMF treatment for 6, 12, and 24 hours, compared with untreated cells. DMF did not affect mitochondrial basal respiration or maximal respiration at 6 **(Figure 4.15A)** or 12 hours **(Figure 4.15B)**. However, following 24 hours of DMF treatment, a significantly decreased in OCR was observed under all the evaluated parameters compared with the control condition, with mitochondrial basal respiration, ATP-linked respiration, maximal respiration, and non-mitochondria respiration reduced by 15%, 19%, 15%, and 15%, respectively **(Figure 4.16)**. These results demonstrate that DMF decreased mitochondria oxygen consumption at the same time point as when the fatty acid oxidation rates were reduced and the glycolytic rates were increased, confirming that DMF induces a metabolic shift in the human cardiomyocytes from oxidative to glycolytic metabolism.

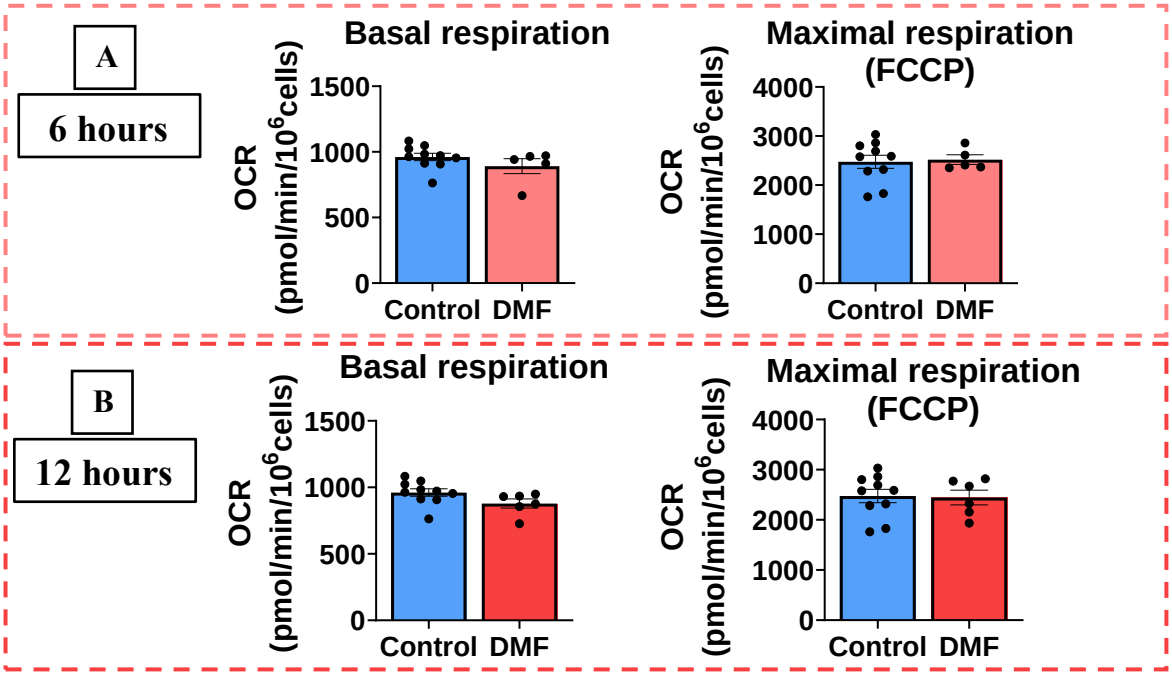

Figure 4.15: Dimethyl fumarate does not affect mitochondrial oxygen consumption at 6 or 12 hours. Oxygen consumption rates (OCR) in hiPSC-CM exposed to dimethyl fumarate (150 µM) (DMF) treatment for **(A)** 6 hours or **(B)**12 hours and compared with untreated cells (Control). * $p < 0.05$ vs. respective control group**.** Each data point represents a biological replicate.

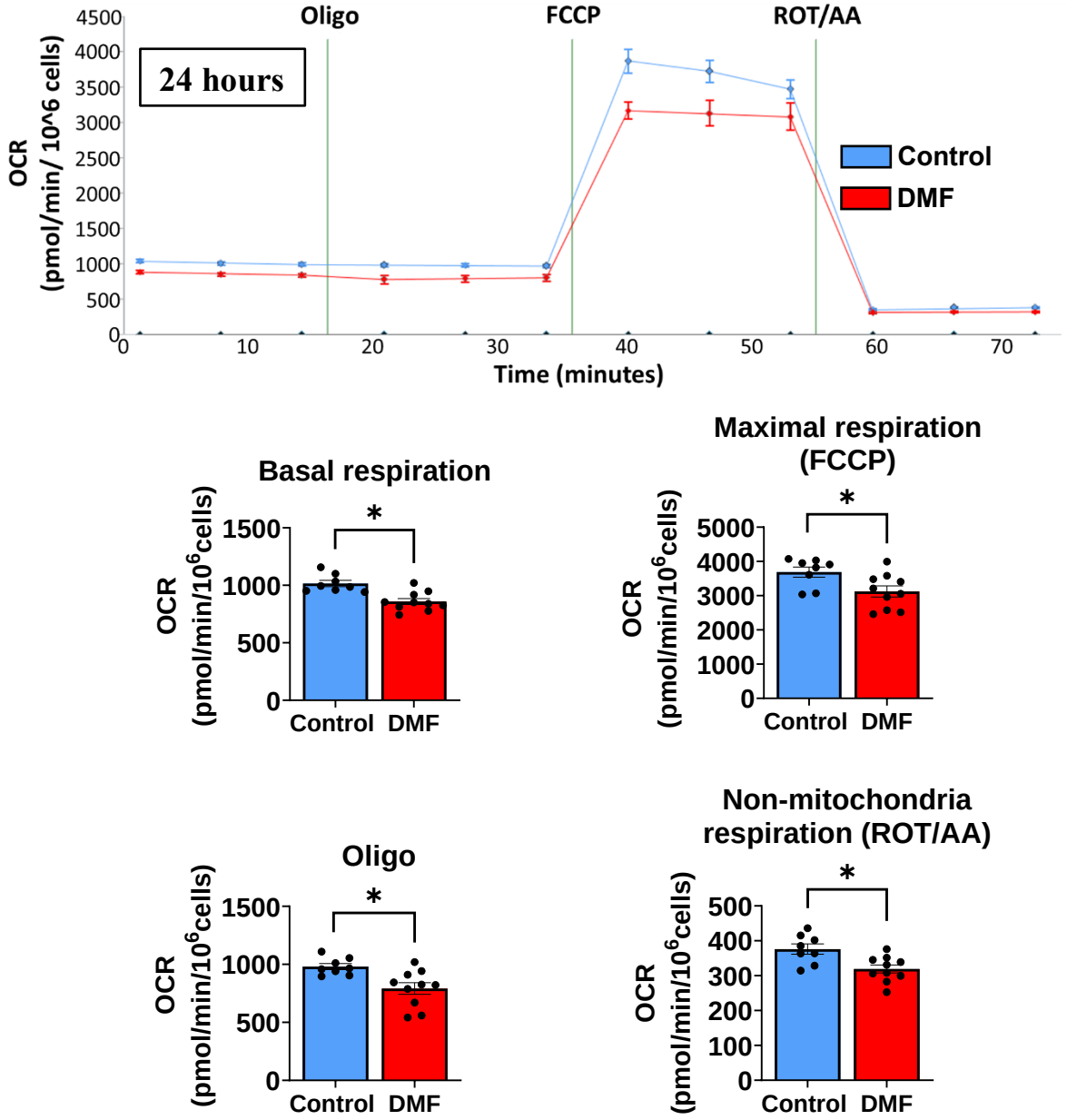

Figure 4.16 Dimethyl fumarate decreases mitochondrial oxygen consumption following 24 hours of treatment. Oxygen consumption rates (OCR) in hiPSC-CM exposed to dimethyl fumarate (150 µM) (DMF) treatment for 24 hours and compared with untreated cells (Control). * $p < 0.05$ vs. respective control group**.** OCR data is represented as the mean ± SEM of the biological replicates. Each data point in the graphs represents a biological replicate.

4.5.7 Sulforaphane and hydrogen peroxide show similar metabolic regulation to dimethyl fumarate.

To determine whether this metabolic regulation was mediated by Nrf2 activation, the well-established Nrf2 activator, sulforaphane (SFN), was used in human cardiomyocytes. SFN induced a similar metabolic response to DMF at the gene level, significantly decreasing the

expression of the fatty acid β-oxidation genes *ACSL1, CPT1B,* and *ECI* by 45%, 45%, and 53%, respectively, compared with the control cells **(Figure 4.17A)**. Interestingly, just 6 hours of SFN treatment (compared with the 24 hours required for DMF treatment) was enough to induce the upregulation of the glycolytic gene GLUT1 by 1.8-fold **(Figure 4.17B)**.

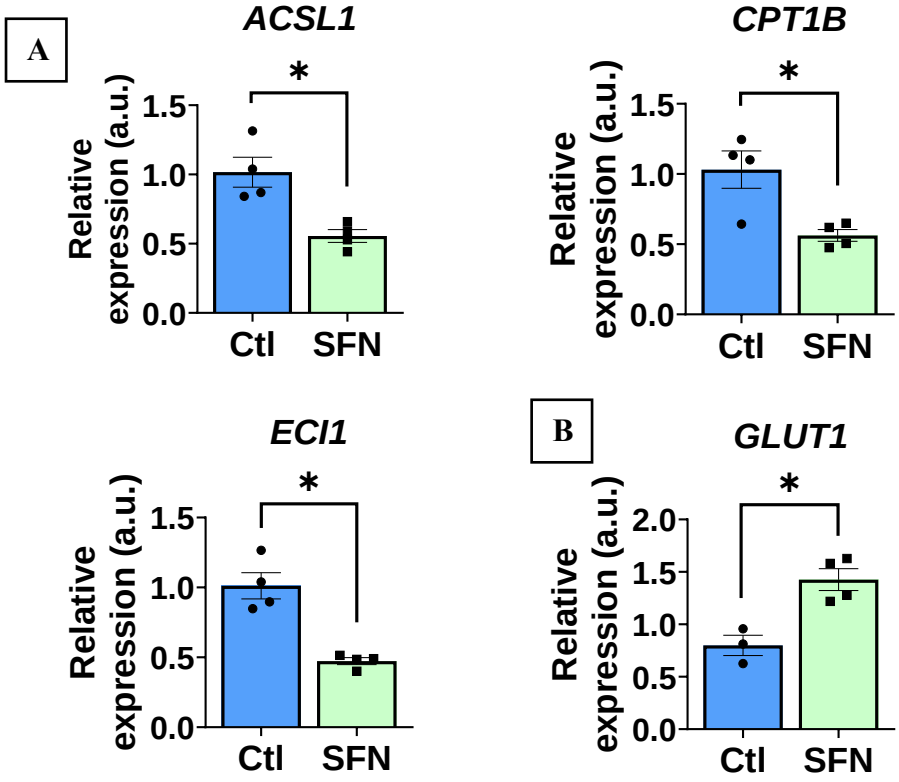

Figure 4.17: Sulforaphane induces similar metabolic gene changes to dimethyl fumarate in hiPSC-CM. Expression of fatty acid β-oxidation and glucose metabolism genes in hiPSC-CM exposed to sulforaphane (5 μM) (SFN) for 6 hours and compared with untreated cells (Ctl). The targets evaluated were: **(A)** Acyl-CoA synthetase long-chain family member 1 (*ACSL1*), carnitine palmitoyltransferase 1B (*CPT1B*), enoyl-CoA delta isomerase 1 (*ECI1*), and **(B)** Glucose transporter 1 (*GLUT1*). * $p < 0.05$ vs. respective control group. a.u., arbitrary units. Each data point represents a biological replicate.

Similar results were obtained when the physiological activator of the Nrf2 pathway, oxidative stress, was induced in the hiPSC-CM using hydrogen peroxide (H_2O_2). In the presence of reactive oxygen species in the cell environment, glutathione is rapidly oxidised to glutathione disulfide (GSSG), therefore, to evaluate the response of these cells to H_2O_2, the ratio of oxidised glutathione (GSSG) to total glutathione (GSH) was measured. H_2O_2

significantly increased GSSG/GSH ratio by 2-fold compared with control cells **(Figure 4.18A)**. Interestingly, when the effect of H_2O_2 on fatty acid β-oxidation genes was evaluated by qPCR, a significant decrease in *CPT1B* and *ECI1* gene expression by 52% and 26% was observed, respectively, while no significant differences were detected for *PGC1A* **(Figure 4.18B)**. Additionally, lactate release into the cell media was significantly increased by 7-fold following H_2O_2 treatment compared with untreated cells **(Figure 4.18C)**.

Both approaches, SFN, as a molecular inductor, and H_2O_2, as the physiological stimulator of the Nrf2 pathway, showed a similar regulation at the gene level to DMF. Therefore, these results suggested that the metabolic changes induced by DMF may be mediated via Nrf2 activation.

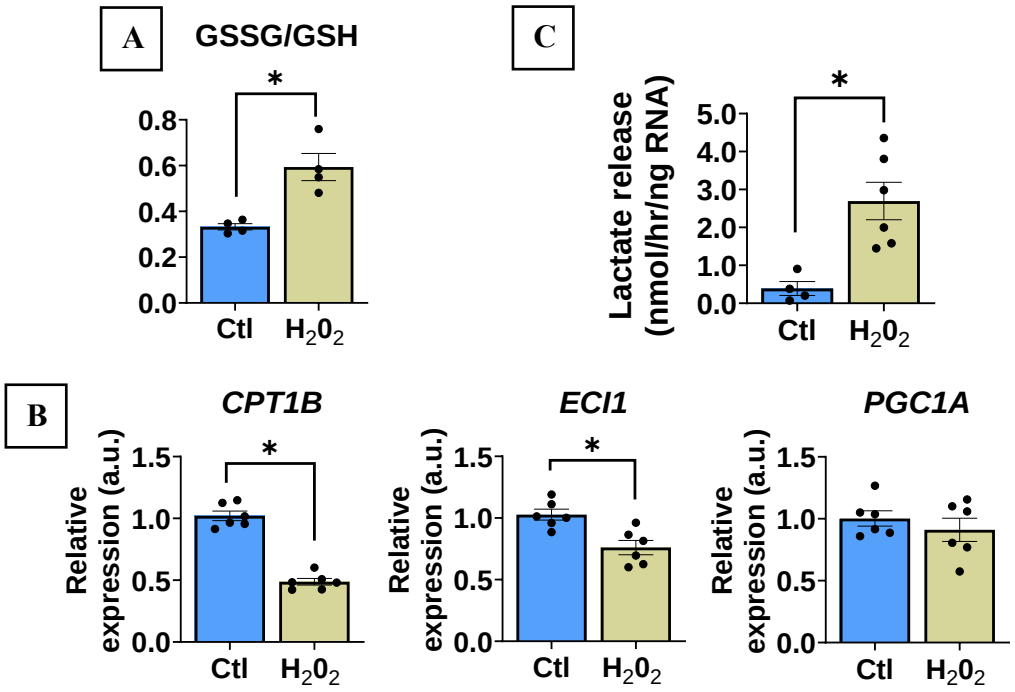

Figure 4.18: Oxidative stress induces similar metabolic gene changes to dimethyl fumarate in hiPSC-CM. hiPSC-CM were exposed to hydrogen peroxide (100 µM) (H_2O_2) for 3 hours and compared with untreated cells (Ctl) **(A)** Oxidised glutathione (GSSG) to total glutathione (GSH) ratio per million cells, as an earlier oxidative stress marker **(B)** Expression of fatty acid β-oxidation genes carnitine palmitoyltransferase 1B (*CPT1B*), enoyl-CoA delta isomerase 1 (*ECI1*), and peroxisome proliferator-activated receptor gamma coactivator-1 alpha (*PGC1A*). **(C)** Lactate release into the cell media following H_2O_2 treatment * $p < 0.05$ vs. respective control group. a.u., arbitrary units. Each data point represents a biological replicate.

4.5.8 Cardiomyocyte-specific *Keap1* mouse model does not regulate metabolic genes in the same way as dimethyl fumarate.

To validate the previous findings, the constitutively activated Nrf2 mouse model (cardiomyocyte-specific *Keap1* knockout mouse) was used, and the expression of the metabolic genes was determined by qPCR. Contrary to expectations, no significant changes in the expression of the fatty acid β-oxidation genes *Cpt1b*, *Acsl1*, *Eci1* or *Pgc1a* **(Figure 4.19A)** or the expression of the glycolytic genes *Glut1*, *Pkm*, or *Pfkm* **(Figure 4.19B)** were observed, with *Glut1* closest to reaching significance with a p-value = 0.0606.

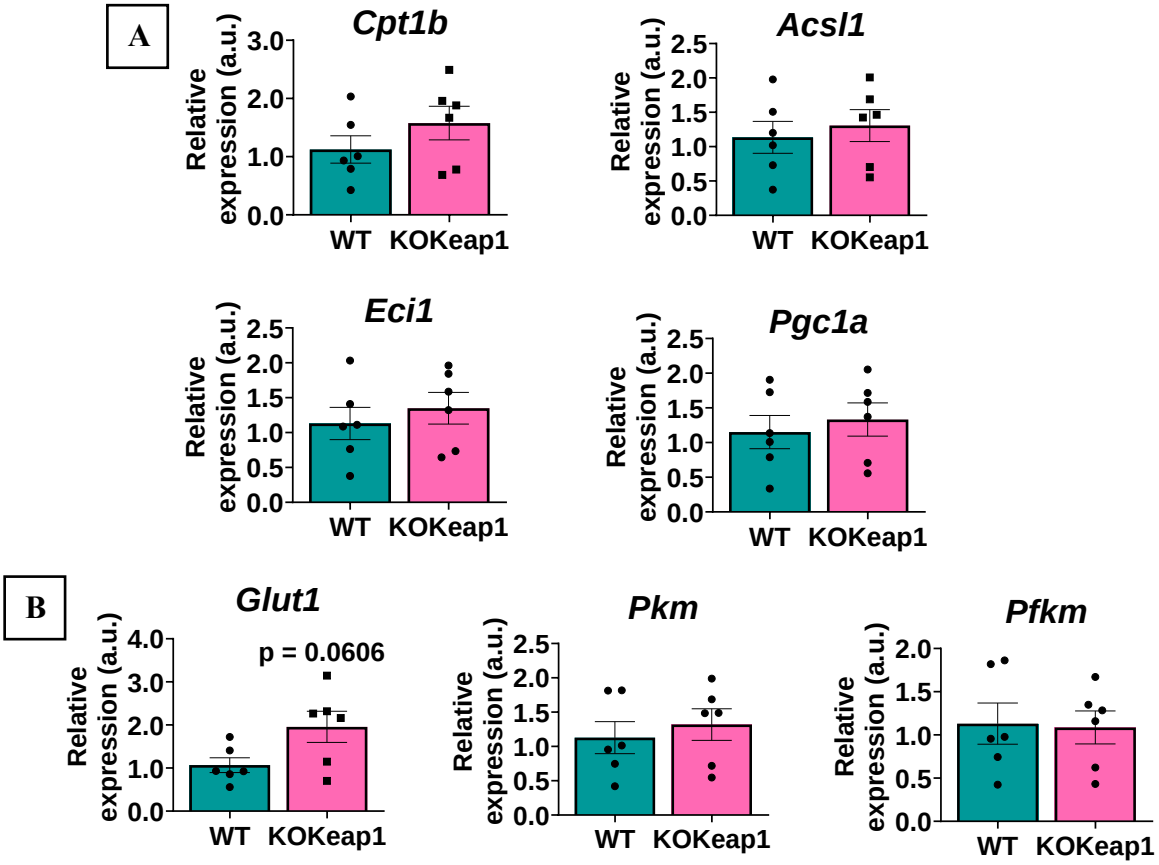

Figure 4.19: Cardiomyocyte-specific *Keap1* knockout does not regulate fatty acid β-oxidation or glycolytic genes in mouse heart. Expression of fatty acid β-oxidation and glucose metabolism genes in cardiomyocyte-specific *Keap1* knockout (KOKeap1) and compared with wild-type (WT) mouse heart. **A)** The targets evaluated from the fatty acid oxidation pathway were acyl-CoA synthetase long-chain family member 1 (*Acsl1*), carnitine palmitoyltransferase 1B (*Cpt1b*), enoyl-CoA delta isomerase 1 (*Eci1*), and peroxisome proliferator-activated receptor gamma coactivator-1 alpha (*Pgc1a*). **(B)** The targets evaluated from the glycolytic pathway were glucose transporter 1 (*Glut1*), pyruvate kinase muscle isoform (*Pkm*), and phosphofructokinase muscle isoform (*Pfkm*). a.u., arbitrary units. Each data point represents a biological replicate.

To investigate whether metabolic pathways were regulated in the KOKeap1 model, a direct comparison between the cardiomyocyte-specific *Keap1* knockout and wild-type mouse hearts was conducted using gene set variation analysis (GSVA) from the previous transcriptomics dataset. The results of this analysis were aligned with different biological pathways extracted from the open science platforms Wikipathway, KEGG and Hallmark gene annotation. Surprisingly, the analysis showed that several metabolic pathways were upregulated in the KOKeap1 model, including glutathione metabolism, glycolysis, fatty acid β-oxidation, amino acid metabolism, pyruvate metabolism, the Krebs cycle, and oxidative phosphorylation **(Figure 4.20)**. On the other hand, the downregulated pathways were mainly involved in the immune system, like the results observed in the previous chapter for DMF.

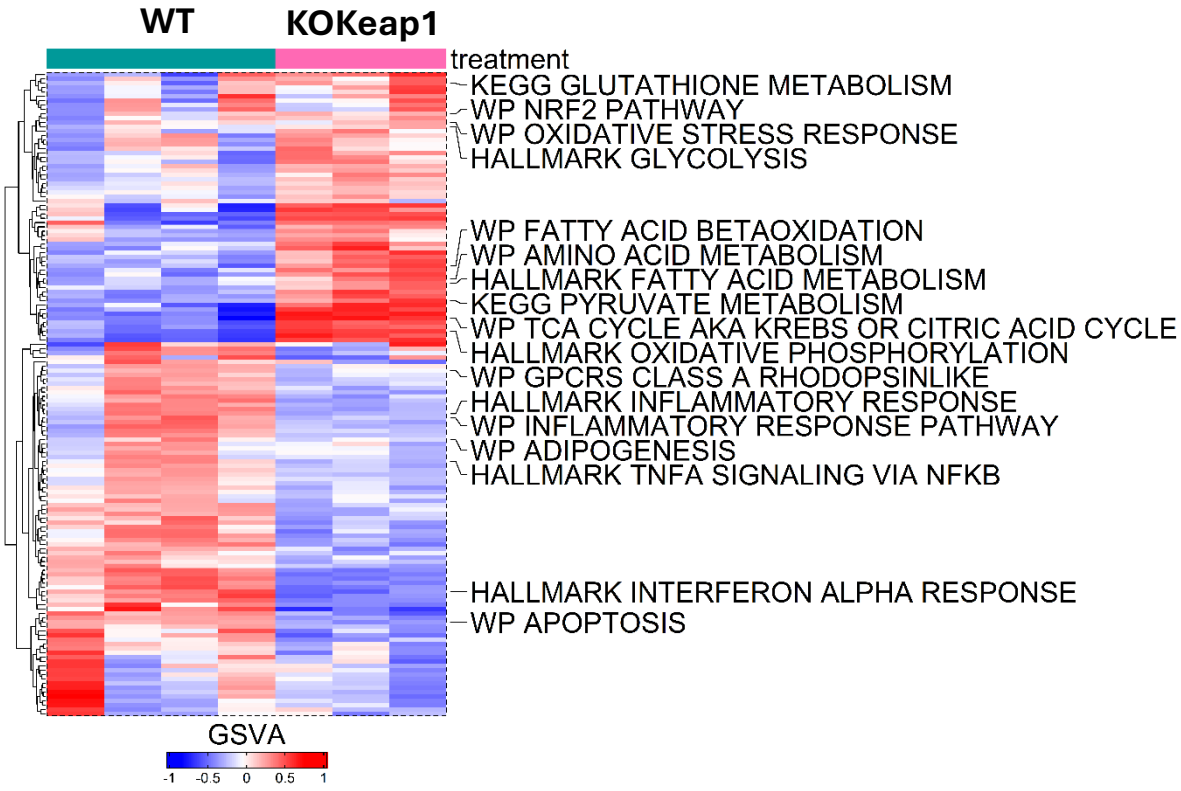

Figure 4.20: Gene set variation analysis comparing cardiomyocyte-specific *Keap1* knockout with wild-type mouse hearts. Transcriptomics analyses were performed in cardiomyocyte-specific *Keap1* knockout (KOKeap1/KO) compared with wild-type (WT) mouse hearts. Each column represents a biological replicate.

It is worth noting that during GSVA, low-count genes were also included in the analysis, the shrinking method in the Log_2fold changes was not applied, and the Log2 Fold change was set to 0. Therefore, even small gene changes were detected and influenced the resulting pathways of this analysis. This effect of different fold changes on gene expression can be visualised in **Figure 4.21**, where, after extracting significant genes with an adjusted p-value <0.05, we observed that when a Log2 Fold cutoff of 1 was applied, differential gene expression (DEG) identified 973 significantly regulated genes in KOKeap1 compared with wild-type mouse hearts **(Figure 4.21A)**. In contrast, when a cutoff of 0 for Log2 Fold change was used, DEG detected 2879 significant regulated genes in the KOKeap1 compared with wild-type mouse hearts **(Figure 4.21B)**.

The impact of different fold change thresholds was further studied by analysing the expression changes of the same genes previously evaluated by qPCR (*Cpt1b*, *Acsl1*, *Eci1*, *Pgc1a*, *Glut1*, *Pkm*, *Pfkm)* **(Figure 4.21C)**. We observed that the fold change for these genes was below 1 (except for Pgc1a, which was identified as non-significant, similar to the qPCR results), which may explain why fatty acid β-oxidation and glycolysis were upregulated in the GSVA, even though no changes were detected by qPCR.

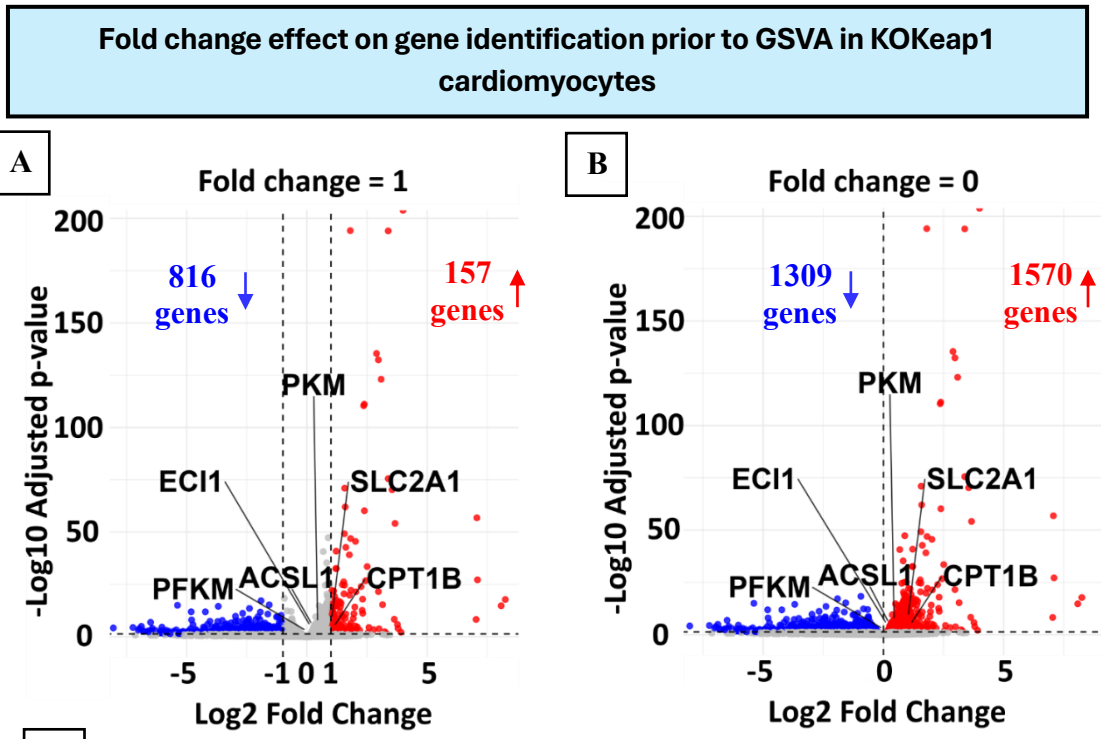

C

Gene	Log2FoldChange
CPT1B	**0.93**
ACSL1	**0.37**
ECI1	**0.31**
PGC1A	**No significant**
GLUT1(SLC2A1)	**0.99**
PKM	**0.45**
PFKM	**0.25**

Figure 4.21: Effect of fold change threshold on gene detection prior to gene set variation analysis. The volcano plots illustrate the impact of different thresholds on the number of significantly regulated genes in cardiomyocyte-specific *Keap1* knockout compared with wild-type mouse hearts. **(A)** Using a p-adjusted value < 0.05, and fold change equal to 1, a total of 973 genes were significantly regulated. **(B)** In contrast, using p-adjusted value < 0.05, and fold change equal to 0, a total of 2879 genes were significantly regulated. Significantly upregulated genes are shown in red, and significantly downregulated genes are shown in blue. **(C)** Differential gene expression fold change for carnitine palmitoyltransferase 1B (*CPT1B*), acyl-CoA synthetase long-chain family member 1 (*ACSL1*), enoyl-CoA delta isomerase 1 (*ECI1*), peroxisome proliferator-activated receptor gamma coactivator-1 alpha (*PGC1A*), glucose transporter 1 (*GLUT1*), pyruvate kinase muscle isoform (*PKM*), and phosphofructokinase muscle isoform (*PFKM*).

Unexpectedly, some of these metabolic processes, especially glycolysis and fatty acid β-oxidation, would be expected to be inversely regulated in the adult heart. However, the increased expression of both these pathways was confirmed by observing an evident

upregulation of fatty acid oxidation and glycolysis genes by generating specific heatmaps for these pathways **(Figure 4.22)**.

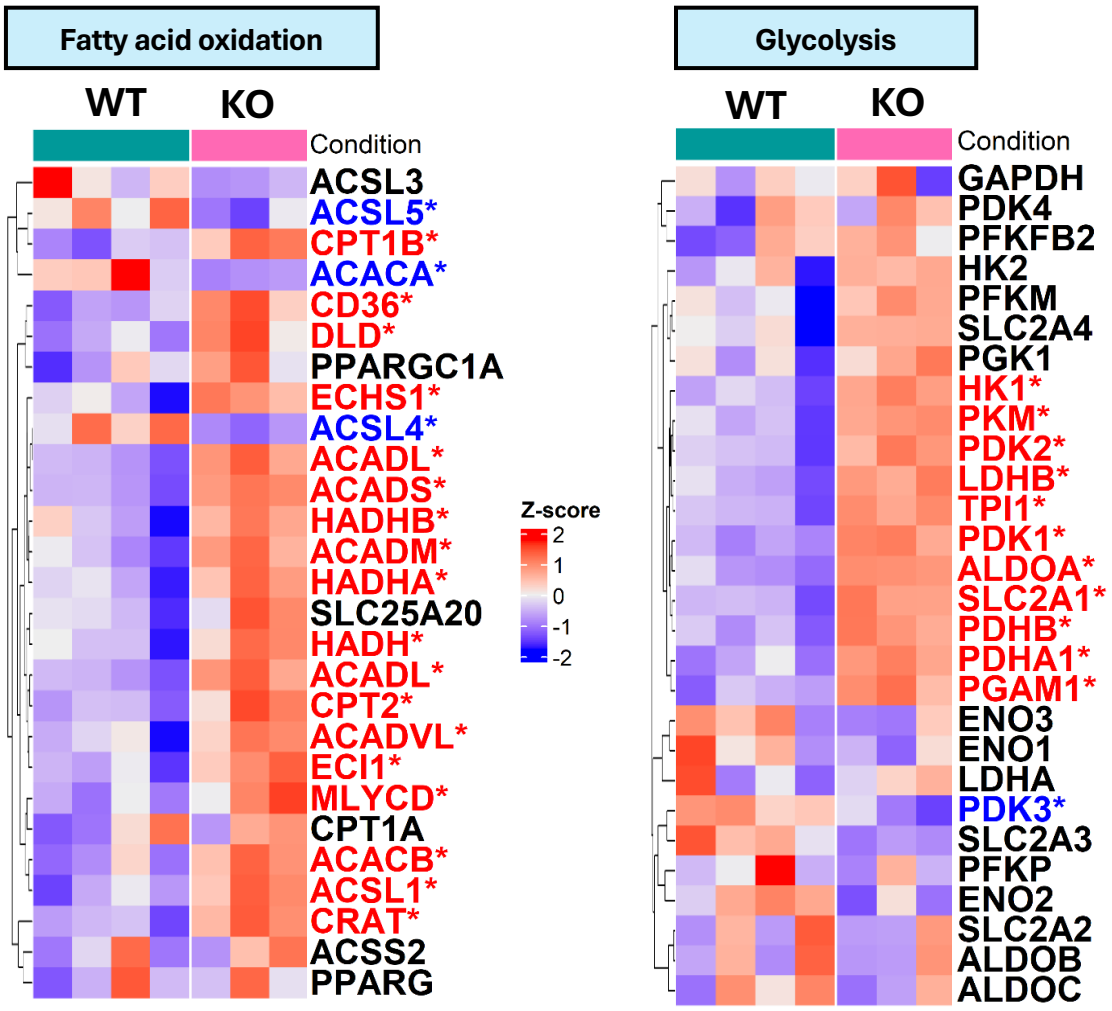

Figure 4.22: Keap1 cardiac-specific knockout upregulates fatty acid oxidation genes in mouse hearts. Fatty acid oxidation and glycolytic pathway heatmaps were generated using normalised counts from the transcriptomics analyses performed in cardiomyocyte-specific *Keap1* knockout (KOKeap1/KO) compared with wild-type (WT) mouse hearts**.** Significantly upregulated genes are shown in red, whereas significantly downregulated genes are shown in blue. * Fold change set as 0 and adjusted p-value < 0.05 vs. respective control group. Each column represents a biological replicate.

The discrepancies observed in the expression of the genes involved in fatty acid β-oxidation, which were decreased in the qPCR data from DMF, SFN and H_2O_2 treatments in hiPSC-CM but slightly increased in the KOKeap1 hearts transcriptomics data, led me to check for the fatty acid oxidation pathway using the previous DMF-treated hiPSC-CM transcriptomics

data. Surprisingly, single sample enrichment scores extracted from GSVA analysis for all the genes involved in the fatty acid β-oxidation pathway, as represented in the open science platform Wikipathway, revealed no significant differences between untreated and DMF-treated hiPSC-CM **(Figure 4.23A)**. Additionally, the fatty acid oxidation heatmap did not show the expected downregulation following DMF treatment **(Figure 4.23B)**. Even more, among the same genes previously measured by qPCR (*CPT1B*, *ACSL1*, *ECI1*, and *PGC1A*), only *PGC1A (PPARGC1A)* presented a significant reduction**.**

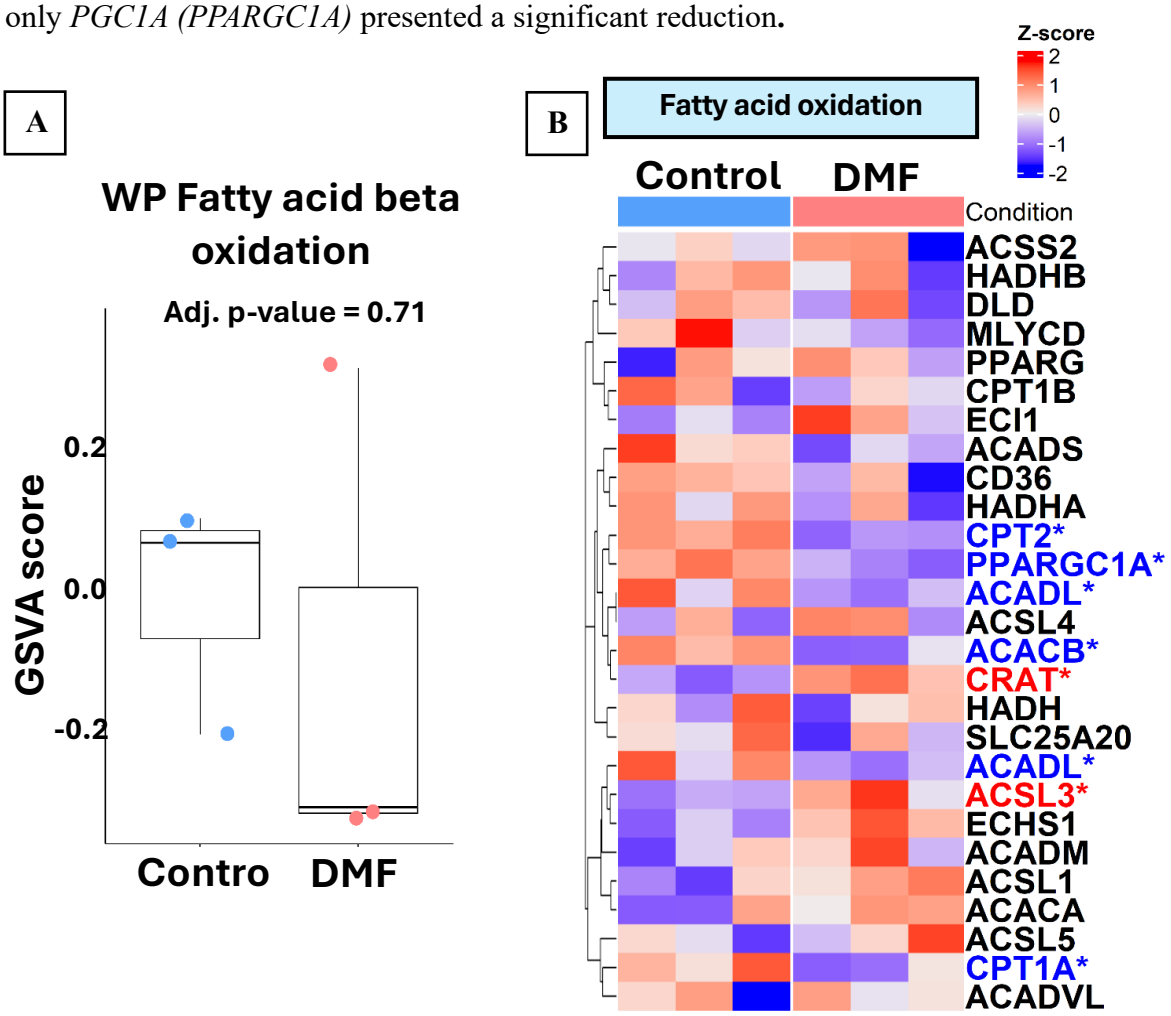

Figure 4.23: Dimethyl fumarate does not modulate fatty acid oxidation genes at the transcriptomics level. HiPSC-CM were exposed to dimethyl fumarate treatment (150 µM) (DMF) for 6 hours and compared with untreated cells (Control). **(A)** Boxplots represent the GSVA scores for all genes in the fatty acid β-oxidation pathway, as defined in Wikipathway (WP). **(B)** Fatty acid oxidation pathway heatmap was generated using normalised counts from the transcriptomics analyses. Significantly upregulated genes are shown in red, whereas significantly downregulated genes are shown in blue. * Fold change set as 0 and adjusted p-value < 0.05 vs. respective control group. Each data point in the graph represents a biological replicate. Each column in the heatmap represents a biological replicate.

In summary, the KOKeap1 model represented a constitutively activated Nrf2 pathway model which was expected to show gene changes in metabolic pathways similar to those observed for DMF treatment. However, contradictory results were shown between the qPCR data from DMF, SFN, and H_2O_2 treatments and transcriptomics results from the KOKeap1 model. These findings suggest that the changes in the metabolic pathway and mitochondria activity following DMF treatment may not be mediated by the Nrf2 pathway, and led me to investigate additional mechanisms involved in these changes.

4.5.9 Dimethyl fumarate is hydrolysed to fumarate in cell media.

Given that metabolic changes at functional levels occurred at the later time points following DMF treatment, we studied the possibility that DMF was being metabolised to another molecule that induced these metabolic changes. Since DMF is a fumarate derivative, and fumarate was the initial focus of this thesis, the hydrolysis of DMF into fumarate was measured. DMF was directly added into cell-free DMEM media for 1, 3, 6, and 24 hours, and the amount of fumarate was semi-quantified relative to a standard using chromatography-mass spectrometry. We observed that after 24 hours, DMF was almost completely hydrolysed into fumarate in the DMEM media, and interestingly, even at time zero, when the DMF was just added to DMEM media, and at earlier time points of incubation, small levels of fumarate were detected. These findings suggested that fumarate could be the molecule inducing the previously observed metabolic changes **(Figure 4.24)**.

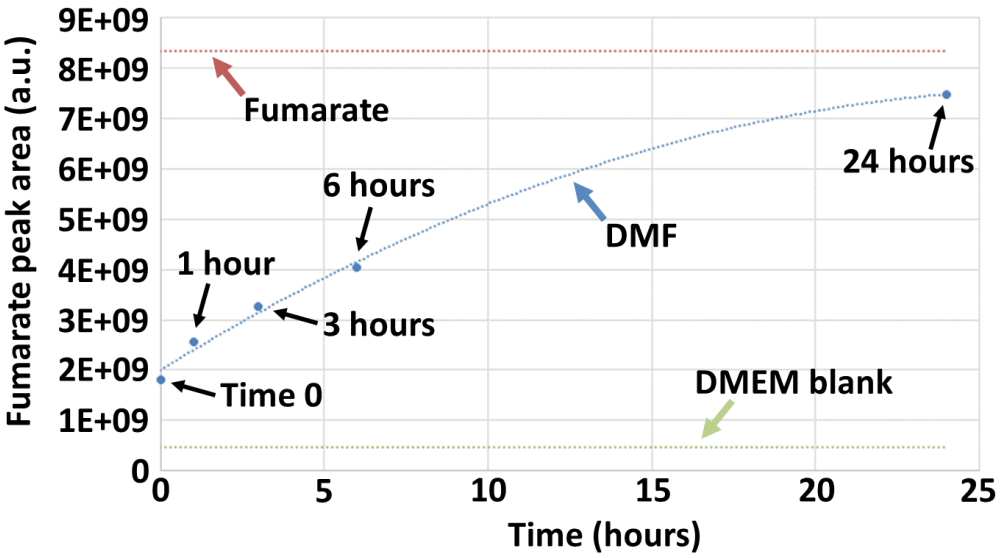

Figure 4.24: Dimethyl fumarate is hydrolysed to fumarate in DMEM media. DMF hydrolysis was studied by adding DMF (150 µM) directly in DMEM media for 1, 3, 6, and 24 hours, and the fumarate levels were measured using chromatography-mass spectrometry. A fumarate standard (150 µM) was used as an internal control.

4.5.10 Fumarate regulates gene expression differently from dimethyl fumarate in hiPSC-CM.

Given that DMF was hydrolysed into fumarate, a transcriptomics analysis was performed in hiPSC-CM, which were treated with fumarate or DMF for 6 hours, to understand whether fumarate induced similar changes to DMF. Principal component analysis (PCA) was used to compare the effect of both molecules with control samples, revealing an evident difference in the effects of both treatments. PC1 accounted for 63% variance and explained the differences observed between conditions along the x-axis, showing that DMF and fumarate were the conditions that were more separated. Both molecules were located at opposite ends of the graph, suggesting that these conditions presented the most prominent differences in gene expression, while the control samples were in the middle, closer to DMF than fumarate samples. On the y-axis, PC2 showed a lower variation of 31% and revealed that DMF and fumarate samples are more likely on this axis than control samples **(Figure 4.25A)**. This sample distribution between both axes, indicated that the three conditions

present unique gene expression profiles. To visualise how the samples were distributed, an inter-sample correlation heatmap using Pearson correlation was generated **(Figure 4.25B)**. The correlation heatmap confirmed similarities between sample members of the same biological group (biological replicates), and similar to the x-axis in the PCA plot, fumarate and DMF conditions were clustered at different ends of the control condition which showed more similitudes with DMF than fumarate.

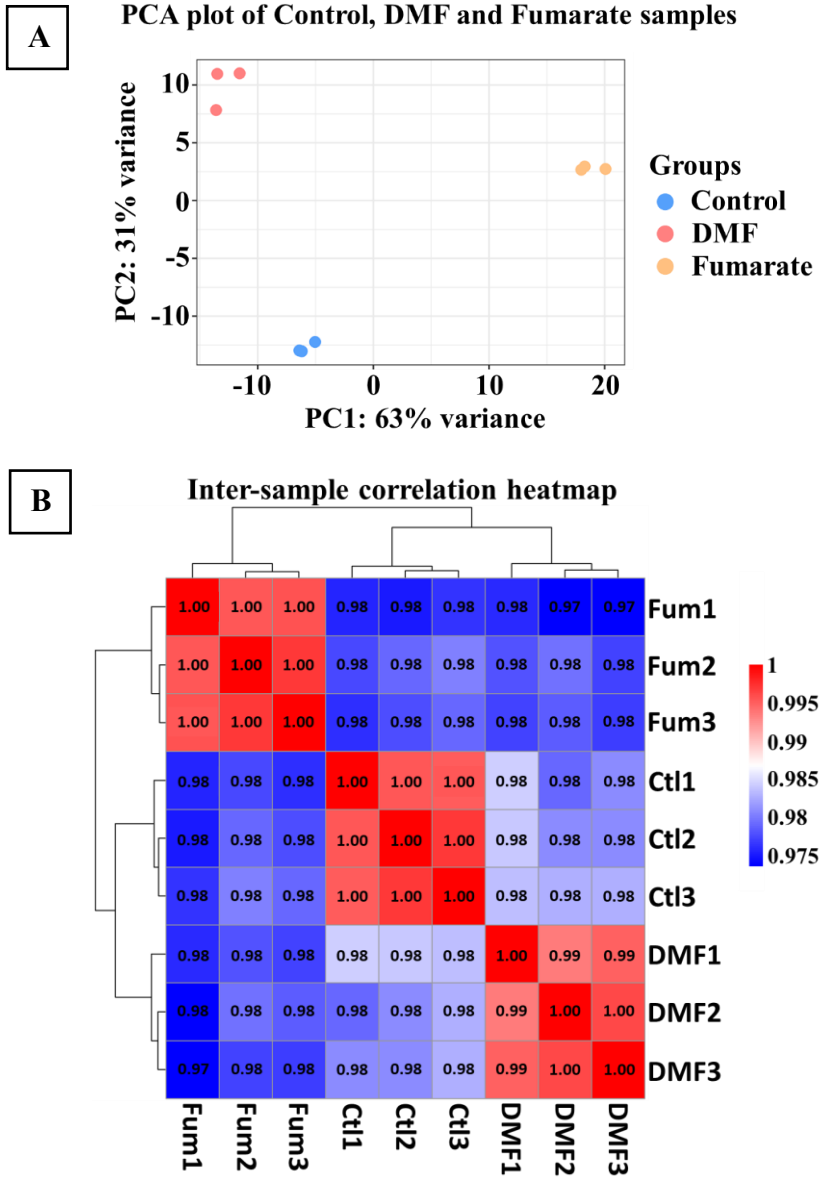

Figure 4.25: Dimethyl fumarate and fumarate induce different effects on hiPSC-CM transcriptomics. Transcriptomics analyses were performed on hiPSC-CM exposed to dimethyl fumarate (150 µM) (DMF) or fumarate (500 µM) (Fum) treatment for 6 hours and compared with untreated cells (Ctl). **(A)** Principal component analyses between control, DMF, and fumarate groups. **(B)** Inter-sample correlation between samples of each condition.

A differential gene expression (DEG) analysis using a p-adjusted value < 0.05 and a strict cutoff of 1 for the Log2 Fold change was performed in a total of 16069 genes comparing fumarate-treated cells and DMF-treated cells with control hiPSC-CM. DEG revealed that fumarate significantly regulated 1327 genes (8% of the total genes), while DMF was significantly modulating 854 genes (5% of the total genes). Venn diagrams were generated for the upregulated and downregulated genes to visualise differences and similarities between both molecules. For the upregulated genes, fumarate increased the expression of 670 genes, while DMF upregulated 377 genes, and between them, there were only 133 common upregulated genes **(Figure 4.26)**. For downregulated genes, fumarate decreased the expression of 657 genes, while DMF downregulated 447 genes, and between them, there were 200 common downregulated genes **(Figure 4.27)**. These results demonstrated that although fumarate and DMF are structurally similar molecules, they regulate gene expression differently and will be explored in the following thesis chapter.

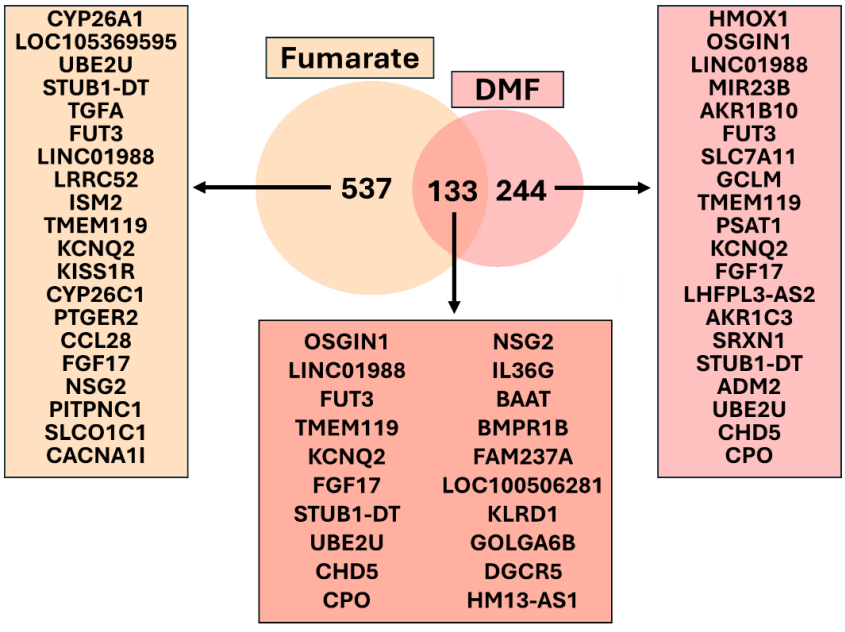

Figure 4.26: Fumarate and dimethyl fumarate induce distinct gene upregulation in hiPSC-CM. Transcriptomics analyses were performed on hiPSC-CM exposed to fumarate (500 µM) (Fum) or dimethyl fumarate (150 µM) (DMF) treatment for 6 hours and compared with untreated cells. Differential gene expression was performed using a Log_2 Fold change equal to 1 and a p-adjusted value < 0.05. The tables represent the top 20 most upregulated genes for fumarate or DMF treatment and the top 20 genes commonly increased by both molecules.

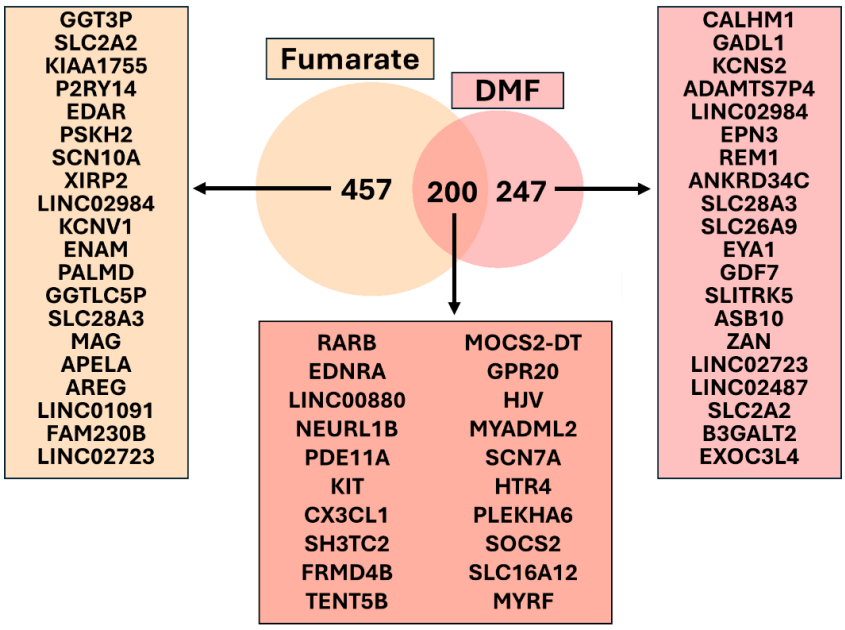

Figure 4.27: Fumarate and dimethyl fumarate induce distinct gene downregulation in hiPSC-CM. Transcriptomics analyses were performed on hiPSC-CM exposed to fumarate (500 µM) (Fum) or dimethyl fumarate (150 µM) (DMF) treatment for 6 hours and compared with untreated cells. Differential gene expression was performed using a Log_2 Fold change equal to 1 and a p-adjusted value < 0.05. The tables represent the top 20 most downregulated genes for fumarate or DMF treatment and the top 20 genes commonly decreased by both molecules.

4.6 Discussion

4.6.1 Mature hiPSC-CM are metabolically flexible, like the adult human heart.

One of the biggest limitations in studying cardiomyocyte metabolism *in vitro* is that commercially available cardiomyocyte cell lines are metabolically immature and do not resemble the adult heart metabolic profile. To address this limitation, an important aspect studied in this chapter was the metabolic profile and flexibility of our human cardiomyocyte model. We observed that, unlike commercial models, our human cardiomyocyte model had the ability to oxidize various substrates, showing metabolic flexibility when a specific metabolic pathway was inhibited. Additionally, we demonstrated that like the adult heart, our hiPSC-CM model also preferentially oxidases long-chain fatty acids, and when this

pathway was impaired, our human cardiomyocyte model rapidly shifted to glycolysis or glucose oxidation to meet the energy demands.

The increased oxidative capacity of our model could be explained by the higher mitochondrial number alongside a more efficient mitochondrial network which results from the maturation process to which our model was exposed, enhancing several fatty acid oxidation components[107, 108]. Conventional cardiomyocyte cell lines are typically incubated in media containing high glucose concentrations, therefore, metabolically, these cells are reliant on glycolysis, and genes involved in fatty acid oxidation are very lowly expressed. In contrast, our model of human cardiomyocytes was exposed to low glucose concentration and long-chain fatty acids, resulting in the upregulation of the genes and protein involved in the fatty acid oxidation pathway, including increased activity of the fatty acid oxidation transcriptional coactivator PGC1A[108]. Therefore, despite the significant limitation of this model, which is that it is a 2D cardiomyocyte model, it appears reliable for studying metabolic mechanisms involved in metabolic diseases and testing pharmacological interventions, as it is metabolically closer to the adult heart than the commercially available cardiomyocytes.

4.6.2 Fumarate derivatives induce a shift from oxidative to glycolytic metabolism in hiPSC-CM.

In this chapter, we identified that the fumarate derivatives, in addition to promoting antioxidant defence mechanisms in human cardiomyocytes, also modulate cardiac metabolism by decreasing fatty acid oxidation and increasing glycolysis. These changes were associated with mitochondrial network fragmentation and accompanied by a reduction in mitochondrial oxygen consumption, indicating that the fumarate derivatives suppress oxidative metabolism and promote glycolysis in our cell model. Interestingly, the metabolic

effect of fumarate derivatives has been reported before in several cell types, which presented a similar or different response to our model, for example, a similar shift toward glycolysis and a decrease in the mitochondria maximal respiration has been reported in human microvascular endothelial cells treated with dimethyl fumarate (DMF)[215]. Furthermore, a decrease in mitochondrial activity and respiration due to a disruption in mitochondrial morphology has been shown in T cells following DMF incubation[216]. Conversely, some studies reported opposite results, for example, peripheral blood mononuclear cells from mice treated with DMF or MMF showed a decrease in the activity of glycolytic enzyme GAPDH, which led to a decrease in glycolysis and ECAR measurements[217]. Moreover, DMF promotes mitochondrial biogenesis in human fibroblasts, increasing mitochondria oxygen consumption[218]. Although the metabolic regulation could differ between different cell types, all these observations indicate that the fumarate derivatives are molecules that can modulate metabolism, especially fatty acid and glucose metabolic pathways, highlighting new insights as potential therapeutic tools in metabolic diseases.

Curiously, when we evaluated the effect of DMF on the fatty acid oxidation genes via qPCR and transcriptomics, we observed a significant decrease in gene expression by qPCR but no changes by RNA-Seq analysis. This discrepancy could be explained by the smaller fold change detected for the fatty acid oxidation genes, and because these small differences can be identified by qPCR and not RNA-seq, it indicates differences in the level of gene detection between both methods. It has been reported that qPCR has higher sensitivity than RNA-seq, detecting small changes between conditions, whereas RNA-seq cannot detect genes with low copy numbers and requires a sufficient number of biological replicates to be reliable[219, 220]. This difference in sensitivity was also verified in our data, where *PGC1A* was the only gene detected as significantly reduced by both methods, probably because it was the gene which presented the more dramatic decrease. Furthermore, another important

difference between both techniques is the normalisation method, while qPCR gene expression is normalised to a stable reference gene, transcriptomic data can be normalised using different computational models, and it has been shown that variations in the normalisation methods can significantly impact transcriptomics results[221, 222]. However, independent of the differences observed at the genetic level with qPCR and transcriptomics analysis, functional measurement revealed that DMF significantly decreased fatty acid oxidation rates and mitochondria oxidative activity and also induced mitochondrial fragmentation. Therefore, we can conclude that at the physiological level, the fumarate derivatives were reducing oxidative metabolism in hiPSC-CM.

4.6.3 Nrf2 may not mediate metabolic changes induced by fumarate derivatives.

In our previous chapter, we determined, using sulforaphane (SFN) as a pharmacological approach and the cardiomyocyte-specific *Keap1* knockout mouse (KOKeap1) as a genetic model, that the upregulation of the antioxidant defence mechanism following fumarate derivatives treatment could be mediated by Nrf2 activation. However, the KOKeap1 data indicate that the overactivation of Nrf2 enhances various metabolic pathways, including glycolysis, fatty acid β-oxidation and oxidative phosphorylation at the gene level, which is contradictory with the decreased fatty acid β-oxidation and mitochondrial oxidative activity observed in the human cardiomyocytes treated with fumarate derivatives, suggesting the possibility that these metabolic changes were not mediated by Nrf2 pathway. This dual effect observed from our cardiomyocyte-specific KOKeap1 model, increasing glycolysis and fatty acid oxidation, has been shown by other researchers using similar *Keap1* knockout mouse approaches in different tissues, where it has been reported that constitutive activation of Nrf2 in fibroblasts increases fatty acid oxidation and mitochondrial maximal respiration[223], and also promoted glycolysis in neurons and astrocytes[224]. Furthermore, other studies have also reported that the Nrf2 pathway upregulates genes involved in both pathways in different cell

models[223, 242] and that Nrf2 activation promotes fatty acid oxidation transport and translocase genes in chronic liver disease to metabolise accumulated lipids and prevent lipotoxicity[225].

The contradictory finding of Nrf2 activation increasing both metabolic pathways in the KOKeap1 model, which are expected to be inversely regulated in the adult heart, could be potentially explained by two different hypotheses: Firstly, Nrf2 may increase fatty acid oxidation and oxidative metabolism as a mechanism to supply cell energy, while the increase in the glycolytic pathway may be for non-energy generation purposes. Instead, glycolysis may be activated alternatively to produce glucose intermediates for other metabolic pathways, such as the pentose phosphate pathway, due to Nrf2 antioxidant role, and amino acids pathway, both significantly upregulated in our KOKeap1 data. Secondly, the constitutive overactivation of Nrf2 in this genetic model may impair the feedback regulation of several cellular mechanisms, including the negative cross-regulation of glucose and fatty acid metabolism through the Randle cycle.

Although KOKeap1 results suggest that the observed metabolic shift in cardiomyocytes may not be mediated by Nrf2, hiPSC-CM treated with the pharmacological activators of Nrf2, SFN and hydrogen peroxide, showed similar metabolic changes to those induced by fumarate derivatives. These findings indicate that Nrf2 activation could still contribute to these metabolic changes. However, as a limitation of this thesis, without more specific experiments, such as genetic Nrf2 silencing in hiPSC-CM or pharmacological inhibitors of this pathway, it is not possible to definitively conclude whether Nrf2 had a role in modulating cardiomyocyte metabolism.

4.6.4 Dimethyl fumarate hydrolysis into fumarate as a potential metabolic regulator.

When we explored other mechanisms that could explain the metabolic changes induced by fumarate derivatives, we found that DMF was hydrolysed into fumarate in free-cell media. This spontaneous hydrolysis of di-esterified metabolites into their mono- and then the non-esterified form has been reported previously for dimethyl-α-ketoglutarate and dimethyl fumarate[226]. These findings position fumarate as the potential molecule that induces the metabolic changes observed for fatty acid oxidation and glycolysis instead of DMF in our human cardiomyocyte model. Both molecules showed a different gene regulation profile, with DMF treatment clustering closer to the control condition than fumarate, indicating that even though the molecular structures between them are very similar, the effect on gene regulation is different. Moreover, we observed the magnitude of the changes induced by fumarate was more considerable than DMF. In-depth studies of the possible mechanisms that fumarate could regulate in human cardiomyocytes were studied in the next chapter.

4.7 Conclusion

This chapter demonstrates that beyond their role in improving antioxidant defence mechanisms, fumarate derivatives also regulate human cardiomyocyte metabolism. These molecules induce a metabolic shift from fatty acid to glucose metabolism by decreasing the expression of genes involved in fatty acid β-oxidation, as well as reducing fatty acid oxidation rates and decreasing mitochondria respiration while upregulating glycolytic genes and increasing lactate production and glycolytic rates. Our results also confirm that Nrf2 may not mediate this metabolic alteration, and the observation of dimethyl fumarate being hydrolysed into fumarate, along with its significant effect on transcriptomics regulation, propose fumarate as a potential regulator of the metabolic profiles observed in this chapter.

Chapter 5

Fumarate as a signalling molecule within the heart

5.1 Abstract

Fumarate has traditionally been studied as a molecule required for energy generation, however, its role beyond the Krebs cycle and the mitochondria is not fully understood. In this chapter, we investigated whether fumarate plays a role in regulating cardiomyocyte biology and metabolism, and we identified novel intracrine and paracrine signalling roles for fumarate.

Elevating fumarate in mature hiPSC-derived cardiomyocytes reprogrammed cardiac metabolism, decreasing genes involved in fatty acid β-oxidation and reducing fatty acid oxidation rates while upregulating genes involved in glucose metabolism and increasing glycolysis rates, measured using radioactive isotopes. Additionally, fumarate decreased mitochondrial respiration in human cardiomyocytes. Using subcellular fractionation and qPCR, we observed that fumarate did not promote Nrf2 nuclear translocation or activation when the metabolic changes occurred, but instead, using transcriptomics analysis, we identified non-metabolic pathways regulated by fumarate, including circadian rhythms and signalling by G protein-coupled receptors (GPCRs). Furthermore, in response to chronic hypoxia, fumarate was released from the cell, which could be blunted by inhibiting the monocarboxylate transporter 1 (MCT1). FRET experiments and *in silico* modelling showed that extracellular fumarate acutely activates the sarcolemmal Gi-coupled hydroxycarboxylic acid receptor 2 (HCA2), decreasing intracellular cAMP levels. Furthermore, prolonged incubation with fumarate also decreased HCA2 gene expression.

In conclusion, fumarate selectively accumulated under hypoxia, acting both intracellularly as a signalling molecule regulating metabolism and circadian rhythm and extracellularly as a paracrine signal via G-protein-coupled receptors, reprogramming neighbouring cells.

5.2 Introduction

In Chapter 4, it was determined that DMF was hydrolysed into fumarate at the same time point that the metabolic changes were observed, suggesting that fumarate may regulate substrate metabolism in its own right. However, traditionally, fumarate uptake has been believed to be minimal or very low[144, 145], making fumarate's effects on cardiomyocyte biology unexpected and novel. Therefore, this chapter mainly focused on investigating the molecular mechanism and signalling pathway modulated by exogenous fumarate and their relationship with cardiac metabolism. To provide context, a brief introduction of the pathways studied in this chapter was incorporated in this introduction:

5.2.1 Circadian rhythm.

Cellular processes are regulated by the oscillation of a 24-hour internal clock, which allows the organism to adapt precisely to external signals like light, temperature and food availability by inducing a specific molecular or hormonal physiological response[227, 228]. This circadian clock relies on many molecular mechanisms where the transcription factors circadian locomoter output cycles protein kaput (CLOCK) and basic helix-loop-helix ARNT like 1 (BMAL1) act as essential core regulators. These two transcription factors, during the early light period heterodimerise, translocate to the nucleus and recognise specific sequences, known as E-boxes, inducing the transcription of plenty of circadian rhythm components, including Period (PER1, PER2, and PER3) and Cryptochrome (CRY1 and CRY2). These components regulate cell processes and, over time, reduce CLOCK:BMAL1 activity by translocating to the nucleus and using a negative feedback mechanism[229]. At night, the PER/CRY heterocomplexes are degraded, reducing their inhibitory effect over the CLOCK:BMAL1 complex, which is activated and translocates to the nucleus and starts a new cycle, a process that repeats rhythmically daily[230].

Circadian rhythm modulates various parameters of the cardiovascular system, including blood pressure, heart rate and metabolism[231], and alteration in the circadian oscillations increase dramatically the risk of arrhythmia and acute myocardial infarction[232, 233], indicating a connection between circadian rhythm and cardiac functionality. Metabolically, the circadian rhythm modulates mitochondrial activity by controlling the oxygen consumption rates and ATP production and regulating the mitochondrial network dynamics via fission and fusion cycles[234]. Circadian rhythm also influences various metabolic pathways via hormone regulation, such as coordinating insulin and glucagon production in β-cells[234, 235]. Disruption of the circadian system significantly impairs glucose and lipid metabolism, increasing the risk of developing a metabolic disorder, including obesity and type 2 diabetes[236, 237]. This critical role of the circadian rhythm in supporting cardiac and metabolic function suggests that identifying molecules capable of regulating circadian rhythm could be a potential therapeutic tool, even more so when this pathway is dysregulated.

5.2.2 G protein-coupled signalling receptors.

The G protein-coupled receptors (GPCRs) are a family of membrane receptors characterised by seven transmembrane domains, which actively participate in cell-to-cell communication and regulate different biological functions, including hormone release, immune response and heart contractility[238]. According to their role and structure, GPCRs are classified into five classes, with class A, also known as rhodopsin-like receptors, involved in the cardiovascular system[239]. Class A GPCRs can bind various ligands, including peptides, amines, nucleotides, melatonin and lipids[239, 240]. Signalling via G proteins involves three different subunits Gα, Gβ, Gγ, which, upon the receptor activation, the subunit Gα dissociates from the other subunits modulating different cellular pathways, where its effect depends on the Gα subtype: Gαs stimulates adenylate cyclases (ACs), Gαi inhibits ACs, Gαq

regulates phospholipase C, and Gα12/13 interacts with Rho nucleotide exchange factors[241, 242].

Among the GPCRs that have an inhibitory effect on AC, a subgroup of these is activated by metabolites, including the hydroxycarboxylic acid receptors (HCA), consisting of HCA1, which is activated by lactate, HCA2, which responds to hydroxy-butyrate and butyrate, and HCA3 whose ligand is hydroxy-octanoic acid[243]. The response to the external stimuli of these receptors begins when a ligand binds to its receptor, inducing subunit Gαi activation by exchanging GDP for GTP. Once activated, Gαi inhibits AC, leading to a decrease in intracellular cAMP levels, and because cAMP is required for PKA activation, this reduction prevents PKA regulation of other targets[244]. The inhibitory effect of Gi protein-coupled receptors positions them as potential therapeutic targets, as is the case for HCA2, where drugs targeting this receptor have been approved for treating cardiovascular and neurological diseases[245]. Furthermore, HCA2 has a potential role in regulating metabolic disorders as its activation inhibits lipolysis in adipocytes[246, 247] by reducing protein kinase A activity and subsequently lowering hormone-lipase activation[248], thereby decreasing serum fatty acid concentrations. Therefore, the potential modulation of these receptors positions the Gi-coupled signalling pathway as a promising candidate to address altered cardiac metabolism.

5.3 Chapter aims

Given the transcriptomics findings from Chapter 4, which demonstrated fumarate's impact on the hiPSC-CM gene profile was greater than the DMF effect, this chapter focused on determining the effects of fumarate in mature hiPSC-CM. This chapter investigated:

1. The effect of fumarate on fatty acid oxidation and glycolytic metabolism in hiPSC-CM and its impact on mitochondrial oxygen consumption rates.

2. The capacity of fumarate to activate the Nrf2 pathway in hiPSC-CM.

3. The role of fumarate on modulating intracellular signalling pathway at transcriptomics level in hiPSC-CM.

4. The role of hypoxia in hiPSC-CM and its relationship with fumarate.

5. The impact of fumarate regulating extracellular signalling pathways in hiPSC-CM.

5.4 Methods

5.4.1 Luciferase reporter for the antioxidant response element.

The generation of viral particles and the stable cell lines expressing the antioxidant response element luciferase reporter vector was performed by Dr Sara Falcone at Oxford University.

5.4.1.1 Viral particle generation.

To generate the antioxidant response element (ARE) luciferase reporter vector (pGF2-ARE), four copies of the ARE sequence were cloned into the pGreenFire2.0 (SBI System Biosciences) vector using XhoI and BmtI restriction enzymes, which allowed the transcription of the luciferase reporter gene rFluc.

Lentiviral particles containing the reporter vector were generated by cotransfecting HEK293T cells with the pGF2-ARE vector and pPACKH1 plasmids (SBI System Biosciences) using the PureFection reagent (SBI System Biosciences). Between 18 to 24 hours before transfection, $3x10^6$ HEK93T cells were seeded in a 10 cm dish containing 9 mL DMEM high glucose (25 mM), pyruvate (1 mM) supplemented with 2 mM L-glutamine, and 10% fetal bovine serum. On the day of transfection, the transfection mixture was prepared by first adding 20 µL of pPACKH1 and 3.5 µg of pGF2-ARE into 800 µL of serum-free DMEM, followed by the addition of 24 µL of PureFection. The solution was mixed by vortexing for 10 seconds, incubated at room temperature for 15 minutes, and then 850 µL added dropwise to the HEK293T dish. The cell media was collected 48 hours and 72 hours post-transfection and centrifuged at 3000 x g for 15 minutes to pellet cell debris. The supernatant was moved to a clean tube, where to concentrate the viral particles, three volumes of medium were incubated with one volume Lenti-X Concentrator (Clontech) for 1 hour at 4°C. The mixture was centrifuged at 1,500 x g for 45 min at 4°C, the pellet was

resuspended in 120 µL of cold PBS, and viral particles were aliquoted in 30 µL aliquots and stored at -80°C until needed.

5.4.1.2 Stable cell lines expressing the antioxidant response element luciferase reporter vector.

For the generation of stable HEK293 and H9c2 cell lines expressing the ARE reporter vector, a total of 10^6 cells were plated in a T75 flask and incubated for 24 hours. Next, 30 µL of viral particles were diluted in 7 mL of DMEM medium containing 8 µg/mL of Polybrene (Santa Cruz) and added to the cells for 24 hours. The cell media was changed for virus-Polybrene-free DMEM and incubated until the cells showed GFP expression. Successfully transduced cells were selected with 1 µg/mL of Puromycin (Sigma) for 14 days.

5.4.1.3 Nrf2 activity quantification using the luciferase reporter vector.

To measure Nrf2 activity, HEK293-ARE and H9c2-ARE cells were seeded into a 96-well plate the day before the drug treatment. The following day, cells were incubated with 80 µL of DMEM high glucose (25 mM) and pyruvate (1 mM) supplemented with 2 mM L-glutamine, 100 U/mL Penicillin-Streptomycin and 10% fetal bovine serum, containing the drugs dimethyl fumarate, sulforaphane, fumarate or none (Control). At the end of drug treatment (6, 12 or 24 hours), cells and ONE-Glo Luciferase Assay System reagent (Promega) were equilibrated to room temperature for 15 minutes. Then 80 µL of ONE-Glo Luciferase Assay System reagent was added to each well, and the plate was mixed on an orbital shaker for 15 minutes. Luminescence, directly proportional to Nrf2 activity **(Figure 5.1)**, was measured using a firefly luciferase luminescence detection protocol with a central wavelength of 580 nm and bandwidth of 80 nm.

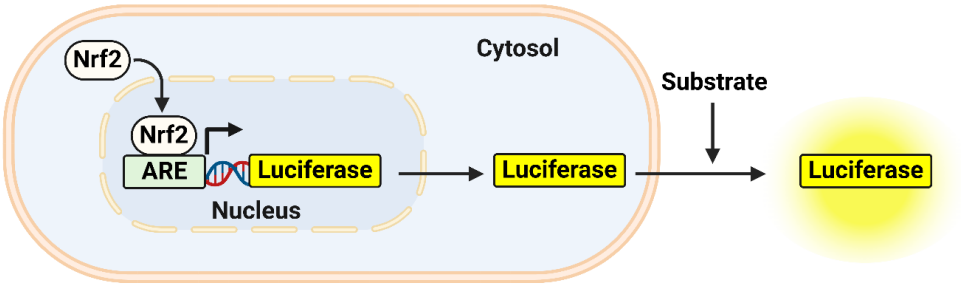

Figure 5.1: Antioxidant response element luciferase reporter. Antioxidant response element sequence is recognised by the Nrf2 transcription factor and induces luciferase gene expression, therefore, the amount of luminescence detected as relative light units (RLU) is directly proportional to Nrf2 activity.

5.4.2 Fumarate release.

Quantification of fumarate in the cell media was performed using two different approaches:

5.4.2.1 Fumarate spectrophotometric kit.

Fumarate levels were measured spectrophotometrically using the Fumarate detection kit (Abcam), following the manufacturer's instructions. Cell media was directly diluted in Assay Buffer, and a 50 µL aliquot was transferred to a 96-well plate where 100 µl of the reaction mix (composed of Assay Buffer, Developer Solution, and Fumarate Enzyme Mix) was added, and solutions were mixed. Finally, the reaction was incubated for 60 minutes at 37°C, the absorbance was measured at 450 nm using a microplate reader, and the fumarate concentration was calculated relative to the standard curve after subtracting the background.

5.4.2.2 Fumarate detection by mass spectrometry.

After cell treatment, cell media was collected, frozen, and sent to Prof Lee Robers at the University of Leeds. The fumarate concentration in the media was determined using their well-established liquid chromatography-triple quadrupole-mass spectrometry targeted metabolomics platform[249].

5.4.3 Lactate dehydrogenase (LDH) release.

LDH content in the cell media was measured using an ABX Pentra 400 system (Horiba ABX diagnostics).

5.4.4 *In silico* target prediction and molecular modelling.

In silico target prediction for fumarate and fumarate derivatives was conducted using the SwissTargetPrediction[250, 251] online tool for small bioactive molecules. Molecular modelling was performed by Dr Pinqi Wang from the Russell group using the Molecular Operating Environment (MOE) docking software[252]. The structure of the human niacin receptor HCA2-Gi protein complex was obtained from the Protein Data Bank under ID 7XK2[253]. Molecular visualisation of fumarate and HCA2 interaction was generated using the PyMOL molecular graphics system.

5.4.5 Neonatal rat ventricular myocytes (NRVMs) isolation and culture.

The isolation of a culture of NRVMs was made possible through collaboration with Prof Manuela Zaccolo's group at Oxford University. Based on their well-established protocol[254], ventricular tissue from 1 to 3-day Wistar rats was enzymatically separated and plated onto 24-mm glass coverslips (previously coated with laminin). Cells were initially cultured in DMEM supplemented with 10% horse serum and 5% newborn calf serum for 24 hours. Subsequently, the media was replaced with DMEM supplemented with 5% horse serum and 0.5% newborn calf serum.

5.4.6 Fluorescence resonance energy transfer (FRET).

FRET experiments were performed by Mr Alexander Demby from the Zaccolo group. Based on their protocol[255-257], NRVMs were infected with EPAC-S-H187 cytosolic FRET sensor[258] using an adenovirus for 24-48 hours. Cells were maintained at room temperature

in Ringer-modified saline solution containing 140 mM NaCl, 3 mM KCl, 10 mM HEPES, 15 mM Glucose, 1 mM $CaCl_2$, and adjusted to pH 7.2), and treated with the adenylyl cyclase activator, forskolin and monomethyl fumarate or fumarate. For imaging, an inverted microscope (Olympus IX71) equipped with an oil immersion objective PlanApoN 60X (NA 1.42, 0.17/FN 26.5) (Olympus) was used with a CoolSNAP HQ2 monochrome camera (Photometrics) and a DV2 beam-splitter (Photometrics). FRET changes were quantified as the ratio of acceptor fluorescence emission (YFP) at 545 nm to donor emission (CFP) at 480 nm, represented as 545 nm/480 nm (YFP/CFP ratio) in the region of interests (ROIs). Images were acquired and analysed using MetaFluor 7.1 software, and values were expressed as a percentage increase over the maximal FRET change.

5.5 Result

5.5.1 Fumarate decreases fatty acid oxidation transporter, transferase and translocase genes while increasing glycolytic genes.

To study which biological pathways were being modulated by fumarate, differential gene expression (DEG) analysis using a p-adjusted value < 0.05 and Log_2Fold change of >1 was performed on a total of 16069 genes comparing fumarate-treated (500 μM fumarate for 6 hours) with control hiPSC-CM. Fumarate significantly upregulated 670 genes and decreased significantly the expression of 657 genes. Enrichment analysis showed that the most enriched pathways associated with the upregulated genes were the HIF pathway, ion transport, response to hormones and nutrients, and circadian clock pathway **(Figure 5.2A)**. Additionally, carbohydrate transport, glucose import, and the solute carrier (SLC) family transporter, which includes various glucose transporters, were also upregulated. In contrast, the main downregulated pathways were involved in heart and muscle development and morphogenesis and signalling by G protein-coupled receptors (GPCR) **(Figure 5.2B)**.

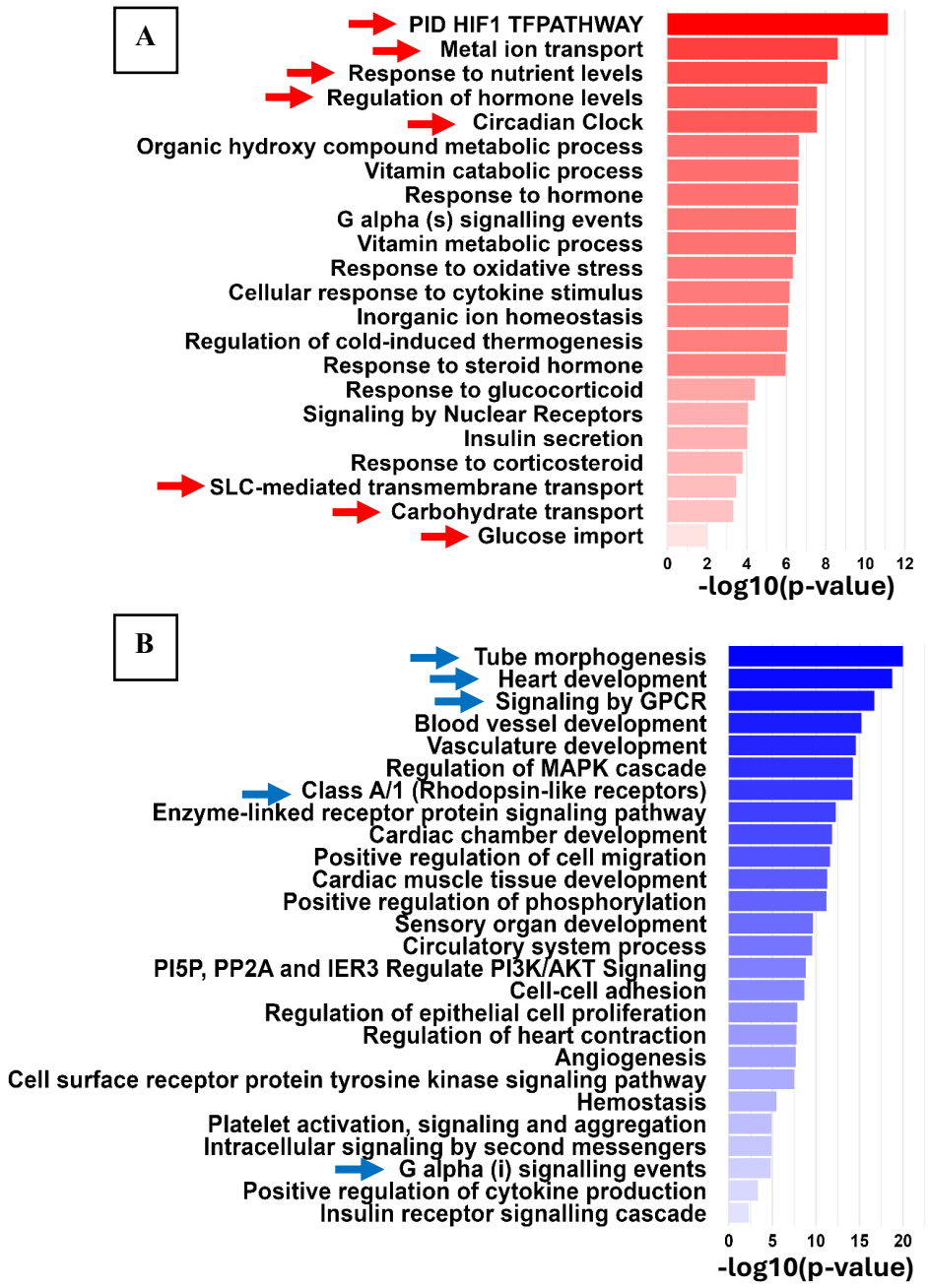

Figure 5.2: Enrichment analysis of differential gene expression in hiPSC-CM exposed to fumarate. Transcriptomics analyses on hiPSC-CM exposed to fumarate treatment (500 µM) for 6 hours and compared with untreated cells. DEG was performed using a Log_2 Fold change equal to 1 and p-adjusted value < 0.05. Enrichment analysis was conducted using metascape, and the graph of enriched terms represents the 670 upregulated **(A)** or 657 downregulated genes **(B)**.

Based on the DEG, the enriched transcription factors modulating the upregulated and downregulated genes following fumarate treatment were visualised using the TRRUST database. Complementing the enriched terms results where the HIF pathway was the most

upregulated pathway, the hypoxia-inducible factor 1 subunit alpha (HIF1A) and the hypoxia-inducible factor 1-beta (ARNT) were detected as upregulated transcription factors **(Figure 5.3A)**. Additionally, CLOCK, neuronal pas domain protein 2 (NPAS2), BMAL1 (ARNTL), and activating transcription factor 4 (ATF4), all implicated in the circadian clock pathway, were also observed. In contrast, the most enriched transcription factors detected for the downregulated genes were the specificity protein 1 (SP1), which plays a role in regulating the cell cycle and specific gene expression during tissue development[259], and the histone deacetylase 1 (HDAC1), which is involved in regulating several epigenetic modifications, and also can bind to SP1 to modulate gene expression[260, 261] **(Figure 5.3B)**. Furthermore, several transcription factors involved in fatty acid oxidation regulation, including the FOXO family (FOXO3, FOXO1, and FOXM1) and the PPAR family (PPARG and PPARA), were also detected downregulated.

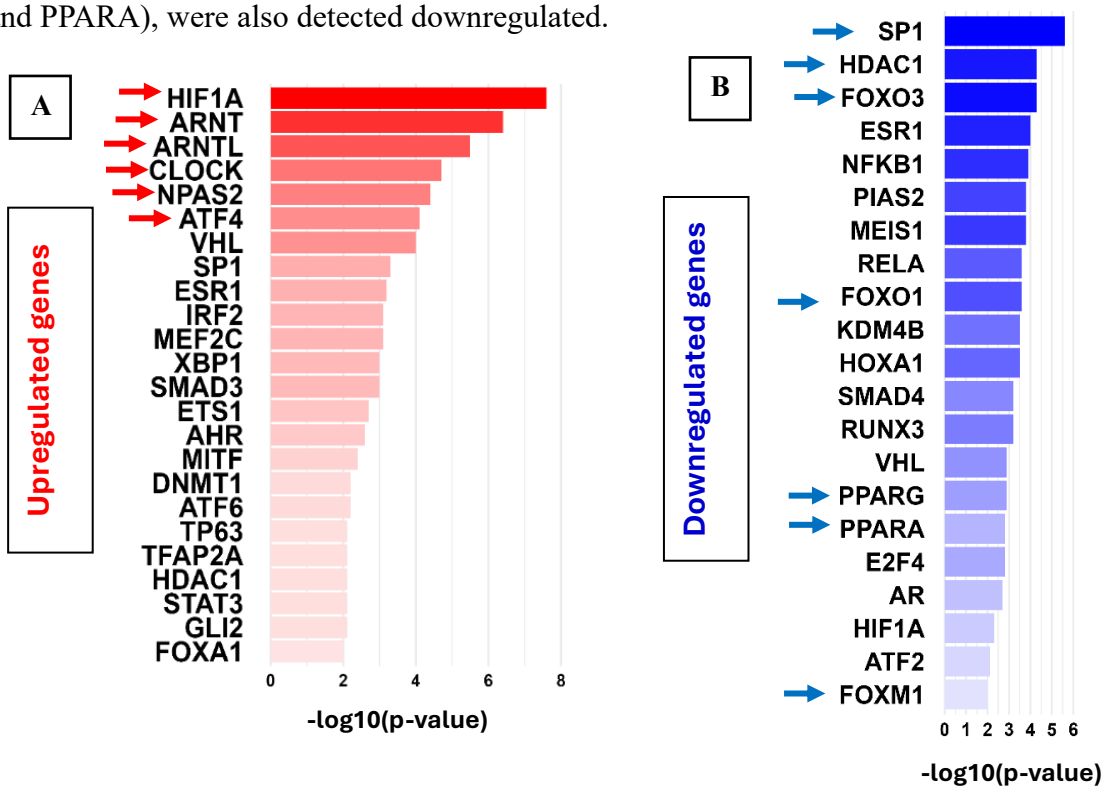

Figure 5.3: Transcription factor enrichment analysis of differential gene expression in hiPSC-CM exposed to fumarate. Transcriptomics analyses on hiPSC-CM exposed to fumarate treatment (500 µM) for 6 hours and compared with untreated cells. DEG was performed using a Log_2 Fold change equal to 1 and p-adjusted value < 0.05. Transcription factor enrichment analysis was conducted using metascape, using the transcriptional regulatory relationships unravelled by sentence-based text mining (TRRUST) database.

Previously, a Log_2 Fold change > 1 was used to identify the genes that presented a considerable difference between conditions, giving us robust results in the biological pathway in which fumarate had a critical impact. However, this approach excluded other potential and important pathways, which also exhibited statistical significance but presented a small-fold change compared with the control condition. The previous enriched terms and transcription factors suggested that fumarate was targeting genes involved in glucose and fatty acid metabolism, therefore, a new DEG was performed using the same p-adjusted value < 0.05 but a Log_2Fold equal to 0 **(Figure 5.4)**. Interestingly, genes involved in fatty acid β-oxidation and glycolysis were identified between the fold changes -1 and 1. When a volcano plot was generated focusing on these metabolic genes, it was possible to observe that fumarate decreased genes involved in fatty acid β-oxidation and increased glycolytic genes.

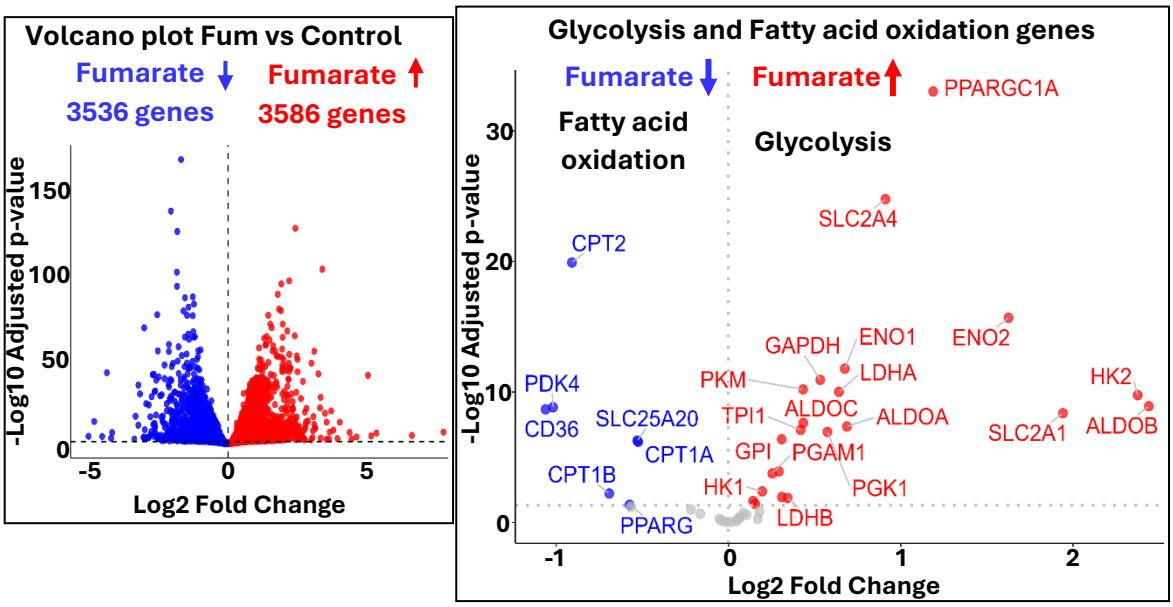

Figure 5.4: Fumarate decreases fatty acid oxidation genes and increases glycolytic genes in hiPSC-CM. Transcriptomics analyses on hiPSC-CM exposed to fumarate treatment (500 µM) for 6 hours and compared with untreated cells. DEG was performed using a Log_2 Fold change equal to 0 and p-adjusted value < 0.05. Significantly upregulated genes are shown in red, and significantly downregulated are shown in blue.

The transcriptional effect of fumarate over the glycolytic pathway was confirmed using a heatmap, which revealed that fumarate significantly upregulated the expression of nearly all the evaluated glycolytic genes. Notably, fumarate also decreased the expression of the glucose metabolism negative regulators pyruvate dehydrogenase kinase (PDK), including the specific cardiac isoform *PDK4* **(Figure 5.5)**.

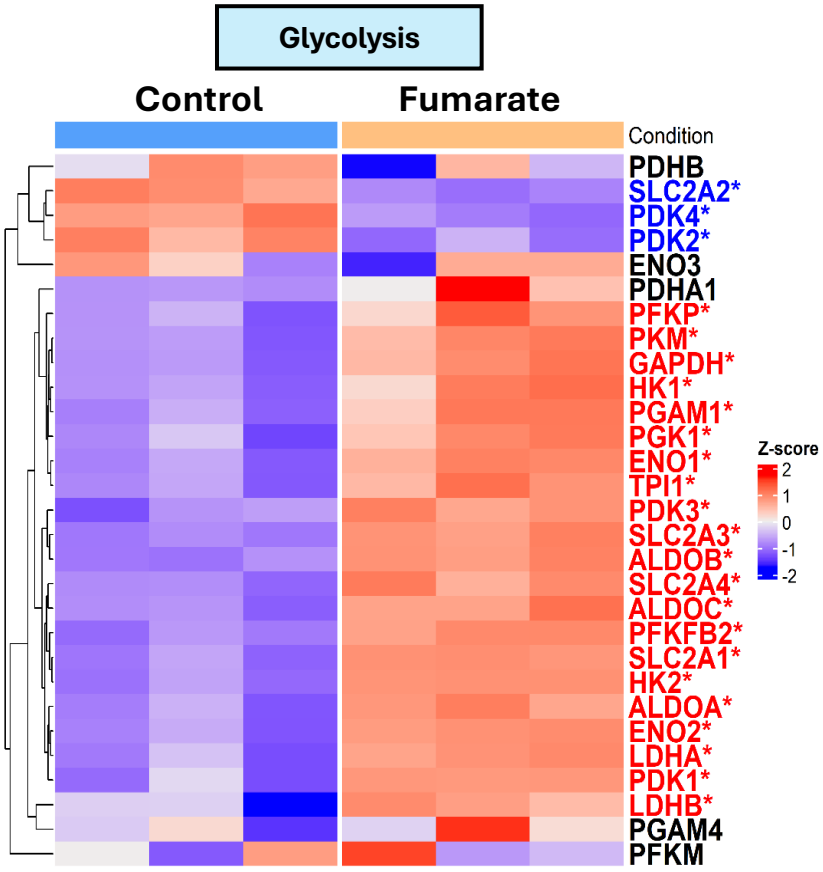

Figure 5.5: Fumarate upregulates glycolytic pathway at the transcriptomics level. Glycolysis pathway heatmap was generated using normalised counts from the transcriptomics analyses on hiPSC-CM exposed to fumarate treatment (500 µM) for 6 hours and compared with untreated cells**.** Significantly upregulated genes are shown in red, and significantly downregulated genes are shown in blue. *p-adjusted value < 0.05. Each column represents a biological replicate.

On the other hand, when the transcriptional effect of fumarate on the fatty acid oxidation pathway was visualised by generating a heatmap, a divergent regulation profile was observed. Some genes, such as the fatty acid oxidation transcriptional coactivator *PGC1A* (*PPARGC1A*), along with genes involved in lipid biosynthesis, acyl-CoA synthetase short-

chain family member 2 (*ACSS2*) and malonyl-CoA decarboxylase (*MLYCD*), were upregulated, while other genes, including all the genes coding for membrane transporters, transferases or translocases involved in fatty acid β-oxidation (*CD36, CPT1A, CPT1B, SLC25A20/CACT*, and *CPT2)* were significantly downregulated **(Figure 5.6)**. Additionally, the magnitude of the changes for the fatty acid β-oxidation membrane targets was visualised using boxplots of the normalised counts comparing fumarate-treated with untreated hiPSC-CM, observing that all the represented genes were significantly downregulated.

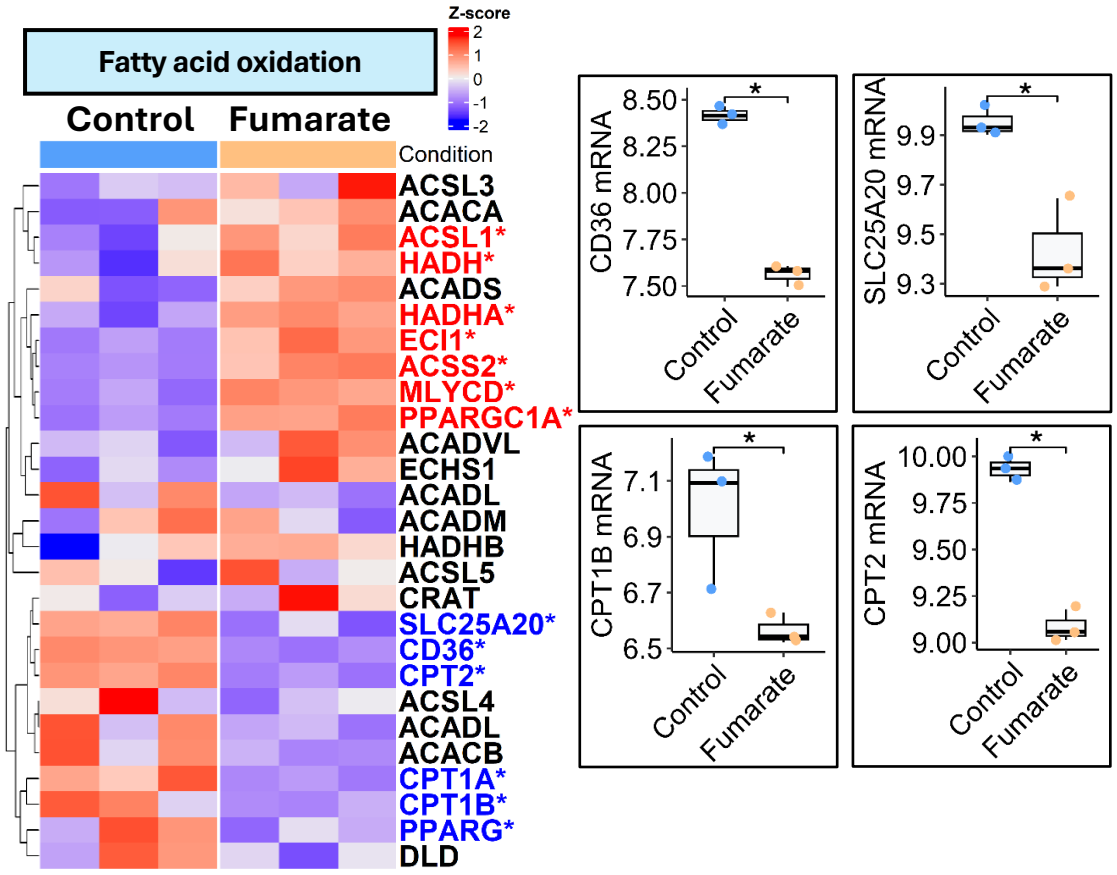

Figure 5.6: Fumarate decreases fatty acid membrane transporters, transferases and translocases genes at transcriptomics level. Fatty acid oxidation pathway heatmap was generated using the normalised counts from the transcriptomics analyses on hiPSC-CM exposed to fumarate treatment (500 µM) for 6 hours and compared with untreated cells**.** Significantly upregulated genes are shown in red, and significantly downregulated genes are shown in blue. Boxplots of the normalised counts for the genes cluster of differentiation 36/fatty acid translocase (*CD36*), carnitine palmitoyltransferase 1B (*CPT1B*), carnitine-acylcarnitine translocase (*SLC25A20/CACT)*, and carnitine palmitoyltransferase 2 (*CPT2*). * $p < 0.05$ adjusted p-value vs. respective control group. Each column in the heatmap represents a biological replicate. Each data point in the graphs represents a biological replicate.

The effect of fumarate on these metabolic pathways was further validated by qPCR, measuring the expression of key genes identified in the transcriptomics data for both fatty acid β-oxidation and glycolysis. Fumarate significantly downregulated all the evaluated fatty acid β-oxidation genes. The expression of the membrane transporter *CD36* was reduced by 51%, the mitochondrial outer membrane acetyltransferase *CPT1B* expression decreased by 24%, and the mitochondrial inner membrane translocase CACT expression was reduced by 16% compared with control cells **(Figure 5.7A)**. In addition, when the effect of fumarate on the glycolytic genes was evaluated, a significant increase in the expression of the cell membrane glucose transporter *GLUT1* by 3-fold was observed and, similarly, the glycolytic gene *HK2* was upregulated by 3-fold compared with control cells **(Figure 5.7B)**.

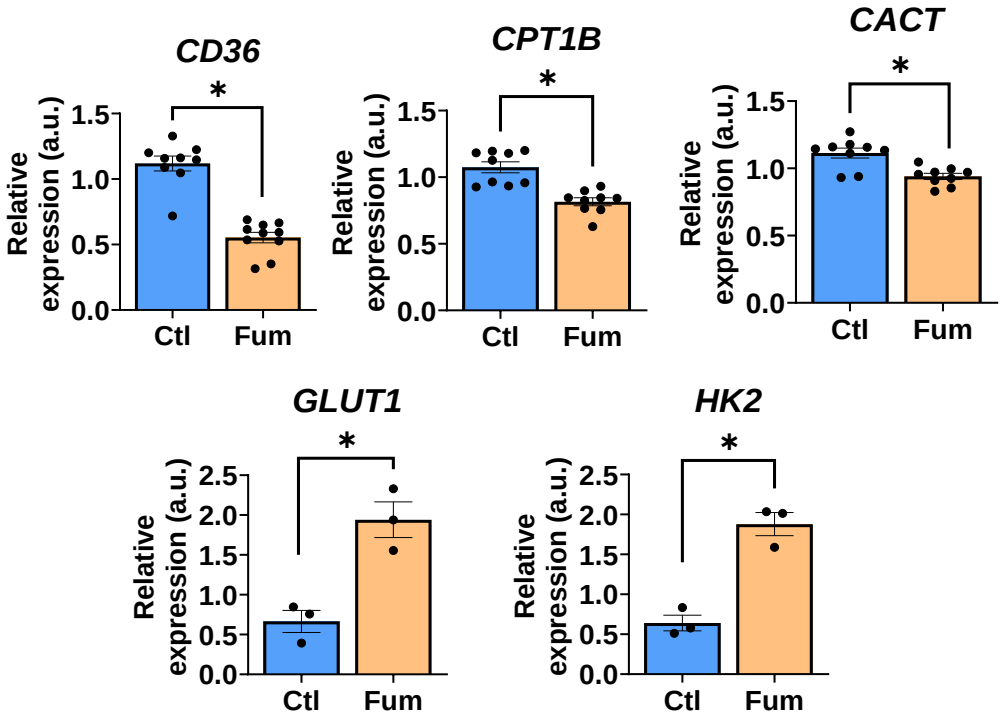

Figure 5.7: Fumarate decreases fatty acid β-oxidation transporters and translocases genes and increases glycolytic genes. Fatty acid β-oxidation and glycolytic gene expression in hiPSC-CM exposed to fumarate treatment (500 µM) for 6 hours (Fum) compared with untreated cells (Ctl). **(A)** The targets evaluated for fatty acid β-oxidation were cluster of differentiation 36/fatty acid translocase (*CD36*), carnitine palmitoyltransferase 1B (*CPT1B*), and carnitine-acylcarnitine translocase (*CACT/SLC25A20).* The targets evaluated for glycolysis were glucose transporter 1 (*GLUT1*) and hexokinase 2 (*HK2*). * $p < 0.05$ vs. respective control group. a.u., arbitrary units. Each data point represents a biological replicate.

In summary, the transcriptomics data revealed that fumarate significantly upregulated the genes involved in glucose transport and glycolytic metabolism while enriching HIF1 and circadian clock pathways. Moreover, fumarate reduced the expression of genes involved in fatty acid β-oxidation, particularly those that code for cell and mitochondrial membrane transporters, transferases and translocases, as well as genes associated with muscle development and GPCR signalling.

5.5.2 Fumarate reduces fatty acid oxidation rates and mitochondrial respiration while increasing glycolytic rates.

The role of fumarate in modulating fatty acid oxidation and glycolysis was further studied at the functional level using radioactive palmitate and glucose. Fumarate treatment rapidly decreased fatty acid oxidation rates by 57% after 6 hours. This effect also persisted after 12 hours of treatment, where fatty acid oxidation rates were significantly reduced by 56% compared with control cells **(Figure 5.8A)**. On the other hand, fumarate treatment significantly increased the glycolytic rate by 26% after 6 hours, but no changes were observed after 12 hours of treatment compared with control cells **(Figure 5.8B)**.

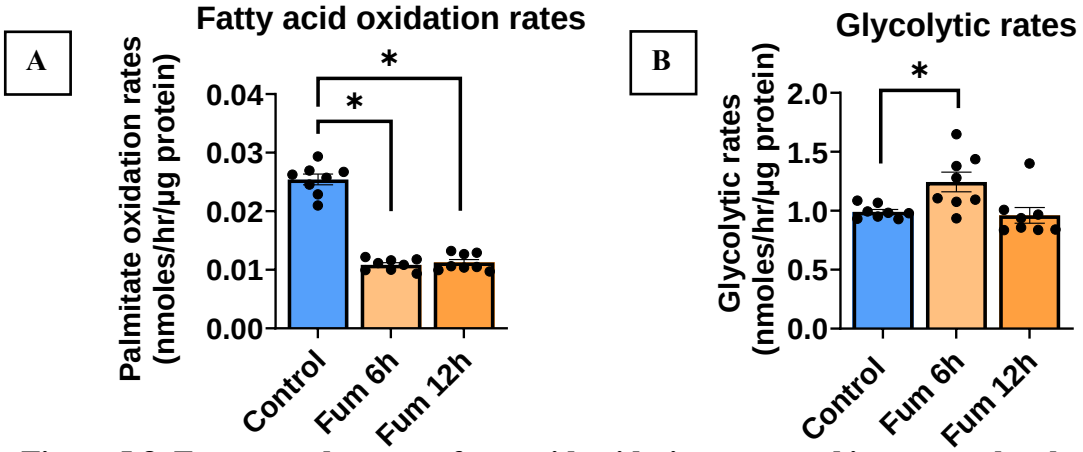

Figure 5.8: Fumarate decreases fatty acid oxidation rates and increases glycolytic rates. Metabolic fluxes in hiPSC-CM exposed to fumarate treatment (500 µM) for 6 or 12 hours (Fum) compared with untreated cells (Control)**. (A)** Fatty acid oxidation rates were measured using [9,10-^{3}H]-palmitate. **(B)** Glycolytic rates were measured using [^{3}H]-glucose. * $p < 0.05$ vs. the respective control group. Each data point represents a biological replicate.

To further investigate whether the shift from oxidative to glycolytic metabolism was associated with changes in mitochondrial function, fumarate's impact on mitochondrial activity was assessed using a Seahorse analyser. Given that the observed changes at the transcriptomics level and in the metabolic rates occurred at 6 and 12 hours, the effect of fumarate on mitochondrial respiration was also studied at these time points. No significant differences were detected following 6 hours of fumarate treatment, although a decreasing trend in mitochondria basal respiration was observed (**Figure 5.9A**). After 12 hours, fumarate treatment significantly decreased mitochondrial basal respiration by 11%, without affecting mitochondrial maximal respiration **(Figure 5.9B)**. Additionally, the effect of fumarate treatment for 24 hours was evaluated, observing that basal respiration, ATP-linked respiration, maximal respiration, and non-mitochondria respiration were significantly reduced by 21%, 30%, 14%, and 14%, respectively compared with the control condition **(Figure 5.10)**.

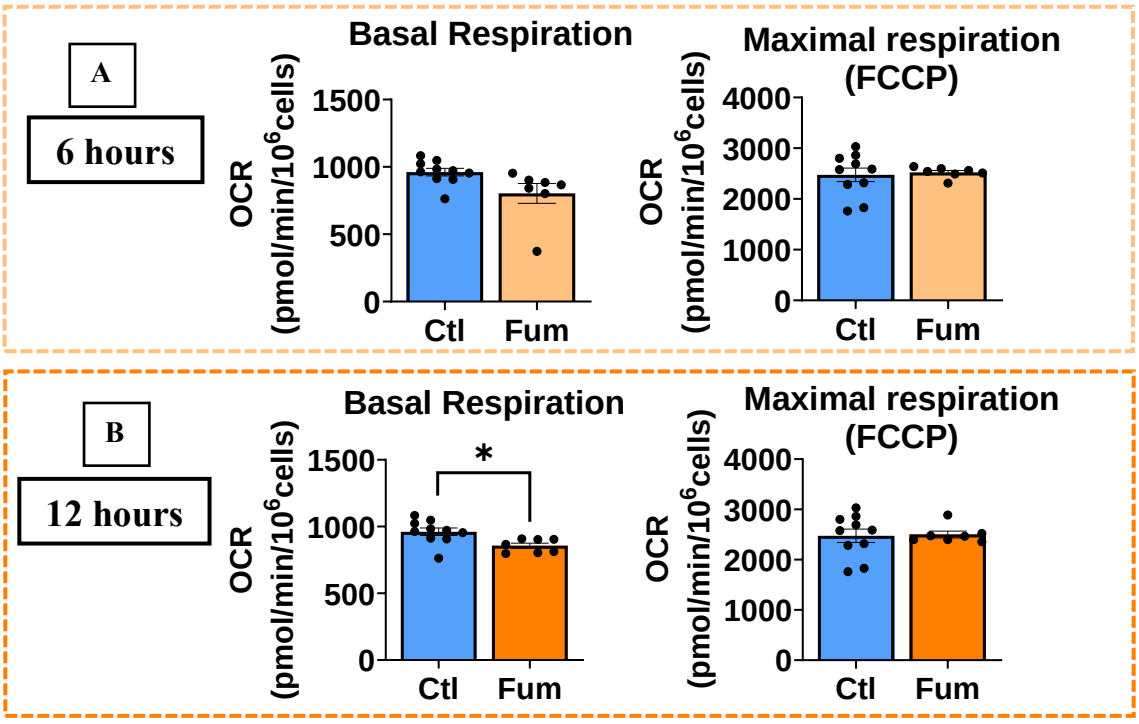

Figure 5.9: Fumarate decreases mitochondria basal respiration following 12 hours of treatment. Oxygen consumption rates (OCR) in hiPSC-CM exposed to fumarate treatment (500 µM) (Fum) for **(A)** 6 hours or **(B)**12 hours * $p < 0.05$ vs. respective control group (Ctl). Each data point represents a biological replicate.

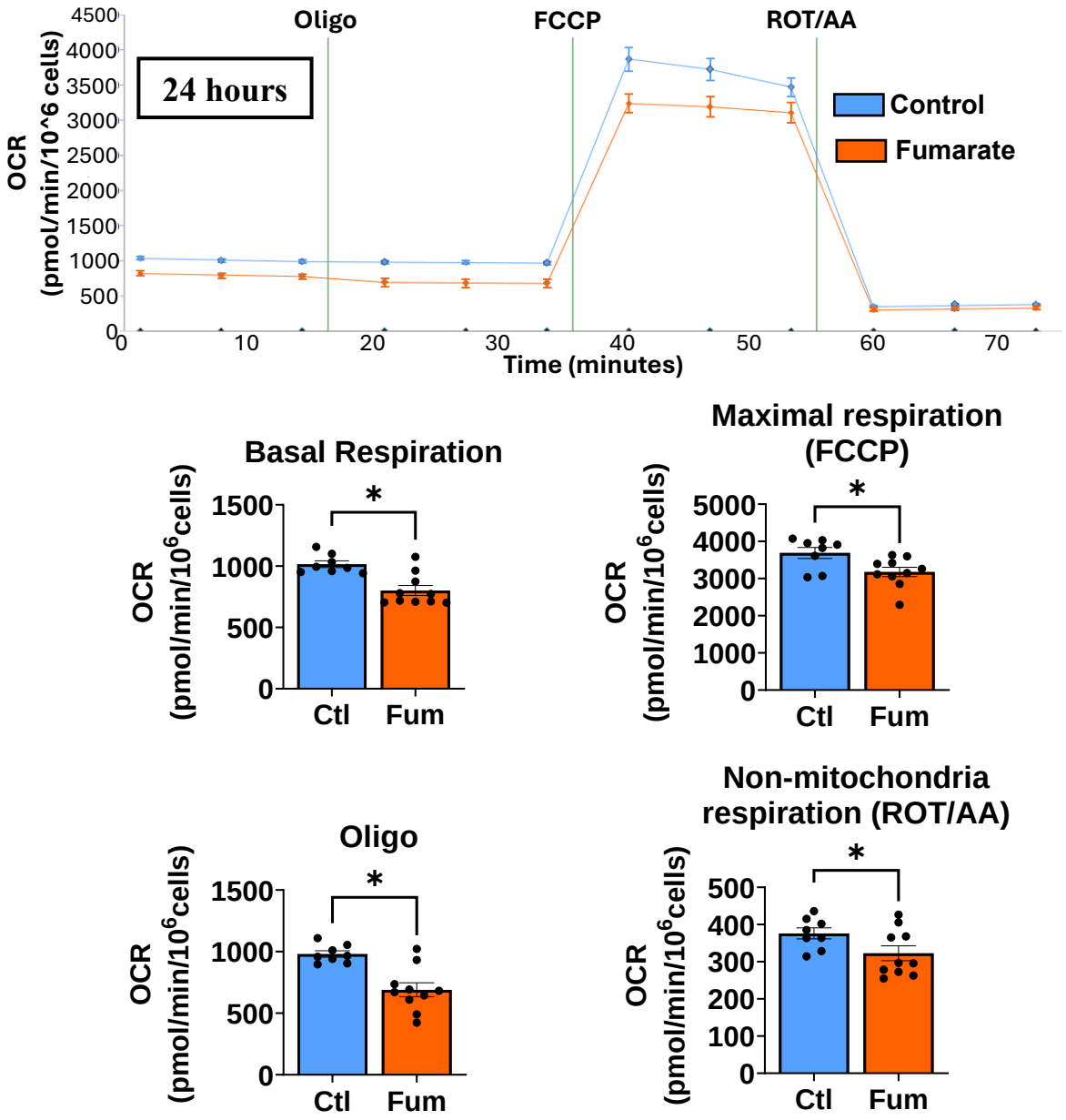

Figure 5.10: Fumarate decreases mitochondria oxygen consumption following 24 hours of treatment. Oxygen consumption rates (OCR) in hiPSC-CM exposed to fumarate treatment (500 µM) (Fum) for 24 hours. * $p < 0.05$ vs. respective control group (Ctl). OCR data is represented as the mean ± SEM of the biological replicates. Each data point in the graphs represents a biological replicate.

Overall, these results indicate that fumarate induced a metabolic reprogramming from oxidative to glycolytic metabolism within the human cardiomyocyte. Fumarate decreased free fatty acid utilisation as an energy source by reducing fatty acid oxidation rates and decreasing mitochondrial activity while increasing the use of glucose as substrate, indicated by the elevated glycolytic rates.

5.5.3 The Nrf2 pathway does not mediate fumarate-induced metabolic changes in fatty acid oxidation and glycolysis.

The next step was to investigate the molecular mechanisms by which fumarate was modulating human cardiomyocyte metabolism. Initially, as studied in the previous chapters for the fumarate derivatives, the potential role of fumarate itself in regulating the Nrf2 pathway was investigated using subcellular fractionation to evaluate Nrf2 nuclear translocation, and qPCR to measure the expression of the Nrf2 antioxidant target genes. The results showed that fumarate neither induced Nrf2 nuclear translocation **(Figure 5.11A)** nor induced significant changes in the expression of the *NQO1, TXNRD1, and HMOX1* genes compared with the control condition **(Figure 5.11B)**.

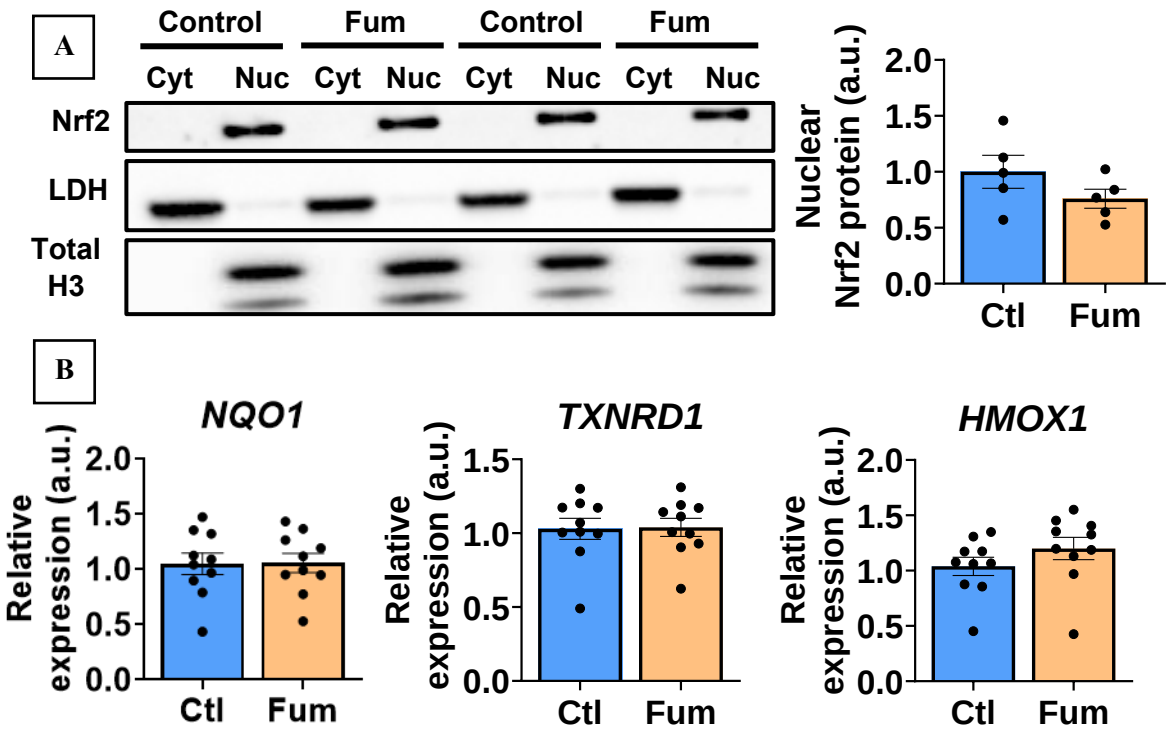

Figure 5.11: Fumarate does not promote Nrf2 nuclear translocation or increase Nrf2 antioxidant target gene expression in hiPSC-CM. Cells were exposed to fumarate treatment (500 µM) (Fum) for 6 hours and compared with untreated cells (Ctl). **(A)** Representative western blot of Nrf2 nuclear translocation **(B)** The evaluated antioxidant genes were NAD(P) dehydrogenase quinone 1 (*NQO1*), thioredoxin reductase 1 (*TXNRD1*), and heme oxygenase 1 (*HMOX1*). a.u., arbitrary units. Each data point represents a biological replicate.

To evaluate whether a different fumarate dose could activate the Nrf2 pathway in human cardiomyocytes, the expression of the antioxidant genes *NQO1*, *TXNRD1*, *HMOX1*, and *SRXN1* in hiPSC-CM treated with 150 µM, 300 µM, 500 µM and 2 mM fumarate for 6 hours was evaluated by qPCR **(Figure 5.12)**. Consistent with the previous qPCR findings, no significant changes were detected for *TXNRD1, HMOX1*, and *SRXN1* genes at any fumarate concentration. *NQO1* showed a significant ANOVA effect between all the conditions, but there was not a significant difference between individual groups (did not reach significance at post hoc analyses).

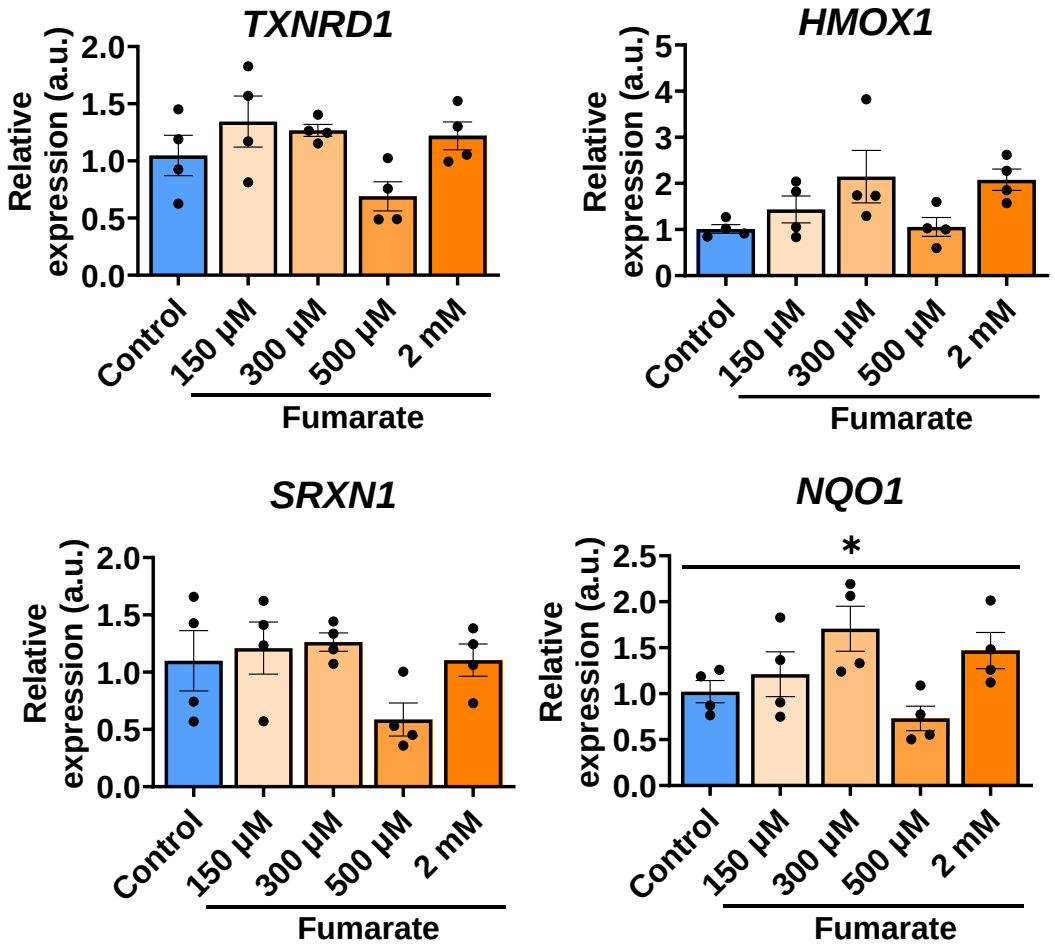

Figure 5.12: Fumarate does not regulate Nrf2 antioxidant target genes in hiPSC-CM, even at different concentrations. hiPSC-CM were exposed to fumarate treatment (150 µM, 300 µM, 500 µM or 2 mM) for 6 hours and compared with untreated cells (Control). The evaluated Nrf2 antioxidant target genes were thioredoxin reductase 1 (*TXNRD1*), heme oxygenase 1 (*HMOX1*), sulfiredoxin 1 (*SRXN1*), and NAD(P) dehydrogenase quinone 1 (*NQO1*). a.u., arbitrary units. * $p < 0.05$ vs. respective control group. Each data point represents a biological replicate.

To further evaluate Nrf2's transcriptional activation, stable HEK293 and H9c2 cell lines constitutively expressing a luciferase reporter vector containing the antioxidant response element (ARE), recognised by nuclear Nrf2, were generated. The effect of dimethyl fumarate (DMF), sulforaphane (SFN), and fumarate in Nrf2 activation was measured using luminescence. HEK293-ARE cells treated with DMF, SFN or fumarate for 6 hours revealed that DMF and SFN rapidly induced a significant increase in Nrf2 activity, while no changes were observed with fumarate treatment at the same time. After 12 hours of treatment, DMF and SFN showed an even more robust Nrf2 activation, whereas fumarate showed a modest significant increase compared with control cells. Following 24 hours of treatment, DMF and SFN massively increased Nrf2 activity by 8- and 5-fold, respectively, compared with control condition, while fumarate significantly increased Nrf2 activity by approximately 2-fold **(Figure 5.13A)**.

The cardiomyocytes H9c2-ARE treated with the same molecules showed that DMF and SFN significantly increased Nrf2 activity after 12 and 24 hours, with the greatest increase observed at 24 hours with a fold change of 3-fold for both molecules compared with the control condition. However fumarate effect on Nrf2 activation was only significantly increased by 16% following 24 hours of treatment compared with the control condition **(Figure 5.13B)**.

These results indicate that DMF, SFN, and fumarate showed a time-dependent effect on Nrf2 activation, with DMF and SFN showing a rapid and increasing impact on Nrf2 activity as the treatment duration was increased. In contrast, fumarate only slightly increased Nrf2 activity at later time points, showing that fumarate did not activate the Nrf2 pathway at the time that the metabolic changes and reduced mitochondria respiration were observed, suggesting that Nrf2 was not the molecular mechanism mediating these changes.

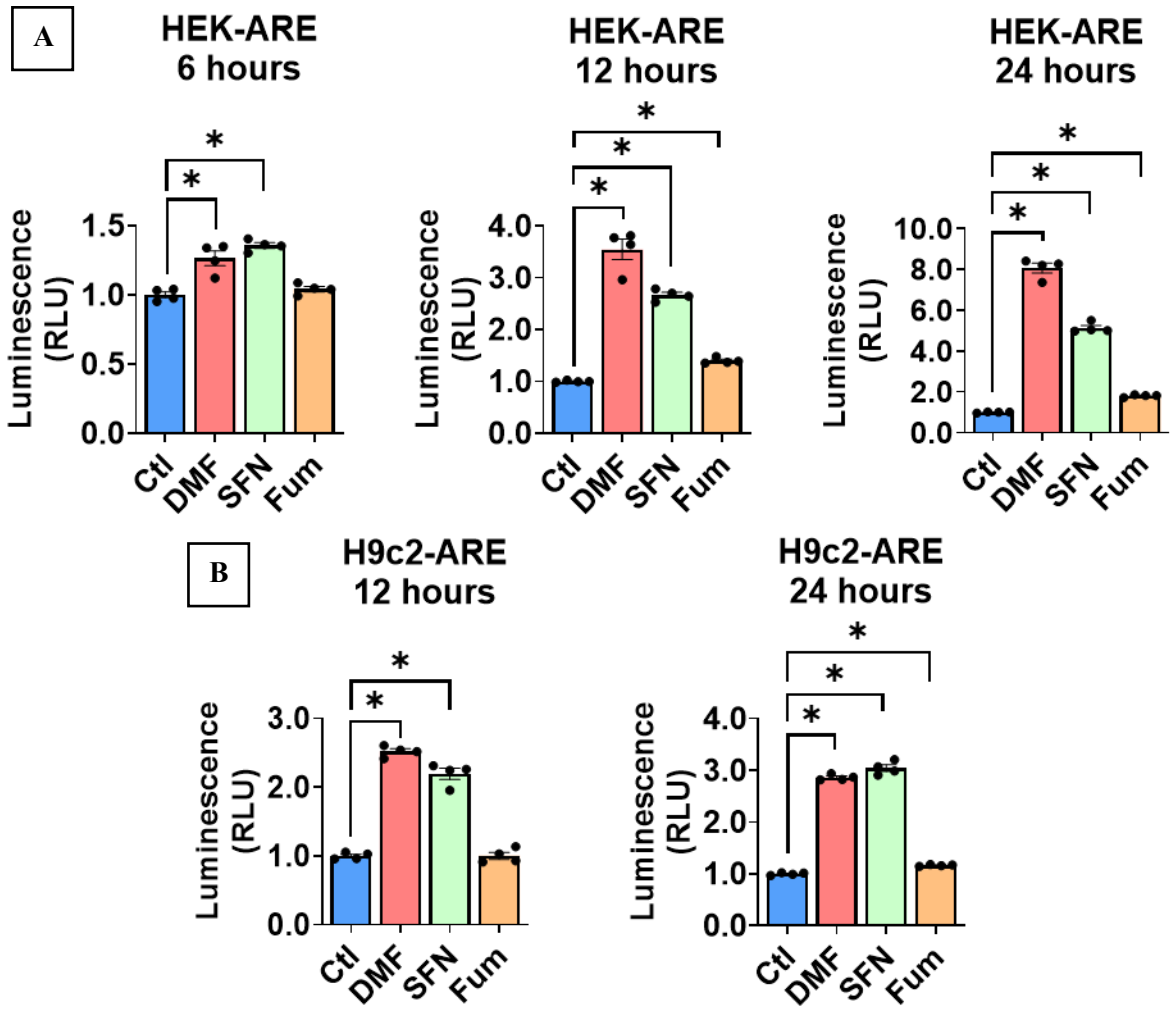

Figure 5.13: Fumarate does not activate Nrf2 at the same time as the metabolic changes were observed in hiPSC-CM. Luciferase reporter vector containing the antioxidant response element (ARE) recognise by Nrf2. Stabe HEK-ARE and H9c2-ARE were exposed to dimethyl fumarate (DMF) (150 µM), sulforaphane (SFN) (5 µM) or fumarate (Fum) (500 µM) treatment for 6, 12 and 24 hours and compared with untreated cells (Ctl). RLU, relative light units. * $p < 0.05$ vs. respective control group. Each data point represents a biological replicate.

5.5.4 Gene set variation analysis shows that fumarate regulates circadian rhythm, hypoxia and G-protein coupled receptor signalling pathway.

Since Nrf2 was not the mechanism by which fumarate modulated the human cardiomyocyte metabolism, gene set variation analysis (GSVA) was performed on the transcriptomics data from fumarate-treated hiPSC-CM to identify possible cellular pathways associated with these changes. GSVA showed that fumarate regulated multiple pathways, including

upregulation of ribosomal proteins, unfolded protein response, mTORC1 signalling, circadian rhythm and hypoxia, as well as the downregulation of GPCRs **(Figure 5.14)**.

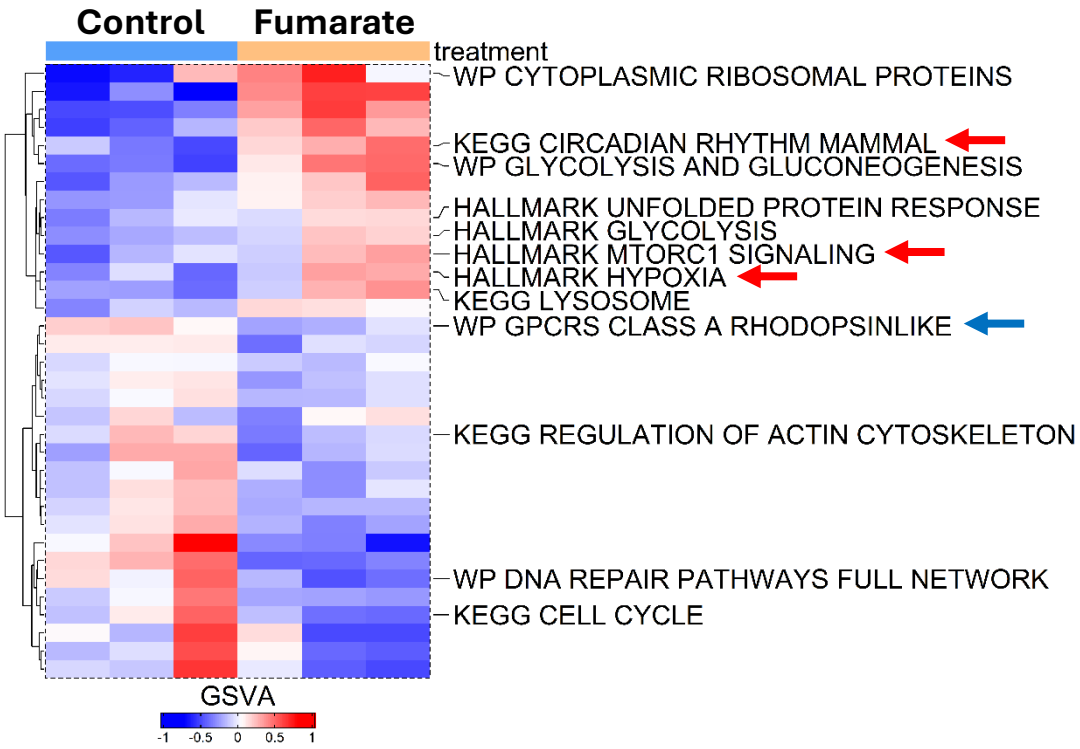

Figure 5.14: Gene set variation analysis comparing fumarate-treated hiPSC-CM with untreated cells. Transcriptomics analyses were performed on hiPSC-CM exposed to fumarate treatment (500 µM) for 6 hours and compared with untreated cells (Control). Arrows indicate the enriched terms that are more relevant to this thesis. Each column represents a biological replicate.

5.5.5 Early fumarate treatment shows that fumarate mainly modulates cell membrane receptor pathways, including the G-protein coupled receptor (GPCR) signalling pathway.

The HIF1 pathway regulates not only metabolic but also several other cellular processes, including apoptotic pathways[262], angiogenesis[263] and cellular survival mechanisms[264], among others. Therefore, to investigate the role of fumarate treatment in upregulating various HIF1-dependent processes, genes from these different pathways were analysed using a heatmap. The results revealed that glycolysis was the only pathway in which all evaluated genes were significantly increased, while "HIF genes" involved in apoptosis,

angiogenesis and survival mechanism were mostly significantly downregulated, or no changes were detected in their expression compared with control cells **(Figure 5.15)**. This selective upregulation of the glycolytic pathway suggested that these genes were misleadingly driving the HIF1 pathway as an upregulated pathway in the fumarate-treated hiPSC-CM transcriptomics data rather than indicating a global increase in the gene expression of the entire pathway. This indicates that a different mechanism may be responsible for the upregulation of the glycolytic metabolism.

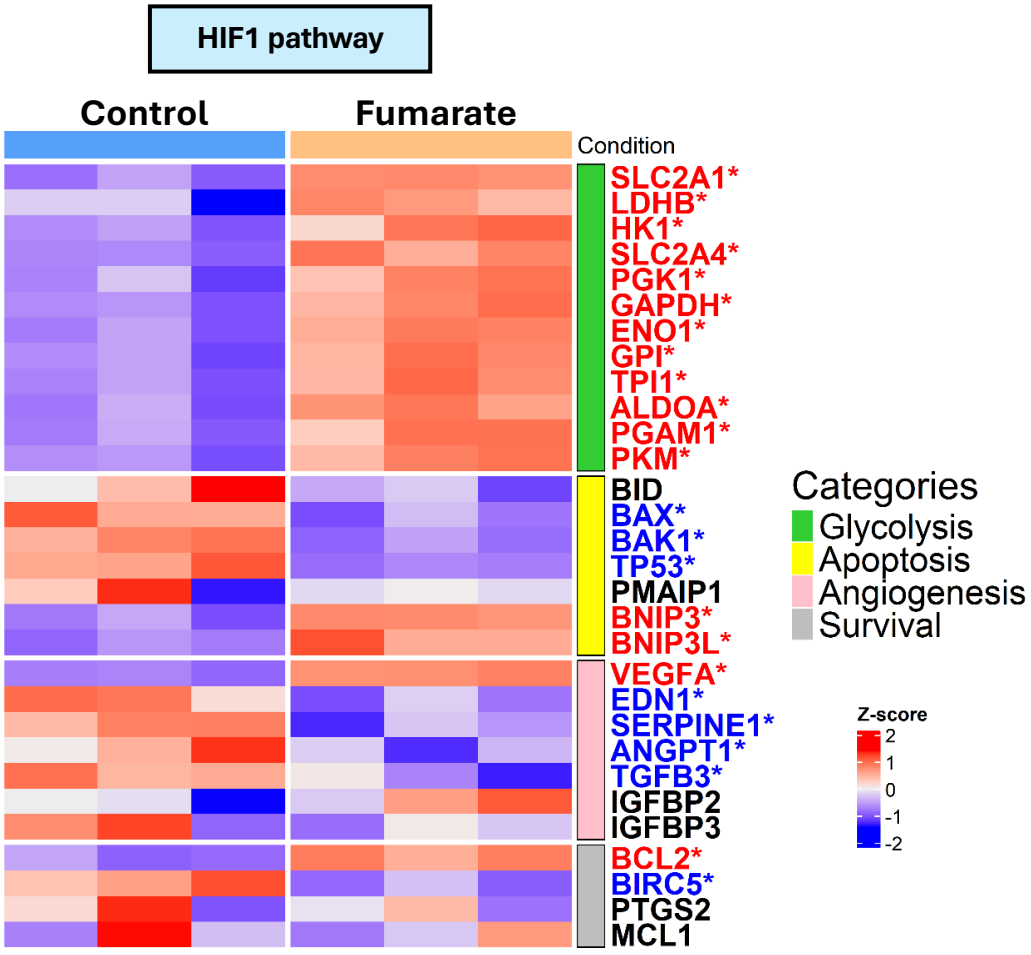

Figure 5.15: Fumarate-induced HIF1 pathway upregulation in hiPSC-CM is specifically driven by the glycolytic genes. Transcriptomics analyses were performed on hiPSC-CM exposed to fumarate treatment (500 µM) for 6 hours and compared with untreated cells (Control). Heatmap representing HIF1 pathway, where the significantly upregulated genes are shown in red, and significantly downregulated genes are shown in blue. *p-adjusted value < 0.05. Each column represents a biological replicate.

The impact of 6 hours fumarate treatment on the circadian rhythm pathway was also evaluated by generating a heatmap of genes involved in this pathway. Fumarate significantly increased the expression of multiple circadian genes compared with the control condition **(Figure 5.16)**. This observation was further corroborated by aligning the list of the significantly regulated genes with the Kyoto Encyclopaedia of Genes and Genomes (KEEG) online database for the circadian rhythm pathway, showing that fumarate was upregulated several genes of this pathway **(Figure 5.17)**.

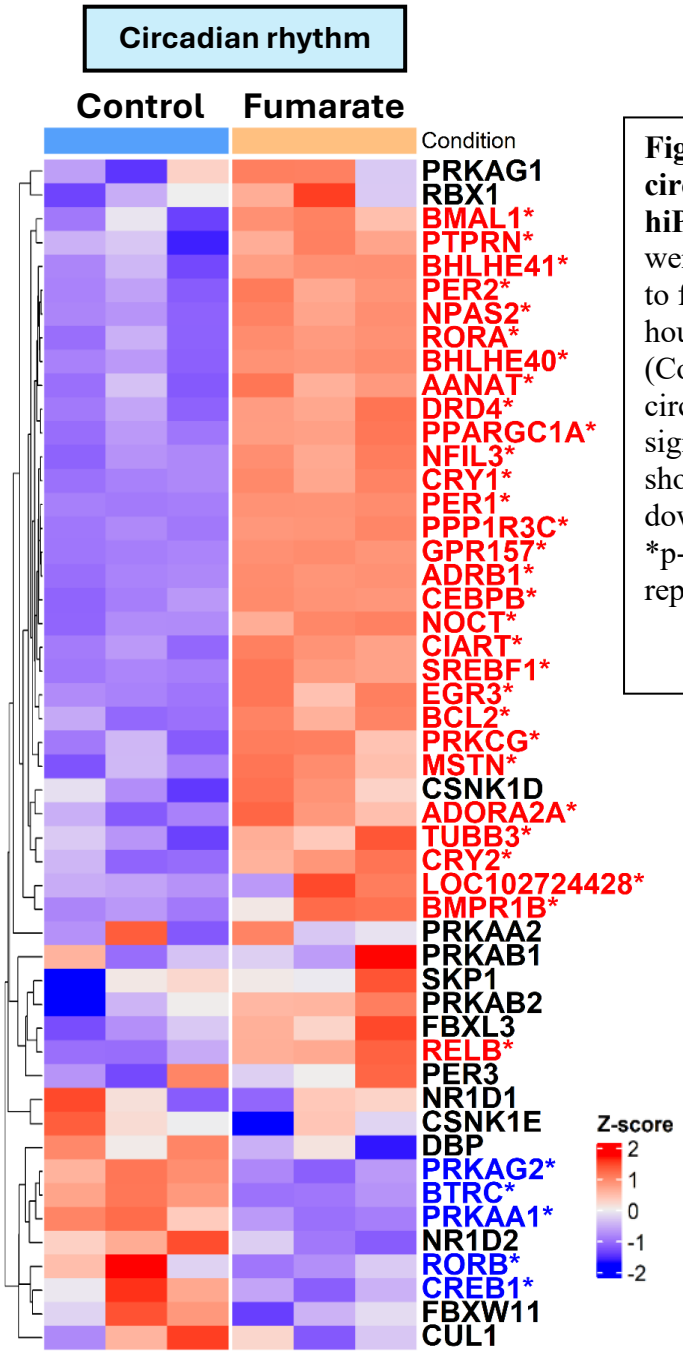

Figure 5.16: Fumarate upregulates circadian rhythm pathway genes in hiPSC-CM. Transcriptomics analyses were performed on hiPSC-CM exposed to fumarate treatment (500 µM) for 6 hours and compared with untreated cells (Control). Heatmap representing circadian rhythm pathway, where the significantly upregulated genes are shown in red, and significantly downregulated genes are shown blue. *p-adjusted value < 0.05. Each column represents a biological replicate.

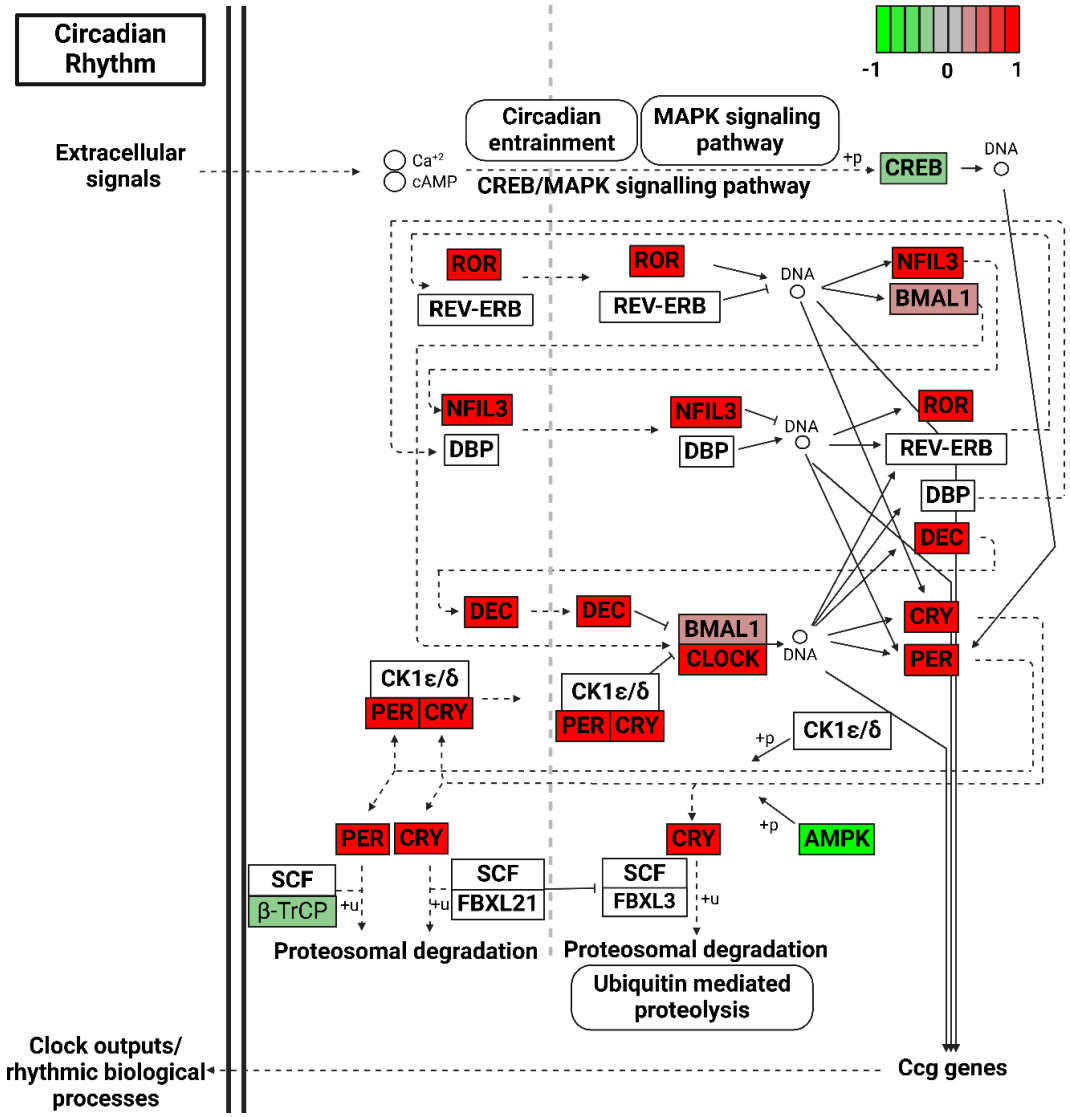

Figure 5.17: Fumarate upregulates circadian rhythm KEGG pathway in hiPSC-CM. Transcriptomics analyses were performed on hiPSC-CM exposed to fumarate treatment (500 µM) for 6 hours and compared with untreated cells (Control). KEGG pathway id hsa04710 was used for circadian rhythm.

If the circadian rhythm pathway were indeed the mechanism driving the metabolic changes observed in the human cardiomyocytes following fumarate treatment, it would be expected that fumarate upregulated the genetic expression of this pathway at a very early time of treatment, prior to the observed metabolic shift. Therefore, to further investigate whether fumarate modulated the circadian rhythm pathway at early times, a new RNA-sequencing experiment was carried out in hiPSC-CM treated with fumarate for only one hour and

compared with untreated cells. Single sample enrichment scores extracted from GSVA analysis for all the circadian rhythm mammal pathway genes, as represented in the open science platform KEGG pathways, revealed no significant differences between untreated and fumarate-treated hiPSC-CM **(Figure 5.18)**.

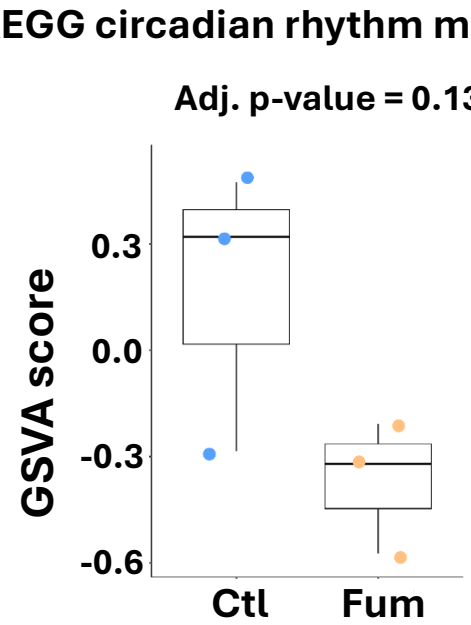

Figure 5.18: One-hour fumarate treatment does not regulate circadian rhythm pathway genes in hiPSC-CM. Transcriptomics analyses were performed on hiPSC-CM exposed to fumarate treatment (500 µM) (Fum) for 1 hour and compared with untreated cells (Ctl). Boxplots represent the GSVA scores for all genes in genes in the circadian rhythm mammal pathway, as defined in KEGG pathways. Each data point represents a biological replicate.

Interestingly, when the effect of one-hour fumarate treatment was studied in the fatty acid oxidation and glycolytic pathways, it was observed that fumarate significantly decreased the expression of the fatty acid oxidation transcriptional coactivator peroxisome proliferator-activated receptor gamma coactivator-1 alpha (*PGC1A/PPARGC1A*), as well as the expression of the glucose metabolism inhibitors pyruvate dehydrogenase kinase (*PDK*), including the cardiac isoform *PDK4* **(Figure 5.19)**. Additionally, fumarate treatment reduced the expression of the free fatty acid transporter *CD36* while increasing the

expression of the glucose transporter *GLUT1* (*SLC2A1*), suggesting that early fumarate treatment modulated the key regulators that may drive the metabolic changes observed at six hours of fumarate treatment.

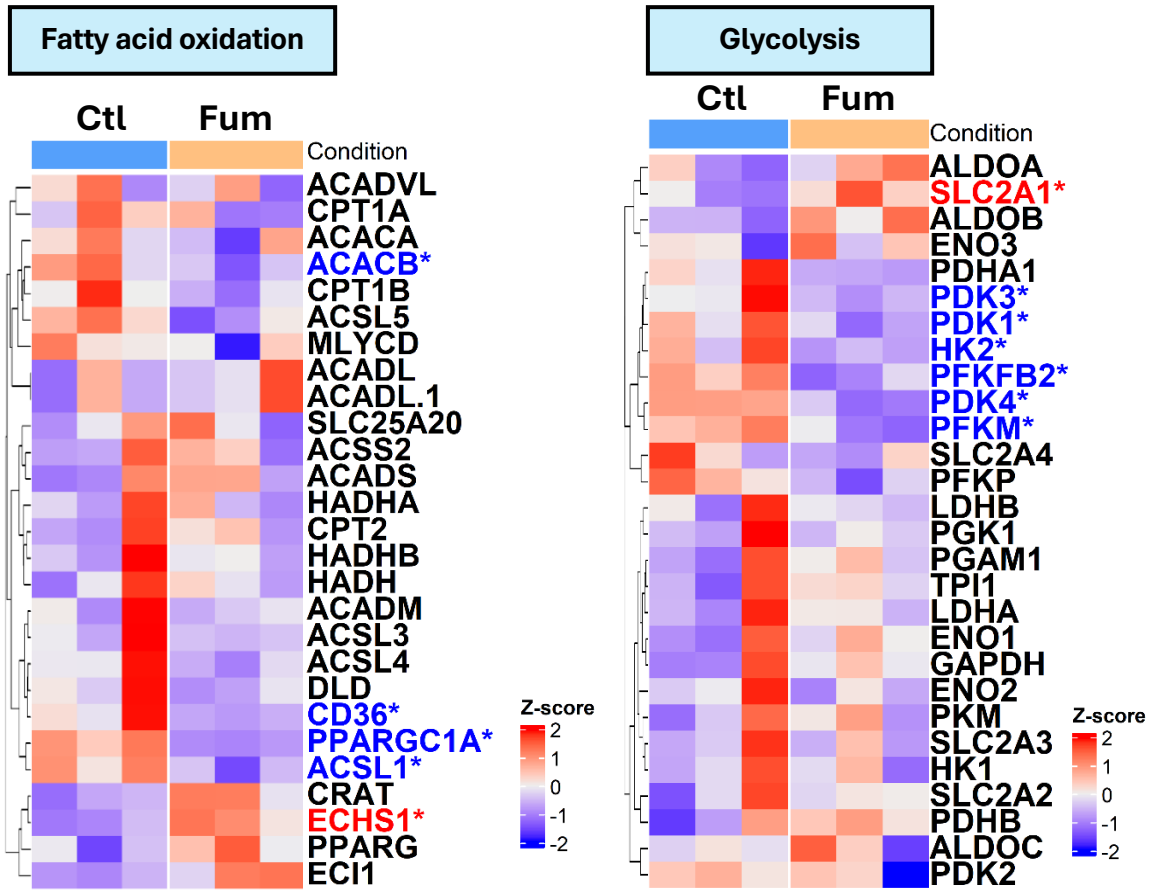

Figure 5.19: One-hour fumarate treatment decreases the expression of the fatty acid transporter CD36, fatty acid oxidation transcriptional coactivator proliferator-activated receptor gamma coactivator-1 alpha, pyruvate dehydrogenase kinase cardiac isoform, and upregulates the glucose transporter 1. Fatty acid oxidation and glycolysis pathway heatmaps were generated using normalised counts from the transcriptomics analyses on hiPSC-CM exposed to fumarate treatment (500 µM) (Fum) for 1 hour and compared with untreated cells (Ctl)**.** Significantly upregulated genes are shown in red, and significantly downregulated genes are shown in blue. *p-adjusted value < 0.05. Each column represents a biological replicate.

GSVA showed that hiPSC-CM exposed to fumarate for one hour presented a significant downregulation of the GPCRs receptor pathway, complemented by a significant reduction of the small ligand GPCRs pathway and other receptor-ligan pathways, such as cytokine receptor interaction, androgen receptor, and glucocorticoid receptor **(Figure 5.20A)**. These

results suggest that early fumarate treatment was modulating various receptor pathways located at the cell membrane. The effect of one-hour fumarate treatment on GPCRs receptor signalling pathway was further measured by generating an enrichment plot using gene set enrichment analysis (GSEA). GSEA showed that just one hour of fumarate treatment significantly reduced GPCRs class A rhodopsin-like pathway with a strong negative normalised enrichment score (NES) of -1.9, and with the lower enrichment score (ES) around -4.6 at the bottom of the ranked genes **(Figure 5.20B)**.

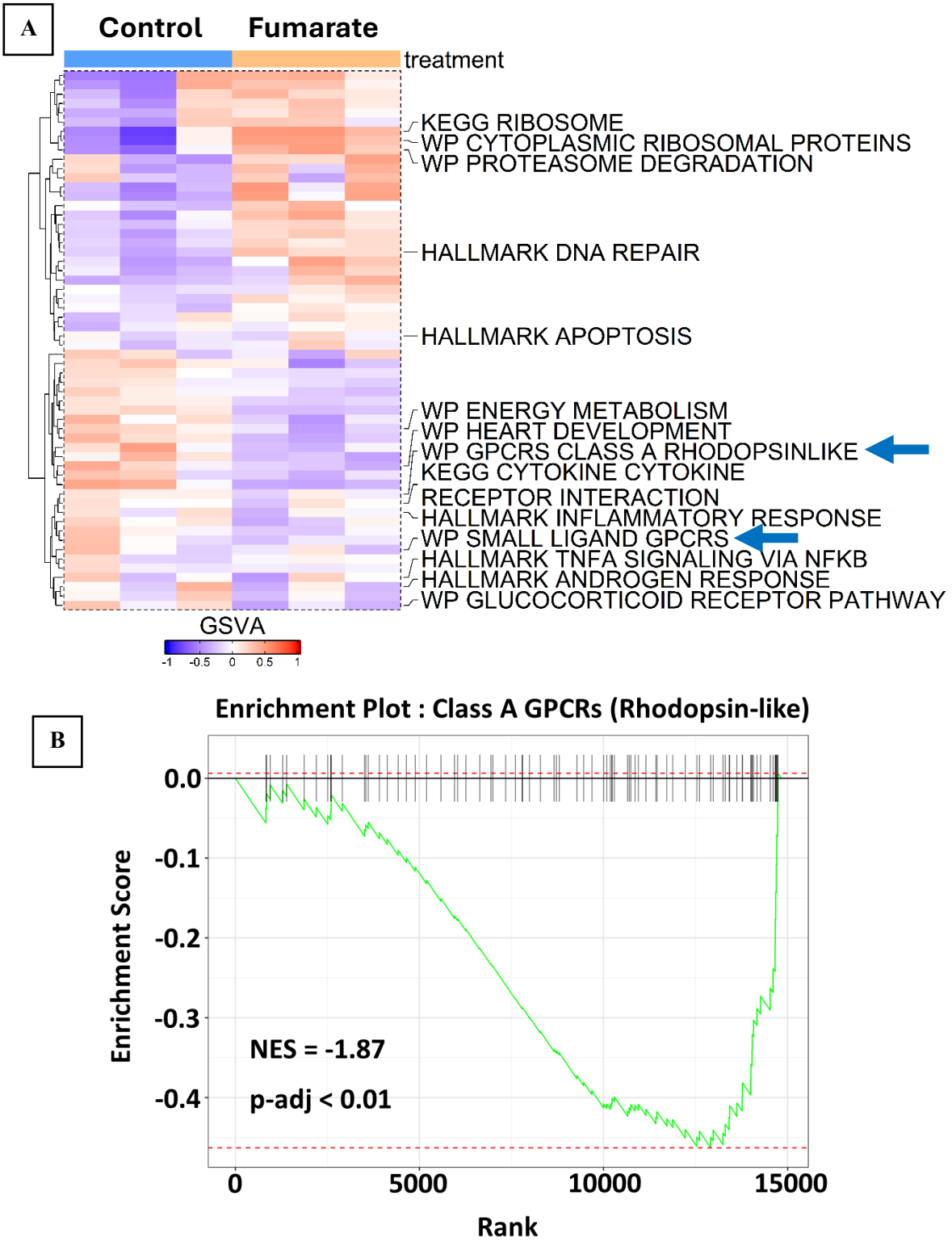

Figure 5.20: One-hour fumarate treatment decreases G-protein coupled membrane receptor signalling pathway. Transcriptomics analyses on hiPSC-CM exposed to fumarate treatment (500 µM) for 1 hour and compared with untreated cells. **(A)** Significant regulated pathways in Gene set variation analysis comparing (GSVA). Each column represents a biological replicate. **(B)** Enrichment plot for GPCRs class A rhodopsin-like pathway extracted from Gene set enrichment analysis (GSEA).

The results of this section suggest that among all the cellular pathways analysed, the GPCRs receptor signalling pathway was consistently identified as a target following both one hour and six hours of fumarate treatments. In contrast, the HIF1 pathway appeared to be enriched just by the expression of the glycolytic genes and not for an overall upregulation of the pathway, and the circadian rhythm pathway only was activated after six hours of fumarate treatment.

5.5.6 Fumarate decreases protein succination in human cardiomyocytes.

Another potential intracellular molecular mechanism through which fumarate could induce metabolic changes was via protein post-translation modifications (PTM). According to the literature, fumarate has been proposed as a molecule which can oxidize the sulfhydryl group in protein cysteine residues into S-(2-succino) cysteine via a Michael addition reaction[144, 265-267], PTM known as succination. This PTM has also been reported as the mechanism by which DMF induces Nrf2 pathway activation[54, 132]. Therefore, the impact of fumarate and DMF on protein succination in hiPSC-CM was evaluated using a total S-(2-succino) cysteine (2SC) antibody and western blotting. Unexpectedly, fumarate significantly reduced the total 2SC protein content by 35%, while, DMF treatment showed a significant increase in 2SC protein levels by 45%, with an additional protein band compared with the control condition **(Figure 5.21)**.

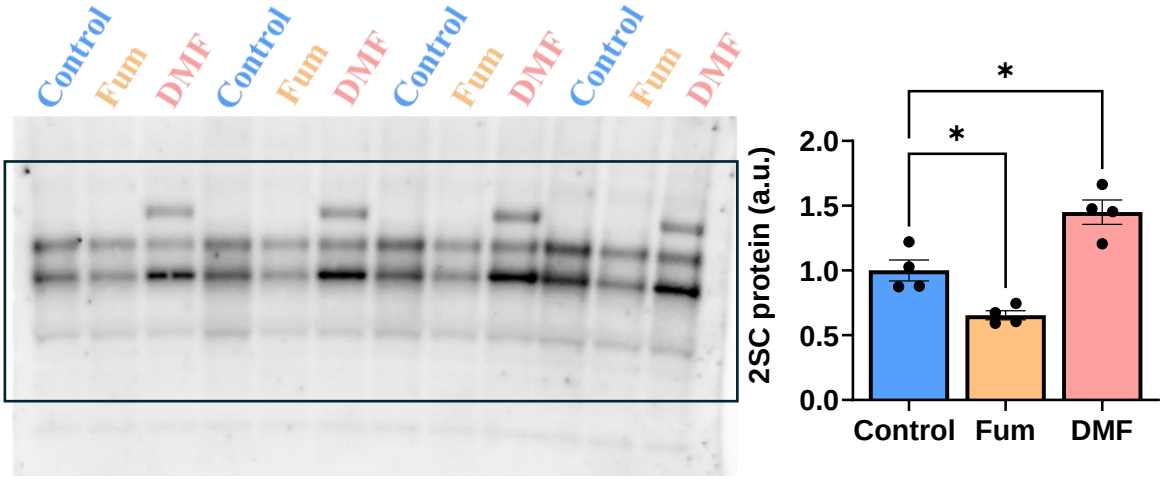

Figure 5.21: Fumarate decreases succination levels, while dimethyl fumarate increases them in hiPSC-CM. S-(2-succino) cysteine (2SC) protein level in hiPSC-CM exposed to fumarate (Fum, 500 µM) or dimethyl fumarate (DMF, 150 µM) for 6 hours and compared with untreated cells hiPSC-CM control. Western blotting densitometry analysis was performed in the area selected by the rectangle. * $p < 0.05$ vs. respective control group. a.u., arbitrary units. Each data point represents a biological replicate.

5.5.7 Fumarate is transported across the sarcolemma by the monocarboxylate transporter 1 in hiPSC-CM.

Previously, we observed in Chapter 3 that fumarate intracellular concentrations within the rat heart increased under hypoxia, but we also questioned whether fumarate remained intracellular or could also be released. However, before measuring fumarate release from the human cardiomyocytes, I evaluated whether our hiPSC-CM model could respond to hypoxic conditions. HiPSC-CM were exposed to 2% O_2 for 16 hours, and the hypoxia response was confirmed by observing an upregulation of glycolytic pathway genes **(Figure 5.22A)**. Additionally, a significant increase in the final product of anaerobic metabolism, lactate, by 2-fold was detected in the cell media from the hypoxic cells compared with the cell media of normoxic cells **(Figure 5.22B)**.

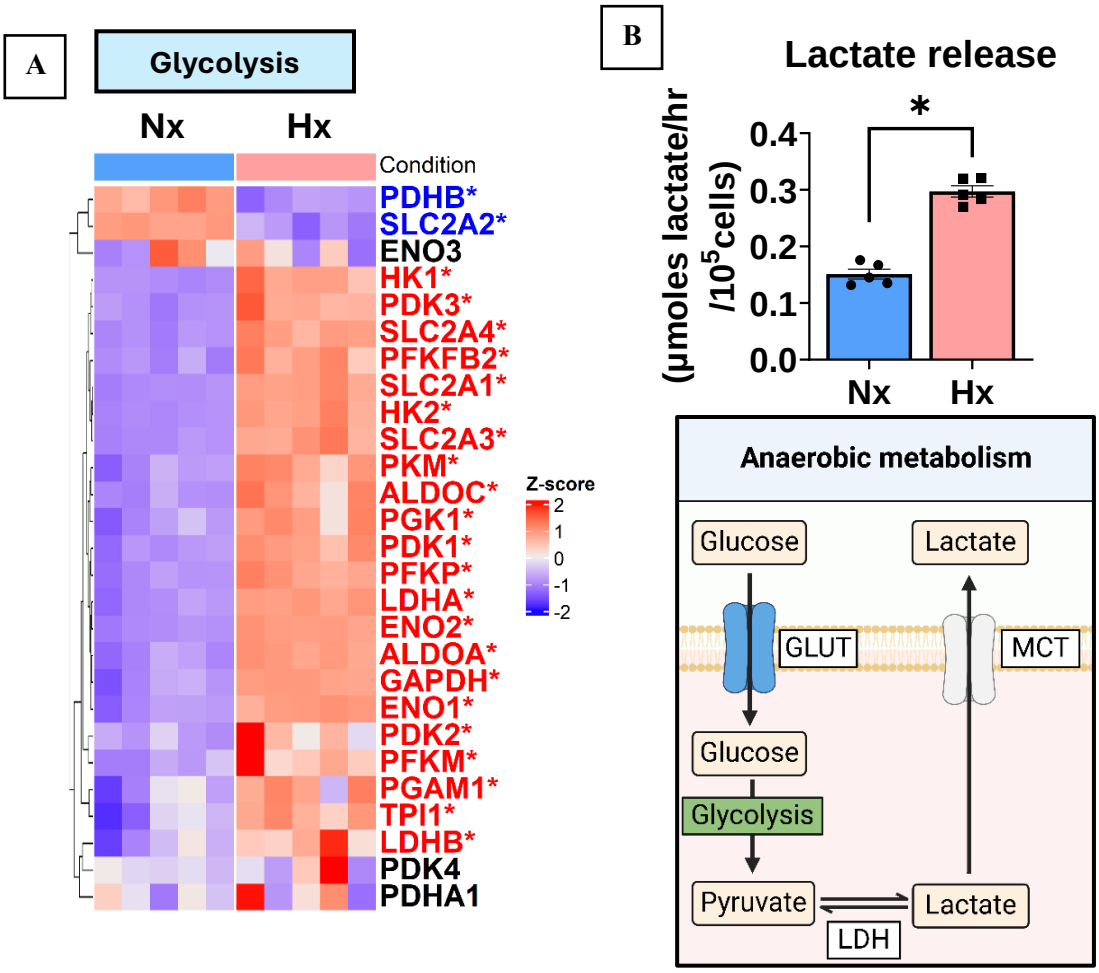

Figure 5.22: Chronic hypoxia upregulates glycolytic metabolism hiPSC-CM. Transcriptomics analyses were performed on hiPSC-CM exposed to hypoxia (2% O_2) (Hx) for 16 hours and compared with normoxic cells (21% O_2) (Nx). **(A)** Glycolysis pathway heatmap representation, where the significantly upregulated genes are shown in red, whereas significantly downregulated genes are shown in blue. *p-adjusted value < 0.05. **(B)** Lactate release into the cell media. * $p < 0.05$ vs. normoxia group. GLUT, glucose transporter. LDH, lactate dehydrogenase. MCT, monocarboxylate transporter. Each column in the heatmap represents a biological replicate. Each data point in the graph represents a biological replicate.

To evaluate whether hiPSC-CM released fumarate under hypoxic conditions, fumarate levels in the cell media were quantified. Hypoxia caused a 54% increase in the fumarate released into the cell media compared with media from normoxia cells. There was no significant difference in the concentration of the cytoplasmatic enzyme lactate dehydrogenase (LDH) in the media, suggesting that the increased extracellular fumarate was

not caused by cell membrane damage but instead exported by a specific membrane transporter **(Figure 5.23)**.

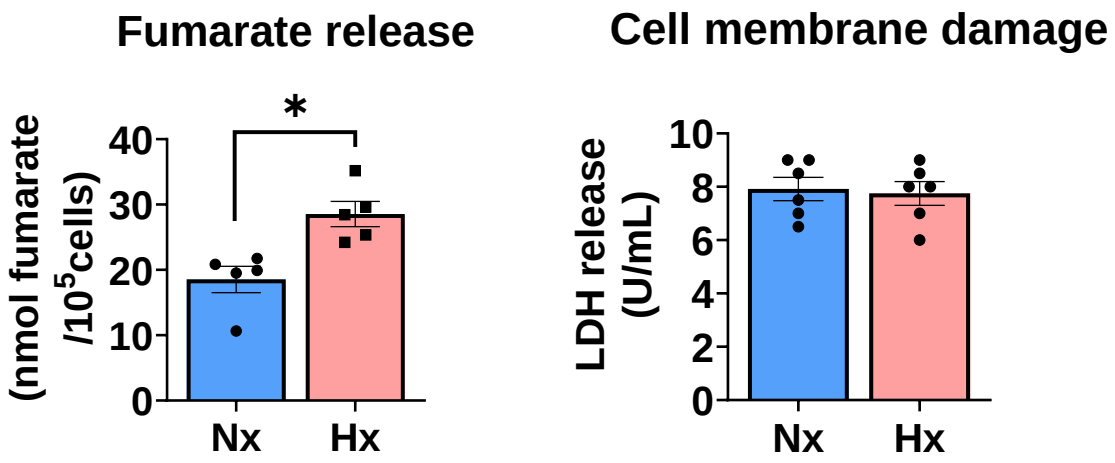

Figure 5.23: Hypoxia causes an increase in fumarate release from hiPSC-CM. hiPSC-CM were exposed to hypoxia (2% O_2) (Hx) for 16 hours, and fumarate levels in the cell media were measured after 16 hours of hypoxic conditions. Media lactate dehydrogenase (LDH) levels were determined after 24 hours of hypoxia and compared with media from normoxic cells (21% O_2) (Nx). * $p < 0.05$ vs. normoxia group. Each data point represents a biological replicate.

The monocarboxylate transporter 1 (MCT1) facilitates the sarcolemmal transport of metabolites structurally similar to fumarate within the heart, including lactate[(268)], malonate[(269)], and succinate[(102)]. Therefore, its role in fumarate release under hypoxia was evaluated using the MCT1 inhibitor AZD396, and fumarate levels in the cell media were quantified using the liquid chromatography-triple quadrupole-mass spectrometry targeted metabolomics **(Figure 5.24)**. Similar to our previous result, hypoxia caused a significant 71% increase in fumarate release into the media compared with normoxia. However, this elevation was dramatically suppressed after MCT1 inhibitor treatment, reducing fumarate extracellular levels by 33% compared with untreated hiPSC-CM under hypoxic conditions. This result demonstrated that under hypoxic conditions, human cardiomyocytes released fumarate into the extracellular space via MCT1.

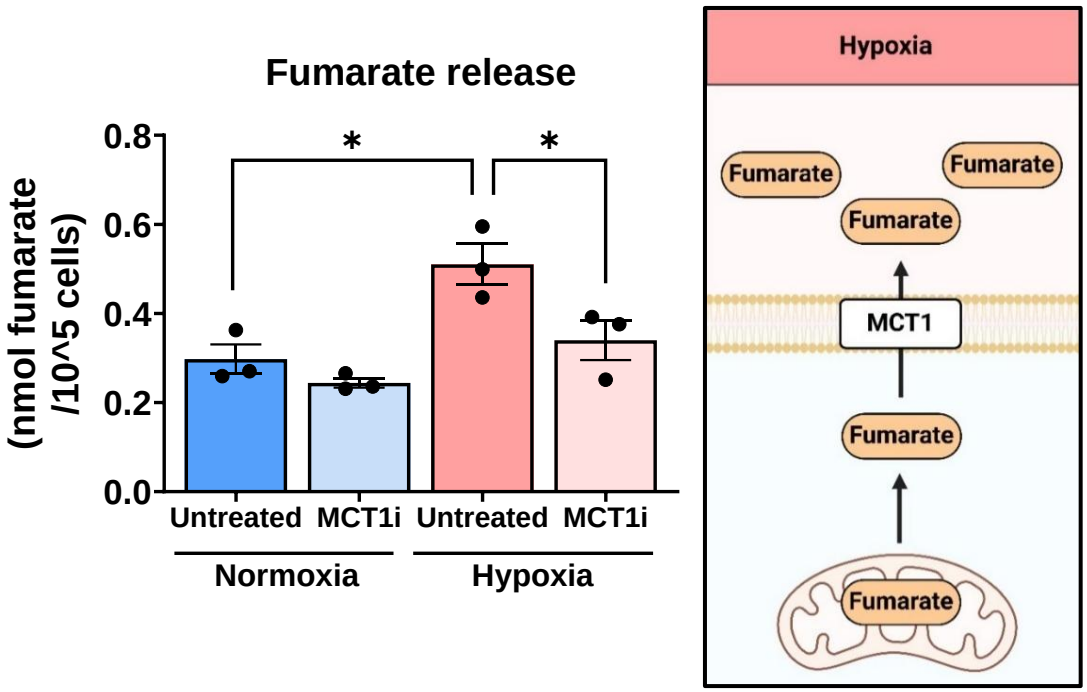

Figure 5.24: Fumarate release into the cell media is mediated by the monocarboxylate transporter 1 in human cardiomyocytes. hiPSC-CM were exposed to the monocarboxylate transporter 1 inhibitor AZD3965 (MCT1i) (100 nM), incubated under hypoxia (2% O2) or normoxia for 16 hours, and compared with untreated cells. * $p < 0.05$ vs. respective control group. Each data point represents a biological replicate.

5.5.8 *In silico* analysis shows the hydroxycarboxylic acid receptor 2 to be a fumarate target.

Given that fumarate is released in the media and that the transcriptomics data showed fumarate regulating genes from various receptor pathways, we questioned whether fumarate could directly modulate membrane receptors. Since both fumarate and DMF transcriptomic analysis showed that G-protein coupled receptor (GPCR) signalling pathways were significantly downregulated, their effect on this pathway was further investigated. To visualise the extent of these molecules modulating membrane receptors, as a first approach, GPCRs pathway genes were extracted from the metascape data of both DMF and fumarate transcriptomics data, and their effect was compared by generating a cnetplot of these genes. This comparison revealed that both molecules downregulated common and unique genes

involved in GPCR signalling pathways, but fumarate significantly regulated a larger population of these genes compared with DMF treatment **(Figure 5.25)**.

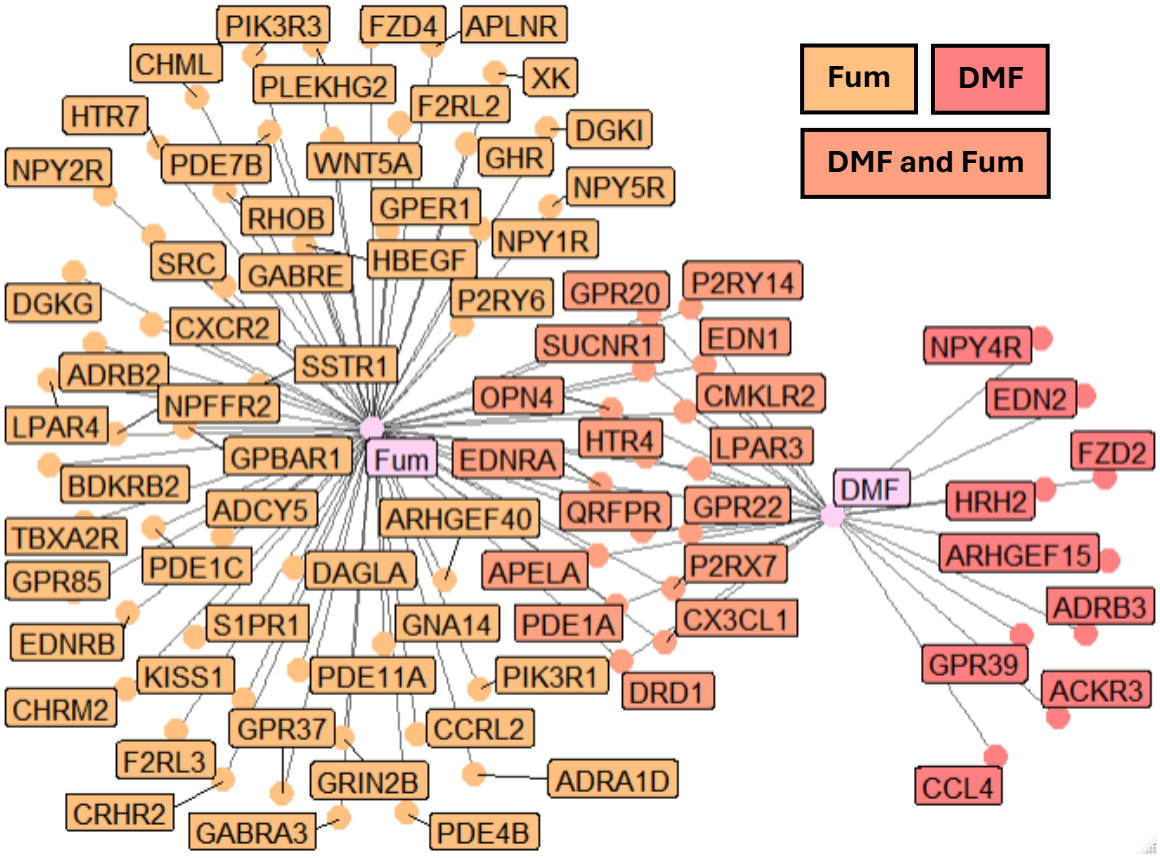

Figure 5.25: Fumarate downregulates a more extensive set of G protein-coupled receptors (GPCRs) genes than dimethyl fumarate in hiPSC-CM. hiPSC-CM were exposed to dimethyl fumarate (DMF) (150 µM) or fumarate (Fum) (500 µM) treatment for 6 hours, and a cnetplot plot was generated to compare the GPCR pathway genes downregulated by fumarate (Fum) and dimethyl fumarate (DMF).

The role of fumarate beyond the genetic regulation of the GPCR pathway was also explored by investigating its physical interaction with this membrane receptors family. For this, the SwissTargetPrediction online tool was used to perform *in silico* target prediction of fumarate and its derivatives with several cellular components. Surprisingly, dimethyl fumarate (DMF), monomethyl fumarate (MMF), and fumarate showed potential *in silico* interaction with a member of the GPCRs family, the hydroxycarboxylic acid receptor 2 (HCA2) **(Figure**

5.26). MMF presented the highest probability of interaction, whereas fumarate the lowest. Interestingly, indolethylamine N-methyltransferase (INMT) was also a common target among DMF, MMF and fumarate, however, INMT is a cytoplasmatic enzyme, therefore the following experiments were focused on HCA2.

DMF	Target	Common name	Target Class	Probability*
	Hydroxycarboxylic acid receptor 2	HCA2	Family A G protein-coupled receptor	
	Indolethylamine N-methyltransferase	INMT	Enzyme	
	Acyl coenzyme A:cholesterol acyltransferase	CES1	Enzyme	
	Carboxylesterase 2	CES2	Enzyme	

MMF	Target	Common name	Target Class	Probability*
	Hydroxycarboxylic acid receptor 2	HCA2	Family A G protein-coupled receptor	
	Indolethylamine N-methyltransferase	INMT	Enzyme	
	Egl nine homolog 3	EGLN3	Enzyme	
	Solute carrier family member 6	SLC22A6	Electrochemical transporter	

Fum	Target	Common name	Target Class	Probability*
	Indolethylamine N-methyltransferase	INMT	Enzyme	
	Carbonic anhydrase II	CA2	Lyase	
	Carbonic anhydrase I	CA1	Lyase	
	Carbonic anhydrase XII	CA12	Lyase	
	Carbonic anhydrase IX	CA9	Lyase	
	Hydroxycarboxylic acid receptor 2	HCA2	Family A G protein-coupled receptor	

Figure 5.26: Fumarate and fumarate derivates interact *in silico* with the hydroxycarboxylic acid receptor 2. Dimethyl fumarate (DMF), monomethyl fumarate (MMF), and fumarate (Fum) *in-silico* target prediction using SwissTargetPrediction online tool.

The interaction between fumarate and its derivatives with the HCA2 membrane receptor was further studied using molecular docking and utilising the HCA2 crystallised structure extracted from the protein database online website (PDB ID 7XK2). The HCA2 receptor

was crystallised bound to the molecule MK-6892, a high-affinity agonist of this receptor, which, after molecular modelling analysis with the extracellular pocket of the receptor, revealed that the amino acid residues arginine 111 (Arg111), tyrosine 284 (Tyr284) and serine 179 (Ser179) were crucial for its interaction with the HCA2 receptor **(Figure 5.27)**.

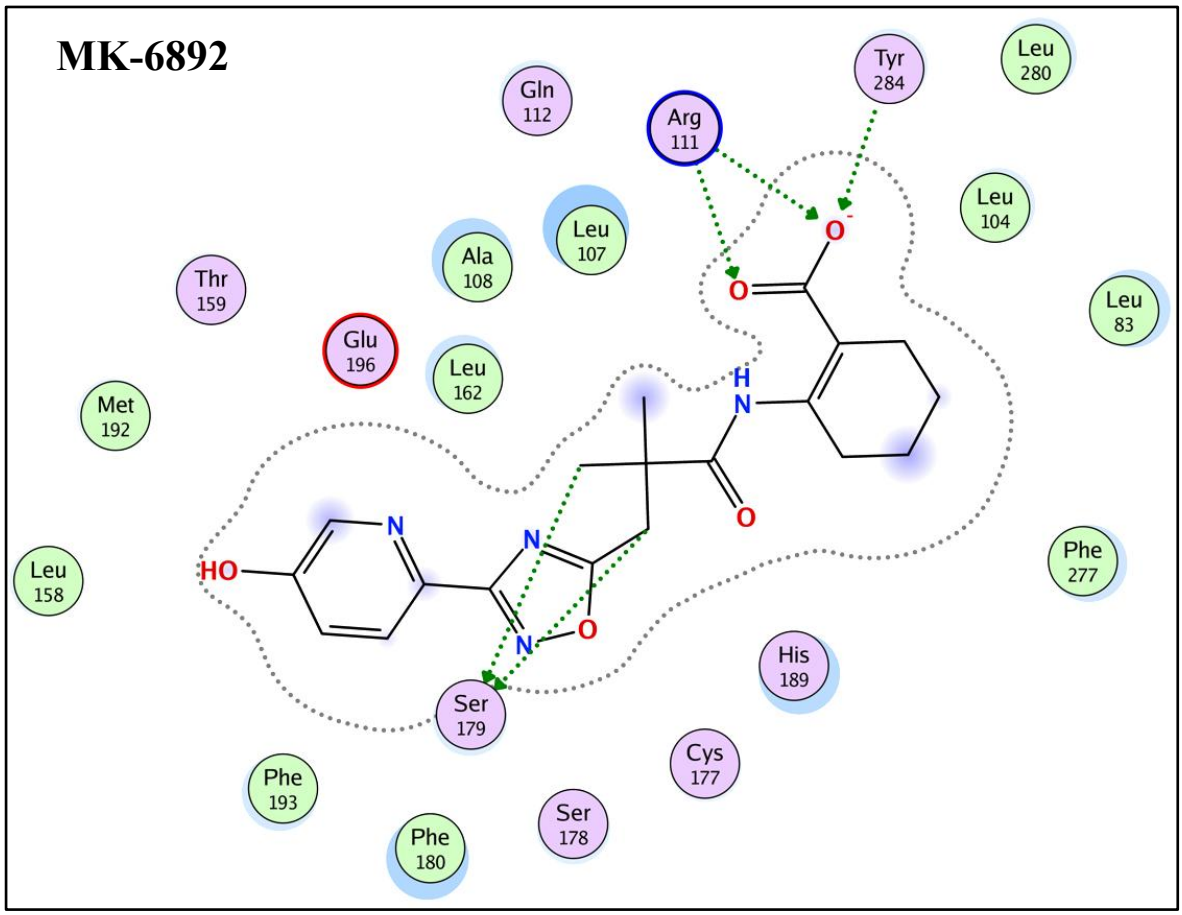

Figure 5.27: Molecular modelling shows that Arg111, Tyr284, and Ser179 residues in the hydroxycarboxylic acid receptor 2 are critical for interacting with its MK-6892 agonist. Molecular docking between MK-6892 and the hydroxycarboxylic acid receptor 2 (HCA2) membrane receptor. HCA2 and MK-6892 structures were obtained from the Protein Data Bank (PDB ID 7XK2).

Molecular docking of monomethyl fumarate (MMF) inside the HCA2 extracellular pocket using the two more favourable orientations identified that MMF could interact with the residues Ser179 and Arg111, the same residues observed before for the agonist MK-6892, suggesting that MMF could act as an agonist of this receptor **(Figure 5.28)**. Similarly,

molecular modelling of fumarate within the extracellular pocket of HCA2 showed this metabolite interacting with the residue Arg111, indicating the critical role of this residue in the fumarate-HCA2 interaction **(Figure 5.29)**. Subsequent structural illustration of this interaction using pyMol determined that the distance between oxygen from the carboxyl group of the fumarate molecule and the hydrogen from the guanide group in the side chain of arginine residue was 2.6 angstroms, a value within the typical range required for a hydrogen bond[270], suggesting that the interaction between fumarate and arginine 111 is very probable.

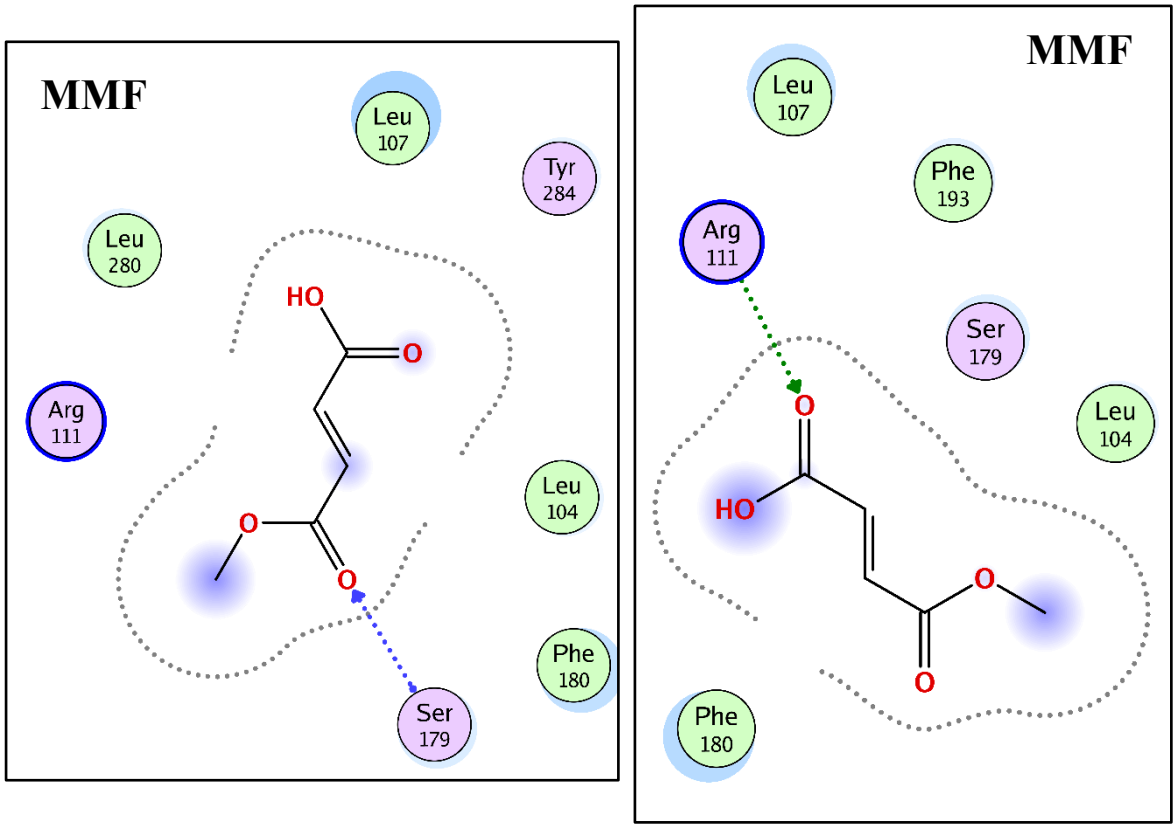

Figure 5.28: Molecular modelling shows that monomethyl fumarate interacts with the hydroxycarboxylic acid receptor 2 similarly to the MK-6892 agonist. Molecular docking between two different orientations of monomethyl fumarate (MMF) and the hydroxycarboxylic acid receptor 2 (HCA2) membrane receptor. HCA2 structure was obtained from the Protein Data Bank (PDB ID 7XK2).

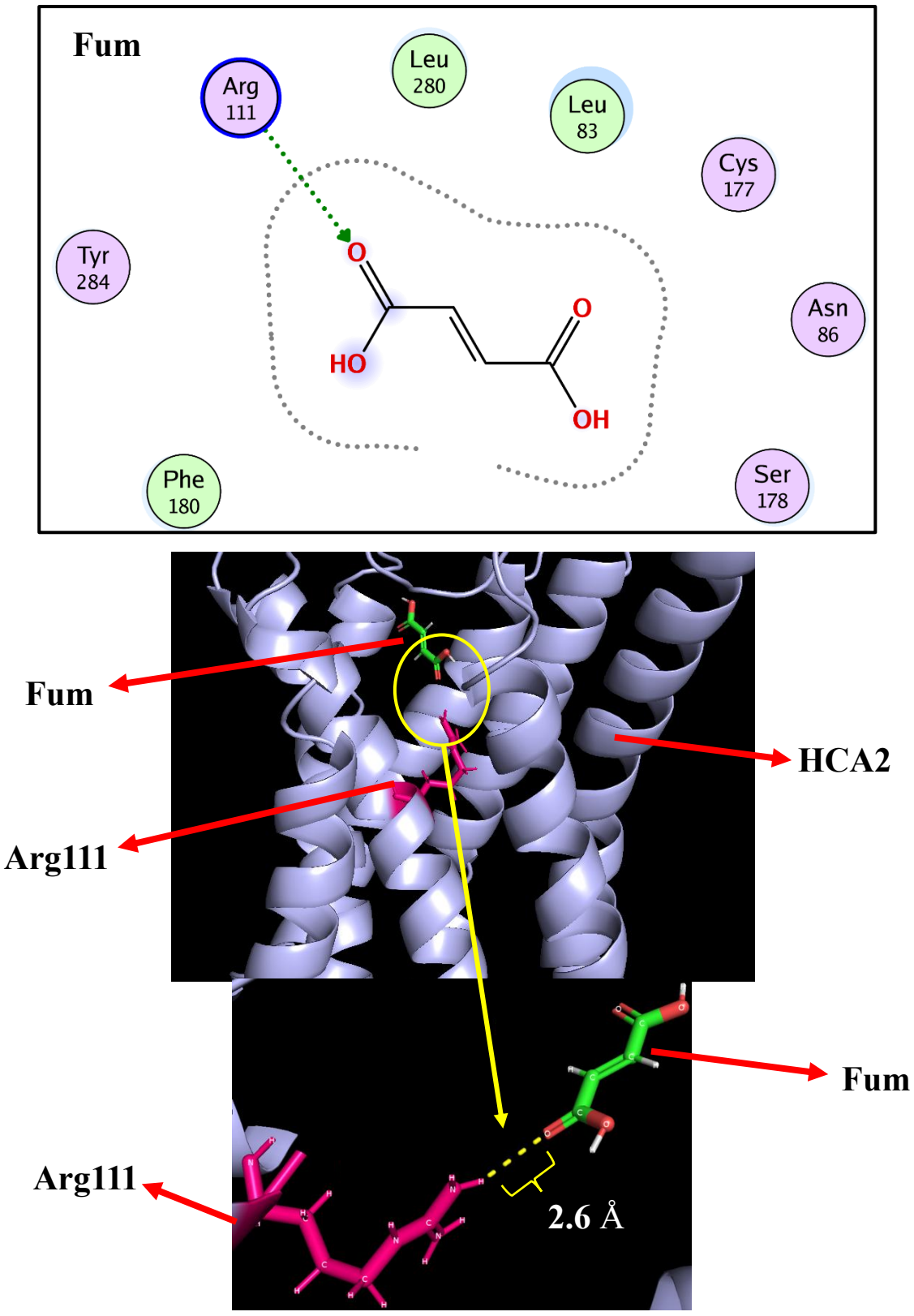

Figure 5.29: Molecular modelling shows that residue arginine 111 is crucial for fumarate interaction with the hydroxycarboxylic acid receptor 2. Molecular modelling between fumarate (Fum) and the hydroxycarboxylic acid receptor 2 (HCA2) membrane receptor. HCA2 structure was obtained from the Protein Data Bank (PDB ID 7XK2).

Fumaric acid has two protonated carboxyl groups with pKa1 =3.03 and pKa2 =4.54[271], hence, both carbonyl groups are deprotonated at physiological pH or pH above these values, generating two carboxylate ions in the fumarate structure (dicarboxylate fumarate). To evaluate whether the pH and fumarate conformation were necessary for its interaction with HCA2, molecular docking of the dicarboxylate fumarate was assessed using four different orientations. The analysis showed that in all the configurations, dicarboxylate fumarate interacted with Arg111. In two assessed positions, dicarboxylate fumarate additionally interacted with Ser179 residue, also observed for HCA2 interaction with the agonist MK-6892, and in one confirmation, fumarate *in silico* was further interacting with histidine 189 (His189) **(Figure 5.30)**.

In silico molecular modelling and docking demonstrated that both MMF and fumarate potentially interact with the extracellular pocket of the GPCR receptor HCA2. Our data showed that the residue arginine 111 on HCA2 was critical for receptor-ligand binding, as was observed comparing these bioactive molecules with the potent HCA2 agonist MK-6892. Finally, after evaluating the potential effect of fumarate deprotonation in its ability to bind to HCA2, we observed that the interaction between the Arg111 in the receptor with fumarate occurred independently of fumarate configuration.

Decarboxylated fumarate (Fum 2-)

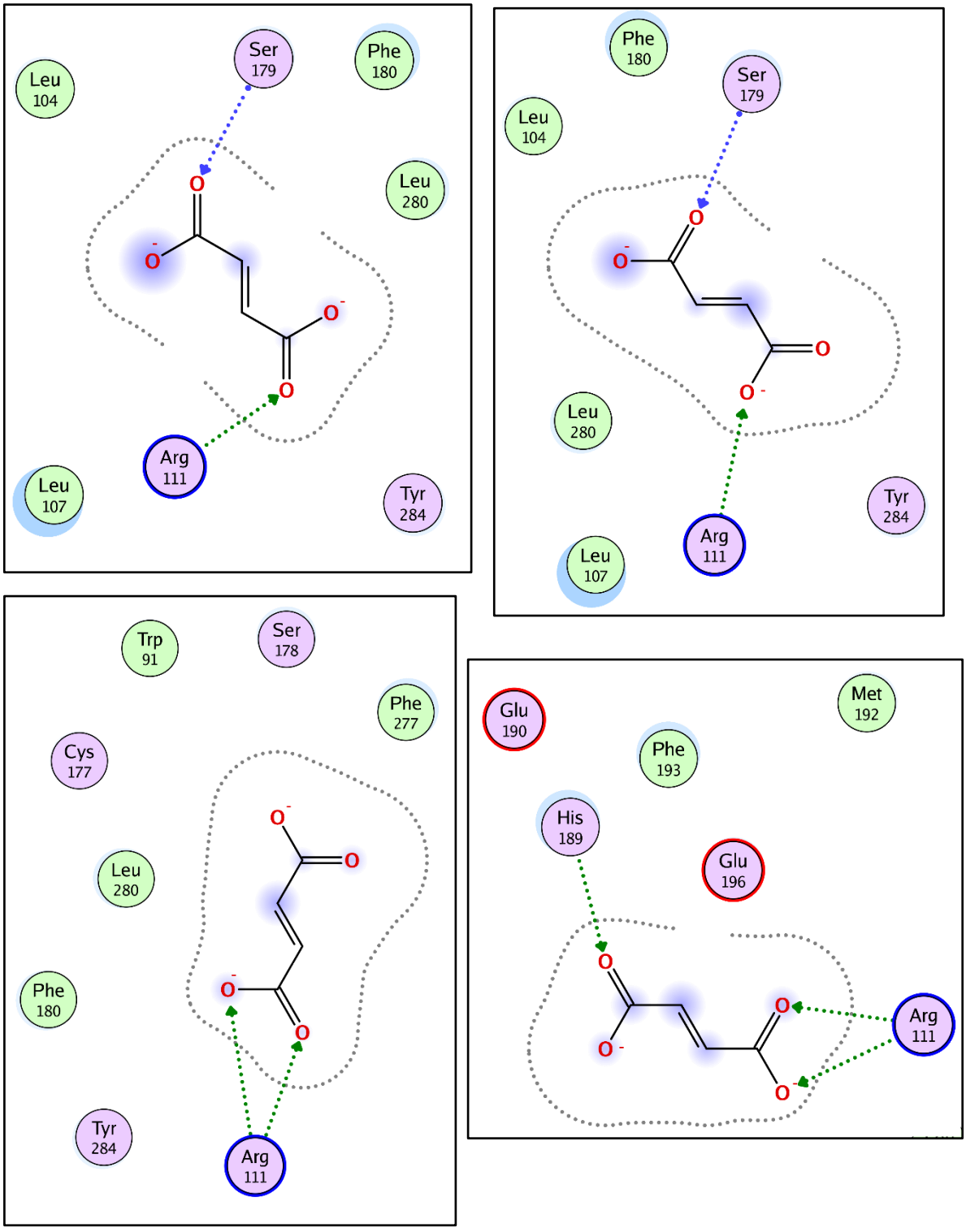

Figure 5.30: Molecular modelling shows that decarboxylated fumarate interacts with residue arginine 111 within the hydroxycarboxylic acid receptor 2, similar to fumaric acid. Molecular modelling of decarboxylated fumarate (Fum 2-) with hydroxycarboxylic acid receptor 2 (HCA2). HCA2 structure was obtained from a protein database (PDB ID 7XK2).

5.5.9 Fumarate decreases cAMP response evoked by forskolin.

HCA2 is a Gi-coupled protein receptor, which means that its activation inhibits adenylyl cyclase and decreases cAMP levels. The role of HCA2 has been mainly studied in adipocytes and immune cells[243], and because its expression in other cell types has not been well described, *HCA2* expression was studied by qPCR in two different cardiomyocyte models **(Figure 5.31)**. *HCA2* gene expression was evaluated as ΔCt (*HCA2* gene expression minus the housekeeping gene expression) in human (mature hiPSC-CM) and rat (H9c2) cardiomyocytes. We observed that both models of cardiomyocytes were expressing the gene that codes for this receptor, and additionally, *HCA2* expression in human cardiomyocytes was significantly higher (lower ΔCt) than in rat cardiomyocytes.

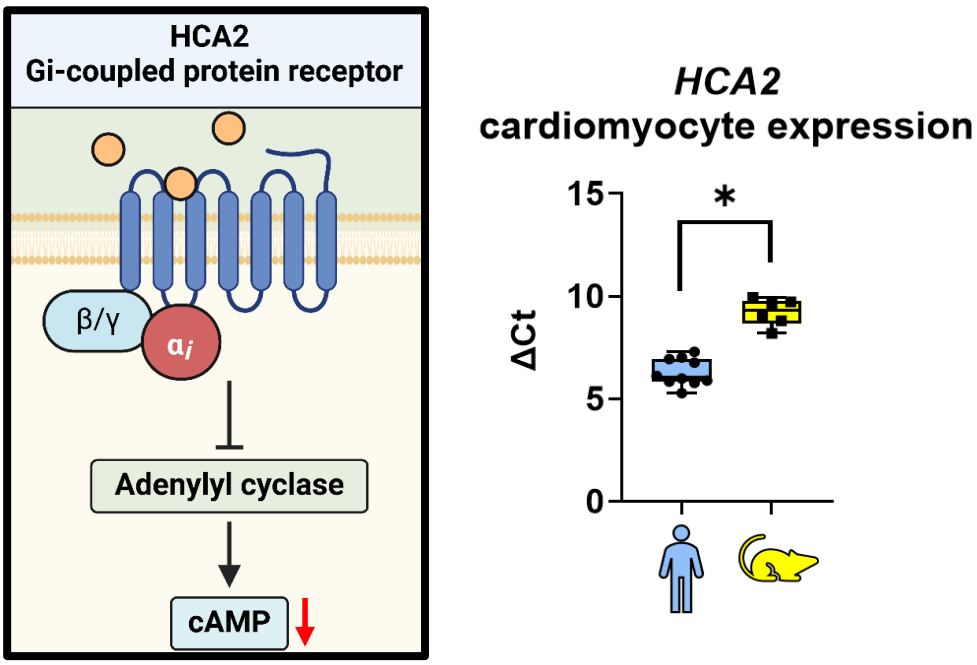

Figure 5.31: Hydroxycarboxylic acid receptor 2 is expressed in both human and rat cardiomyocytes. Hydroxycarboxylic acid receptor 2 (*HCA2*) genes expression in mature hiPSC-CM and H9c2 rat cardiomyocyte cells. * $p < 0.05$ vs. hiPSC-CM expression. Each data point represents a biological replicate.

To evaluate whether fumarate derivatives and fumarate could acutely activate Gi-coupled signalling, an EPAC (exchange protein directly activated by cAMP) FRET sensor assay was used in neonatal rat ventricular cardiomyocytes to quantify the intracellular cAMP concentration. cAMP formation was stimulated using forskolin, an adenylyl cyclase activator, and when 150 µM of MMF was added, a decrease of around 30% in cAMP levels was detected **(Figure 5.32A)**. Next, the effect of fumarate itself on the intracellular cAMP levels was evaluated using the same concentration as MMF, but no changes were observed in intracellular cAMP content **(Figure 5.32B)**. However, when the fumarate concentration was doubled to 300 µM, a rapid and dramatic decrease of 80% in intracellular cAMP was observed **(Figure 5.32C)**, confirming that fumarate extracellular accumulation acutely activates sarcolemmal Gi-coupled pathways decreasing cAMP levels.

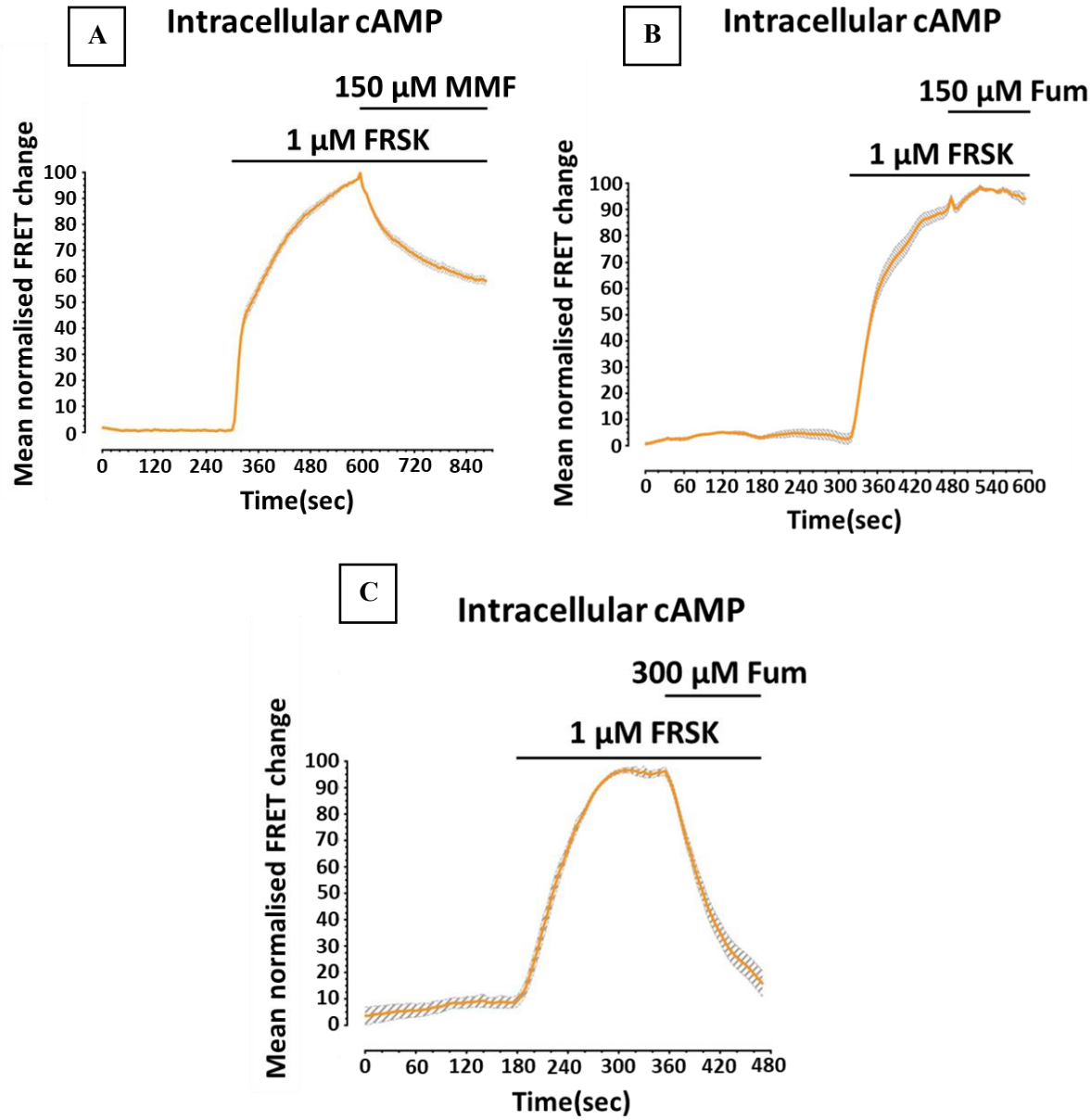

Figure 5.32: Monomethyl fumarate and fumarate itself acutely decrease cAMP levels. Fluorescence resonance energy transfer (FRET) in neonatal rat ventricular cardiomyocytes (NRVMs) expressing EPAC (exchange protein directly activated by cAMP) to quantify cAMP intracellular levels. **(A)** 150 µM monomethyl fumarate (MMF). **(B)** 150 µM fumarate (Fum). **(C)** 300 µM fumarate (Fum). Data represent the average of 6 biological replicates.

The chronic effect of fumarate on HCA2 receptor was also observed by detecting a significant 52% reduction in *HCA2* receptor gene expression in human cardiomyocytes after 6 hours of fumarate treatment **(Figure 5.33).**

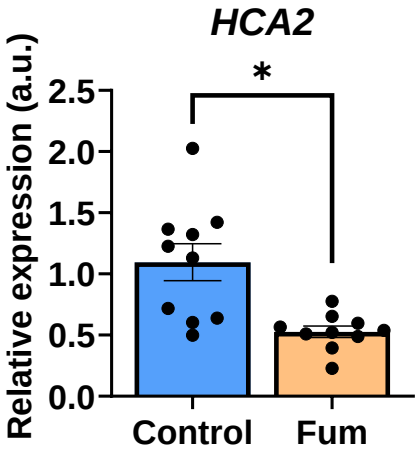

Figure 5.33: Fumarate decreases the expression of hydroxycarboxylic acid receptor 2. Hydroxycarboxylic acid receptor 2 (*HCA2*) gene expression in hiPSC-CM exposed to fumarate treatment (500 µM) (Fum) for 6 hours and compared with untreated cells. * $p < 0.05$ vs. respective control group. Each data point represents a biological replicate.

5.6 Discussion

5.6.1 Fumarate induces a metabolic shift from fatty acid oxidation to glucose metabolism within the cardiomyocyte.

Our results show that fumarate induces a metabolic shift from fatty acid oxidation to glucose metabolism within the human cardiomyocyte, reassembling the metabolic phenotype observed in the heart in response to limited oxygen levels[62, 272]. These findings suggest that the elevated intracellular fumarate content detected within the heart in response to acute hypoxia (as observed in this thesis) and during ischemia[159], may drive these metabolic adaptations. Interestingly, our data revealed that the decrease in fatty acid oxidation was also accompanied by a reduction in mitochondrial oxygen consumption, indicating that fumarate was suppressing broadly oxidative metabolism. Similar changes have been reported in bone marrow-derived macrophages in which the Krebs cycle enzyme fumarate hydratase (FH) was inhibited, leading to increased fumarate levels and suppression of the mitochondria

respiration[273]. Furthermore, hematopoietic cells extracted from *Fh* knockout mice also presented a reduction in mitochondria activity[274], and human *FH* null renal cell lines showed an increased fumarate content, with decreased mitochondrial activity followed by increased glucose uptake, glycolytic rates and lactate production compared with wild-type cells[275, 276].

A possible mechanism associated with this metabolic shift from fatty acid oxidation to glucose metabolism observed with fumarate treatment may involve the Randle cycle regulation[28]. In our metabolic rate data, the magnitude of the reduction in fatty acid oxidation was more dramatic than the increase in glycolytic rate, suggesting that fumarate may initially inhibit the fatty acid oxidation pathway and then, removing the negative feedback regulation, promote glycolysis.

5.6.2 Fumarate does not modulate the Nrf2 or HIF1 pathway but promotes the circadian rhythm pathway.

In the search for signalling pathways that could explain the metabolic changes, our data demonstrates that in human cardiomyocytes, fumarate did not activate the Nrf2 pathway at the same time point when the metabolic changes were induced. Enriched terms and transcription factors in the transcriptomics data identified the HIF pathway as a potential candidate causing these changes. However, we discarded that HIF1 mediated these changes because we found that other genes from non-metabolic pathways regulated by HIF1 were not significantly upregulated, such as the angiogenesis pathway, whose expression has been reported to be enhanced by HIF1α[277, 278]. Furthermore, in the literature, the evaluated genes for this pathway, *EDN1*[279], *SERPINE1*[280], *ANGPT1*[281], *TGFB3*[282], and *IGFBP3*[283], are upregulated by HIF1, whereas with fumarate treatment, their expression was either downregulated or did not change.

The circadian rhythm pathway was the next most enriched signalling pathway, with a larger set of circadian genes upregulated following fumarate treatment. Among these, *PER2* has been identified as a critical gene behind the metabolic adaptations observed during myocardial ischemia, where it facilitates the shift toward glycolysis[284], as well as decreases fatty acid oxidation components[284, 285] and also acts as a PPAR repressor in adipocytes[286]. Additional studies in a double knockout mouse model for the genes *Cry1* and *Cry2* (genes also upregulated after fumarate treatment) presented impaired glucose tolerance and were unable to restore normal blood glucose levels after feeding compared with wild-type mice[287], suggesting a relationship between circadian rhythm and glucose metabolism. Similarly, the circadian rhythm transcription factor NPAS2 (also enriched following fumarate treatment) promoted glycolytic gene and protein expression while suppressing mitochondrial biogenesis and oxidative phosphorylation by reducing PGC1A levels in human cells[288]. While our study did not determine the exact mechanism by which fumarate upregulates the circadian rhythm genes, our GSVA data indicate an increase in the mTORC1 signalling pathway. mTORC1 has been described to modulate circadian clock components, including promoting activation of ATF4[289, 290]-and then PER2[291]-, and increasing CRY1, CLOCK and BMAL1 [292-294], which were increased in our transcriptomics data.

5.6.3 Fumarate activates the Gi-coupled signalling pathway and reduces intracellular cAMP levels.

The interaction between Krebs cycle metabolites and Gi-coupled receptors has been documented previously for succinate and the SUCNR1 receptor[295]. In this thesis, we identified, using *in silico* target prediction, that fumarate and its derivatives can bind to the hydroxycarboxylic acid receptor 2 (HCA2) in human cardiomyocytes. Moreover, using molecular docking, we observed that the residue arginine 111 (Arg111) in the extracellular pocket of HCA2 is essential for this interaction. The critical role of this residue in HCA2 for

binding bioactive molecules was also found indispensable in a recent publication where researchers tested several HCA2 agonists and observed that all of them interacted with Arg111[296]. Furthermore, using molecular visualisation, we determined that, under physiological pH, the distance between the oxygen from the carboxyl group of the fumarate molecule and the hydrogen from the guanidine group in the side chain of Arg111 is within the range to generate a hydrogen bond. Additionally, we discovered that this potential interaction could be driven not just by a covalent interaction but also by ionic interaction, as we observed that the dicarboxylate form of fumarate (containing two negative charges) interacted with Arg111 in all the tested orientations and with histidine 189 (His189) in one orientation. The pKa of the arginine guanidinium group is around 13.8[297], meaning that at physiological pH, it is protonated and carries a positive charge, which may explain its interaction with the negatively charged carboxylate ions. In contrast, the pKa of the histidine imidazole group is around 6.9[298], hence, at physiological pH, histidine remains deprotonated with a neutral charge, making its interaction with decarboxylated fumarate unlike to occur.

The role of MMF as an agonist of the HCA2 receptor has been previously documented[243, 296]. Additionally, it has been demonstrated that MMF competes with the HCA2 endogenous ligand, nicotinic acid, for the binding site[299]. Here, we presented a novel finding for fumarate decreasing intracellular cAMP content, and there is no literature on the direct interaction between fumarate itself and the HCA2 receptor or Gi-coupled signalling pathways, as most studies have focussed on fumarate derivatives. However, one limitation of this chapter is that we did not measure whether the reduced intracellular cAMP content following fumarate treatment was specifically mediated by HCA2 in cardiomyocytes, and this was not studied as there are no HCA2 antagonists currently available[300]. Nevertheless,

our group recently established a protocol for performing siRNA experiments in hiPSC-CM and NRVMs, therefore, this is a key experiment for future investigation.

Interestingly, increasing levels of cAMP have been shown to induce PGC1α deacetylation and activation by SIRT1, promoting fatty acid oxidation in mouse fibroblast[301]. A similar response mechanism has also been observed in primary hepatocytes[302], suggesting that promoting HCA2 activation may inhibit fatty acid oxidation. Additionally, high levels of cAMP inhibit mTOR complex 1 and 2[303, 304] via PKA activation. Notably, in our data mTOR signalling pathway was not observed in the GSVA plot following one-hour fumarate treatment but appeared at six hours. This may indicate that the increase in the mTOR pathway observed at six hours is a consequence of fumarate activating HCA2 at one hour.

5.6.4 Fumarate is released to extracellular space via the monocarboxylate transporter 1 under hypoxic conditions.

Our results showed that under hypoxic conditions, fumarate is not only accumulated intracellularly but also released extracellularly via the monocarboxylate transporter 1 (MCT1). We noticed that the suppression of fumarate efflux using an MCT1 inhibitor was specific for hypoxia but not normoxia, suggesting that hypoxia may induce physiological cell changes that enhanced MCT1's affinity for fumarate. A similar response has been reported for MCT1-mediated succinate efflux, where it was determined that a pH gradient between the intracellular (more acidic) and extracellular spaces was necessary for succinate release by MCT1[102]. This finding indicates that in our cardiomyocyte model, hypoxia not only increases fumarate intracellular levels but also likely generates the required acidic environment necessary for fumarate release via MCT1.

5.6.5 Fumarate proposed mechanism of action in human cardiomyocytes.

Based on the results generated in this chapter and the complementary observations from the literature, we propose the following cellular signalling hypothesis, excluding any additional PTM or molecular mechanism involved in fumarate-mediated metabolic changes (**Figure 5.34**): Under hypoxic conditions, intracellular fumarate concentrations rise and the intracellular pH decreases, which generates a proton gradient between the intra- and extracellular spaces. This pH gradient enhances MCT1's affinity for fumarate, increasing fumarate release into the extracellular space where fumarate binds and activates G-protein couples signalling pathways via HCA2 receptor, on neighbouring normoxic or hypoxic cells, as well as on the same hypoxic cell from which it was released. HCA2 activation inhibits adenylyl cyclase, decreasing cAMP intracellular content. Potential mechanisms downstream of decreased intracellular cAMP concentration (not demonstrated in this thesis) could include the reduction of fatty acid β-oxidation, which potentially may drive glycolysis by removing the negative feedback regulation (Randle cycle), and activation of mTOR, which hypothetically could regulate the circadian rhythm pathway. However, further investigation is required to determine the precise mechanism involved in fumarate-induced metabolic reprogramming.

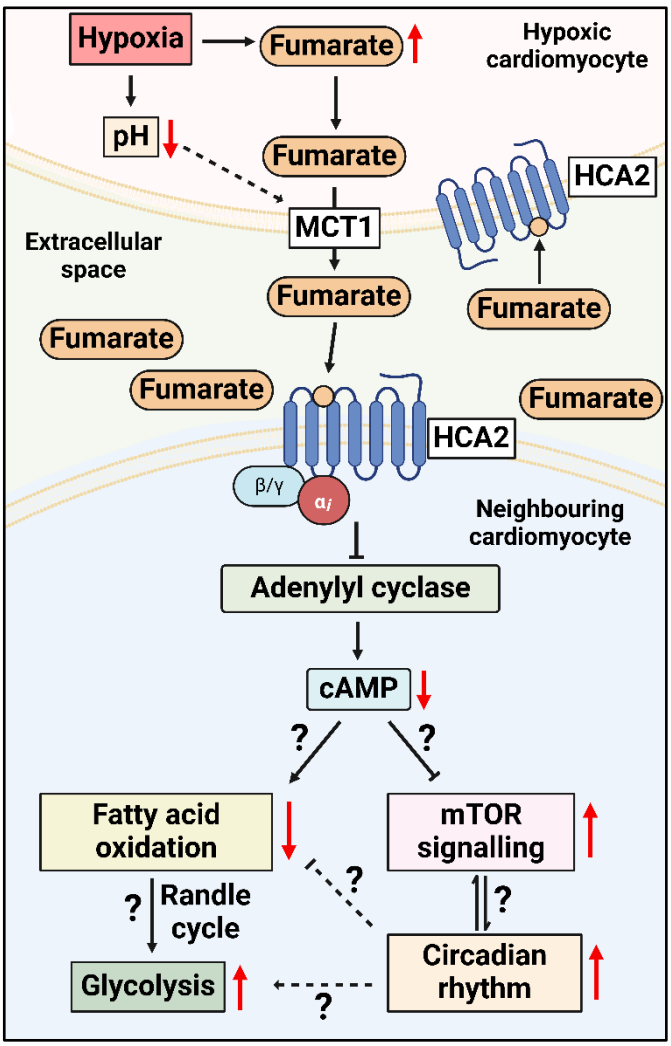

Figure 5.34: Fumarate proposed mechanism of action.

The illustration represents a hypothetical signalling mechanism regulated by fumarate to induce metabolic changes. Hypoxic conditions increase fumarate levels and acidify the intracellular space, promoting fumarate release via the monocarboxylate transporter 1 (MCT1). Extracellular fumarate binds and activates the hydroxycarboxylic acid receptor 2 (HCA2), lowering cAMP level, which decreases fatty acid oxidation and, by Randle cycle regulation, increases glycolysis. Reduced cAMP content also activates mTOR signalling, promoting the circadian rhythm pathway and modulating human cardiomyocyte metabolism.

5.7 Conclusion

Fumarate is a Krebs cycle metabolite that selectively accumulates under hypoxia, acting intracellularly as a signalling molecule, regulating cardiomyocyte metabolism, where fumarate induces a metabolic shift from fatty acid oxidation to glucose metabolism impairing mitochondria respiration, and additionally upregulating circadian rhythm component. Under hypoxic conditions, fumarate is also released from the human cardiomyocytes via MCT1, where it has an extracellular role as a paracrine signal via G-protein coupled receptors, reprogramming neighbouring cells.

Chapter 6

Fumarate derivatives and their potential therapeutic role in type 2 diabetic hearts

6.1 Abstract

Type 2 diabetes is a metabolic disorder that significantly disrupts the functionality of various organs, including the heart, with cardiovascular diseases being the main cause of death among diabetic patients. Glucose intolerance and insulin resistance lead to fat overload within the heart, increasing fatty acid β-oxidation and lipid accumulation. These alterations promote reactive oxygen species generation, resulting in oxidative stress and damage that contribute to the progression of type 2 diabetes complications. Dimethyl fumarate (DMF) is clinically approved for human use to treat autoimmune diseases and enhances antioxidant defence enzymes by activating Nrf2. Therefore this chapter was focused on evaluating the potential therapeutic use of DMF in type 2 diabetes, repurposing the clinical use of this molecule.

Using type 2 diabetic rat hearts, we observed an impaired hypoxic response in the content of the Krebs cycle metabolites compared with healthy hearts. Notably, fumarate elevation was blunted in the diabetic hearts, and it was accompanied by increased oxidative stress. Using an insulin-resistant hiPSC-CM model, we observed that insulin resistance induced a large global gene expression change in human cardiomyocytes, increasing the expression of genes involved in fatty acid β-oxidation while decreasing antioxidant genes regulated by Nrf2. Both long and short incubation with DMF treatment significantly reversed some aspects of the diabetic phenotype by upregulating the antioxidant genes regulated by Nrf2, while short-term incubation also decreased the expression of fatty acid β-oxidation genes.

In conclusion, DMF promoted antioxidant defences and reduced the expression of fatty acid β-oxidation genes in insulin-resistant cardiomyocytes, reversing key aspects of this phenotype and repurposing the use of fumarate derivatives for treating metabolic cardiac disorders in humans.

6.2 Introduction

Type 2 diabetes (T2D) is the most prevalent form of diabetes mellitus, characterised as a metabolic disorder marked by persistent hyperglycaemia, insulin resistance, and β-cell dysfunction[305, 306]. This metabolic disorder has a projected adult global prevalence of 10.2% by 2030[307], making diabetes one of the biggest challenges to human health. T2D leads to dysfunction in several organs and tissues, however, the primary cause of death among T2D patients is cardiovascular diseases, particularly myocardial infarction, where T2D increases the risk of developing these diseases by 2- to 4-fold[308, 309].

6.2.1 Cardiac metabolism in type 2 diabetes.

Under healthy conditions, insulin regulates glucose and fatty acid metabolism within the heart. Glucose metabolism is modulated through various mechanisms that directly enhance glucose uptake and metabolism. Insulin promotes GLUT4 membrane translocation to the sarcolemma, enhances glycogen synthesis and increases glycolysis[310, 311]. Additionally, insulin stimulates long-chain fatty acid uptake in the heart by increasing CD36/FAT sarcolemmal translocation[312] and promotes fatty acid storage in adipose tissue while decreasing lipolysis and circulating plasma fatty acid[313].

In insulin-resistance conditions, the suppression of lipolysis by insulin is reduced, significantly increasing plasma fatty acids[314]. The increased circulating fatty acids promote the preference and use of long-fatty acids by the heart for energy generation and leading a reduction in glucose uptake and oxidation[315]. Furthermore, T2DM and insulin resistance are associated with the accumulation of ectopic lipids within the heart, and due to the heart's low capacity to store triglycerides, this increased lipid accumulation contributes to lipotoxicity and cardiac dysfunction[314, 316, 317].

6.2.2 Type 2 diabetes and oxidative stress.

The metabolic changes within the diabetic heart are associated with alteration in reactive oxygen species (ROS) levels. Increased plasma glucose promotes ROS generation by different mechanisms, including [318-320]: (1) depletion of the antioxidant cofactor NADPH due to the overactivation of the polyol pathway, where the excessive glucose is converted into fructose; (2) increased advanced glycation end-products (AGEs) that upon binding their receptors activate the NADPH-oxidase (NOX) enzymes; (3) and activating protein kinase C (PKC), which also increases NOX activity. Additionally, under diabetes condition, antioxidant enzyme activity is decreased[321], glutathione synthesis is impaired[322], and cardiac mitochondria become dysfunctional, significantly increasing the endogenous level of hydrogen peroxide[323]. Oxidative stress, resulting from increased ROS accumulation, has been suggested as an important cause behind the development of insulin resistance, β-cell dysfunction, glucose intolerance and T2DM development[324]. High levels of ROS and oxidative stress have also been linked to the progression of diabetes complications at the microvascular and cardiovascular level[325].

As we observed in **Chapter 3**, fumarate derivatives enhance the antioxidant defence mechanisms in healthy human cardiomyocytes. Therefore, this chapter focused on evaluating the potential therapeutic use of the exogenous fumarate derivative dimethyl fumarate as a protective agent against oxidative stress in the diabetic heart.

6.3 Chapter aims

Type 2 diabetes impairs cardiac metabolism, increasing reactive oxygen species and oxidative stress, which significantly exacerbates diabetes complications and causes oxidative damage in various organs, including the heart. Dimethyl fumarate is a drug already approved for use in humans for the treatment of autoimmune diseases, which promotes Nrf2 activation and enhances antioxidant defence mechanisms in several cell types, including, as observed in previous chapters, human cardiomyocytes. However, despite the benefits the Nrf2 pathway and fumarate derivatives could have on diabetic patients, decreasing oxidative stress and diabetes complications, it remains unclear whether exogenous fumarate derivatives could benefit the diabetic heart. Therefore, this chapter investigated:

1. Fumarate intracellular concentration in perfused diabetic rat hearts exposed to acute hypoxia compared with normoxia.

2. Diabetic heart oxidative stress levels and antioxidant profile.

3. The effect of dimethyl fumarate oral administration in global gene expression on rat hearts.

4. The effect of insulin-resistance condition on the metabolic and antioxidant gene profiles in hiPSC-CM.

5. The effect of exogenous dimethyl fumarate on the expression of antioxidant and fatty acid oxidation genes in insulin-resistant hiPSC-CM.

6.4 Methods

6.4.1 Type 2 Diabetes rat model.

Heart tissue from the type 2 diabetic rats used for the metabolomics experiment was generated by Dr Latt Mansor. Heart tissue from the type 2 diabetic rats used for the western blotting and glutathione experiments was generated by Dr Matthew Kerr. Type 2 diabetes was induced in rats using a high-fat diet and low-dose streptozotocin[104]. Male Wistar rats were fed with a high-fat diet ad libitum, and on day 14, they received a single intraperitoneal injection of low-dose streptozotocin (25 mg/kg body weight) (prepared in citrate buffer, pH 4). Control (non-diabetic) rats were fed a conventional chow diet and received only a single intraperitoneal injection of citrate buffer. The corresponding diets were maintained for five additional weeks. For the metabolomics experiments, five rats were used per condition, except for the healthy group under normoxia, which included six rats. For western blotting and glutathione measurement, six rats were used per condition.

6.4.2 Protein carbonylation.

During long-term oxidative stress, proteins are modified, and carbonyl groups are attached to them, a process known as protein carbonylation. Levels of protein carbonylation were determined using the OxyBlot Protein Oxidation Detection Kit (Millipore) following the manufacturer's instructions. This kit utilises the enzymatic activity of 2,4-dinitrophenylhydrazine to modify the attached carbonyl groups into 2,4-dinitrophenylhydrazone, allowing subsequent detection by western blotting using a specific 2,4-dinitrophenylhydrazone antibody. Protein was extracted from 30 µg of frozen healthy or diabetic heart tissue, following the protein lysis protocol from **Section 2.3.1.**

6.4.3 *In vivo* dimethyl fumarate administration.

In vivo dimethyl fumarate experiments were performed with the assistance of Ms Claudia Montes Aparicio and Dr Kaitlyn Dennis. Male Wister rats were purchased from Envigo (UK) and randomly assigned to Control and DMF-treated groups. Both groups were fed with a chow diet and water ad libitum. Drug administration was carried out by mixing DMF (in powder form) with jelly in a weighing boat, while control rats received plain jelly. The effects of in vivo DMF were evaluated in two different studies: in the first one, rats were given 25 mg DMF/kg twice daily for 5 days, and in the second one, 80 mg DMF/kg was given once daily for 12 days. Four rats per condition were used for the first pilot experiment, while seven rats (four for the Control group and three for the DMF-treated group) were used for the second pilot experiment. All investigations were conformed to UK Home Office guidelines under The Animal (Scientific Procedures) Act, 1986.

6.4.4 Insulin-resistance human-induced pluripotent stem cell-derived cardiomyocyte generation.

Human-induced Pluripotent Stem Cells (hiPSC) (IMR90) were differentiated into cardiomyocytes and matured following the protocol in **Section 2.1.1**, then insulin resistance was induced in hiPSC-CM following a six-day protocol[107]. On day one, mature hiPSC-CM were changed from maturation media to glucose-free insulin-resistance media, consisting of DMEM no glucose (Gibco) supplemented 1.7 µM insulin, 10% heat-inactivated horse serum, 0.2 mM palmitic acid:BSA (bound 6:1, Sigma Aldrich), 5 µg/mL vitamin B12, 0.5 mM vitamin C, 0.84 µM biotin, 0.1X penicillin/Streptomycin , and 1X nonessential amino acids. On day two, the media was replaced with fresh glucose-free insulin-resistant media and kept until day three. On day four, hiPSC-CMs media was replaced with the glucose-enriched insulin-resistant media, identical to the previous media but containing 12 mM

glucose and 3.4 µM insulin. On day five, the media was replaced with fresh glucose-enriched insulin-resistance media and was kept for days five and six. Non-insulin-resistant cells were cultured for six days in maturation media.

Insulin sensitivity was confirmed by measuring the pAkt/Akt ratio. The media from insulin-resistant and control hiPSC-CM was removed, and the cells were washed with DPBS 1X to ensure complete removal of the cell media components. Then DMEM 1 g/L glucose supplemented with 1.7 µM insulin was added, and the cells were incubated for 30 minutes at 37°C. Protein extraction and western blotting followed the protocol set out in **Section 2.3**.

After confirming that the hiPSC-CM were insulin-resistant, dimethyl fumarate (DMF) treatment was conducted for 16 hours to perform transcriptomics analysis in collaboration with Dr Ryan Carter or for 6 hours to carry out qPCR experiments **(Figure 6.1)**.

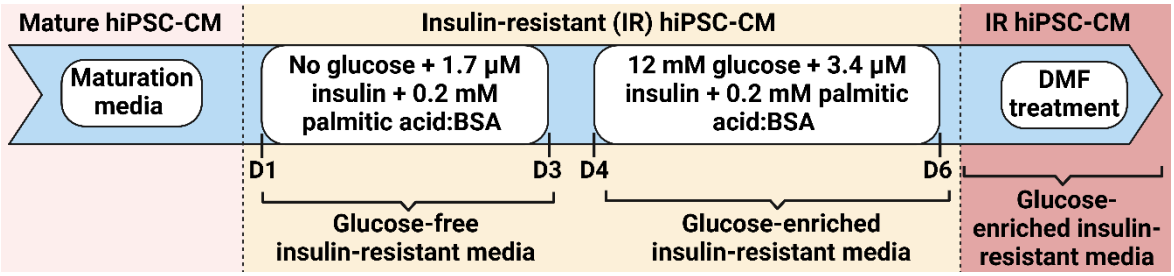

Figure 6.1: Protocol for generating the insulin-resistant hiPSC-CM. Insulin-resistant hiPSC-CM (IR) were generated from mature hiPSC-CM using a six-day protocol involving glucose-free and glucose-enriched insulin-resistant media. After completing the insulin-resistant protocol, cells were treated with 200 µM dimethyl fumarate (DMF) for 16 hours for transcriptomics analysis or 150 µM DMF for 6 hours for evaluating gene expression by qPCR.

6.5 Results

6.5.1 Acute hypoxia does not increase intracellular fumarate levels within the diabetic rat hearts (in contrast to control hearts).

The effect of hypoxia on the diabetic heart was evaluated using in-depth metabolomics screening in isolated diabetic rat hearts perfused under acute hypoxic conditions (Po_2 = 90 ± 10 mmHg for 32 minutes) or normoxia conditions (Po_2 = 413 ± 15 mmHg). Notably, the impact of hypoxia in the diabetic heart differed from that previously observed in healthy hearts. While fumarate intracellular levels were significantly increased in hypoxia within the healthy heart, no differences in fumarate content were observed when hypoxia was compared with normoxia within the diabetic **(Figure 6.2A)**. Interestingly, the magnitude of accumulation after hypoxia for the same metabolite differed between healthy and diabetic hearts, as was the case for succinate intracellular levels. Under normoxia, the average area peak detected for succinate was 1.7-fold higher in the diabetic heart compared with the healthy heart. However, after acute hypoxia exposure, the succinate accumulation within the diabetic heart was half of the increase observed within the healthy heart, suggesting an impaired metabolic response to hypoxia **(Figure 6.2B)**. On the other hand, the significantly decreased metabolites from the diabetic heart showed a pronounced reduction compared with the healthy heart, as exemplified by succinyl-CoA, which decrease was 26% greater in the diabetic condition **(Figure 6.2C)**.

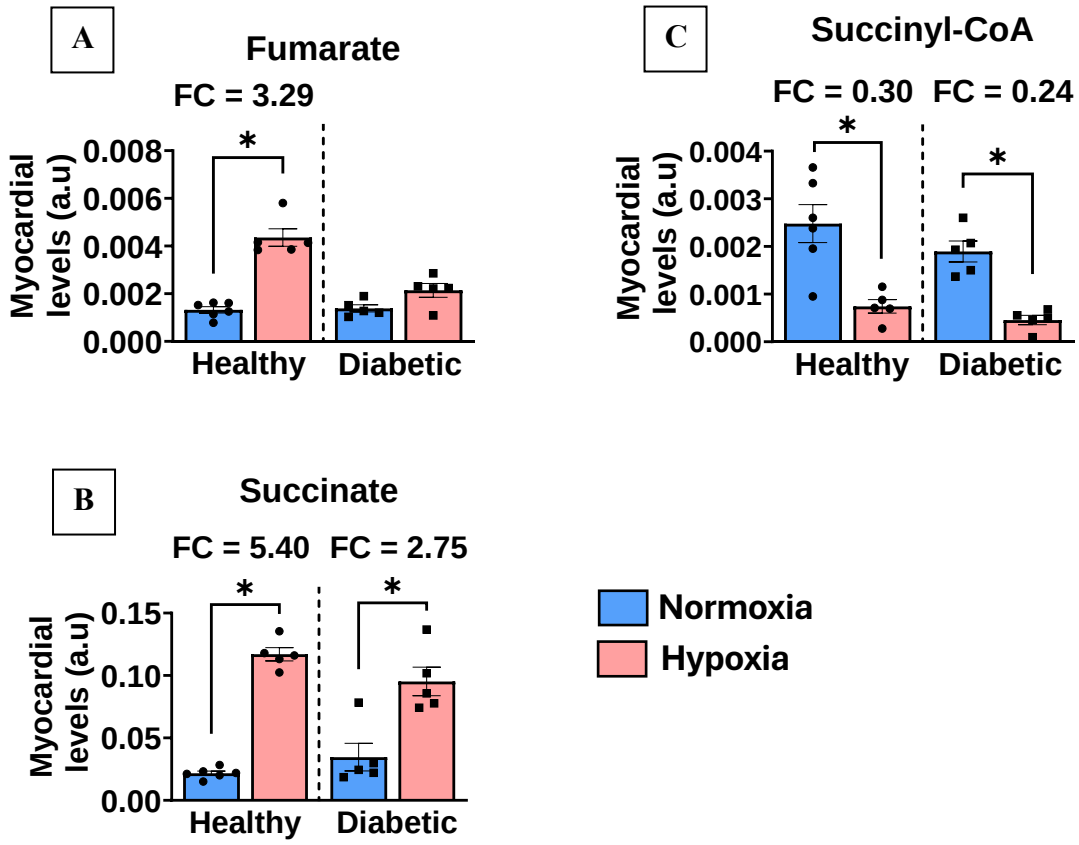

Figure 6.2: Myocardia content of fumarate, succinate and succinyl-CoA from healthy and diabetic hearts under normoxia or hypoxia. Krebs cycle metabolite fumarate (**A**), succinate (**B**) and succinyl-CoA (**C**) levels following normoxia and acute hypoxia within the healthy and diabetic rat heart. Data was expressed as peak area ratio. Data was normalised to tissue weight. FC, fold change represented the ratio between mean hypoxia and mean normoxia for each metabolite. * $p < 0.05$ vs. respective normoxia group. a.u., arbitrary units. Each data point represents a biological replicate.

To further understand whether the differences in the metabolite content in response to hypoxia were dependent on the healthy or diabetic phenotype of the heart, a two-way ANOVA was performed on the significant metabolites from both studies, using as factors heart condition (healthy or diabetic) and oxygen levels (normoxia or hypoxia) **(Figure 6.3)**. The ANOVA analysis revealed that the oxygen levels were the primary or unique source of variation for most of the significant metabolites. Surprisingly, just three metabolites, fumarate, malate and succinyl-CoA, showed significant differences depending on the heart condition factor, oxygen levels factor, and the interaction between these factors, suggesting

that one factor influenced the other. Fumarate content was significantly elevated in the healthy heart under hypoxia but not in the diabetic heart, indicating that the oxygen levels factor depends on the heart condition factor for this metabolite. The quantitative influence of each factor for each one of the significant regulated metabolites was represented in **Supplementary Table 9.1**.

These results show that acute hypoxia induces significant changes in diabetic cardiac metabolite content. However, key metabolites, like fumarate, remained unchanged, contrasting with the response observed for hypoxia in healthy hearts. Statistical analysis further confirmed that the heart condition (healthy or diabetic) influences the elevation of intracellular fumarate under hypoxia.

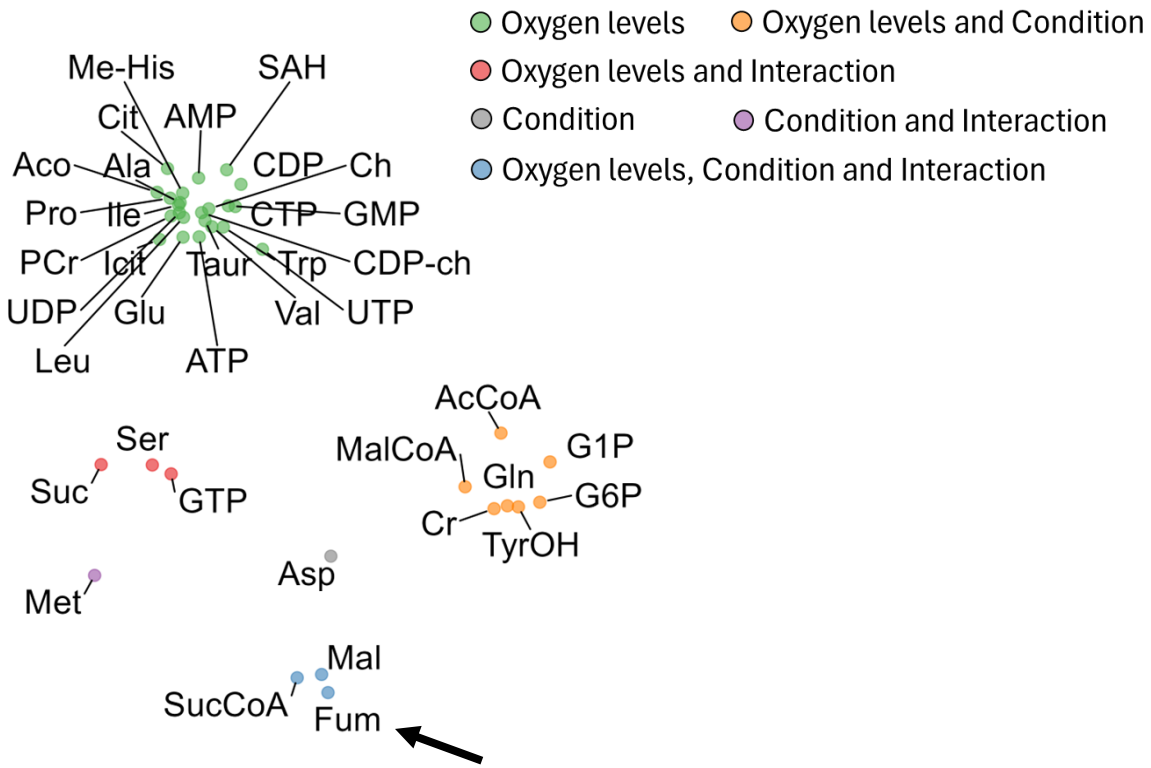

Figure 6.3: Hypoxia-induced fumarate elevation depends on the heart phenotype. To determine which factors were triggering the changes in metabolite content within the healthy and diabetic heart exposed to hypoxia, the statistical source of variation in the regulated metabolites was determined by two-way ANOVA. The analysis used oxygen levels (normoxia or hypoxia) and heart condition (healthy or diabetic) as dependent factors, observing that fumarate was influenced by the oxygen levels, heart condition and interaction between both factors.

6.5.2 Diabetes increases oxidative stress without affecting antioxidant protein levels within the heart.

The role of fumarate derivatives in modulating the antioxidant response, previously observed in Chapter 3, led to the study of how impaired fumarate elevation under hypoxia affects the diabetic heart by measuring its oxidative state. Oxidative stress was assessed using two established markers: the glutathione redox content and protein carbonylation. Under oxidative stress, reactive oxygen species in the cellular environment directly modify the antioxidant molecule glutathione, which is rapidly oxidised to glutathione disulfide (GSSG). Similarly, long-term exposure to oxidative stress induces modifications in several cellular components, including carbonyl groups binding to the proteins, a process called protein carbonylation.

The ratio of oxidised glutathione (GSSG) to total glutathione (GSH), used as a marker of oxidative stress, significantly increased by 11% in the diabetic heart (D) compared with the healthy heart (Control (C)) **(Figure 6.4A)**. In contrast, no significant differences were observed in the protein carbonylation content between conditions **(Figure 6.4B)**. Notably, western blot analysis showed that the GSSG/GSH ratio change was not associated with changes in TXNRD1, HMOX1, or NQO1 protein levels **(Figure 6.5)**. These results indicated that the healthy and diabetic hearts present similar levels of antioxidant components under basal conditions, however, the elevated GSSG/GSH was an indicator of increased oxidative stress within the diabetic heart.

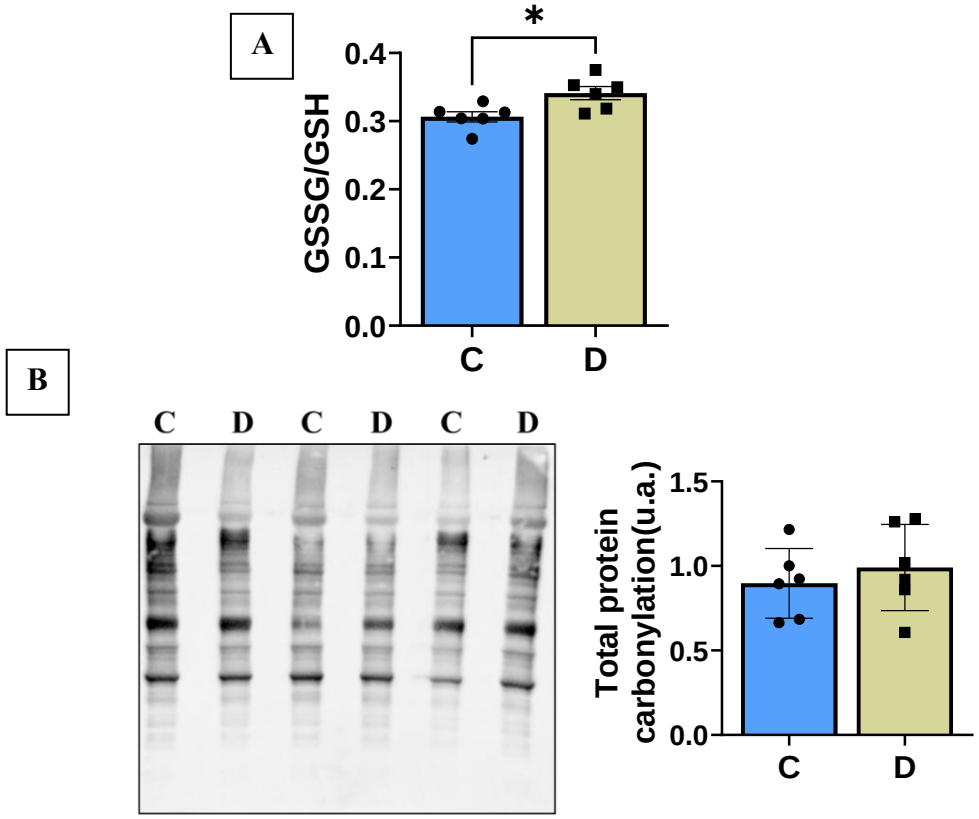

Figure 6.4: Diabetes increases early oxidative stress response in the heart tissue. **(A)** Oxidised glutathione (GSSG) to total glutathione (GSH) ratio per mg of tissue as an earlier oxidative stress marker. **(B)** Representative western blot of total protein carbonylation as a long-term oxidative stress marker. C, control. D, diabetic.* $p < 0.05$ vs. respective control. a.u., arbitrary units. Each data point represents a biological replicate.

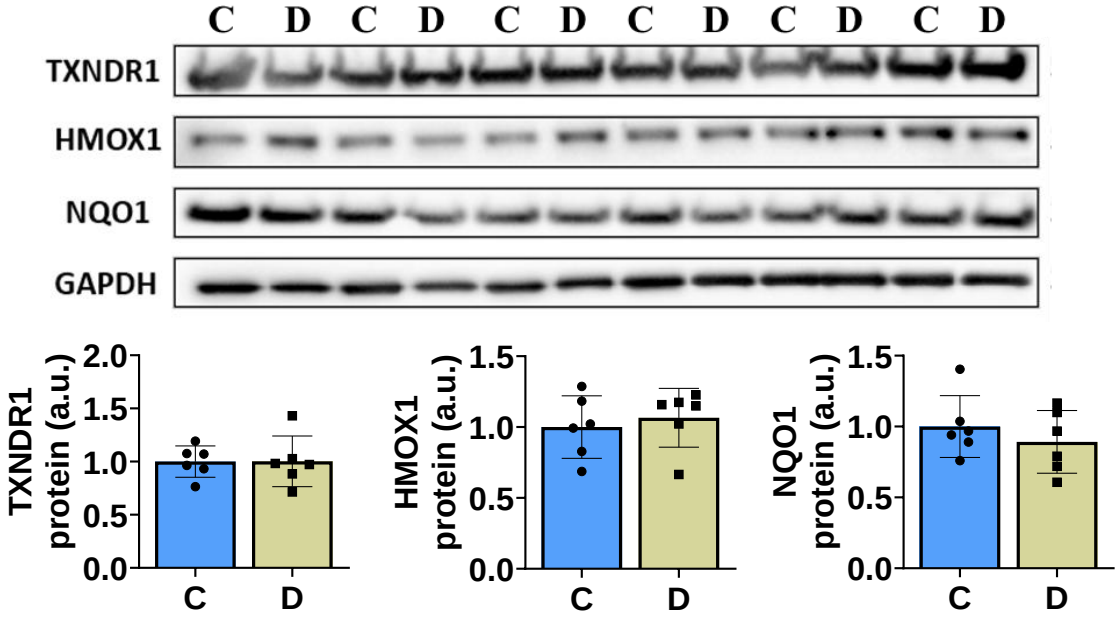

Figure 6.5: Diabetic heart shows a similar antioxidant profile to the healthy heart tissue. Protein levels of the antioxidant enzymes thioredoxin Reductase 1 (TXRND1), heme oxygenase 1 (HMOX1), and NAD(P) dehydrogenase quinone 1 (NQO1). Glyceraldehyde-3-phosphate dehydrogenase (GAPDH) was used as a loading control. C, control. D, diabetic a.u., arbitrary units. Each data point represents a biological replicate.

6.5.3 Oral dimethyl fumarate administration shows no effect on antioxidant gene expression within rat hearts.

To evaluate whether exogenous fumarate derivatives could help revert the oxidative state within the diabetic heart, a pilot study in rats was carried out to explore the effect of oral dimethyl fumarate (DMF) administration on antioxidant gene expression within the heart. Initially, Wister rats were fed 25mg/kg DMF twice daily for 5 days, however, no significant differences were detected by qPCR in the cardiac expression of the antioxidant genes *Nqo1*, *Txnrd1,* or *Hmox1* compared with the control condition **(Figure 6.6A)**.

Due to the failure of the first pilot study, a second pilot study was carried out using a higher dose and duration of DMF (80 mg /kg DMF once daily for 12 days). Despite an increased trend in the gene expression of *Nqo1*, *Txnrd1,* and *Hmox1* in the DMF-fed rat hearts was observed, no significant differences were reached compared with the control condition **(Figure 6.6B)**.

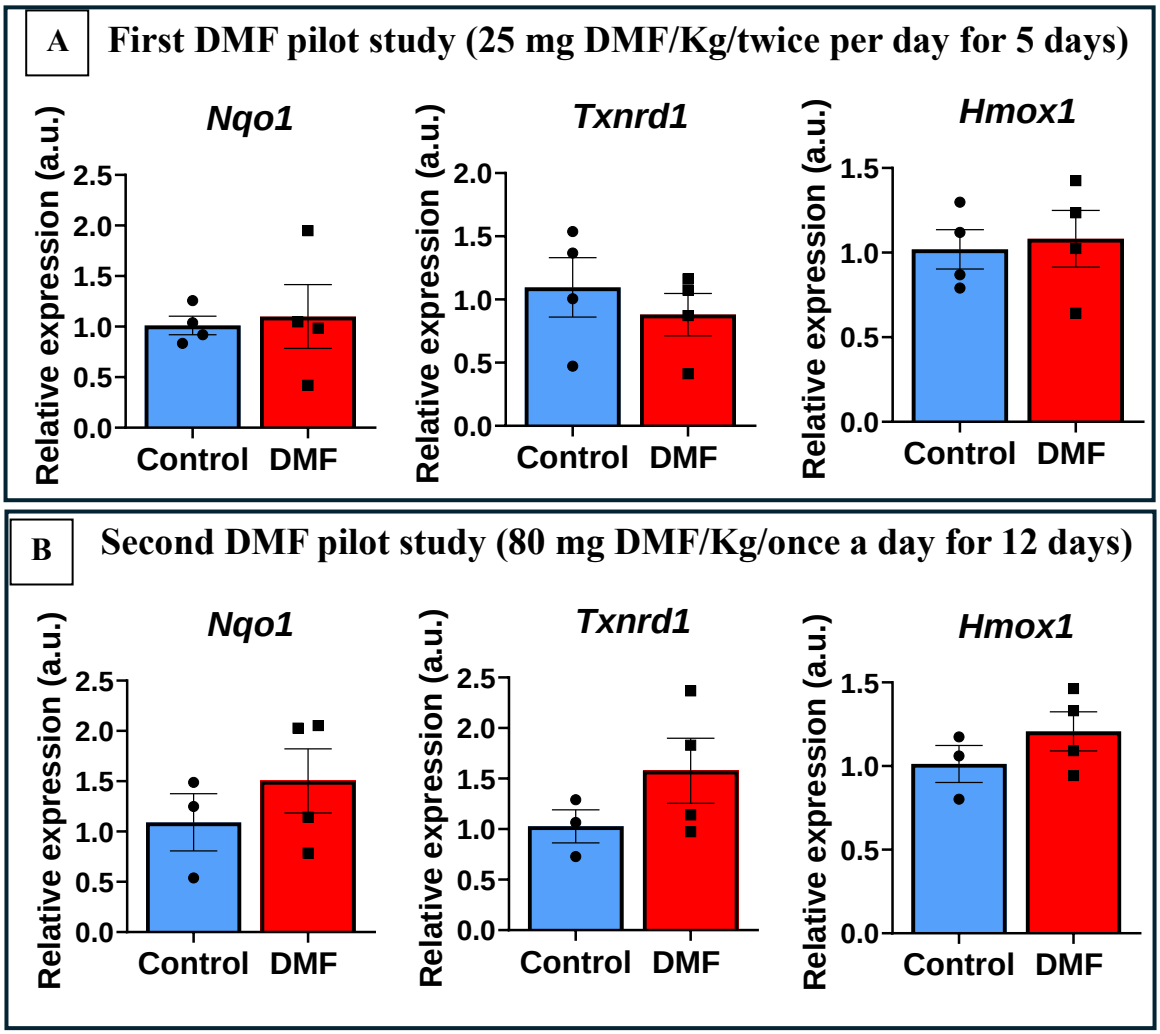

Figure 6.6: Dimethyl fumarate does not upregulate antioxidant gene expression in rat hearts. Gene expression analyses of Nrf2 target genes in control and dimethyl fumarate (DMF)-treated rats. **(A)** 25 mg/kg DMF was administered twice daily for 5 days. **(B)** 80 mg/kg DMF was administrated once daily for 12 days. The evaluated targets were NAD(P) dehydrogenase quinone 1 (*Nqo1*), thioredoxin reductase 1 (*Txnrd1*), and heme oxygenase 1 (*Hmox1*). a.u., arbitrary units. Each data point represents a biological replicate.

To analyse whether the DMF treatment was affecting specific antioxidant targets, an in-depth RNA-Seq and transcriptomics analysis were performed on the heart tissue from Control and DMF-fed rats from the second pilot study. The PCA plot showed a different profile for each component **(Figure 6.7A)**, where the higher variation was in PC1, with a 61% variance, occasioned by the distribution of the samples through the x-axis, whereas PC2 identified a 16% variance through the y-axis. No evident pattern in the sample

distribution was observed, indicating that samples from both Control and DMF-fed groups were highly similar, and no apparent differences were detected. This was confirmed by observing a similar distribution in the inter-sample correlation heatmap **(Figure 6.7B)**, where components from different groups were clustered together.

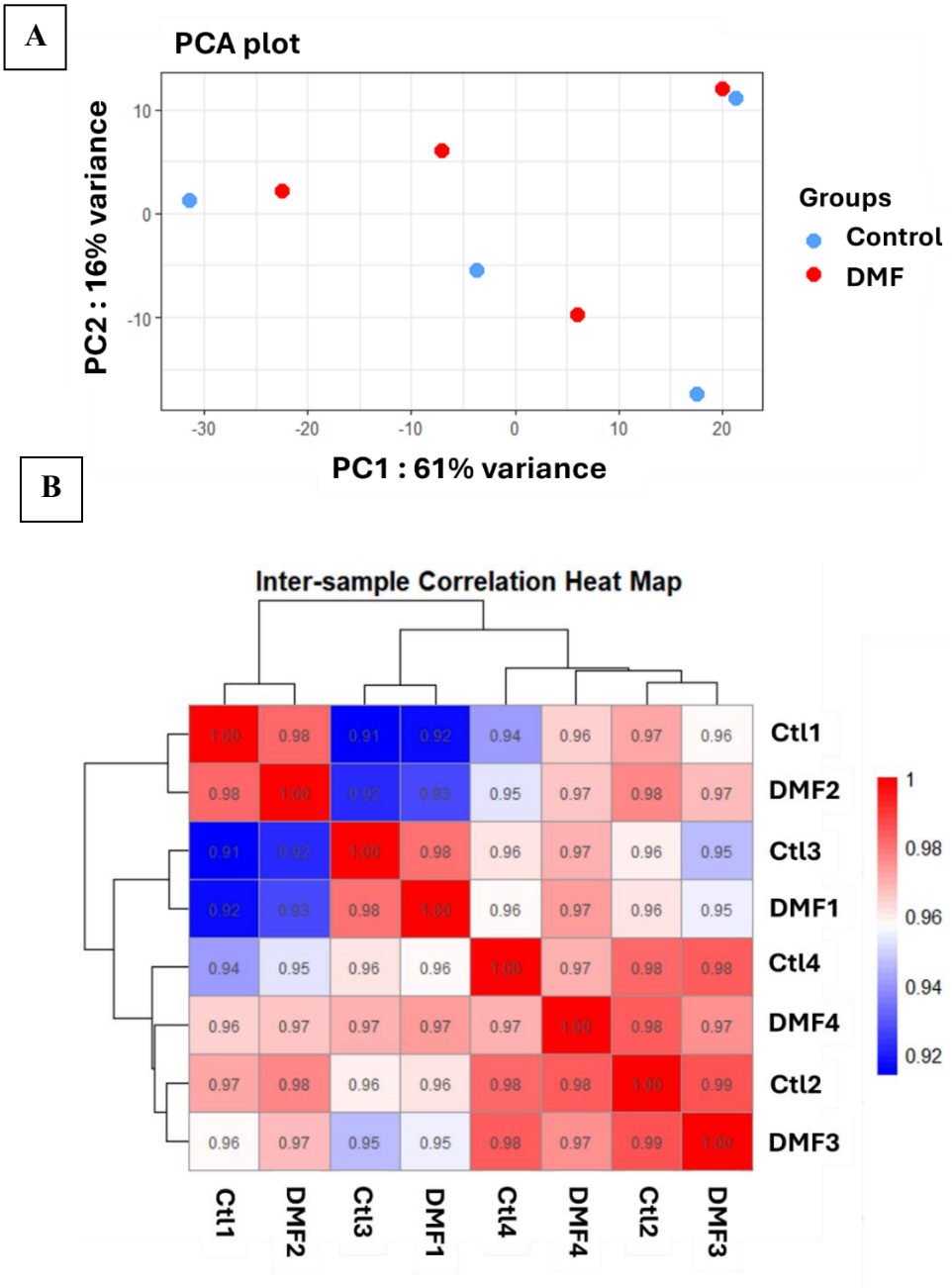

Figure 6.7: Oral dimethyl fumarate administration does not modulate global gene expression within the rat hearts. Transcriptomics analyses were performed on rat hearts following in vivo DMF treatment (80 mg/kg DMF once daily) for 12 days and compared with untreated control. **(A)** Principal component analyses between control and DMF groups. **(B)** Inter-sample correlation between samples of each condition.

Differential gene expression (DEG) was performed on 13244 genes using a p-adjusted value < 0.05 and a Log2Fold change equal to 1. However, DEG showed that only 17 genes were significantly regulated when DMF-fed were compared with control rats. To generate a larger data set for enriched terms analysis, the DEG was generated again, but using less strict parameters, the p-adjusted value was changed for p-value < 0.05, and a Log2Fold change was set as 0. Under these parameters, DEG detected 374 significantly regulated genes, with 109 upregulated genes mainly involved in muscle contraction, development, and membrane transporter processes **(Figure 6.8A)**. Interestingly, the 265 downregulated genes were mostly associated with autoimmune processes **(Figure 6.8B)**, supporting the clinical human use of DMF to treat autoimmune diseases. These findings suggested that although DMF did not modulate any antioxidant or Nrf2 target gene in the heart tissue, it modified the autoimmune system. However, since the classic DMF response was not observed, it was impossible to conclude whether the molecule reached the cardiomyocyte or another cell type in the heart which was generating these effects.

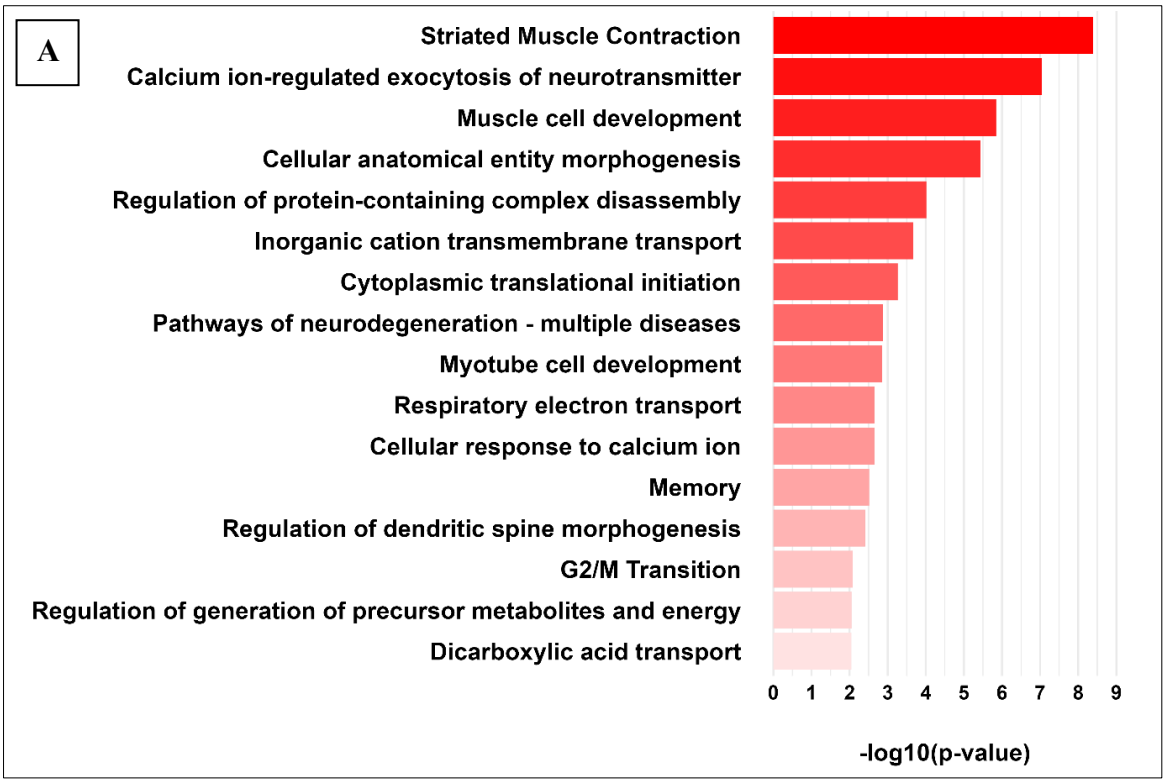

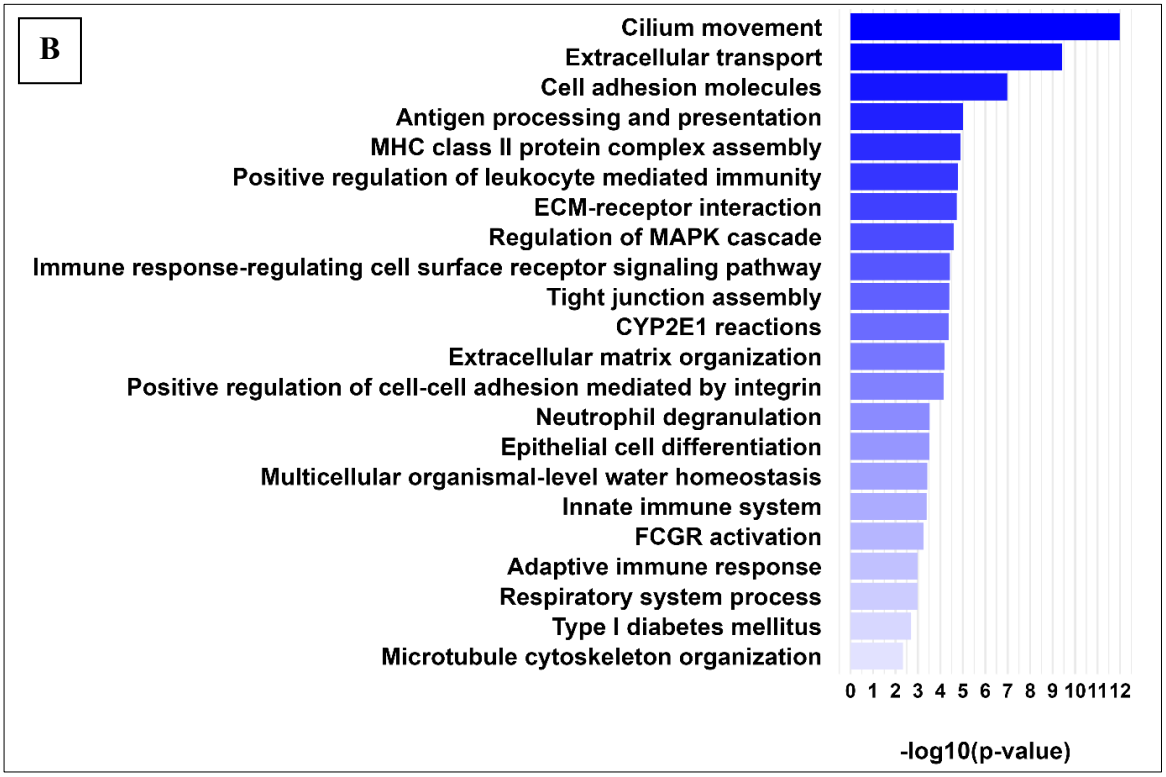

Figure 6.8: Enrichment analysis of differential gene expression comparing dimethyl fumarate-treated with untreated hearts. Transcriptomics analyses were performed on rat hearts exposed to in vivo DMF treatment (80 mg/kg DMF once daily) for 12 days and compared with untreated control. DEG was performed using a Log_2 Fold change equal to 0 and p-value < 0.05. Enrichment analysis was conducted using metascape, and the graph of enriched terms represents the 109 upregulated **(A)** or 265 downregulated genes **(B)**.

6.5.4 Insulin-resistant hiPSC-CM have impaired insulin sensitivity and increased fatty acid oxidation genes.

The previous DMF studies were performed using doses reported in the literature[168, 326], however, no canonical or well-known effects of DMF treatment on the heart were observed using these concentrations and administration times. To understand whether fumarate derivatives had a potential therapeutic role in modulating antioxidant profiles in diabetic conditions, a different approach was utilised, and an insulin-resistant model of the hiPSC-CM was employed[107].

The main difference between the maturation (control) and insulin-resistant media compositions was that insulin-resistant media contained palmitate and twice the insulin concentration, while maturation media contained oleate. Two different concentrations of palmitate, 100 and 200 μM, were tested to generate the insulin-resistant (IR) model in the hiPSC-CM. The protocol's efficacy was evaluated by stimulating both healthy and IR hiPSC-CM with the same dose of insulin for a short time and measuring the phosphorylation status of the insulin response marker Akt **(Figure 6.9)**. Healthy hiPSC-CM incubated in maturation media exhibited an evident and pronounced increase in the p-Akt levels after insulin stimulation, whereas a blunted response to exogenous insulin was detected in hiPSC-CM incubated in IR media with either 100 or 200 μM palmitate. Due to 200 μM palmitate closely reflecting the physiological fatty acid concentration observed in T2D patients[327], further IR experiments were performed using this concentration.

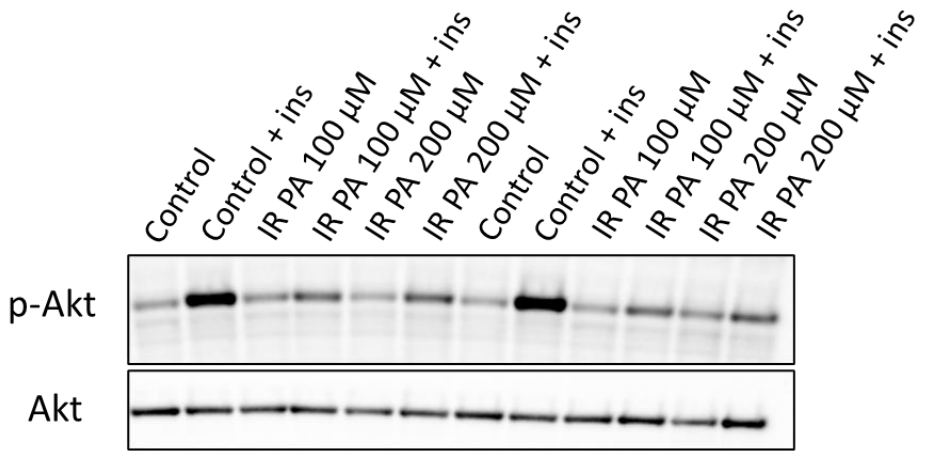

Figure 6.9: Insulin-resistant protocol decreases p-Akt protein levels after exogenous insulin stimulation. Mature hiPSC-CM were incubated in maturation media (Control) or insulin-resistant (IR) media for 1 week, and exogenous insulin was added for 30 minutes, and pAkt was measured as an insulin response marker. Total Akt was used as a loading control. PA, palmitate conjugated to BSA(6:1). ins, insulin.

The metabolic phenotype of the IR cells was studied at the genetic level by performing an RNA-seq, transcriptomics analysis, and gene set variation analysis (GSVA) on these cells, and the resulting gene data was aligned with different biological pathways extracted from the open science platform WikiPathways. Interestingly, among the top significantly upregulated pathways under IR conditions, fatty acid β-oxidation and roles of ceramides in the development of insulin resistance, two critical metabolic pathways overactivated in type 2 diabetes, were identified **(Figure 6.10)**. Notable, among the top significant downregulated pathways, GSVA detected glutathione metabolism and the pentose phosphate pathway, two essential antioxidant pathways highly regulated by Nrf2.

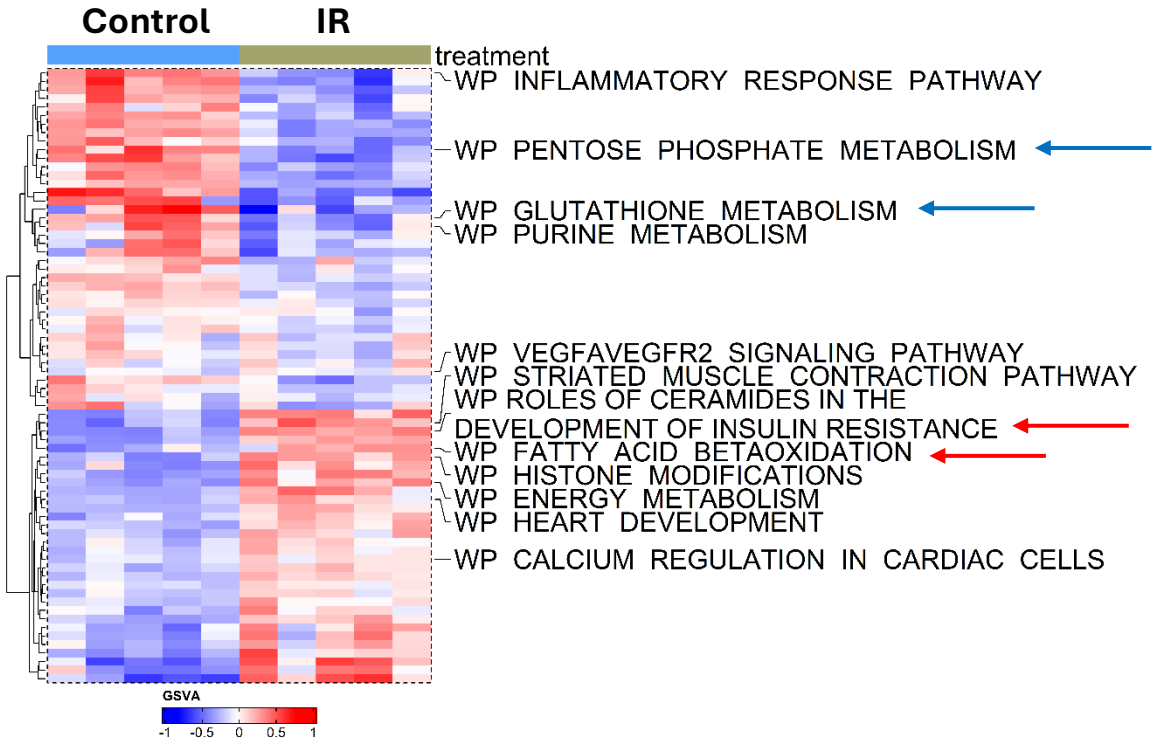

Figure 6.10: Gene set variation analysis detected upregulation of fatty acid β-oxidation metabolism in insulin-resistant compared with healthy hiPSC-CM. Transcriptomics analyses were performed on healthy (Control) or insulin-resistant (IR) hiPSC-CM. Each column represents a biological replicate.

The magnitude of the changes in the fatty acid β-oxidation pathway genes was visualised by generating boxplots of the mRNA levels for *CD36*, *ACSL1*, *CPT1B*, and *SLC25A20* (*CACT*), showing a significant increase of these targets in the IR condition compared with the healthy condition **(Figure 6.11)**. This genetic upregulation was also accompanied by a significant increase in the expression of the fatty acid oxidation master regulator *PGC1A* and the glucose metabolism negative regulator *PDK4*. These findings indicate that hiPSC-CM exposed to insulin-resistance media presented many of the metabolic characteristics observed in the T2D heart, including an upregulation of the fatty acid β-oxidation pathway and downregulation of glutathione metabolism[328, 329], which complemented the observed increased ratio of GSSG/GSH in the diabetic heart.

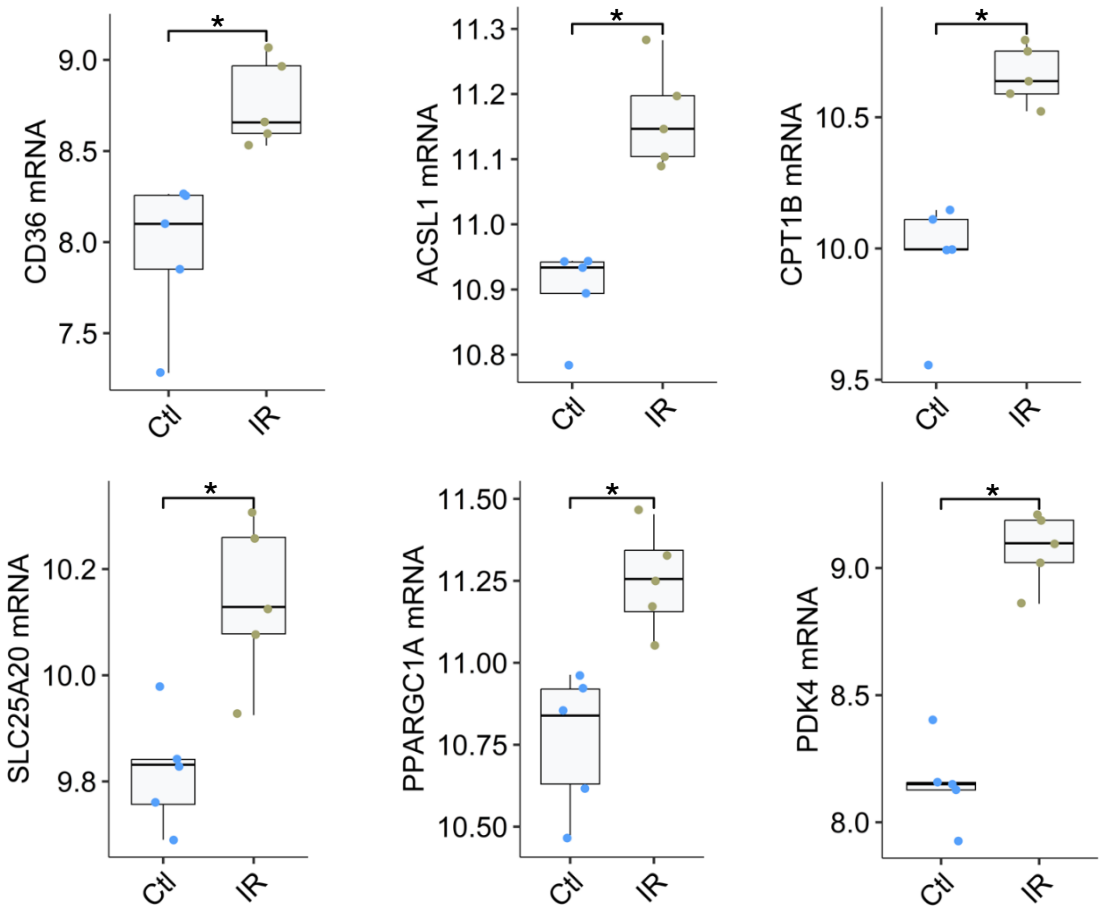

Figure 6.11: Insulin-resistant conditions increase genes involved in fatty acid β-oxidation in hiPSC-CM at the transcriptomics level. Boxplots for fatty acid oxidation genes extracted from the transcriptomics analyses performed on healthy (Ctl) or insulin-resistant (IR) hiPSC-CM. The evaluated genes were cluster of differentiation 36/fatty acid translocase (*CD36*), acyl-CoA synthetase long-chain family member 1 (*ACSL1*) carnitine palmitoyltransferase 1B (*CPT1B*), carnitine-acylcarnitine translocase (*SLC25A20/CACT)*, peroxisome proliferator-activated receptor gamma coactivator-1 alpha (*PPARGC1A*/*PGC1A*), and pyruvate dehydrogenase kinase 4 (*PDK4*). * Adjusted p-value < 0.05 vs. respective control group. Each data point represents a biological replicate.

6.5.5 Insulin-resistant hiPSC-CM show a decrease in Nrf2's antioxidant target genes.

The extent of the genetic changes induced by the IR condition was explored through a principal component analysis (PCA) that revealed a large separation between healthy and IR hiPSC-CM **(Figure 6.12A)**. The majority of the differences between samples were due to the first principal component (PC1), which represented the difference in cell media composition and showed a 57% variance with an evident separation between the samples of

each group, confirming the strong effect that the IR media had on the cells. The second principal component (PC2), which represented differences not associated with the cell media, accounted for a small 9%, suggesting that this component had almost no impact on the data distribution. An inter-sample correlation heatmap using Pearson correlation **(Figure 6.12B)** confirmed similarities between sample members of the same biological group (biological replicates) when healthy hiPSC-CM were compared with IR cells.

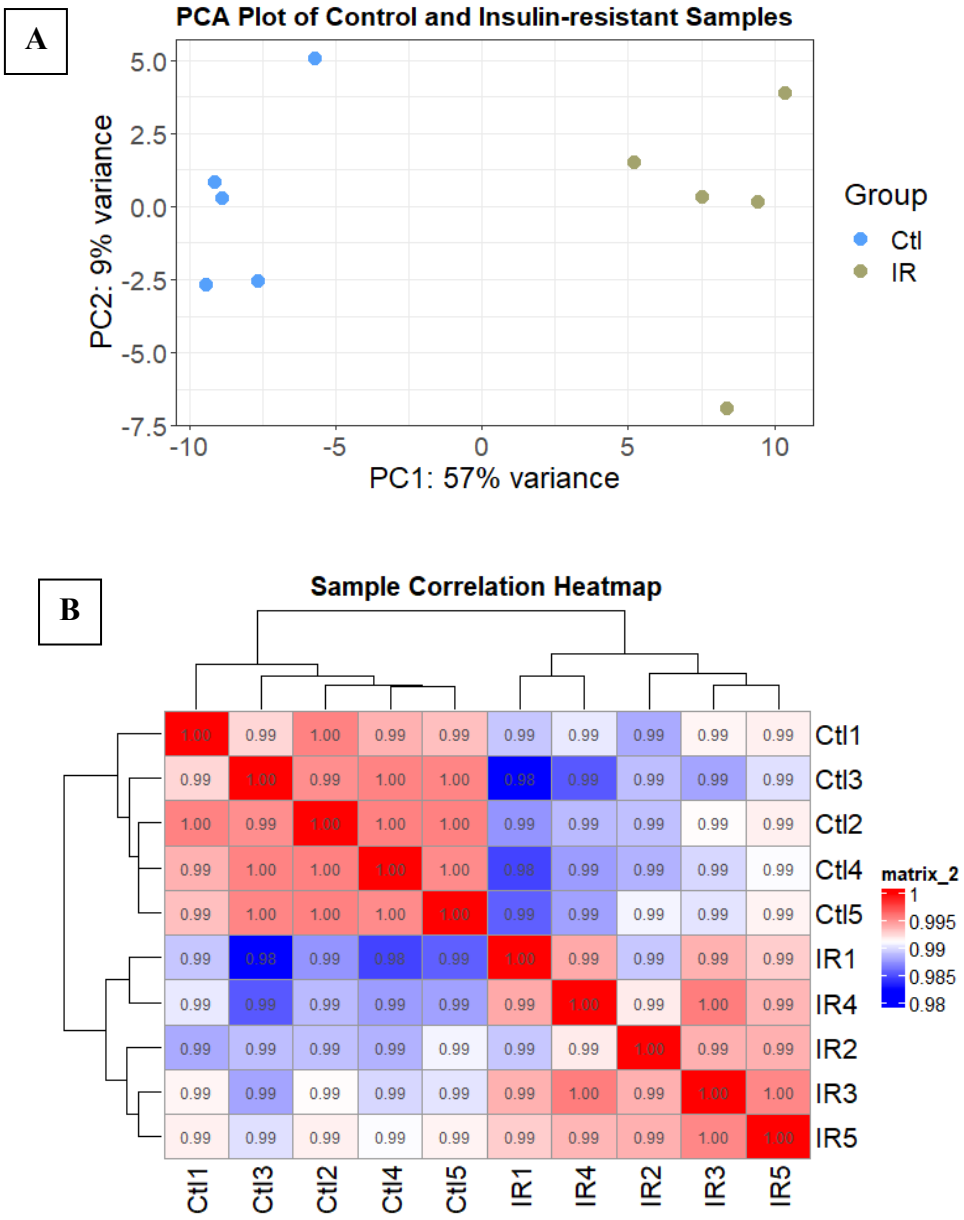

Figure 6.12: Insulin-resistant condition induces a larger gene expression changes in hiPSC-CM compared with control cells. Transcriptomics analyses were performed on healthy (Ctl) and insulin-resistant (IR) hiPSC-CM. **(A)** Principal component analyses between Ctl and IR groups. **(B)** Inter-sample correlation between samples of each condition.

At the beginning of this chapter, it was observed that type 2 diabetes induced an increase in the GSSG/GSH ratio within the heart, however, this was not accompanied by changes in the protein levels of antioxidant enzymes. These findings suggested that while oxidative stress was elevated in the diabetic heart, its ability to respond by increasing the antioxidant protein content was impaired. To determine whether this was occurring at the gene level, the impact of IR condition on the Nrf2 pathway gene expression was visualised by creating a heatmap that showed that IR condition induced a significant downregulation of specific Nrf2-regulated genes **(Figure 6.13).**

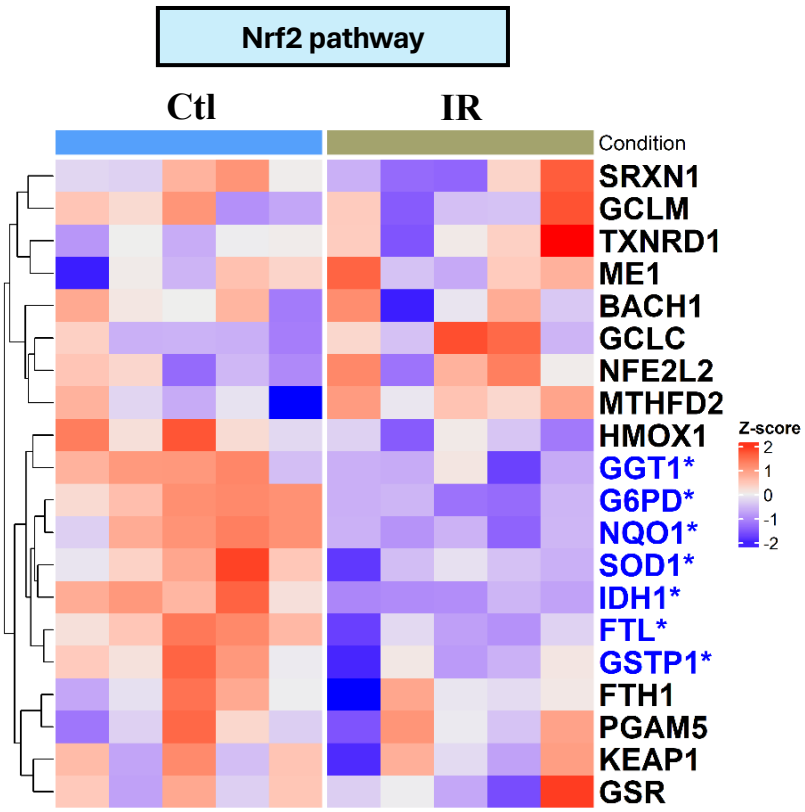

Figure 6.13: Insulin-resistant condition decreases Nrf2's antioxidant target genes in hiPSC-CM. Nrf2 pathway heatmap was generated using normalised counts from the transcriptomics analyses on insulin-resistant (IR) hiPSC-CM compared with healthy cells (Ctl). Significantly downregulated genes are shown in blue. * Fold change set as 0 and adjusted p-value vs. respective control group. Each column represents a biological replicate.

6.5.6 Dimethyl fumarate enhances the Nrf2 pathway and decreases fatty acid oxidation genes in insulin-resistant hiPSC-CM.

To evaluate whether fumarate derivatives could improve antioxidant mechanisms under insulin-resistant conditions, IR cells were treated with dimethyl fumarate (DMF) maintaining all IR reagents in the cell media. PCA analysis between healthy (Ctl), insulin-resistant (IR), and DMF-treated insulin-resistant (DMF_IR) hiPSC-CM showed a distinctive separation between groups **(Figure 6.14A)**. The majority of the differences between samples were due to the first principal component (PC1), which reflected the difference in cell media composition and revealed a 57% variance, confirming a unique effect of the IR media and DMF treatment on the cells. The second principal component (PC2) variation was 17%, suggesting that this component had a lower impact on the data distribution compared with PC1, however, on this component, DMF_IR changes were aligned closer to Ctl than with IR. Interestingly, DMF long-term treatment (16 hours) did not reverse the IR gene profile back to a healthy profile, but instead, it generated a unique gene profile.

An inter-sample correlation heatmap using Pearson correlation **(Figure 6.14B)** confirmed similarities between sample members of the same biological group (biological replicates) when Ctl, IR and DMF_IR were compared. Notably, this result showed that Ctl and IR samples are more similar to each other than to DMF_IR, but as in the previous case, DMF_IR was more closely related to the Ctl group than IR.

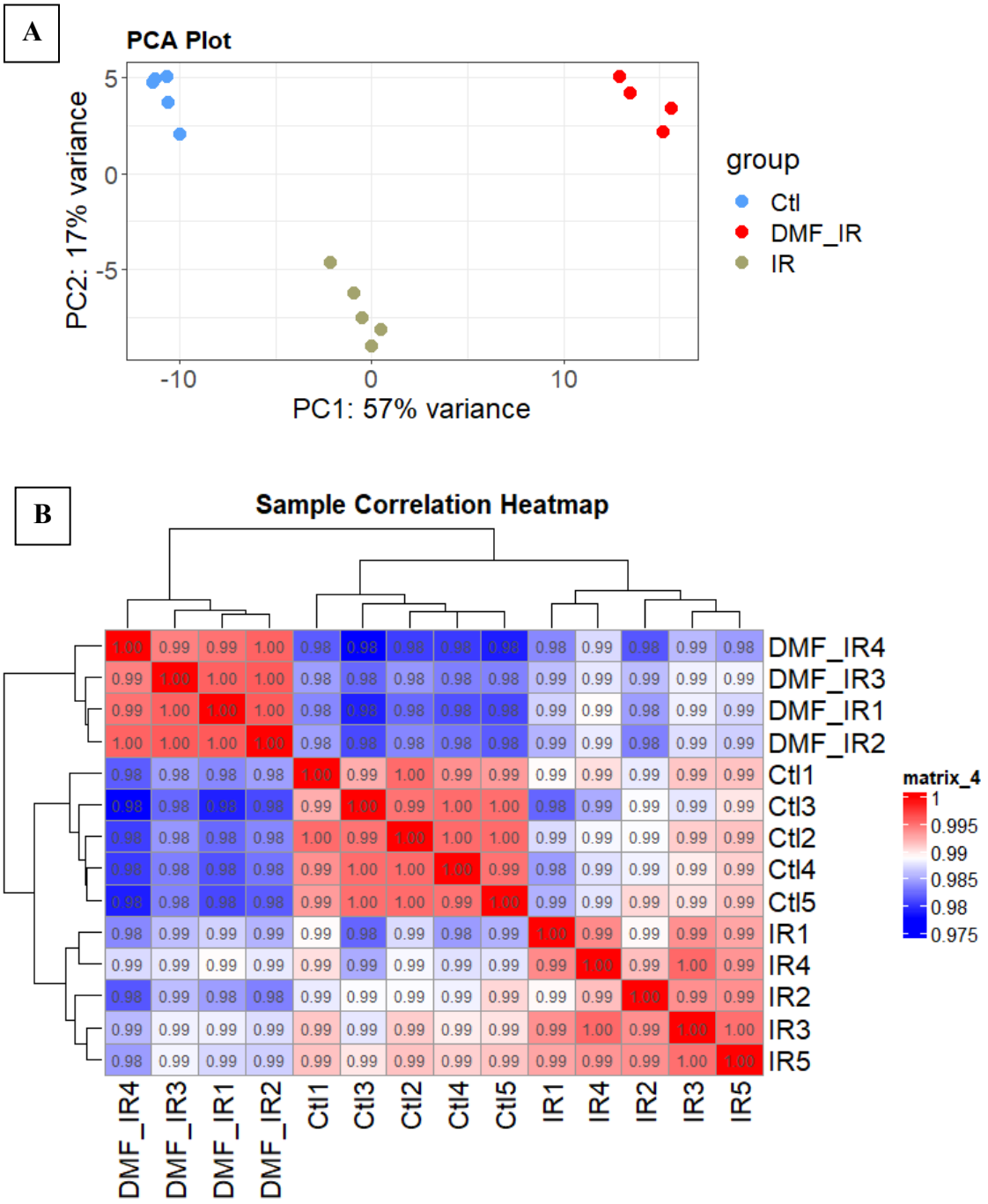

Figure 6.14: Dimethyl fumarate produces a larger gene change in insulin-resistant hiPSC-CM. Transcriptomics analyses were performed on healthy (Ctl), insulin-resistant (IR), or insulin-resistant hiPSC-CM exposed to DMF treatment (200 µM) for 16 hours (DMF_IR) **(A)** Principal component analyses between groups. **(B)** Inter-sample correlation between samples of each condition.

The impact of DMF treatment on the Nrf2 pathway in IR cells was visualised by generating a heatmap from the transcriptomics analysis comparing IR with DMF_IR hiPSC-CM. This heatmap showed that DMF induced a larger upregulation of practically all the Nrf2 pathways

(Figure 6.15), including the genes which were previously observed significantly reduced in IR cells.

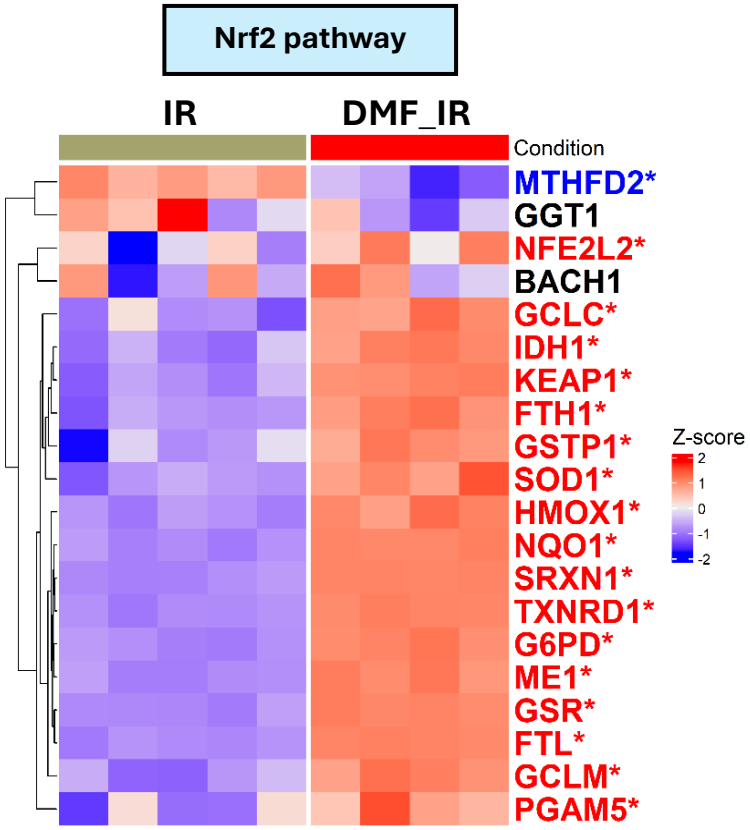

Figure 6.15: Dimethyl fumarate reverses Nrf2's antioxidant target genes impairment in insulin-resistant hiPSC-CM. Nrf2 pathway heatmap was generated using normalised counts from the transcriptomics analyses on insulin-resistant hiPSC-CM exposed to DMF treatment (200 µM) for 16 hours (DMF_IR) and compared with untreated insulin-resistant cells (IR). Significantly upregulated genes are shown in red and significantly downregulated genes are shown in blue. * Fold change set as 0 and adjusted p-value vs. respective IR group. Each column represents a biological replicate.

To further evaluate which biological processes DMF was regulating in the IR hiPSC-CM, gene set variation analysis (GSVA) was performed on DMF-treated and untreated insulin-resistant cells **(Figure 6.16)**. Complementary to the previous results, DMF significantly upregulates the Nrf2 pathway, as well as the pentose phosphate pathway, suggesting that DMF not only enhances the Nrf2's antioxidant target but also improves other critical pathways required to upregulate the antioxidant defence mechanisms. Interestingly, DMF also increased pathways involved in the DNA repair mechanism, including the ATR signalling pathway, which has also been involved in protection against apoptosis[330].

Notable, among the top significant downregulated pathways, GSVA detected that DMF decreased Krebs cycle enzyme genes and reduced adipogenesis and cholesterol biosynthesis, suggesting a potential role in obesity and diabetes.

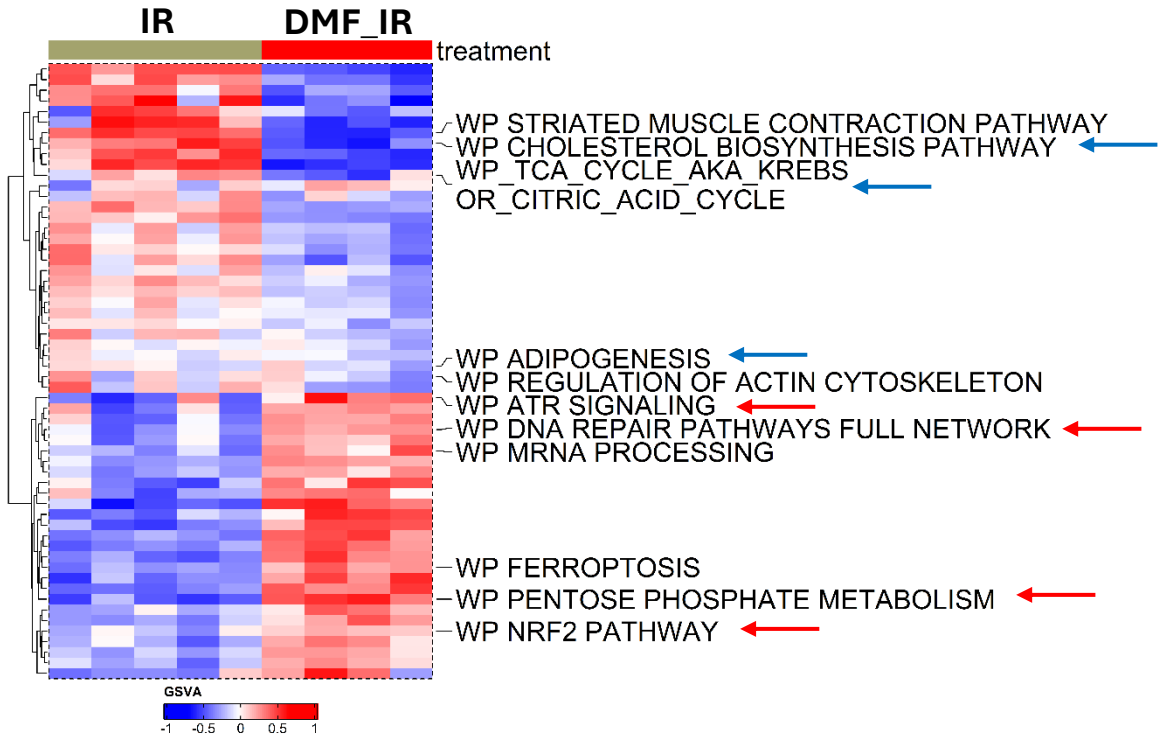

Figure 6.16 Gene set variation analysis detected upregulation of Nrf2 and pentose phosphate pathway metabolism in insulin-resistant hiPSC-CM exposed to dimethyl fumarate. Transcriptomics analyses were performed on insulin-resistant hiPSC-CM exposed to DMF treatment (200 µM) for 16 hours (DMF_IR) and compared with untreated insulin-resistant cells (IR). Each column represents a biological replicate.

In the previous chapters, it was observed that the antioxidant and metabolic changes occurred with short-term exposure (6 hours) to fumarate or fumarate derivatives treatment. Therefore, to evaluate whether similar regulation could happen in IR cells, the acute effect of DMF on the antioxidant genes was evaluated by qPCR. DMF significantly increased the expression of the genes *NQO1*, *TXNRD1*, *HMOX1*, and *SRXN1* by 2, 4, 32, and 6-fold, respectively, compared with the untreated IR hiPSC-CM **(Figure 6.17)**.

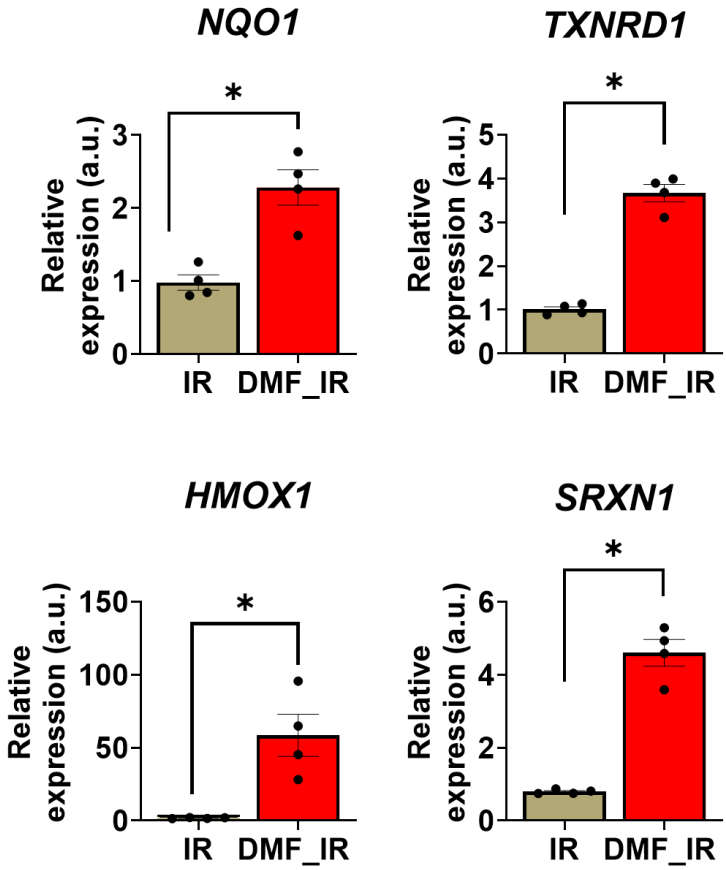

Figure 6.17: Short-term dimethyl fumarate treatment increases antioxidant genes in insulin-resistant hiPSC-CM. Insulin-resistant hiPSC-CM were exposed to DMF (150 µM) for 6 hours (DMF_IR) and compared with untreated insulin-resistant cells (IR). The evaluated genes by qPCR were NAD(P) dehydrogenase quinone 1 (*NQO1*), thioredoxin reductase 1 (*TXNRD1*), heme oxygenase 1 (*HMOX1*), and sulfiredoxin 1 (*SRXN*1). * $p < 0.05$ vs. respective IR group. a.u., arbitrary units. Each data point represents a biological replicate.

Finally, since fatty acid oxidation upregulation is a metabolic hallmark of T2D heart and because, in previous chapters, short-term DMF treatment decreased the expression of genes involved in fatty acid β-oxidation, the impact of DMF on key genes involved in this pathway was evaluated by qPCR. DMF significantly reduced *ACSL1*, *CPT1B*, *ECI,* and *PGC1A* gene expression by 49%, 49%, 51%, and 73%, respectively, compared with untreated IR hiPSC-CM **(Figure 6.18)**.

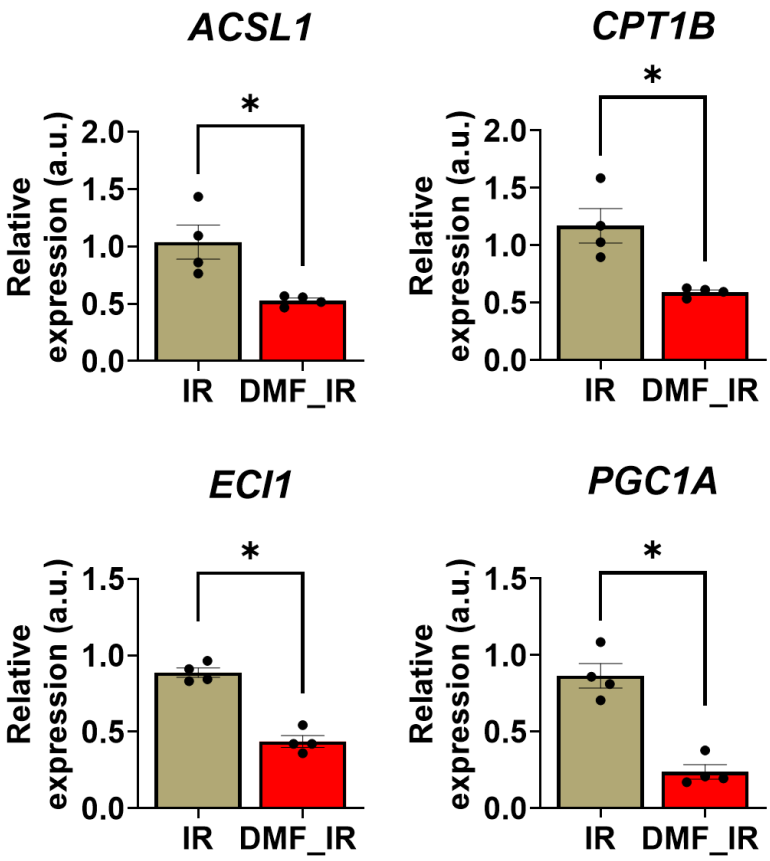

Figure 6.18: Short-term dimethyl fumarate treatment decreases fatty acid β-oxidation genes in insulin-resistant hiPSC-CM. Insulin-resistant hiPSC-CM were exposed to DMF (150 µM) for 6 hours (DMF_IR) and compared with untreated insulin-resistant cells (IR). The evaluated genes by qPCR were acyl-CoA synthetase long-chain family member 1 (*ACSL1*), carnitine palmitoyltransferase 1B (*CPT1B*), enoyl-CoA delta isomerase 1 (*ECI1*), and peroxisome proliferator-activated receptor gamma coactivator-1 alpha (*PGC1A*). * $p < 0.05$ vs. respective IR group. a.u., arbitrary units. Each data point represents a biological replicate.

Overall, these findings indicate that the insulin-resistant condition induced a large number of genetic changes within the human cardiomyocytes, including the impairment of the antioxidant enzymes and cellular pathways required for the correct functionality of the antioxidant defence mechanism. Dimethyl fumarate countered some genetic changes by enhancing Nrf2's antioxidant target genes at short- and long-term exposure, promoting other antioxidant and protective pathways while decreasing genes involved in oxidative metabolism, including fatty acid β-oxidation and Krebs cycle enzymes.

6.6 Discussion

6.6.1 Type 2 diabetes impairs metabolic adaptation in response to hypoxia within the heart.

Our results demonstrate that acute hypoxia significantly changes the intracellular concentration of metabolites within the diabetic heart but not to the same extent that we previously observed for the healthy heart. Interestingly, while some metabolites were significantly increased in both conditions, the magnitude of this increase in response to hypoxia was different in the healthy and diabetic heart, as was the case of fumarate and succinate intracellular levels. Notably, succinate levels in normoxia were higher in the diabetic heart, however after being exposed to acute hypoxia, its accumulation was only half as much as within the healthy heart. This reduction in the intracellular accumulation of succinate in diabetes has also been observed in ischemic diabetic rat hearts compared with non-diabetic hearts[331]. It has been reported that elevated circulating fatty acid in insulin-resistant cardiomyocytes suppressed succinate accumulation during hypoxia by inhibiting glycolysis and then succinate generation via the malate-aspartate shuttle[58].

In contrast, the significant reduction in some metabolites from the diabetic heart was more dramatic than in the healthy heart, as exemplified by succinyl-CoA. This may be a consequence of well-reported decrease in the activity of the mitochondrial enzyme succinyl-CoA:3-ketoacid-CoA transferase under type 2 diabetes[332, 333]. This enzyme generates succinyl-CoA by transferring the coenzyme-A from acetoacetyl-CoA to succinate, suggesting that these differences in the metabolite content may result from the inhibition of the anaplerotic pathways in diabetes.

The significant hypoxia-induced fumarate elevation within the healthy heart was suppressed in the diabetic heart, and the precise cellular and molecular mechanism associated with this

blunted response is unknown and exceeds the scope of this thesis. However, the ANOVA results indicate that fumarate accumulation depends on both oxygen levels (normoxia or hypoxia) and the heart condition (healthy or diabetic), given that the hypoxia intensity and duration were consistent in both experiments, this impairment is likely associated with the diabetic condition. A potential mechanism for this impairment involves the Krebs cycle enzyme fumarate hydratase (FH), which under healthy conditions, oxidises fumarate into malate. Studies have reported that FH depletion in β-cells promotes glucose intolerance and diabetes development, as well as that diabetic islets present decreased FH gene expression[334, 335]. These observations suggest a link between diabetes and decreased FH activity or levels. Notably, under hypoxic conditions, the Krebs cycle operates in reverse, therefore the impaired FH activity observed in T2D would be expected to reduce fumarate generation from malate. Furthermore, as mentioned before, inhibition of glycolysis by elevated fatty acid concentration impaired malate-aspartate shuttle[58], which could also limit fumarate production.

6.6.2 Nrf2 antioxidant response is blunted in the diabetic heart.

Our results show that type 2 diabetes increases the oxidative marker GSSG/GSH within the rat heart without altering the antioxidant protein content. Significant increases in GSSG content and decreases in GSH concentration have been reported in plasma from type 2 diabetic patients[336] and rat ventricular cardiomyocytes[337]. Consistent with these findings, our IR cell model also showed downregulation in the glutathione metabolism pathway, an event previously reported under diabetes condition for various cell types, including hepatocytes[338], cardiomyocyte models[328, 329], and even for erythrocytes from type 2 diabetic patients[339]. Notably, we did not detect any difference in the protein content of the antioxidant protein levels, however, it has been reported that diabetes decreases the activity of several antioxidant enzymes[340-342], and this alteration increases oxidative stress and

cellular dysfunction[343, 344]. The differences observed regarding the antioxidant enzymes levels between diabetic patients and our diabetic rat model could be due to the fact that our model represents a mild and early-stage type 2 diabetic condition[345]. While it recapitulates the cardiac metabolic alteration observed in T2D patients, the rats may not have been exposed to the T2D condition long enough to develop all the oxidative stress alterations observed in patients. This could explain why only differences between diabetic and control hearts for the early oxidative stress marker, GSSG/GSH ratio, were detected but not for protein carbonylation or antioxidant enzyme levels.

The results observed in our insulin-resistant cardiomyocyte suggest that the increased oxidative stress may be caused by a decrease in the antioxidant enzyme activity. Our data showed that the pentose phosphate pathway was downregulated under insulin-resistant conditions, implying a decrease in the NADPH cofactor pool required for plenty of the antioxidant enzyme functionality. Similar dysregulation has been described for other diabetic models, where a downregulation in the activity of the glucose-6-phosphate dehydrogenase, a key rate-limiting enzyme in the pentose phosphate pathway, was reported accompanied by a reduction in NADPH production and an increase in oxidative stress[346-349].

Our data was focused on the genetic expression in insulin-resistant condition, and we observed that Nrf2's antioxidant genes were downregulated. The Nrf2 pathway has been reported to be impaired in diabetes[350, 351], and it has been observed that two critical hallmarks of type 2 diabetes, insulin resistance and β-cell dysfunction, can also prevent Nrf2 pathway activation[352]. This disruption involves several altered mechanisms, including the increase in the protein levels and binding capacity of the Nrf2's suppressor KEAP1 in diabetic rat primary fibroblasts[353], as well as upregulation of BACH1 and FYN protein

content, two inhibitors of the nuclear Nrf2 activity as a transcription factor in db/db mouse heart[354].

6.6.3 Dimethyl fumarate as a therapeutical tool to enhance antioxidant defences and reverse fatty acid metabolism within the diabetic heart.

In our *in vivo* pilot studies using dimethyl fumarate (DMF), no changes in the cardiac antioxidant enzymes were observed, an unexpected result that we attribute to the delivery method rather than the dose or duration used for DMF. While most of the *in vivo* animal studies commonly used oral gavage for DMF delivery[168, 326, 355-358], we considered this method as invasive and stressful for the animals. To avoid generating variability in the baseline stress state of the animals, we decided to add the DMF directly to pots containing jelly. However, to prevent DMF from being hydrolysed into fumarate in an aqueous solution, (as we aimed to study DMF effect), we did not pre-mix DMF into the jelly, but instead, we added DMF in the powdered form directly to the jelly just immediately before feeding it to the animals. Although initially, this method worked, rats gradually stopped consuming the jelly, likely due to taste and odour alterations caused by DMF, as this issue was not observed in control animals fed with plain jelly.

Given the dysregulation of Nrf2 under diabetes and insulin-resistant conditions, we explored the potential use of the fumarate derivative, DMF, as a therapeutic molecule to reverse the diabetic phenotype using insulin-resistant human cardiomyocytes. Our data showed that both short- and long-term treatments with DMF significantly upregulate the Nrf2 pathway at the gene level, demonstrating that DMF can enhance the antioxidant enzyme system in insulin-resistant condition.

The potential therapeutic use of DMF in diabetes has been studied in different diabetic models, observing that DMF significantly reduces diabetes onset[170], accelerate wound

healing[359], and reverse cardiac dysfunction[360] in diabetic mice. Furthermore, DMF also increases HDL content and reduces glycated haemoglobin, total cholesterol and advanced glycation end product (AGEs) in serum from diabetic rats[361]. Similarly, the Nrf2 activator sulforaphane (SFN) has been reported to decrease diabetes alterations by reducing glucose levels and glucose intolerance in type 2 diabetes patients[362]. SFN also decreased oxidative stress, serum triglycerides, cholesterol, LDL, insulin, and insulin resistance in clinical studies in type 2 diabetes patients[363, 364].

Numerous anti-diabetic drugs directly or indirectly affect fatty acid oxidation. Metformin, the gold-standard drug for type 2 diabetes treatment, reduces lipid accumulation by increasing fatty acid oxidation[365, 366]. In contrast, the hypoglycaemic drugs glyburide and tolbutamide have been shown to inhibit carnitine palmitoyl transferase 1, decreasing fatty acid oxidation[367, 368]. The role of Nrf2 in regulating fatty acid oxidation in diabetic conditions has not been well documented, and here we observed that short-term treatment with DMF significantly decreased the gene expression of essential fatty acid β-oxidation components. However, as demonstrated in previous chapters, this reduction may not result directly from DMF effect, but rather from fumarate generation and its previously observed downregulation of this pathway. This represents a limitation of this chapter because the role of fumarate itself was not studied in our insulin-resistant hiPSC-CM model, indicating that this is a key experiment for future investigation.

6.7 Conclusion

Type 2 diabetes and insulin resistance conditions altered several cellular processes and metabolic pathways in the heart, impairing the cellular response to oxidative stress by inducing a dysregulation of the Nrf2 and its antioxidant-related pathways. Here, we demonstrate that the FDA-approved drug dimethyl fumarate can reverse this phenotype by

enhancing the Nrf2 pathway and upregulating other antioxidant cellular components within the insulin-resistant human cardiomyocyte. Dimethyl fumarate can also decrease the overactivated fatty acid oxidation metabolic profile of these cells, suggesting that dimethyl fumarate has potential therapeutic use for the treatment of cardiac metabolic disorders.

Chapter 7

General discussion

Hypoxia induces alterations in the intracellular content of several metabolites within the heart, including an increase in intracellular fumarate concentrations. However, fumarate elevation is suppressed within the type 2 diabetic heart, and the consequences of this blunted response are unknown. Whether this limited fumarate accumulation under hypoxia is related to the detrimental effects on cardiac health and function described for this metabolic disorder[104] remains unclear. Understanding the role of fumarate beyond its energetic function in the Krebs cycle and identifying signalling pathways that fumarate regulates was one of the key aims of this thesis. Moreover, given the therapeutic approval of fumarate derivates for human use, this work also investigated their potential use of fumarate derivatives in human cardiomyocytes, comparing their effect with fumarate itself, and furthermore their benefit for insulin-resistant cardiomyocytes.

7.1 Fumarate derivatives modulate cardiomyocyte metabolism, potentially through their hydrolysis into fumarate.

We observed that fumarate derivatives modulated cardiac metabolism by shifting from oxidative to anaerobic metabolism, specifically decreasing fatty acid β-oxidation and mitochondria activity while enhancing the glycolytic pathway. Dimethyl fumarate (DMF) results **(Chapter 4)** demonstrated that changes in glycolytic gene expression and rates, lactate release, mitochondrial respiration, and fatty acid oxidation rates occurred after 24 hours of treatment, whereas fumarate itself **(Chapter 5)** induced similar metabolic changes within just 6 hours of treatment. This rapid fumarate effect, combined with our observation that DMF was hydrolysed into fumarate in cell media following 24 hours, suggests that the metabolic changes observed with DMF treatment were potentially induced by fumarate itself. It is important to note that a limitation of our hydrolysis experiment is that it was performed in cell-free media at 25°C for technical reasons. However, under physiological

conditions, DMF would be incorporated into the cardiomyocytes, where its hydrolysis into fumarate would likely occur more rapidly due to the presence of cell esterases.

In the search for intracellular signalling pathways associated with fumarate-induced metabolic changes, we ruled out HIF1 as the only ‘‘HIF1-regulated genes’’ that we detected upregulated were the glycolytic genes. In contrast, other non-metabolic genes did not show the same regulation. This suggests that the glycolytic genes were misleadingly driving the HIF1 pathway as an upregulated pathway.

Using a genetic cardiac model with constitutive Nrf2 activation, we determined that Nrf2 may not mediate the observed metabolic changes. This finding was further supported by luciferase assays showing that fumarate did not activate the Nrf2 pathway at the same time point as the metabolic changes were observed. However, conflicting data showed that the Nrf2 activators, sulforaphane and hydrogen peroxide, induced similar metabolic changes to those observed for the fumarate derivatives, potentially implicating that Nrf2 could be involved in this metabolic reprogramming. Therefore, without additional genetic models or specific pharmacological inhibitors of Nrf2, it is not possible to determine whether this transcription factor is involved in these metabolic changes.

The circadian rhythm was another process that was upregulated by fumarate. However, the specific role of this pathway in modulating cardiomyocyte metabolism was not evaluated in this thesis. While the upregulation of this pathway was detected at the same time point that the fumarate-induced metabolic changes occurred (6 hours), no effect on this pathway was observed after one-hour fumarate treatment. Interestingly, one-hour fumarate treatment downregulated *PGC1A* expression, suggesting that fumarate-induced metabolic shift could be a direct consequence of fumarate modulating fatty acid β-oxidation. However, despite having identified several molecular and signalling targets of fumarate, the mechanism

behind fumarate-induced metabolic reprogramming remains unknown, and further experiments are required to elucidate how this metabolic shift occurs.

7.2 Dimethyl fumarate and fumarate activate distinct signalling pathways and induce different effects on protein succination.

Fumarate derivatives have historically been used as molecules to study fumarate's effect across different models, and in this thesis, we demonstrated that the effect of a metabolite prodrug could differ from the effect of the metabolite itself. Our data demonstrates that in human cardiomyocytes, fumarate did not activate Nrf2 pathway at the same time point that DMF, observing that Nrf2 activation occurs later and with a smaller fold change compared with DMF.

Furthermore, we detected a differential regulation of PTM mediated by both molecules, observing that DMF increased protein succination, whereas exogenous fumarate decreased the total protein succination content compared with the control condition in our human cardiomyocyte model. Even though human protein succination induced by fumarate has been reported *in vitro* previously, this was only observed at extremely high fumarate concentrations and under specific pH conditions[369]. Similar differences were reported in adipocytes, in which protein succination was detected to increase following DMF but did not change following fumarate treatment[370]. Interestingly, one study in activated human and mouse macrophages and lymphocytes showed that the fumarate derivatives DMF and monomethyl fumarate (MMF) induce GAPDH succination and inhibition, thereby reducing aerobic glycolysis[217]. This suggests that fumarate's upregulation of glycolytic metabolism could be mediated in part by its negative modulation of this PTM in cardiomyocytes.

We identified distinct pathways regulated by each of these molecules: DMF mainly enhanced the antioxidant defence mechanisms, including the Nrf2 pathway, pentose

phosphate pathway (including NADPH regeneration), and glutathione metabolism **(Chapter 3)**, whereas fumarate promoted the circadian rhythm pathway **(Chapter 5)**. The differences in cellular process regulation between DMF and fumarate are presented in **Table 7.1**.

Table 7.1. Comparative summary of the effect of dimethyl fumarate (DMF) and fumarate in cardiomyocytes.

Cell process	DMF	Fumarate
Nrf2 Activation	↑ **6, 12 and 24 hours**	↑ **24 hours**
Succination	↑ **6 hours**	↓ **6 hours**
Distinct enhanced pathways	**Pentose phosphate pathway.** **NADPH regeneration.** **Glutathione metabolism.**	**Circadian rhythm.**
Glycolytic rates	↑ **24 and 48 hours**	↑ **6 hours**
Fatty acid oxidation rates	↓ **24 hours**	↓ **6 and 12 hours**
Mitochondria oxygen consumption	↓ **24 hours**	↓ **12 and 24 hours**

7.3 Fumarate as a novel Gi-protein-coupled signalling activator.

In contrast with the previous upregulated pathways comparison, we identified common downregulated pathways for both molecules, including heart development and signalling by G-coupled signalling receptors (GPCR). Interestingly, GPCR signalling was the only pathway that was downregulated in the GSVA results for human cardiomyocytes for DMF and both fumarate treatments (one hour and six hours). Notably, we also detected that the

number of downregulated genes for GPCR signalling pathway was more dramatic following fumarate treatment compared with DMF **(Chapter 5)**.

While the role of fumarate derivatives activating the HCA2 receptor has been previously reported[243, 296, 299], we identified a novel role for fumarate in modulating cAMP levels via G-coupled signalling pathways. This finding suggests an important paracrine role of the cardiomyocytes regulating other cells by realising fumarate. Notably, in the diabetic heart, we detected an impaired ability to elevate fumarate levels in response to hypoxia **(Chapter 6)**, suggesting that this metabolic disorder could also suppress this paracrine signalling role of the cardiomyocyte. Gi-receptor depletion in mice adipocytes, a cell type that highly expresses HCA2[243], increases lipolysis, promotes insulin resistance and disrupts glucose homeostasis[371]. Additionally, high fatty acid levels blunt hypoxia-driven metabolic adaptation in diabetic heart and insulin-resistant cardiomyocytes, resulting in cardiac dysfunction[58]. These observations suggest that the suppressed ability of the diabetic heart to elevate fumarate levels in response to hypoxia may be partly responsible for the increased circulating fatty acid due to the lack of fumarate-mediated paracrine modulation via G-protein-coupled signalling pathways.

HCA2 agonists, including niacin and its derivates acipimox and acifran, are clinically used to treat dyslipidemia[296, 372, 373]. However, the use of niacin for treating type 2 diabetes patients dyslipidemia has been considered as a ‘‘double-edged sword’’, as it also increases fasting blood glucose levels[374]. In contrast, our findings show that fumarate acts extracellularly as an HCA2 agonist and increases glucose uptake and utilisation intracellularly **(Chapter 5)**. This suggests a potential role of exogenous fumarate as a therapeutic molecule in type 2 diabetes patients, reversing the lipotoxicity and glucotoxicity phenotypes characteristic of this disease.

7.4 Repurposing fumarate derivatives treatment for type 2 diabetes patients.

We identified that fumarate derivatives enhanced Nrf2 pathway activation and upregulated antioxidant gene expression in both healthy **(Chapter 3)** and insulin-resistant **(Chapter 6)** human cardiomyocytes. Furthermore, fumarate derivatives (likely due to their hydrolysis intro fumarate) were shown to decrease fatty acid oxidation and mitochondria oxygen consumption while promoting glycolytic metabolism **(Chapter 4)**.

Interestingly, a rodent study demonstrated that fumarate derivatives have an important impact on metabolic disorders such as obesity, where these molecules reduce weight gain in high-fat/high-sucrose diet-inducing obesity, decreasing glucose intolerance and improving insulin sensitivity[375]. Furthermore, patients under DMF treatment showed increased serum adiponectin levels and reduced fatty acid binding protein FABP4[376]. Adiponectin, a hormone secreted by adipocytes, plays an important role in improving insulin sensitivity and modulating anti-inflammatory processes[377], and notable low levels of this hormone are associated with type 2 diabetes and pre-diabetes[378, 379].

Our findings, along with these observations, indicate a potential therapeutic role for the fumarate derivatives in the treatment of metabolic disorders. Our data shows the potential of these molecules to reverse the cardiac metabolic phenotype associated with type 2 diabetes, including its increased oxidative stress resulting from lipotoxicity and glucotoxicity[314, 317-320, 380], mitochondria dysfunction[323, 381, 382], and reduced antioxidant activity[372-374] as well as its metabolic alterations characterised by increasing fatty acid β-oxidation and suppressing glucose metabolism[315] **(Figure 7.1)**.

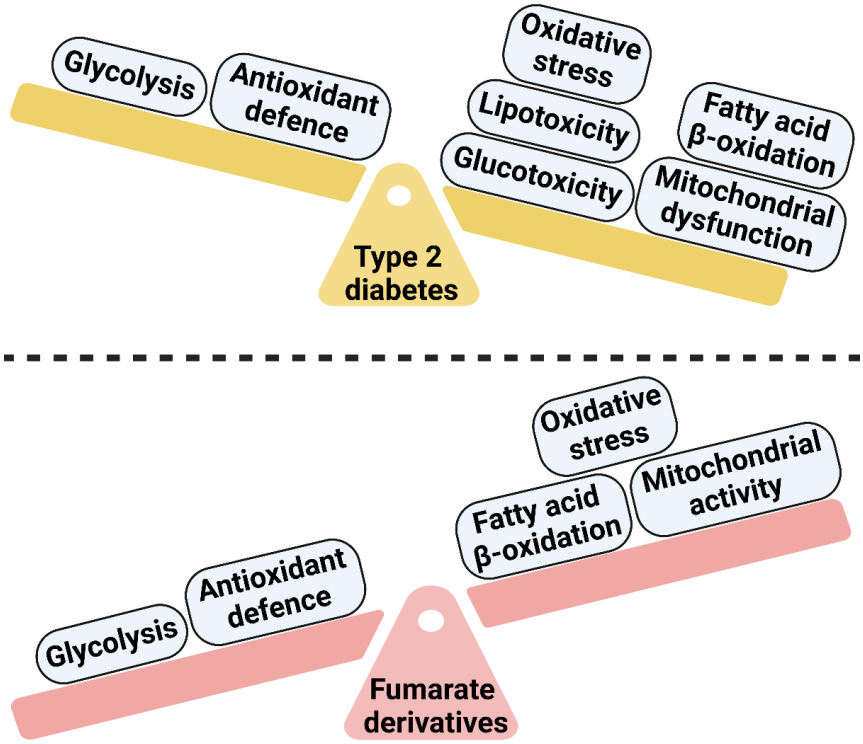

Figure 7.1: Fumarate derivatives as potential therapeutic molecules for the type 2 diabetic heart. Type 2 diabetes (T2D) promotes preferential fatty acid utilisation, increasing fatty acid β-oxidation, cardiac lipid accumulation, lipotoxicity and inducing mitochondrial dysfunction. T2D also decreases glucose metabolism, increasing circulating glucose, and induces glucotoxicity. These disarrangements, in addition to the reduced antioxidant defence mechanisms, increase reactive oxygen species and induce oxidative damage. In contrast, fumarate derivatives induce a metabolic shift from fatty acid to glucose metabolism within the cardiomyocyte, reducing mitochondrial activity and enhancing the antioxidant defence pathway, thereby decreasing oxidative stress. These findings suggest a potential therapeutic role for fumarate derivatives in reversing the cardiac metabolic dysfunction observed in the T2D heart.

7.5 Conclusion.

The work presented in this thesis has furthered the understanding of physiological processes and molecular pathways modulated in the heart in response to hypoxia. Specifically, it showed a novel role for the Krebs cycle metabolite fumarate as a signalling molecule regulating cardiomyocyte metabolism and Gi-protein-coupled signalling pathway. Furthermore, this work explored the potential therapeutic role of fumarate derivatives in addressing insulin-resistant disarrangements in human cardiomyocytes, presenting an

intriguing capacity to reverse the metabolic alterations and the reduced antioxidant response characteristic of the type 2 diabetic heart. The summary of this thesis's findings on signalling pathways regulated by fumarate and its derivatives in human cardiomyocytes is presented in **Figure 7.2**.

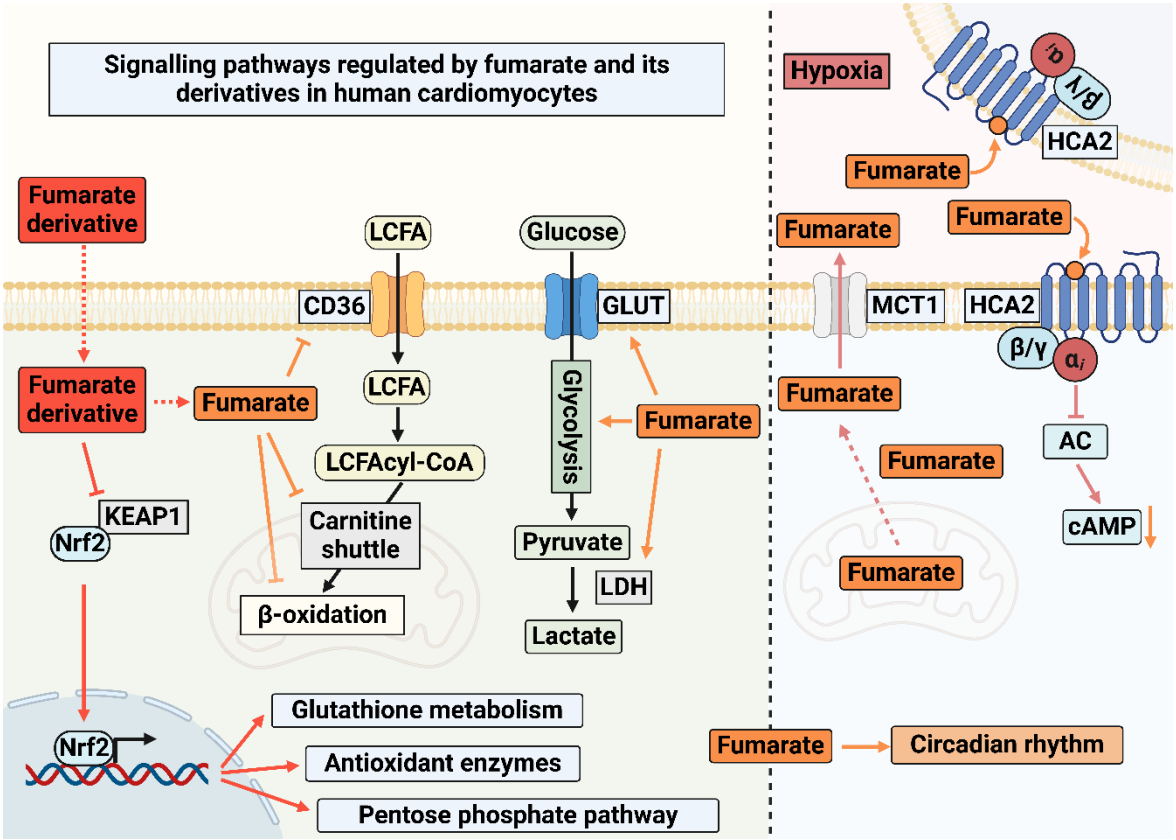

Figure 7.2: Summary of thesis findings on signalling pathways regulated by fumarate and its derivatives in human cardiomyocytes. Fumarate derivatives promoted Nrf2 nuclear translocation, thereby enhancing antioxidant defence mechanisms, including glutathione metabolism, antioxidant enzymes and pentose phosphate pathway. Fumarate derivatives were hydrolysed into fumarate, which induced a metabolic shift within the cardiomyocyte, decreasing fatty acid oxidation and mitochondrial activity, while increasing glycolytic metabolism. Additionally, fumarate was shown to activate circadian rhythm. Finally, under hypoxia condition, fumarate accumulated intracellularly, and it was released into the extracellular space by the monocarboxylate transporter 1 (MCT1), where it modulated Gi-couple signalling pathway via the hydroxycarboxylic acid receptor 2 (HCA2), inducing adenyl cyclase (AC) inactivation, and then decreasing cAMP levels. Nrf2, nuclear factor erythroid 2 [NF-E2]-related factor 2. KEAP1, Kelch-like erythroid cell-derived protein with CNC homology [ECH]-associated protein 1. CD36, cluster of differentiation 36/fatty acid translocase. LCFA, long-chain fatty acids. LCFAcyl-CoA, long-chain fatty acyl-CoA. GLUT, glucose transporter. LDH, lactate dehydrogenase. mTORC1, mammalian target of rapamycin complex 1.

8. Bibliography

1. Avram R, Tison GH, Aschbacher K, Kuhar P, Vittinghoff E, Butzner M, et al. Real-world heart rate norms in the Health eHeart study. NPJ Digit Med. 2019;2:58.

2. Ingwall JS. ATP and the Heart. Cardiologist BSft, editor. Boston, MA.: Springer Science & Business Media; 2002. 244 p.

3. Doenst T, Nguyen TD, Abel ED. Cardiac metabolism in heart failure: implications beyond ATP production. Circ Res. 2013;113(6):709-24.

4. Lopaschuk GD, Karwi QG, Tian R, Wende AR, Abel ED. Cardiac Energy Metabolism in Heart Failure. Circulation Research. 2021;128(10):1487-513.

5. Abel ED. Glucose transport in the heart. Front Biosci. 2004;9:201-15.

6. Frayn KN, Evans RD. Human metabolism : a regulatory perspective. Hoboken, NJ: John Wiley & Sons, Inc.; 2019. Available from: https://search.ebscohost.com/login.aspx?direct=true&scope=site&db=nlebk&db=nlabk&AN=2089009.

7. Castro-Guarda M, Evans RD. Human metabolism: metabolic pathways and clinical aspects. Surgery - Oxford International Edition.

8. Schulze PC, Drosatos K, Goldberg IJ. Lipid Use and Misuse by the Heart. Circ Res. 2016;118(11):1736-51.

9. Hauton D, Bennett MJ, Evans RD. Utilisation of triacylglycerol and non-esterified fatty acid by the working rat heart: myocardial lipid substrate preference. Biochimica et Biophysica Acta (BBA) - Molecular and Cell Biology of Lipids. 2001;1533(2):99-109.

10. Pulinilkunnil T, Qi D, Ghosh S, Cheung C, Yip P, Varghese J, et al. Circulating triglyceride lipolysis facilitates lipoprotein lipase translocation from cardiomyocyte to myocardial endothelial lining. Cardiovascular Research. 2003;59(3):788-97.

11. Luiken JJFP, Schaap FG, van Nieuwenhoven FA, van der Vusse GJ, Bonen A, Glatz JFC. Cellular fatty acid transport in heart and skeletal muscle as facilitated by proteins. Lipids. 1999;34(S1Part2):S169-S75.

12. Chabowski A, Górski J, Glatz JF, JJ PL, Bonen A. Protein-mediated Fatty Acid Uptake in the Heart. Curr Cardiol Rev. 2008;4(1):12-21.

13. Salway JG. Metabolism at a Glance: Wiley; 2017.

14. Talley JT, Mohiuddin SS. Biochemistry, Fatty Acid Oxidation: StatPearls Publishing, Treasure Island (FL); 2023 2023.

15. Tran DH, Wang ZV. Glucose Metabolism in Cardiac Hypertrophy and Heart Failure. J Am Heart Assoc. 2019;8(12):e012673.

16. Depre C, Vanoverschelde J-LJ, Taegtmeyer H. Glucose for the Heart. Circulation. 1999;99(4):578-88.

17. Patel MS, Korotchkina LG. Regulation of mammalian pyruvate dehydrogenase complex by phosphorylation: complexity of multiple phosphorylation sites and kinases. Experimental & Molecular Medicine. 2001;33(4):191-7.

18. Postic C, Dentin R, Denechaud PD, Girard J. ChREBP, a transcriptional regulator of glucose and lipid metabolism. Annu Rev Nutr. 2007;27:179-92.

19. Heidenreich S, Weber P, Stephanowitz H, Petricek KM, Schütte T, Oster M, et al. The glucose-sensing transcription factor ChREBP is targeted by proline hydroxylation. J Biol Chem. 2020;295(50):17158-68.

20. Lei Y, Zhou S, Hu Q, Chen X, Gu J. Carbohydrate response element binding protein (ChREBP) correlates with colon cancer progression and contributes to cell proliferation. Scientific Reports. 2020;10(1):4233.

21. Georgiadi A, Kersten S. Mechanisms of Gene Regulation by Fatty Acids. Advances in Nutrition. 2012;3(2):127-34.

22. Fatehi-Hassanabad Z, Chan CB. Transcriptional regulation of lipid metabolism by fatty acids: a key determinant of pancreatic beta-cell function. Nutr Metab (Lond). 2005;2(1):1.

23. Huang R, Zhang J, Li M, Yan P, Yin H, Zhai S, et al. The Role of Peroxisome Proliferator-Activated Receptors (PPARs) in Pan-Cancer. PPAR Res. 2020;2020:6527564.

24. Tyagi S, Gupta P, Saini AS, Kaushal C, Sharma S. The peroxisome proliferator-activated receptor: A family of nuclear receptors role in various diseases. J Adv Pharm Technol Res. 2011;2(4):236-40.

25. Kersten S. Integrated physiology and systems biology of PPARα. Mol Metab. 2014;3(4):354-71.

26. Hu P, Li K, Peng X, Kan Y, Li H, Zhu Y, et al. Nuclear Receptor PPARα as a Therapeutic Target in Diseases Associated with Lipid Metabolism Disorders. Nutrients. 2023;15(22):4772.

27. Garland PB, Newsholme EA, Randle PJ. Effect of Fatty Acids, Ketone Bodies, Diabetes and Starvation on Pyruvate Metabolism in Rat Heart and Diaphragm Muscle. Nature. 1962;195(4839):381-3.

28. Randle PJ, Garland PB, Hales CN, Newsholme EA. THE GLUCOSE FATTY-ACID CYCLE ITS ROLE IN INSULIN SENSITIVITY AND THE METABOLIC DISTURBANCES OF DIABETES MELLITUS. The Lancet. 1963;281(7285):785-9.

29. Hue L, Taegtmeyer H. The Randle cycle revisited: a new head for an old hat. Am J Physiol Endocrinol Metab. 2009;297(3):E578-91.

30. Lesnefsky EJ, Chen Q, Tandler B, Hoppel CL. Mitochondrial Bioenergetics in the Heart. In: Vasan RS, Sawyer DB, editors. Encyclopedia of Cardiovascular Research and Medicine. Oxford: Elsevier; 2018. p. 365-80.

31. Krebs H, Johnson W. The role of citric acid in intermediate metabolism in animal tissues. Enzymologia. 1937;4:148–56.

32. Arnold PK, Finley LWS. Regulation and function of the mammalian tricarboxylic acid cycle. Journal of Biological Chemistry. 2023;299(2):102838.

33. Owen OE, Kalhan SC, Hanson RW. The Key Role of Anaplerosis and Cataplerosis for Citric Acid Cycle Function *. Journal of Biological Chemistry. 2002;277(34):30409-12.

34. Inigo M, Deja S, Burgess SC. Ins and Outs of the TCA Cycle: The Central Role of Anaplerosis. Annu Rev Nutr. 2021;41:19-47.

35. Nolfi-Donegan D, Braganza A, Shiva S. Mitochondrial electron transport chain: Oxidative phosphorylation, oxidant production, and methods of measurement. Redox Biol. 2020;37:101674.

36. Zhao RZ, Jiang S, Zhang L, Yu ZB. Mitochondrial electron transport chain, ROS generation and uncoupling (Review). Int J Mol Med. 2019;44(1):3-15.

37. Hamilton JP. Epigenetics: principles and practice. Dig Dis. 2011;29(2):130-5.

38. Salminen A, Kauppinen A, Hiltunen M, Kaarniranta K. Krebs cycle intermediates regulate DNA and histone methylation: Epigenetic impact on the aging process. Ageing Research Reviews. 2014;16:45-65.

39. Huergo LF, Dixon R. The Emergence of 2-Oxoglutarate as a Master Regulator Metabolite. Microbiol Mol Biol Rev. 2015;79(4):419-35.

40. Salminen A, Kauppinen A, Kaarniranta K. 2-Oxoglutarate-dependent dioxygenases are sensors of energy metabolism, oxygen availability, and iron homeostasis: potential role in the regulation of aging process. Cell Mol Life Sci. 2015;72(20):3897-914.

41. Liu X, Si W, He L, Yang J, Peng Y, Ren J, et al. The existence of a nonclassical TCA cycle in the nucleus that wires the metabolic-epigenetic circuitry. Signal Transduction and Targeted Therapy. 2021;6(1):375.

42. Ashbrook MJ, McDonough KL, Pituch JJ, Christopherson PL, Cornell TT, Selewski DT, et al. Citrate modulates lipopolysaccharide-induced monocyte inflammatory responses. Clin Exp Immunol. 2015;180(3):520-30.

43. Williams NC, O'Neill LAJ. A Role for the Krebs Cycle Intermediate Citrate in Metabolic Reprogramming in Innate Immunity and Inflammation. Frontiers in Immunology. 2018;9.

44. Zhang W, Lang R. Succinate metabolism: a promising therapeutic target for inflammation, ischemia/reperfusion injury and cancer. Front Cell Dev Biol. 2023;11:1266973.

45. Mills E, O'Neill LAJ. Succinate: a metabolic signal in inflammation. Trends in Cell Biology. 2014;24(5):313-20.

46. Xiao Y, Chen X, Wang Z, Quan J, Zhao X, Tang H, et al. Succinate Is a Natural Suppressor of Antiviral Immune Response by Targeting MAVS. Frontiers in Immunology. 2022;13.

47. Peace CG, O'Carroll SM, O'Neill LAJ. Fumarate hydratase as a metabolic regulator of immunity. Trends in Cell Biology. 2024;34(6):442-50.

48. Ryan DG, Murphy MP, Frezza C, Prag HA, Chouchani ET, O'Neill LA, et al. Coupling Krebs cycle metabolites to signalling in immunity and cancer. Nat Metab. 2019;1:16-33.

49. Cheng J, Liu Y, Yan J, Zhao L, Zhou Y, Shen X, et al. Fumarate suppresses B-cell activation and function through direct inactivation of LYN. Nature Chemical Biology. 2022;18(9):954-62.

50. Galdieri L, Zhang T, Rogerson D, Lleshi R, Vancura A. Protein acetylation and acetyl coenzyme a metabolism in budding yeast. Eukaryot Cell. 2014;13(12):1472-83.

51. Diskin C, Ryan TAJ, O'Neill LAJ. Modification of Proteins by Metabolites in Immunity. Immunity. 2021;54(1):19-31.

52. Zhang Z, Tan M, Xie Z, Dai L, Chen Y, Zhao Y. Identification of lysine succinylation as a new post-translational modification. Nature Chemical Biology. 2011;7(1):58-63.

53. Kinch L, Grishin NV, Brugarolas J. Succination of Keap1 and activation of Nrf2-dependent antioxidant pathways in FH-deficient papillary renal cell carcinoma type 2. Cancer Cell. 2011;20(4):418-20.

54. Saidu NEB, Kavian N, Leroy K, Jacob C, Nicco C, Batteux F, et al. Dimethyl fumarate, a two-edged drug: Current status and future directions. Medicinal Research Reviews. 2019;39(5):1923-52.

55. Kane AE, Sinclair DA. Sirtuins and NAD⁺ in the Development and Treatment of Metabolic and Cardiovascular Diseases. Circulation Research. 2018;123(7):868-85.

56. Durán RV, MacKenzie ED, Boulahbel H, Frezza C, Heiserich L, Tardito S, et al. HIF-independent role of prolyl hydroxylases in the cellular response to amino acids. Oncogene. 2013;32(38):4549-56.

57. Selak MA, Armour SM, MacKenzie ED, Boulahbel H, Watson DG, Mansfield KD, et al. Succinate links TCA cycle dysfunction to oncogenesis by inhibiting HIF-α prolyl hydroxylase. Cancer Cell. 2005;7(1):77-85.

58. Dodd MS, Sousa Fialho MdL, Montes Aparicio CN, Kerr M, Timm KN, Griffin JL, et al. Fatty Acids Prevent Hypoxia-Inducible Factor-1α Signaling Through Decreased Succinate in Diabetes. JACC: Basic to Translational Science. 2018;3(4):485-98.

59. Bailey PSJ, Nathan JA. Metabolic Regulation of Hypoxia-Inducible Transcription Factors: The Role of Small Molecule Metabolites and Iron. Biomedicines. 2018;6(2):60.

60. Chouchani ET, Pell VR, Gaude E, Aksentijević D, Sundier SY, Robb EL, et al. Ischaemic accumulation of succinate controls reperfusion injury through mitochondrial ROS. Nature. 2014;515(7527):431-5.

61. Sörnmo L, Laguna P. Chapter 6 - The Electrocardiogram—A Brief Background. In: Sörnmo L, Laguna P, editors. Bioelectrical Signal Processing in Cardiac and Neurological Applications. Burlington: Academic Press; 2005. p. 411-52.

62. Zuurbier CJ, Bertrand L, Beauloye CR, Andreadou I, Ruiz-Meana M, Jespersen NR, et al. Cardiac metabolism as a driver and therapeutic target of myocardial infarction. J Cell Mol Med. 2020;24(11):5937-54.

63. Dengler F. Activation of AMPK under Hypoxia: Many Roads Leading to Rome. Int J Mol Sci. 2020;21(7).

64. Hunter RW, Treebak JT, Wojtaszewski JF, Sakamoto K. Molecular mechanism by which AMP-activated protein kinase activation promotes glycogen accumulation in muscle. Diabetes. 2011;60(3):766-74.

65. Janzen NR, Whitfield J, Hoffman NJ. Interactive Roles for AMPK and Glycogen from Cellular Energy Sensing to Exercise Metabolism. Int J Mol Sci. 2018;19(11).

66. Kim J, Yang G, Kim Y, Kim J, Ha J. AMPK activators: mechanisms of action and physiological activities. Experimental & Molecular Medicine. 2016;48(4):e224-e.

67. Dennis KMJH, Heather LC. Post-translational palmitoylation of metabolic proteins. Frontiers in Physiology. 2023;14.

68. Knutson AK, Williams AL, Boisvert WA, Shohet RV. HIF in the heart: development, metabolism, ischemia, and atherosclerosis. J Clin Invest. 2021;131(17).

69. Masoud GN, Li W. HIF-1α pathway: role, regulation and intervention for cancer therapy. Acta Pharm Sin B. 2015;5(5):378-89.

70. Lin S-C, Liao W-L, Lee J-C, Tsai S-J. Hypoxia-regulated gene network in drug resistance and cancer progression. Experimental Biology and Medicine. 2014;239(7):779-92.

71. Sim J, Cowburn AS, Palazon A, Madhu B, Tyrakis PA, Macías D, et al. The Factor Inhibiting HIF Asparaginyl Hydroxylase Regulates Oxidative Metabolism and Accelerates Metabolic Adaptation to Hypoxia. Cell Metabolism. 2018;27(4):898-913.e7.

72. Lancaster DE, McNeill LA, McDonough MA, Aplin RT, Hewitson KS, Pugh CW, et al. Disruption of dimerization and substrate phosphorylation inhibit factor inhibiting hypoxia-inducible factor (FIH) activity. Biochem J. 2004;383(Pt. 3):429-37.

73. Fan L, Li J, Yu Z, Dang X, Wang K. The Hypoxia-Inducible Factor Pathway, Prolyl Hydroxylase Domain Protein Inhibitors, and Their Roles in Bone Repair and Regeneration. BioMed Research International. 2014;2014(1):239356.

74. Semenza GL, Roth PH, Fang HM, Wang GL. Transcriptional regulation of genes encoding glycolytic enzymes by hypoxia-inducible factor 1. J Biol Chem. 1994;269(38):23757-63.

75. Riddle SR, Ahmad A, Ahmad S, Deeb SS, Malkki M, Schneider BK, et al. Hypoxia induces hexokinase II gene expression in human lung cell line A549. Am J Physiol Lung Cell Mol Physiol. 2000;278(2):L407-16.

76. Mirtschink P, Krek W. Hypoxia-driven glycolytic and fructolytic metabolic programs: Pivotal to hypertrophic heart disease. Biochimica et Biophysica Acta (BBA) - Molecular Cell Research. 2016;1863(7, Part B):1822-8.

77. Spinicci K, Jacquet P, Powathil G, Stéphanou A. Modeling the role of HIF in the regulation of metabolic key genes LDH and PDH: Emergence of Warburg phenotype. Computational and Systems Oncology. 2022;2(3):e1040.

78. Kim J-w, Tchernyshyov I, Semenza GL, Dang CV. HIF-1-mediated expression of pyruvate dehydrogenase kinase: A metabolic switch required for cellular adaptation to hypoxia. Cell Metabolism. 2006;3(3):177-85.

79. Taylor CT, Scholz CC. The effect of HIF on metabolism and immunity. Nature Reviews Nephrology. 2022;18(9):573-87.

80. Fukuda R, Zhang H, Kim JW, Shimoda L, Dang CV, Semenza GL. HIF-1 regulates cytochrome oxidase subunits to optimize efficiency of respiration in hypoxic cells. Cell. 2007;129(1):111-22.

81. Jucht AE, Scholz CC. PHD1-3 oxygen sensors in vivo—lessons learned from gene deletions. Pflügers Archiv - European Journal of Physiology. 2024;476(9):1307-37.

82. Pajuelo Reguera D, Čunátová K, Vrbacký M, Pecinová A, Houštěk J, Mráček T, et al. Cytochrome c Oxidase Subunit 4 Isoform Exchange Results in Modulation of Oxygen Affinity. Cells. 2020;9(2):443.

83. Semenza GL. Hypoxia-inducible factor 1 and cardiovascular disease. Annu Rev Physiol. 2014;76:39-56.

84. Masoud GN, Li W. HIF-1α pathway: role, regulation and intervention for cancer therapy. Acta Pharmaceutica Sinica B. 2015;5(5):378-89.

85. Kung-Chun Chiu D, Pui-Wah Tse A, Law C-T, Ming-Jing Xu I, Lee D, Chen M, et al. Hypoxia regulates the mitochondrial activity of hepatocellular carcinoma cells through HIF/HEY1/PINK1 pathway. Cell Death & Disease. 2019;10(12):934.

86. Schieber M, Chandel NS. ROS function in redox signaling and oxidative stress. Curr Biol. 2014;24(10):R453-62.

87. Sharma P, Jha AB, Dubey RS, Pessarakli M. Reactive Oxygen Species, Oxidative Damage, and Antioxidative Defense Mechanism in Plants under Stressful Conditions. Journal of Botany. 2012;2012(1):217037.

88. Kobayashi EH, Suzuki T, Funayama R, Nagashima T, Hayashi M, Sekine H, et al. Nrf2 suppresses macrophage inflammatory response by blocking proinflammatory cytokine transcription. Nature Communications. 2016;7(1):11624.

89. Ngo V, Duennwald ML. Nrf2 and Oxidative Stress: A General Overview of Mechanisms and Implications in Human Disease. Antioxidants (Basel). 2022;11(12).

90. Kolamunne RT, Dias IH, Vernallis AB, Grant MM, Griffiths HR. Nrf2 activation supports cell survival during hypoxia and hypoxia/reoxygenation in cardiomyoblasts; the roles of reactive oxygen and nitrogen species. Redox Biol. 2013;1(1):418-26.

91. Bae T, Hallis SP, Kwak M-K. Hypoxia, oxidative stress, and the interplay of HIFs and NRF2 signaling in cancer. Experimental & Molecular Medicine. 2024;56(3):501-14.

92. Ashrafian H, Czibik G, Bellahcene M, Aksentijević D, Smith Anthony C, Mitchell Sarah J, et al. Fumarate Is Cardioprotective via Activation of the Nrf2 Antioxidant Pathway. Cell Metabolism. 2012;15(3):361-71.

93. Deng C, Sun Z, Tong G, Yi W, Ma L, Zhao B, et al. α-Lipoic acid reduces infarct size and preserves cardiac function in rat myocardial ischemia/reperfusion injury through activation of PI3K/Akt/Nrf2 pathway. PLoS One. 2013;8(3):e58371.

94. Huang D, Li T, Li X, Zhang L, Sun L, He X, et al. HIF-1-mediated suppression of acyl-CoA dehydrogenases and fatty acid oxidation is critical for cancer progression. Cell Rep. 2014;8(6):1930-42.

95. Samovski D, Sun J, Pietka T, Gross RW, Eckel RH, Su X, et al. Regulation of AMPK activation by CD36 links fatty acid uptake to β-oxidation. Diabetes. 2015;64(2):353-9.

96. Zhou S, Sun W, Zhang Z, Zheng Y. The role of Nrf2-mediated pathway in cardiac remodeling and heart failure. Oxid Med Cell Longev. 2014;2014:260429.

97. Zuberi S, Rafi H, Hussain A, Hashmi S. Upregulation of Nrf2 in myocardial infarction and ischemia-reperfusion injury of the heart. PLoS One. 2024;19(3):e0299503.

98. Livak KJ, Schmittgen TD. Analysis of Relative Gene Expression Data Using Real-Time Quantitative PCR and the 2−ΔΔCT Method. Methods. 2001;25(4):402-8.

99. Zhang J, Wang YT, Miller JH, Day MM, Munger JC, Brookes PS. Accumulation of Succinate in Cardiac Ischemia Primarily Occurs via Canonical Krebs Cycle Activity. Cell Rep. 2018;23(9):2617-28.

100. Kohlhauer M, Dawkins S, Costa ASH, Lee R, Young T, Pell VR, et al. Metabolomic Profiling in Acute ST-Segment-Elevation Myocardial Infarction Identifies Succinate as an Early Marker of Human Ischemia-Reperfusion Injury. J Am Heart Assoc. 2018;7(8).

101. Pell VR, Spiroski AM, Mulvey J, Burger N, Costa ASH, Logan A, et al. Ischemic preconditioning protects against cardiac ischemia reperfusion injury without affecting succinate accumulation or oxidation. J Mol Cell Cardiol. 2018;123:88-91.

102. Prag HA, Gruszczyk AV, Huang MM, Beach TE, Young T, Tronci L, et al. Mechanism of succinate efflux upon reperfusion of the ischaemic heart. Cardiovasc Res. 2021;117(4):1188-201.

103. Kula-Alwar D, Prag HA, Krieg T. Targeting Succinate Metabolism in Ischemia/Reperfusion Injury. Circulation. 2019;140(24):1968-70.

104. Mansor LS, Sousa Fialho MDL, Yea G, Coumans WA, West JA, Kerr M, et al. Inhibition of sarcolemmal FAT/CD36 by sulfo-N-succinimidyl oleate rapidly corrects metabolism and restores function in the diabetic heart following hypoxia/reoxygenation. Cardiovasc Res. 2017;113(7):737-48.

105. Kenny HC, Abel ED. Heart Failure in Type 2 Diabetes Mellitus. Circulation Research. 2019;124(1):121-41.

106. Jain V, Qamar A, Matsushita K, Vaduganathan M, Ashley KE, Khan MS, et al. Impact of Diabetes on Outcomes in Patients Hospitalized With Acute Myocardial Infarction: Insights From the Atherosclerosis Risk in Communities Study Community Surveillance. Journal of the American Heart Association. 2023;12(10):e028923.

107. Sousa Fialho MDL, Purnama U, Dennis K, Montes Aparicio CN, Castro-Guarda M, Massourides E, et al. Activation of HIF1alpha Rescues the Hypoxic Response and Reverses Metabolic Dysfunction in the Diabetic Heart. Diabetes. 2021;70(11):2518-31.

108. Lopez CA, Al-Siddiqi H, Purnama U, Iftekhar S, Bruyneel AAN, Kerr M, et al. Physiological and pharmacological stimulation for in vitro maturation of substrate metabolism in human induced pluripotent stem cell-derived cardiomyocytes. Sci Rep. 2021;11(1):7802.

109. Zhao M, Tang Y, Zhou Y, Zhang J. Deciphering Role of Wnt Signalling in Cardiac Mesoderm and Cardiomyocyte Differentiation from Human iPSCs: Four-dimensional control of Wnt pathway for hiPSC-CMs differentiation. Sci Rep. 2019;9(1):19389.

110. Ramirez-Calderon G, Colombo G, Hernandez-Bautista CA, Astro V, Adamo A. Heart in a Dish: From Traditional 2D Differentiation Protocols to Cardiac Organoids. Front Cell Dev Biol. 2022;10:855966.

111. Carey MF, Peterson CL, Smale ST. Dignam and Roeder nuclear extract preparation. Cold Spring Harb Protoc. 2009;2009(12):pdb prot5330.

112. Lopaschuk GD, Barr RL. Measurements of fatty acid and carbohydrate metabolism in the isolated working rat heart. Mol Cell Biochem. 1997;172(1-2):137-47.

113. Parkhomchuk D, Borodina T, Amstislavskiy V, Banaru M, Hallen L, Krobitsch S, et al. Transcriptome analysis by strand-specific sequencing of complementary DNA. Nucleic Acids Res. 2009;37(18):e123.

114. Mortazavi A, Williams BA, McCue K, Schaeffer L, Wold B. Mapping and quantifying mammalian transcriptomes by RNA-Seq. Nat Methods. 2008;5(7):621-8.

115. Love MI, Huber W, Anders S. Moderated estimation of fold change and dispersion for RNA-seq data with DESeq2. Genome Biol. 2014;15(12):550.

116. Lin SM, Du P, Huber W, Kibbe WA. Model-based variance-stabilizing transformation for Illumina microarray data. Nucleic Acids Res. 2008;36(2):e11.

117. Zhu A, Ibrahim JG, Love MI. Heavy-tailed prior distributions for sequence count data: removing the noise and preserving large differences. Bioinformatics. 2019;35(12):2084-92.

118. Xu S, Hu E, Cai Y, Xie Z, Luo X, Zhan L, et al. Using clusterProfiler to characterize multiomics data. Nat Protoc. 2024.

119. Wu T, Hu E, Xu S, Chen M, Guo P, Dai Z, et al. clusterProfiler 4.0: A universal enrichment tool for interpreting omics data. Innovation (Camb). 2021;2(3):100141.

120. Yu G, Wang LG, Han Y, He QY. clusterProfiler: an R package for comparing biological themes among gene clusters. OMICS. 2012;16(5):284-7.

121. Luo W, Brouwer C. Pathview: an R/Bioconductor package for pathway-based data integration and visualization. Bioinformatics. 2013;29(14):1830-1.

122. H W. Ggplot2: Elegant graphics for data analysis. 2nd ed ed. Switzerland:: Springer International Publishing; 2016.

123. Blighe K, Rana S, Lewis M. EnhancedVolcano: Publication-ready volcano plots with enhanced colouring and labeling. R package version. 2019;1(0):10.18129.

124. Gu Z, Eils R, Schlesner M. Complex heatmaps reveal patterns and correlations in multidimensional genomic data. Bioinformatics. 2016;32(18):2847-9.

125. Gu Z. Complex heatmap visualization. Imeta. 2022;1(3):e43.

126. Zhou Y, Zhou B, Pache L, Chang M, Khodabakhshi AH, Tanaseichuk O, et al. Metascape provides a biologist-oriented resource for the analysis of systems-level datasets. Nat Commun. 2019;10(1):1523.

127. Han H, Cho JW, Lee S, Yun A, Kim H, Bae D, et al. TRRUST v2: an expanded reference database of human and mouse transcriptional regulatory interactions. Nucleic Acids Res. 2018;46(D1):D380-D6.

128. Korotkevich G, Sukhov V, Budin N, Shpak B, Artyomov MN, Sergushichev A. Fast gene set enrichment analysis. bioRxiv. 2021:060012.

129. Hanzelmann S, Castelo R, Guinney J. GSVA: gene set variation analysis for microarray and RNA-seq data. BMC Bioinformatics. 2013;14:7.

130. Zoccarato A, Smyrnias I, Reumiller CM, Hafstad AD, Chong M, Richards DA, et al. NRF2 activation in the heart induces glucose metabolic reprogramming and mediates cardioprotection via upregulation of the pentose phosphate pathway. bioRxiv. 2023:2023.05.12.540342.

131. Le Belle JE, Harris NG, Williams SR, Bhakoo KK. A comparison of cell and tissue extraction techniques using high-resolution 1H-NMR spectroscopy. NMR Biomed. 2002;15(1):37-44.

132. Brennan MS, Matos MF, Li B, Hronowski X, Gao B, Juhasz P, et al. Dimethyl Fumarate and Monoethyl Fumarate Exhibit Differential Effects on KEAP1, NRF2 Activation, and Glutathione Depletion In Vitro. PLOS ONE. 2015;10(3):e0120254.

133. Kourakis S, Timpani CA, de Haan JB, Gueven N, Fischer D, Rybalka E. Dimethyl Fumarate and Its Esters: A Drug with Broad Clinical Utility? Pharmaceuticals (Basel). 2020;13(10).

134. Hosseini A, Masjedi A, Baradaran B, Hojjat-Farsangi M, Ghalamfarsa G, Anvari E, et al. Dimethyl fumarate: Regulatory effects on the immune system in the treatment of multiple sclerosis. Journal of Cellular Physiology. 2019;234(7):9943-55.

135. Majkutewicz I. Dimethyl fumarate: A review of preclinical efficacy in models of neurodegenerative diseases. European Journal of Pharmacology. 2022;926:175025.

136. Bresciani G, Manai F, Davinelli S, Tucci P, Saso L, Amadio M. Novel potential pharmacological applications of dimethyl fumarate—an overview and update. Frontiers in Pharmacology. 2023;14.

137. Kienhöfer D, Boeltz S, Hoffmann MH. Reactive oxygen homeostasis – the balance for preventing autoimmunity. Lupus. 2016;25(8):943-54.

138. Pisetsky DS. Pathogenesis of autoimmune disease. Nature Reviews Nephrology. 2023;19(8):509-24.

139. Souliotis VL, Vlachogiannis NI, Pappa M, Argyriou A, Ntouros PA, Sfikakis PP. DNA Damage Response and Oxidative Stress in Systemic Autoimmunity. Int J Mol Sci. 2019;21(1).

140. Robledinos-Antón N, Fernández-Ginés R, Manda G, Cuadrado A. Activators and Inhibitors of NRF2: A Review of Their Potential for Clinical Development. Oxid Med Cell Longev. 2019;2019:9372182.

141. Canning P, Sorrell FJ, Bullock AN. Structural basis of Keap1 interactions with Nrf2. Free Radic Biol Med. 2015;88(Pt B):101-7.

142. Tong KI, Kobayashi A, Katsuoka F, Yamamoto M. Two-site substrate recognition model for the Keap1-Nrf2 system: a hinge and latch mechanism. Biol Chem. 2006;387(10-11):1311-20.

143. Satoh T, Lipton S. Recent advances in understanding NRF2 as a druggable target: development of pro-electrophilic and non-covalent NRF2 activators to overcome systemic side effects of electrophilic drugs like dimethyl fumarate. F1000Res. 2017;6:2138.

144. Guberovic I, Frezza C. Functional implications of fumarate-induced cysteine succination. Trends in Biochemical Sciences. 2024;49(9):775-90.

145. Wang Y-P, Sharda A, Xu S-N, van Gastel N, Man CH, Choi U, et al. Malic enzyme 2 connects the Krebs cycle intermediate fumarate to mitochondrial biogenesis. Cell Metabolism. 2021;33(5):1027-41.e8.

146. Takimoto JK, Xiang Z, Kang J-Y, Wang L. Esterification of an Unnatural Amino Acid Structurally Deviating from Canonical Amino Acids Promotes Its Uptake and Incorporation into Proteins in Mammalian Cells. ChemBioChem. 2010;11(16):2268-72.

147. Mrowietz U, Morrison PJ, Suhrkamp I, Kumanova M, Clement B. The Pharmacokinetics of Fumaric Acid Esters Reveal Their In Vivo Effects. Trends in Pharmacological Sciences. 2018;39(1):1-12.

148. Li M, Thorne RF, Shi R, Zhang XD, Li J, Li J, et al. DDIT3 Directs a Dual Mechanism to Balance Glycolysis and Oxidative Phosphorylation during Glutamine Deprivation. Advanced Science. 2021;8(11):2003732.

149. Li T, Su L, Lei Y, Liu X, Zhang Y, Liu X. DDIT3 and KAT2A Proteins Regulate TNFRSF10A and TNFRSF10B Expression in Endoplasmic Reticulum Stress-mediated Apoptosis in Human Lung Cancer Cells*. Journal of Biological Chemistry. 2015;290(17):11108-18.

150. Yu X, Xu X, Dong W, Yang C, Luo Y, He Y, et al. DDIT3/CHOP mediates the inhibitory effect of ER stress on chondrocyte differentiation by AMPKalpha-SIRT1 pathway. Biochim Biophys Acta Mol Cell Res. 2022;1869(8):119265.

151. Jauhiainen A, Thomsen C, Strombom L, Grundevik P, Andersson C, Danielsson A, et al. Distinct cytoplasmic and nuclear functions of the stress induced protein DDIT3/CHOP/GADD153. PLoS One. 2012;7(4):e33208.

152. Behrens AN, Iacovino M, Lohr JL, Ren Y, Zierold C, Harvey RP, et al. Nkx2-5 mediates differential cardiac differentiation through interaction with Hoxa10. Stem Cells Dev. 2013;22(15):2211-20.

153. Lescroart F, Zaffran S. Hox and Tale transcription factors in heart development and disease. Int J Dev Biol. 2018;62(11-12):837-46.

154. Mak TW, Hauck L, Grothe D, Billia F. p53 regulates the cardiac transcriptome. Proc Natl Acad Sci U S A. 2017;114(9):2331-6.

155. Men H, Cai H, Cheng Q, Zhou W, Wang X, Huang S, et al. The regulatory roles of p53 in cardiovascular health and disease. Cell Mol Life Sci. 2021;78(5):2001-18.

156. Wang YX. PPARs: diverse regulators in energy metabolism and metabolic diseases. Cell Res. 2010;20(2):124-37.

157. Weber LW, Boll M, Stampfl A. Maintaining cholesterol homeostasis: sterol regulatory element-binding proteins. World J Gastroenterol. 2004;10(21):3081-7.

158. Eberle D, Hegarty B, Bossard P, Ferre P, Foufelle F. SREBP transcription factors: master regulators of lipid homeostasis. Biochimie. 2004;86(11):839-48.

159. Goetzman E, Gong Z, Rajasundaram D, Muzumdar I, Goodchild T, Lefer D, et al. Serum Metabolomics Reveals Distinct Profiles during Ischemia and Reperfusion in a Porcine Model of Myocardial Ischemia-Reperfusion. Int J Mol Sci. 2022;23(12).

160. Huang H, Taraboletti A, Shriver LP. Dimethyl fumarate modulates antioxidant and lipid metabolism in oligodendrocytes. Redox Biol. 2015;5:169-75.

161. Ahuja M, Ammal Kaidery N, Yang L, Calingasan N, Smirnova N, Gaisin A, et al. Distinct Nrf2 Signaling Mechanisms of Fumaric Acid Esters and Their Role in Neuroprotection against 1-Methyl-4-Phenyl-1,2,3,6-Tetrahydropyridine-Induced Experimental Parkinson's-Like Disease. J Neurosci. 2016;36(23):6332-51.

162. Scannevin RH, Chollate S, Jung MY, Shackett M, Patel H, Bista P, et al. Fumarates promote cytoprotection of central nervous system cells against oxidative stress via the nuclear factor (erythroid-derived 2)-like 2 pathway. J Pharmacol Exp Ther. 2012;341(1):274-84.

163. Carlstrom KE, Ewing E, Granqvist M, Gyllenberg A, Aeinehband S, Enoksson SL, et al. Therapeutic efficacy of dimethyl fumarate in relapsing-remitting multiple sclerosis associates with ROS pathway in monocytes. Nat Commun. 2019;10(1):3081.

164. McGuire VA, Ruiz-Zorrilla Diez T, Emmerich CH, Strickson S, Ritorto MS, Sutavani RV, et al. Dimethyl fumarate blocks pro-inflammatory cytokine production via inhibition of TLR induced M1 and K63 ubiquitin chain formation. Sci Rep. 2016;6:31159.

165. Meseguer-Ripolles J, Lucendo-Villarin B, Tucker C, Ferreira-Gonzalez S, Homer N, Wang Y, et al. Dimethyl fumarate reduces hepatocyte senescence following paracetamol exposure. iScience. 2021;24(6):102552.

166. Abu-Halaka D, Shpaizer A, Zeigerman H, Kanner J, Tirosh O. DMF-Activated Nrf2 Ameliorates Palmitic Acid Toxicity While Potentiates Ferroptosis Mediated Cell Death: Protective Role of the NO-Donor S-Nitroso-N-Acetylcysteine. Antioxidants (Basel). 2023;12(2).

167. Kuang Y, Zhang Y, Xiao Z, Xu L, Wang P, Ma Q. Protective effect of dimethyl fumarate on oxidative damage and signaling in cardiomyocytes. Mol Med Rep. 2020;22(4):2783-90.

168. Hu X, Li C, Wang Q, Wei Z, Chen T, Wang Y, et al. Dimethyl Fumarate Ameliorates Doxorubicin-Induced Cardiotoxicity By Activating the Nrf2 Pathway. Front Pharmacol. 2022;13:872057.

169. Gendy A, Soubh A, Al-Mokaddem A, Kotb El-Sayed M. Dimethyl fumarate protects against intestinal ischemia/reperfusion lesion: Participation of Nrf2/HO-1, GSK-3β and Wnt/β-catenin pathway. Biomedicine & Pharmacotherapy. 2021;134:111130.

170. Li S, Vaziri ND, Swentek L, Takasu C, Vo K, Stamos MJ, et al. Prevention of Autoimmune Diabetes in NOD Mice by Dimethyl Fumarate. Antioxidants. 2021;10(2):193.

171. Cho H, Hartsock MJ, Xu Z, He M, Duh EJ. Monomethyl fumarate promotes Nrf2-dependent neuroprotection in retinal ischemia-reperfusion. Journal of Neuroinflammation. 2015;12(1):239.

172. Dwivedi DK, Jena G, Kumar V. Dimethyl fumarate protects thioacetamide-induced liver damage in rats: Studies on Nrf2, NLRP3, and NF-kappaB. J Biochem Mol Toxicol. 2020;34(6):e22476.

173. Zhen X, Jindong L, Yang Z, Yashi R, Wei G, Wei J, et al. Activation of Nrf2 Pathway by Dimethyl Fumarate Attenuates Renal Ischemia-Reperfusion Injury. Transplant Proc. 2021;53(7):2133-9.

174. Ahmed AA, Ahmed AAE, El Morsy EM, Nofal S. Dimethyl fumarate interferes with MyD88-dependent toll-like receptor signalling pathway in isoproterenol-induced cardiac hypertrophy model. J Pharm Pharmacol. 2018;70(11):1521-30.

175. Bai Y, Wang X, Zhao S, Ma C, Cui J, Zheng Y. Sulforaphane Protects against Cardiovascular Disease via Nrf2 Activation. Oxid Med Cell Longev. 2015;2015:407580.

176. Bose C, Alves I, Singh P, Palade PT, Carvalho E, Børsheim E, et al. Sulforaphane prevents age-associated cardiac and muscular dysfunction through Nrf2 signaling. Aging Cell. 2020;19(11):e13261.

177. Apopa PL, He X, Ma Q. Phosphorylation of Nrf2 in the transcription activation domain by casein kinase 2 (CK2) is critical for the nuclear translocation and transcription activation function of Nrf2 in IMR-32 neuroblastoma cells. J Biochem Mol Toxicol. 2008;22(1):63-76.

178. Kawai Y, Garduño L, Theodore M, Yang J, Arinze IJ. Acetylation-deacetylation of the transcription factor Nrf2 (nuclear factor erythroid 2-related factor 2) regulates its transcriptional activity and nucleocytoplasmic localization. J Biol Chem. 2011;286(9):7629-40.

179. Walters TS, McIntosh DJ, Ingram SM, Tillery L, Motley ED, Arinze IJ, et al. SUMO-Modification of Human Nrf2 at K(110) and K(533) Regulates Its Nucleocytoplasmic Localization, Stability and Transcriptional Activity. Cell Physiol Biochem. 2021;55(2):141-59.

180. Chen PH, Smith TJ, Wu J, Siesser PF, Bisnett BJ, Khan F, et al. Glycosylation of KEAP1 links nutrient sensing to redox stress signaling. Embo j. 2017;36(15):2233-50.

181. Mills EL, Ryan DG, Prag HA, Dikovskaya D, Menon D, Zaslona Z, et al. Itaconate is an anti-inflammatory metabolite that activates Nrf2 via alkylation of KEAP1. Nature. 2018;556(7699):113-7.

182. Ibrahim L, Stanton C, Nutsch K, Nguyen T, Li-Ma C, Ko Y, et al. Succinylation of a KEAP1 sensor lysine promotes NRF2 activation. bioRxiv. 2023.

183. Song Y, Qu Y, Mao C, Zhang R, Jiang D, Sun X. Post-translational modifications of Keap1: the state of the art. Frontiers in Cell and Developmental Biology. 2024;11.

184. Unni S, Deshmukh P, Krishnappa G, Kommu P, Padmanabhan B. Structural insights into the multiple binding modes of Dimethyl Fumarate (DMF) and its analogs to the Kelch domain of Keap1. The FEBS Journal. 2021;288(5):1599-613.

185. Lv Y, Lv X, Zhang J, Cao G, Xu C, Zhang B, et al. BRD4 Targets the KEAP1-Nrf2-G6PD Axis and Suppresses Redox Metabolism in Small Cell Lung Cancer. Antioxidants. 2022;11(4):661.

186. Yang Q, Yan R, Zhang J, Zhang T, Kong Q, Zhang X, et al. Reductive stress induced by NRF2/G6PD through glucose metabolic reprogramming promotes malignant transformation in Arsenite-exposed human keratinocytes. Sci Total Environ. 2023;896:165207.

187. Shen A, Kim HJ, Oh GS, Lee SB, Lee S, Pandit A, et al. Pharmacological stimulation of NQO1 decreases NADPH levels and ameliorates acute pancreatitis in mice. Cell Death Dis. 2018;10(1):5.

188. Calandria JM, Bhattacharjee S, Kala-Bhattacharjee S, Mukherjee PK, Feng Y, Vowinckel J, et al. Elovanoid-N34 modulates TXNRD1 key in protection against oxidative stress-related diseases. Cell Death Dis. 2023;14(12):819.

189. Ju HQ, Lin JF, Tian T, Xie D, Xu RH. NADPH homeostasis in cancer: functions, mechanisms and therapeutic implications. Signal Transduct Target Ther. 2020;5(1):231.

190. Sablina AA, Budanov AV, Ilyinskaya GV, Agapova LS, Kravchenko JE, Chumakov PM. The antioxidant function of the p53 tumor suppressor. Nat Med. 2005;11(12):1306-13.

191. Hoogendoorn A, Avery TD, Li J, Bursill C, Abell A, Grace PM. Emerging Therapeutic Applications for Fumarates. Trends Pharmacol Sci. 2021;42(4):239-54.

192. Rasheed MSU, Cherry FR, Grace PM. Opioid-sparing Effects of the Nrf2 Activator Diroximel Fumarate in Mice. The Journal of Pain. 2022;23(5, Supplement):60-1.

193. Wundes A, Wray S, Gold R, Singer BA, Jasinska E, Ziemssen T, et al. Improved gastrointestinal profile with diroximel fumarate is associated with a positive impact on quality of life compared with dimethyl fumarate: results from the randomized, double-blind, phase III EVOLVE-MS-2 study. Ther Adv Neurol Disord. 2021;14:1756286421993999.

194. Palte MJ, Wehr A, Tawa M, Perkin K, Leigh-Pemberton R, Hanna J, et al. Improving the Gastrointestinal Tolerability of Fumaric Acid Esters: Early Findings on Gastrointestinal Events with Diroximel Fumarate in Patients with Relapsing-Remitting Multiple Sclerosis from the Phase 3, Open-Label EVOLVE-MS-1 Study. Adv Ther. 2019;36(11):3154-65.

195. Piroli GG, Manuel AM, Clapper AC, Walla MD, Baatz JE, Palmiter RD, et al. Succination is Increased on Select Proteins in the Brainstem of the NADH dehydrogenase (ubiquinone) Fe-S protein 4 (Ndufs4) Knockout Mouse, a Model of Leigh Syndrome*. Molecular & Cellular Proteomics. 2016;15(2):445-61.

196. Hu C, Eggler AL, Mesecar AD, van Breemen RB. Modification of Keap1 Cysteine Residues by Sulforaphane. Chemical Research in Toxicology. 2011;24(4):515-21.

197. Ali M, Bonay M, Vanhee V, Vinit S, Deramaudt TB. Comparative effectiveness of 4 natural and chemical activators of Nrf2 on inflammation, oxidative stress, macrophage polarization, and bactericidal activity in an in vitro macrophage infection model. PLoS One. 2020;15(6):e0234484.

198. Ebihara S, Tajima H, Ono M. Nuclear factor erythroid 2-related factor 2 is a critical target for the treatment of glucocorticoid-resistant lupus nephritis. Arthritis Research & Therapy. 2016;18(1):139.

199. Martín Ortega AM, Segura Campos MR. Chapter 4 - Phytochemicals in cancer treatment. In: Campos MRS, Ortega AMM, editors. Oncological Functional Nutrition: Academic Press; 2021. p. 125-60.

200. Rajendran P, Williams DE, Ho E, Dashwood RH. Metabolism as a key to histone deacetylase inhibition. Critical Reviews in Biochemistry and Molecular Biology. 2011;46(3):181-99.

201. Kamal MM, Akter S, Lin CN, Nazzal S. Sulforaphane as an anticancer molecule: mechanisms of action, synergistic effects, enhancement of drug safety, and delivery systems. Arch Pharm Res. 2020;43(4):371-84.

202. Su X, Jiang X, Meng L, Dong X, Shen Y, Xin Y. Anticancer Activity of Sulforaphane: The Epigenetic Mechanisms and the Nrf2 Signaling Pathway. Oxid Med Cell Longev. 2018;2018:5438179.

203. Jiang Y, Park P, Hong SM, Ban K. Maturation of Cardiomyocytes Derived from Human Pluripotent Stem Cells: Current Strategies and Limitations. Mol Cells. 2018;41(7):613-21.

204. Liu SJ, Melchert RB. 6.07 - In Vitro Cultured Cardiomyocytes for Evaluating Cardiotoxicity. In: McQueen CA, editor. Comprehensive Toxicology (Second Edition). Oxford: Elsevier; 2010. p. 113-31.

205. Nguyen PD, Hsiao ST, Sivakumaran P, Lim SY, Dilley RJ. Enrichment of neonatal rat cardiomyocytes in primary culture facilitates long-term maintenance of contractility in vitro. American Journal of Physiology-Cell Physiology. 2012;303(12):C1220-C8.

206. Kiani AK, Pheby D, Henehan G, Brown R, Sieving P, Sykora P, et al. Ethical considerations regarding animal experimentation. J Prev Med Hyg. 2022;63(2 Suppl 3):E255-e66.

207. Kumar A, Katz LS, Schulz AM, Kim M, Honig LB, Li L, et al. Activation of Nrf2 Is Required for Normal and ChREBPα-Augmented Glucose-Stimulated β-Cell Proliferation. Diabetes. 2018;67(8):1561-75.

208. Chorley BN, Campbell MR, Wang X, Karaca M, Sambandan D, Bangura F, et al. Identification of novel NRF2-regulated genes by ChIP-Seq: influence on retinoid X receptor alpha. Nucleic Acids Research. 2012;40(15):7416-29.

209. Hayes JD, Dinkova-Kostova AT. The Nrf2 regulatory network provides an interface between redox and intermediary metabolism. Trends Biochem Sci. 2014;39(4):199-218.

210. Schneider CA, Rasband WS, Eliceiri KW. NIH Image to ImageJ: 25 years of image analysis. Nat Methods. 2012;9(7):671-5.

211. Schindelin J, Arganda-Carreras I, Frise E, Kaynig V, Longair M, Pietzsch T, et al. Fiji: an open-source platform for biological-image analysis. Nat Methods. 2012;9(7):676-82.

212. Valente AJ, Maddalena LA, Robb EL, Moradi F, Stuart JA. A simple ImageJ macro tool for analyzing mitochondrial network morphology in mammalian cell culture. Acta Histochem. 2017;119(3):315-26.

213. Chaudhry A, Shi R, Luciani DS. A pipeline for multidimensional confocal analysis of mitochondrial morphology, function and dynamics in pancreatic β-cells. bioRxiv. 2019:687749.

214. Wiemerslage L, Lee D. Quantification of mitochondrial morphology in neurites of dopaminergic neurons using multiple parameters. J Neurosci Methods. 2016;262:56-65.

215. Ocana MC, Bernal M, Yang C, Caro C, Dominguez A, Vu HS, et al. New insights in the targets of action of dimethyl fumarate in endothelial cells: effects on energetic metabolism and serine synthesis in vitro and in vivo. Commun Biol. 2023;6(1):1084.

216. Liebmann M, Korn L, Janoschka C, Albrecht S, Lauks S, Herrmann AM, et al. Dimethyl fumarate treatment restrains the antioxidative capacity of T cells to control autoimmunity. Brain. 2021;144(10):3126-41.

217. Kornberg MD, Bhargava P, Kim PM, Putluri V, Snowman AM, Putluri N, et al. Dimethyl fumarate targets GAPDH and aerobic glycolysis to modulate immunity. Science. 2018;360(6387):449-53.

218. Hayashi G, Jasoliya M, Sahdeo S, Sacca F, Pane C, Filla A, et al. Dimethyl fumarate mediates Nrf2-dependent mitochondrial biogenesis in mice and humans. Hum Mol Genet. 2017;26(15):2864-73.

219. Kolodziejczyk AA, Lönnberg T. Global and targeted approaches to single-cell transcriptome characterization. Brief Funct Genomics. 2018;17(4):209-19.

220. Coenye T. Do results obtained with RNA-sequencing require independent verification? Biofilm. 2021;3:100043.

221. van Lingen HJ, Suarez-Diez M, Saccenti E. Normalization of gene counts affects principal components-based exploratory analysis of RNA-sequencing data. Biochimica et Biophysica Acta (BBA) - Gene Regulatory Mechanisms. 2024;1867(4):195058.

222. Evans C, Hardin J, Stoebel DM. Selecting between-sample RNA-Seq normalization methods from the perspective of their assumptions. Brief Bioinform. 2018;19(5):776-92.

223. Ludtmann MH, Angelova PR, Zhang Y, Abramov AY, Dinkova-Kostova AT. Nrf2 affects the efficiency of mitochondrial fatty acid oxidation. Biochem J. 2014;457(3):415-24.

224. Esteras N, Blacker TS, Zherebtsov EA, Stelmashuk OA, Zhang Y, Wigley WC, et al. Nrf2 regulates glucose uptake and metabolism in neurons and astrocytes. Redox Biol. 2023;62:102672.

225. Park JS, Rustamov N, Roh YS. The Roles of NFR2-Regulated Oxidative Stress and Mitochondrial Quality Control in Chronic Liver Diseases. Antioxidants (Basel). 2023;12(11).

226. Parker SJ, Encarnación-Rosado J, Hollinshead KER, Hollinshead DM, Ash LJ, Rossi JAK, et al. Spontaneous hydrolysis and spurious metabolic properties of α-ketoglutarate esters. Nature Communications. 2021;12(1):4905.

227. Elkhenany H, AlOkda A, El-Badawy A, El-Badri N. Tissue regeneration: Impact of sleep on stem cell regenerative capacity. Life Sciences. 2018;214:51-61.

228. Ruan W, Yuan X, Eltzschig HK. Circadian rhythm as a therapeutic target. Nature Reviews Drug Discovery. 2021;20(4):287-307.

229. Ayyar VS, Sukumaran S. Circadian rhythms: influence on physiology, pharmacology, and therapeutic interventions. Journal of Pharmacokinetics and Pharmacodynamics. 2021;48(3):321-38.

230. Reschke L, McCarthy R, Herzog ED, Fay JC, Jungheim ES, England SK. Chronodisruption: An untimely cause of preterm birth? Best Practice & Research Clinical Obstetrics & Gynaecology. 2018;52:60-7.

231. Lecacheur M, Ammerlaan DJM, Dierickx P. Circadian rhythms in cardiovascular (dys)function: approaches for future therapeutics. npj Cardiovascular Health. 2024;1(1):21.

232. Crnko S, Du Pré BC, Sluijter JPG, Van Laake LW. Circadian rhythms and the molecular clock in cardiovascular biology and disease. Nat Rev Cardiol. 2019;16(7):437-47.

233. Lin J, Kuang H, Jiang J, Zhou H, Peng L, Yan X, et al. Circadian Rhythms in Cardiovascular Function: Implications for Cardiac Diseases and Therapeutic Opportunities. Med Sci Monit. 2023;29:e942215.

234. Reinke H, Asher G. Crosstalk between metabolism and circadian clocks. Nature Reviews Molecular Cell Biology. 2019;20(4):227-41.

235. Petrenko V, Saini C, Giovannoni L, Gobet C, Sage D, Unser M, et al. Pancreatic α- and β-cellular clocks have distinct molecular properties and impact on islet hormone secretion and gene expression. Genes Dev. 2017;31(4):383-98.

236. Qian J, Scheer F. Circadian System and Glucose Metabolism: Implications for Physiology and Disease. Trends Endocrinol Metab. 2016;27(5):282-93.

237. Sinturel F, Spaleniak W, Dibner C. Circadian rhythm of lipid metabolism. Biochem Soc Trans. 2022;50(3):1191-204.

238. Calebiro D, Koszegi Z, Lanoiselée Y, Miljus T, O'Brien S. G protein-coupled receptor-G protein interactions: a single-molecule perspective. Physiological Reviews. 2021;101(3):857-906.

239. Zhang M, Chen T, Lu X, Lan X, Chen Z, Lu S. G protein-coupled receptors (GPCRs): advances in structures, mechanisms and drug discovery. Signal Transduction and Targeted Therapy. 2024;9(1):88.

240. Foster SR, Hauser AS, Vedel L, Strachan RT, Huang XP, Gavin AC, et al. Discovery of Human Signaling Systems: Pairing Peptides to G Protein-Coupled Receptors. Cell. 2019;179(4):895-908.e21.

241. Syrovatkina V, Alegre KO, Dey R, Huang XY. Regulation, Signaling, and Physiological Functions of G-Proteins. J Mol Biol. 2016;428(19):3850-68.

242. Rysiewicz B, Błasiak E, Mystek P, Dziedzicka-Wasylewska M, Polit A. Beyond the G protein α subunit: investigating the functional impact of other components of the Gαi3 heterotrimers. Cell Communication and Signaling. 2023;21(1):279.

243. Offermanns S. Hydroxy-Carboxylic Acid Receptor Actions in Metabolism. Trends in Endocrinology & Metabolism. 2017;28(3):227-36.

244. Zhao J, Deng Y, Jiang Z, Qing H. G Protein-Coupled Receptors (GPCRs) in Alzheimer's Disease: A Focus on BACE1 Related GPCRs. Frontiers in Aging Neuroscience. 2016;8.

245. Suzuki S, Tanaka K, Nishikawa K, Suzuki H, Oshima A, Fujiyoshi Y. Structural basis of hydroxycarboxylic acid receptor signaling mechanisms through ligand binding. Nature Communications. 2023;14(1):5899.

246. Taggart AK, Kero J, Gan X, Cai TQ, Cheng K, Ippolito M, et al. (D)-beta-Hydroxybutyrate inhibits adipocyte lipolysis via the nicotinic acid receptor PUMA-G. J Biol Chem. 2005;280(29):26649-52.

247. Ahmed K. Biological roles and therapeutic potential of hydroxy-carboxylic Acid receptors. Front Endocrinol (Lausanne). 2011;2:51.

248. Li Z, McCafferty KJ, Judd RL. Role of HCA(2) in Regulating Intestinal Homeostasis and Suppressing Colon Carcinogenesis. Front Immunol. 2021;12:606384.

249. Taylor GS, Smith K, Scragg J, McDonald TJ, Shaw JA, West DJ, et al. The metabolome as a diagnostic for maximal aerobic capacity during exercise in type 1 diabetes. Diabetologia. 2024;67(7):1413-28.

250. Daina A, Michielin O, Zoete V. SwissTargetPrediction: updated data and new features for efficient prediction of protein targets of small molecules. Nucleic Acids Res. 2019;47(W1):W357-W64.

251. Gfeller D, Grosdidier A, Wirth M, Daina A, Michielin O, Zoete V. SwissTargetPrediction: a web server for target prediction of bioactive small molecules. Nucleic Acids Res. 2014;42(Web Server issue):W32-8.

252. ULC CCG. Molecular Operating Environment (MOE). 2024.

253. Yang Y, Kang HJ, Gao R, Wang J, Han GW, DiBerto JF, et al. Structural insights into the human niacin receptor HCA2-Gi signalling complex. Nature Communications. 2023;14(1):1692.

254. Zaccolo M, Pozzan T. Discrete microdomains with high concentration of cAMP in stimulated rat neonatal cardiac myocytes. Science. 2002;295(5560):1711-5.

255. Zaccolo M, De Giorgi F, Cho CY, Feng L, Knapp T, Negulescu PA, et al. A genetically encoded, fluorescent indicator for cyclic AMP in living cells. Nat Cell Biol. 2000;2(1):25-9.

256. Stangherlin A, Gesellchen F, Zoccarato A, Terrin A, Fields LA, Berrera M, et al. cGMP signals modulate cAMP levels in a compartment-specific manner to regulate catecholamine-dependent signaling in cardiac myocytes. Circ Res. 2011;108(8):929-39.

257. Musheshe N. Understanding compartmentalized cAMP signaling for potential therapeutic approaches in cardiac disease: University of Groningen; 2018.

258. Klarenbeek J, Goedhart J, van Batenburg A, Groenewald D, Jalink K. Fourth-generation epac-based FRET sensors for cAMP feature exceptional brightness, photostability and dynamic range: characterization of dedicated sensors for FLIM, for ratiometry and with high affinity. PLoS One. 2015;10(4):e0122513.

259. O'Connor L, Gilmour J, Bonifer C. The Role of the Ubiquitously Expressed Transcription Factor Sp1 in Tissue-specific Transcriptional Regulation and in Disease. Yale J Biol Med. 2016;89(4):513-25.

260. Doetzlhofer A, Rotheneder H, Lagger G, Koranda M, Kurtev V, Brosch G, et al. Histone deacetylase 1 can repress transcription by binding to Sp1. Mol Cell Biol. 1999;19(8):5504-11.

261. Hung JJ, Wang YT, Chang WC. Sp1 deacetylation induced by phorbol ester recruits p300 to activate 12(S)-lipoxygenase gene transcription. Mol Cell Biol. 2006;26(5):1770-85.

262. Greijer AE, van der Wall E. The role of hypoxia inducible factor 1 (HIF-1) in hypoxia induced apoptosis. J Clin Pathol. 2004;57(10):1009-14.

263. Zimna A, Kurpisz M. Hypoxia-Inducible Factor-1 in Physiological and Pathophysiological Angiogenesis: Applications and Therapies. Biomed Res Int. 2015;2015:549412.

264. Loor G, Schumacker PT. Role of hypoxia-inducible factor in cell survival during myocardial ischemia–reperfusion. Cell Death & Differentiation. 2008;15(4):686-90.

265. Alderson NL, Wang Y, Blatnik M, Frizzell N, Walla MD, Lyons TJ, et al. S-(2-Succinyl)cysteine: A novel chemical modification of tissue proteins by a Krebs cycle intermediate. Archives of Biochemistry and Biophysics. 2006;450(1):1-8.

266. Jové M, Pradas I, Mota-Martorell N, Cabré R, Ayala V, Ferrer I, et al. Succination of Protein Thiols in Human Brain Aging. Frontiers in Aging Neuroscience. 2020;12.

267. Blatnik M, Thorpe SR, Baynes JW. Succination of proteins by fumarate: mechanism of inactivation of glyceraldehyde-3-phosphate dehydrogenase in diabetes. Ann N Y Acad Sci. 2008;1126:272-5.

268. Jóhannsson E, Lunde PK, Heddle C, Sjaastad I, Thomas MJ, Bergersen L, et al. Upregulation of the Cardiac Monocarboxylate Transporter MCT1 in a Rat Model of Congestive Heart Failure. Circulation. 2001;104(6):729-34.

269. Prag HA, Aksentijevic D, Dannhorn A, Giles AV, Mulvey JF, Sauchanka O, et al. Ischemia-Selective Cardioprotection by Malonate for Ischemia/Reperfusion Injury. Circ Res. 2022;131(6):528-41.

270. Kyte J. Structure in Protein Chemistry. 2nd Edition ed. New York: Garland Science; 2006. 832 p.

271. National Center for Biotechnology Information (2024). PubChem Compound Summary for CID 444972, Fumaric Acid [Internet]. [cited November 7, 2024]. Available from: https://pubchem.ncbi.nlm.nih.gov/compound/Fumaric-Acid.

272. Li X, Wu F, Günther S, Looso M, Kuenne C, Zhang T, et al. Publisher Correction: Inhibition of fatty acid oxidation enables heart regeneration in adult mice. Nature. 2023;623(7986):E7-E.

273. Jeridi A, Kapellos TS, Yildirim AÖ. Fumarate hydratase: a new checkpoint of metabolic regulation in inflammatory macrophages. Signal Transduction and Targeted Therapy. 2023;8(1):332.

274. Guitart AV, Panagopoulou TI, Villacreces A, Vukovic M, Sepulveda C, Allen L, et al. Fumarate hydratase is a critical metabolic regulator of hematopoietic stem cell functions. Journal of Experimental Medicine. 2017;214(3):719-35.

275. Yang Y, Lane AN, Ricketts CJ, Sourbier C, Wei MH, Shuch B, et al. Metabolic reprogramming for producing energy and reducing power in fumarate hydratase null cells from hereditary leiomyomatosis renal cell carcinoma. PLoS One. 2013;8(8):e72179.

276. Tong W-H, Sourbier C, Kovtunovych G, Jeong Suh Y, Vira M, Ghosh M, et al. The Glycolytic Shift in Fumarate-Hydratase-Deficient Kidney Cancer Lowers AMPK Levels, Increases Anabolic Propensities and Lowers Cellular Iron Levels. Cancer Cell. 2011;20(3):315-27.

277. Ziello JE, Jovin IS, Huang Y. Hypoxia-Inducible Factor (HIF)-1 regulatory pathway and its potential for therapeutic intervention in malignancy and ischemia. Yale J Biol Med. 2007;80(2):51-60.

278. Wlodarczyk J, Leng A, Abadchi SN, Shababi N, Mokhtari-Esbuie F, Gheshlaghi S, et al. Transfection of hypoxia-inducible factor-1α mRNA upregulates the expression of genes encoding angiogenic growth factors. Scientific Reports. 2024;14(1):6738.

279. Belaidi E, Joyeux-Faure M, Ribuot C, Launois SH, Levy P, Godin-Ribuot D. Major role for hypoxia inducible factor-1 and the endothelin system in promoting myocardial infarction and hypertension in an animal model of obstructive sleep apnea. J Am Coll Cardiol. 2009;53(15):1309-17.

280. Azimi I, Petersen RM, Thompson EW, Roberts-Thomson SJ, Monteith GR. Hypoxia-induced reactive oxygen species mediate N-cadherin and SERPINE1 expression, EGFR signalling and motility in MDA-MB-468 breast cancer cells. Scientific Reports. 2017;7(1):15140.

281. Kaur B, Khwaja FW, Severson EA, Matheny SL, Brat DJ, Van Meir EG. Hypoxia and the hypoxia-inducible-factor pathway in glioma growth and angiogenesis. Neuro Oncol. 2005;7(2):134-53.

282. Schäffer L, Scheid A, Spielmann P, Breymann C, Zimmermann R, Meuli M, et al. Oxygen-regulated expression of TGF-beta 3, a growth factor involved in trophoblast differentiation. Placenta. 2003;24(10):941-50.

283. Shih H-J, Chang H-F, Chen C-L, Torng P-L. Differential expression of hypoxia-inducible factors related to the invasiveness of epithelial ovarian cancer. Scientific Reports. 2021;11(1):22925.

284. Eckle T, Hartmann K, Bonney S, Reithel S, Mittelbronn M, Walker LA, et al. Adora2b-elicited Per2 stabilization promotes a HIF-dependent metabolic switch crucial for myocardial adaptation to ischemia. Nat Med. 2012;18(5):774-82.

285. Bonney S, Kominsky D, Brodsky K, Eltzschig H, Walker L, Eckle T. Cardiac Per2 Functions as Novel Link between Fatty Acid Metabolism and Myocardial Inflammation during Ischemia and Reperfusion Injury of the Heart. PLOS ONE. 2013;8(8):e71493.

286. Grimaldi B, Bellet MM, Katada S, Astarita G, Hirayama J, Amin RH, et al. PER2 Controls Lipid Metabolism by Direct Regulation of PPARγ. Cell Metabolism. 2010;12(5):509-20.

287. Lamia KA, Papp SJ, Yu RT, Barish GD, Uhlenhaut NH, Jonker JW, et al. Cryptochromes mediate rhythmic repression of the glucocorticoid receptor. Nature. 2011;480(7378):552-6.

288. Yuan P, Yang T, Mu J, Zhao J, Yang Y, Yan Z, et al. Circadian clock gene NPAS2 promotes reprogramming of glucose metabolism in hepatocellular carcinoma cells. Cancer Letters. 2020;469:498-509.

289. Byles V, Cormerais Y, Kalafut K, Barrera V, Hughes Hallett JE, Sui SH, et al. Hepatic mTORC1 signaling activates ATF4 as part of its metabolic response to feeding and insulin. Molecular Metabolism. 2021;53:101309.

290. Li TY, Wang Q, Gao AW, Li X, Sun Y, Mottis A, et al. Lysosomes mediate the mitochondrial UPR via mTORC1-dependent ATF4 phosphorylation. Cell Discovery. 2023;9(1):92.

291. Koyanagi S, Hamdan AM, Horiguchi M, Kusunose N, Okamoto A, Matsunaga N, et al. cAMP-response Element (CRE)-mediated Transcription by Activating Transcription Factor-4 (ATF4) Is Essential for Circadian Expression of the Period2 Gene*. Journal of Biological Chemistry. 2011;286(37):32416-23.

292. Ramanathan C, Kathale ND, Liu D, Lee C, Freeman DA, Hogenesch JB, et al. mTOR signaling regulates central and peripheral circadian clock function. PLoS Genet. 2018;14(5):e1007369.

293. Singla R, Mishra A, Cao R. The trilateral interactions between mammalian target of rapamycin (mTOR) signaling, the circadian clock, and psychiatric disorders: an emerging model. Translational Psychiatry. 2022;12(1):355.

294. Lipton JO, Yuan ED, Boyle LM, Ebrahimi-Fakhari D, Kwiatkowski E, Nathan A, et al. The Circadian Protein BMAL1 Regulates Translation in Response to S6K1-Mediated Phosphorylation. Cell. 2015;161(5):1138-51.

295. Littlewood-Evans A, Sarret S, Apfel V, Loesle P, Dawson J, Zhang J, et al. GPR91 senses extracellular succinate released from inflammatory macrophages and exacerbates rheumatoid arthritis. Journal of Experimental Medicine. 2016;213(9):1655-62.

296. Shenol A, Tenente R, Lückmann M, Frimurer TM, Schwartz TW. Multiple recent HCAR2 structures demonstrate a highly dynamic ligand binding and G protein activation mode. Nature Communications. 2024;15(1):5364.

297. Fitch CA, Platzer G, Okon M, Garcia-Moreno BE, McIntosh LP. Arginine: Its pKa value revisited. Protein Sci. 2015;24(5):752-61.

298. Pogostin BH, Malmendal A, Londergan CH, Åkerfeldt KS. pKa Determination of a Histidine Residue in a Short Peptide Using Raman Spectroscopy. Molecules. 2019;24(3).

299. Tang H, Lu JY-L, Zheng X, Yang Y, Reagan JD. The psoriasis drug monomethylfumarate is a potent nicotinic acid receptor agonist. Biochemical and Biophysical Research Communications. 2008;375(4):562-5.

300. Hydroxycarboxylic acid receptors in GtoPdb v.2023.1. IUPHAR/BPS Guide to Pharmacology CITE. 2023;2023(1).

301. Gerhart-Hines Z, Dominy John E, Jr., Blättler Sharon M, Jedrychowski Mark P, Banks Alexander S, Lim J-H, et al. The cAMP/PKA Pathway Rapidly Activates SIRT1 to Promote Fatty Acid Oxidation Independently of Changes in NAD⁺. Molecular Cell. 2011;44(6):851-63.

302. Lv S, Qiu X, Li J, Liang J, Li W, Zhang C, et al. Glucagon-induced extracellular cAMP regulates hepatic lipid metabolism. Journal of Endocrinology. 2017;234(2):73-87.

303. Xie J, Ponuwei GA, Moore CE, Willars GB, Tee AR, Herbert TP. cAMP inhibits mammalian target of rapamycin complex-1 and -2 (mTORC1 and 2) by promoting complex dissociation and inhibiting mTOR kinase activity. Cell Signal. 2011;23(12):1927-35.

304. Jewell JL, Fu V, Hong AW, Yu F-X, Meng D, Melick CH, et al. GPCR signaling inhibits mTORC1 via PKA phosphorylation of Raptor. eLife. 2019;8:e43038.

305. Hameed I, Masoodi SR, Mir SA, Nabi M, Ghazanfar K, Ganai BA. Type 2 diabetes mellitus: From a metabolic disorder to an inflammatory condition. World J Diabetes. 2015;6(4):598-612.

306. Association AD. Diagnosis and Classification of Diabetes Mellitus. Diabetes Care. 2010;33(Supplement_1):S62-S9.

307. Saeedi P, Petersohn I, Salpea P, Malanda B, Karuranga S, Unwin N, et al. Global and regional diabetes prevalence estimates for 2019 and projections for 2030 and 2045: Results from the International Diabetes Federation Diabetes Atlas, 9(th) edition. Diabetes Res Clin Pract. 2019;157:107843.

308. Ma C-X, Ma X-N, Guan C-H, Li Y-D, Mauricio D, Fu S-B. Cardiovascular disease in type 2 diabetes mellitus: progress toward personalized management. Cardiovascular Diabetology. 2022;21(1):74.

309. Raghavan S, Vassy JL, Ho YL, Song RJ, Gagnon DR, Cho K, et al. Diabetes Mellitus–Related All-Cause and Cardiovascular Mortality in a National Cohort of Adults. Journal of the American Heart Association. 2019;8(4):e011295.

310. Bertrand L, Horman S, Beauloye C, Vanoverschelde J-L. Insulin signalling in the heart. Cardiovascular Research. 2008;79(2):238-48.

311. Lee SH, Park SY, Choi CS. Insulin Resistance: From Mechanisms to Therapeutic Strategies. Diabetes Metab J. 2022;46(1):15-37.

312. Luiken JJFP, Koonen DPY, Willems J, Zorzano A, Becker C, Fischer Y, et al. Insulin Stimulates Long-Chain Fatty Acid Utilization by Rat Cardiac Myocytes Through Cellular Redistribution of FAT/CD36. Diabetes. 2002;51(10):3113-9.

313. Dimitriadis G, Mitrou P, Lambadiari V, Maratou E, Raptis SA. Insulin effects in muscle and adipose tissue. Diabetes Res Clin Pract. 2011;93 Suppl 1:S52-9.

314. Abel ED, O'Shea KM, Ramasamy R. Insulin Resistance: Metabolic Mechanisms and Consequences in the Heart. Arteriosclerosis, Thrombosis, and Vascular Biology. 2012;32(9):2068-76.

315. Bayeva M, Sawicki KT, Ardehali H. Taking diabetes to heart--deregulation of myocardial lipid metabolism in diabetic cardiomyopathy. J Am Heart Assoc. 2013;2(6):e000433.

316. DeFronzo RA. Insulin resistance, lipotoxicity, type 2 diabetes and atherosclerosis: the missing links. The Claude Bernard Lecture 2009. Diabetologia. 2010;53(7):1270-87.

317. Wende AR, Abel ED. Lipotoxicity in the heart. Biochim Biophys Acta. 2010;1801(3):311-9.

318. Bajaj S, Khan A. Antioxidants and diabetes. Indian J Endocrinol Metab. 2012;16(Suppl 2):S267-71.

319. Volpe CMO, Villar-Delfino PH, dos Anjos PMF, Nogueira-Machado JA. Cellular death, reactive oxygen species (ROS) and diabetic complications. Cell Death & Disease. 2018;9(2):119.

320. Cepas V, Collino M, Mayo JC, Sainz RM. Redox Signaling and Advanced Glycation Endproducts (AGEs) in Diet-Related Diseases. Antioxidants. 2020;9(2):142.

321. Laight DW, Carrier MJ, Änggård EE. Antioxidants, diabetes and endothelial dysfunction. Cardiovascular Research. 2000;47(3):457-64.

322. Sekhar RV, McKay SV, Patel SG, Guthikonda AP, Reddy VT, Balasubramanyam A, et al. Glutathione synthesis is diminished in patients with uncontrolled diabetes and restored by dietary supplementation with cysteine and glycine. Diabetes Care. 2011;34(1):162-7.

323. Kaludercic N, Di Lisa F. Mitochondrial ROS Formation in the Pathogenesis of Diabetic Cardiomyopathy. Frontiers in Cardiovascular Medicine. 2020;7.

324. Wright E, Jr., Scism-Bacon JL, Glass LC. Oxidative stress in type 2 diabetes: the role of fasting and postprandial glycaemia. Int J Clin Pract. 2006;60(3):308-14.

325. Giacco F, Brownlee M, Schmidt AM. Oxidative Stress and Diabetic Complications. Circulation Research. 2010;107(9):1058-70.

326. Ibrahim SG, El-Emam SZ, Mohamed EA, Abd Ellah MF. Dimethyl fumarate and curcumin attenuate hepatic ischemia/reperfusion injury via Nrf2/HO-1 activation and anti-inflammatory properties. International Immunopharmacology. 2020;80:106131.

327. Clore JN, Allred J, White D, Li J, Stillman J. The role of plasma fatty acid composition in endogenous glucose production in patients with type 2 diabetes mellitus. Metabolism - Clinical and Experimental. 2002;51(11):1471-7.

328. Raza H, John A, Howarth FC. Alterations in Glutathione Redox Metabolism, Oxidative Stress, and Mitochondrial Function in the Left Ventricle of Elderly Zucker Diabetic Fatty Rat Heart. International Journal of Molecular Sciences. 2012;13(12):16241-54.

329. Li S, Li X, Li YL, Shao CH, Bidasee KR, Rozanski GJ. Insulin regulation of glutathione and contractile phenotype in diabetic rat ventricular myocytes. Am J Physiol Heart Circ Physiol. 2007;292(3):H1619-29.

330. Wang J, He J, Su F, Ding N, Hu W, Yao B, et al. Repression of ATR pathway by miR-185 enhances radiation-induced apoptosis and proliferation inhibition. Cell Death & Disease. 2013;4(6):e699-e.

331. Jespersen NR, Hjortbak MV, Lassen TR, Stottrup NB, Johnsen J, Tonnesen PT, et al. Cardioprotective effect of succinate dehydrogenase inhibition in rat hearts and human myocardium with and without diabetes mellitus. Sci Rep. 2020;10(1):10344.

332. Hasan NM, Longacre MJ, Seed Ahmed M, Kendrick MA, Gu H, Ostenson CG, et al. Lower succinyl-CoA:3-ketoacid-CoA transferase (SCOT) and ATP citrate lyase in pancreatic islets of a rat model of type 2 diabetes: knockdown of SCOT inhibits insulin release in rat insulinoma cells. Arch Biochem Biophys. 2010;499(1-2):62-8.

333. Turko IV, Marcondes S, Murad F. Diabetes-associated nitration of tyrosine and inactivation of succinyl-CoA:3-oxoacid CoA-transferase. Am J Physiol Heart Circ Physiol. 2001;281(6):H2289-94.

334. Adam J, Ramracheya R, Chibalina MV, Ternette N, Hamilton A, Tarasov AI, et al. Fumarate Hydratase Deletion in Pancreatic β Cells Leads to Progressive Diabetes. Cell Rep. 2017;20(13):3135-48.

335. Haythorne E, Rohm M, van de Bunt M, Brereton MF, Tarasov AI, Blacker TS, et al. Diabetes causes marked inhibition of mitochondrial metabolism in pancreatic β-cells. Nature Communications. 2019;10(1):2474.

336. Calabrese V, Cornelius C, Leso V, Trovato-Salinaro A, Ventimiglia B, Cavallaro M, et al. Oxidative stress, glutathione status, sirtuin and cellular stress response in type 2 diabetes. Biochimica et Biophysica Acta (BBA) - Molecular Basis of Disease. 2012;1822(5):729-36.

337. Xu Z, Patel KP, Lou MF, Rozanski GJ. Up-regulation of K+ channels in diabetic rat ventricular myocytes by insulin and glutathione. Cardiovascular Research. 2002;53(1):80-8.

338. McLennan SV, Heffernan S, Wright L, Rae C, Fisher E, Yue DK, et al. Changes in Hepatic Glutathione Metabolism in Diabetes. Diabetes. 1991;40(3):344-8.

339. Murakami K, Takahito K, Ohtsuka Y, Fujiwara Y, Shimada M, Kawakami Y. Impairment of glutathione metabolism in erythrocytes from patients with diabetes mellitus. Metabolism. 1989;38(8):753-8.

340. Sheweita SA, Mashaly S, Newairy AA, Abdou HM, Eweda SM. Changes in Oxidative Stress and Antioxidant Enzyme Activities in Streptozotocin-Induced Diabetes Mellitus in Rats: Role of Alhagi maurorum Extracts. Oxidative Medicine and Cellular Longevity. 2016;2016(1):5264064.

341. Shabalala SC, Johnson R, Basson AK, Ziqubu K, Hlengwa N, Mthembu SXH, et al. Detrimental Effects of Lipid Peroxidation in Type 2 Diabetes: Exploring the Neutralizing Influence of Antioxidants. Antioxidants. 2022;11(10):2071.

342. Jandrić-Balen M, Božikov V, Bozikov J, Metelko Ž, Jandrić I, Romić Ž. Impact of glycemic control on antioxidant enzyme activity in patients with type 2 diabetes mellitus. Diabetologia Croatica. 2004;33:131-5.

343. Asmat U, Abad K, Ismail K. Diabetes mellitus and oxidative stress-A concise review. Saudi Pharm J. 2016;24(5):547-53.

344. Tiwari BK, Pandey KB, Abidi AB, Rizvi SI. Markers of Oxidative Stress during Diabetes Mellitus. J Biomark. 2013;2013:378790.

345. Mansor LS, Gonzalez ER, Cole MA, Tyler DJ, Beeson JH, Clarke K, et al. Cardiac metabolism in a new rat model of type 2 diabetes using high-fat diet with low dose streptozotocin. Cardiovasc Diabetol. 2013;12:136.

346. Xu Y, Osborne BW, Stanton RC. Diabetes causes inhibition of glucose-6-phosphate dehydrogenase via activation of PKA, which contributes to oxidative stress in rat kidney cortex. American Journal of Physiology-Renal Physiology. 2005;289(5):F1040-F7.

347. Zhang Z, Liew CW, Handy DE, Zhang Y, Leopold JA, Hu J, et al. High glucose inhibits glucose-6-phosphate dehydrogenase, leading to increased oxidative stress and beta-cell apoptosis. Faseb j. 2010;24(5):1497-505.

348. Mahmoud AA, Nor El-Din AKA. Glucose-6-Phosphate Dehydrogenase Activity and Protein Oxidative Modification in Patients with Type 2 Diabetes Mellitus. Journal of Biomarkers. 2013;2013(1):430813.

349. Katare R, Oikawa A, Cesselli D, Beltrami AP, Avolio E, Muthukrishnan D, et al. Boosting the pentose phosphate pathway restores cardiac progenitor cell availability in diabetes. Cardiovascular Research. 2012;97(1):55-65.

350. Lou Y, Kong M, Li L, Hu Y, Zhai W, Qi X, et al. Inhibition of the Keap1/Nrf2 Signaling Pathway Significantly Promotes the Progression of Type 1 Diabetes Mellitus. Oxid Med Cell Longev. 2021;2021:7866720.

351. Chi H, Sun Y, Lin P, Zhou J, Zhang J, Yang Y, et al. Glucose Fluctuation Inhibits Nrf2 Signaling Pathway in Hippocampal Tissues and Exacerbates Cognitive Impairment in Streptozotocin-Induced Diabetic Rats. Journal of Diabetes Research. 2024;2024(1):5584761.

352. David JA, Rifkin WJ, Rabbani PS, Ceradini DJ. The Nrf2/Keap1/ARE Pathway and Oxidative Stress as a Therapeutic Target in Type II Diabetes Mellitus. J Diabetes Res. 2017;2017:4826724.

353. Bitar MS, Al-Mulla F. A defect in Nrf2 signaling constitutes a mechanism for cellular stress hypersensitivity in a genetic rat model of type 2 diabetes. Am J Physiol Endocrinol Metab. 2011;301(6):E1119-29.

354. Peake BF, Nicholson CK, Lambert JP, Hood RL, Amin H, Amin S, et al. Hydrogen sulfide preconditions the db/db diabetic mouse heart against ischemia-reperfusion injury by activating Nrf2 signaling in an Erk-dependent manner. Am J Physiol Heart Circ Physiol. 2013;304(9):H1215-24.

355. Pitarokoili K, Ambrosius B, Meyer D, Schrewe L, Gold R. Dimethyl Fumarate Ameliorates Lewis Rat Experimental Autoimmune Neuritis and Mediates Axonal Protection. PLOS ONE. 2015;10(11):e0143416.

356. Li S, Vaziri ND, Swentek L, Takasu C, Vo K, Stamos MJ, et al. Prevention of Autoimmune Diabetes in NOD Mice by Dimethyl Fumarate. Antioxidants (Basel). 2021;10(2).

357. Yan N, Xu Z, Qu C, Zhang J. Dimethyl fumarate improves cognitive deficits in chronic cerebral hypoperfusion rats by alleviating inflammation, oxidative stress, and ferroptosis via NRF2/ARE/NF-κB signal pathway. International Immunopharmacology. 2021;98:107844.

358. Lin R, Cai J, Kostuk EW, Rosenwasser R, Iacovitti L. Fumarate modulates the immune/inflammatory response and rescues nerve cells and neurological function after stroke in rats. Journal of Neuroinflammation. 2016;13(1):269.

359. Li Y, Ma F, Li H, Song Y, Zhang H, Jiang Z, et al. Dimethyl fumarate accelerates wound healing under diabetic condition. J Mol Endocrinol. 2018;61(4):163-72.

360. Hu X, Rajesh M, Zhang J, Zhou S, Wang S, Sun J, et al. Protection by dimethyl fumarate against diabetic cardiomyopathy in type 1 diabetic mice likely via activation of nuclear factor erythroid-2 related factor 2. Toxicology Letters. 2018;287:131-41.

361. Amin FM, Abdelaziz RR, Hamed MF, Nader MA, Shehatou GSG. Dimethyl fumarate ameliorates diabetes-associated vascular complications through ROS-TXNIP-NLRP3 inflammasome pathway. Life Sciences. 2020;256:117887.

362. Axelsson AS, Tubbs E, Mecham B, Chacko S, Nenonen HA, Tang Y, et al. Sulforaphane reduces hepatic glucose production and improves glucose control in patients with type 2 diabetes. Sci Transl Med. 2017;9(394).

363. Bahadoran Z, Mirmiran P, Azizi F. Potential efficacy of broccoli sprouts as a unique supplement for management of type 2 diabetes and its complications. J Med Food. 2013;16(5):375-82.

364. Mohamadi N, Baradaran Rahimi V, Fadaei MR, Sharifi F, Askari VR. A mechanistic overview of sulforaphane and its derivatives application in diabetes and its complications. Inflammopharmacology. 2023;31(6):2885-99.

365. Kim H-S, Ren G, Kim T, Bhatnagar S, Yang Q, Bahk YY, et al. Metformin reduces saturated fatty acid-induced lipid accumulation and inflammatory response by restoration of autophagic flux in endothelial cells. Scientific Reports. 2020;10(1):13523.

366. Wang C, Liu F, Yuan Y, Wu J, Wang H, Zhang L, et al. Metformin suppresses lipid accumulation in skeletal muscle by promoting fatty acid oxidation. Clin Lab. 2014;60(6):887-96.

367. Patel TB. Effect of sulfonylureas on hepatic fatty acid oxidation. American Journal of Physiology-Endocrinology and Metabolism. 1986;251(2):E241-E6.

368. Cook GA. The hypoglycemic sulfonylureas glyburide and tolbutamide inhibit fatty acid oxidation by inhibiting carnitine palmitoyltransferase. J Biol Chem. 1987;262(11):4968-72.

369. Kulkarni RA, Bak DW, Wei D, Bergholtz SE, Briney CA, Shrimp JH, et al. A chemoproteomic portrait of the oncometabolite fumarate. Nat Chem Biol. 2019;15(4):391-400.

370. Manuel AM, Frizzell N. Adipocyte protein modification by Krebs cycle intermediates and fumarate ester-derived succination. Amino Acids. 2013;45(5):1243-7.

371. Wang L, Pydi SP, Zhu L, Barella LF, Cui Y, Gavrilova O, et al. Adipocyte Gi signaling is essential for maintaining whole-body glucose homeostasis and insulin sensitivity. Nature Communications. 2020;11(1):2995.

372. Cheng L, Sun S, Wang H, Zhao C, Tian X, Liu Y, et al. Orthosteric ligand selectivity and allosteric probe dependence at Hydroxycarboxylic acid receptor HCAR2. Signal Transduction and Targeted Therapy. 2023;8(1):364.

373. Yadav MK, Sarma P, Maharana J, Ganguly M, Mishra S, Zaidi N, et al. Structure-guided engineering of biased-agonism in the human niacin receptor via single amino acid substitution. Nature Communications. 2024;15(1):1939.

374. Grundy SM, Vega GL, McGovern ME, Tulloch BR, Kendall DM, Fitz-Patrick D, et al. Efficacy, safety, and tolerability of once-daily niacin for the treatment of dyslipidemia associated with type 2 diabetes: results of the assessment of diabetes control and evaluation of the efficacy of niaspan trial. Arch Intern Med. 2002;162(14):1568-76.

375. Valenca HdM, Mota EC, Silva ACdFA, Figueiredo-Junior AT, Verdini F, Romana-Souza B, et al. Therapeutic Potential of Dimethyl Fumarate for the Treatment of High-Fat/High-Sucrose Diet-Induced Obesity. Antioxidants. 2024;13(12):1496.

376. Baharnoori M, Wilson R, Saxena S, Gonzalez CT, Sotiropoulos MG, Keyhanian K, et al. Altered adipokine levels are associated with dimethyl fumarate treatment in multiple sclerosis patients. Multiple Sclerosis and Related Disorders. 2021;56.

377. Begum M, Choubey M, Tirumalasetty MB, Arbee S, Mohib MM, Wahiduzzaman M, et al. Adiponectin: A Promising Target for the Treatment of Diabetes and Its Complications. Life. 2023;13(11):2213.

378. Hong X, Zhang X, You L, Li F, Lian H, Wang J, et al. Association between adiponectin and newly diagnosed type 2 diabetes in population with the clustering of obesity, dyslipidaemia and hypertension: a cross-sectional study. BMJ Open. 2023;13(2):e060377.

379. Weyer C, Funahashi T, Tanaka S, Hotta K, Matsuzawa Y, Pratley RE, et al. Hypoadiponectinemia in obesity and type 2 diabetes: close association with insulin resistance and hyperinsulinemia. J Clin Endocrinol Metab. 2001;86(5):1930-5.

380. DeFronzo RA. Insulin resistance, lipotoxicity, type 2 diabetes and atherosclerosis: the missing links. The Claude Bernard Lecture 2009. Diabetologia. 2010;53(7):1270-87.

381. Liu M, Lv J, Pan Z, Wang D, Zhao L, Guo X. Mitochondrial dysfunction in heart failure and its therapeutic implications. Frontiers in Cardiovascular Medicine. 2022;9.

382. Kerr M, Miller JJ, Thapa D, Stiewe S, Timm KN, Aparicio CNM, et al. Rescue of myocardial energetic dysfunction in diabetes through the correction of mitochondrial hyperacetylation by honokiol. JCI Insight. 2020;5(17).

9. Supplementary figures

Table 9.1. Fold change between hypoxia and normoxia of the significantly regulated metabolites and their source of variation, determined by the factors oxygen levels (normoxia or hypoxia), condition (healthy or diabetes), and interaction between these factors.

Metabolite	Healthy heart	Diabetic heart	% Oxygen levels	% Condition	% Interaction
Succinate	5.40	2.75	79.9 (*)	0.26 (ns)	4.0 (*)
Fumarate	3.29	No change	51.32 (*)	16.63 (*)	18.49 (*)
Isoleucine	2.62	1.75	72.37 (*)	0.090 (ns)	3.77 (ns)
Valine	2.42	1.77	70.52 (*)	1.21 (ns)	1.66 (ns)
Leucine	2.40	No change	63.98 (*)	0.06 (ns)	4.26 (ns)
Cytidine diphosphate-cholin	2.29	No change	56.22 (*)	3.11 (ns)	0.51 (ns)
S-Adenosylhomocysteine	2.15	No change	33.18 (*)	9.33 (ns)	5.21 (ns)
Malate	2.08	No change	49.73 (*)	22.92 (*)	15.92 (*)
Taurine	2.02	No change	50.06 (*)	0.16 (ns)	0.41 (ns)
Alanine	2.02	No change	50.07 (*)	0.16 (ns)	0.40 (ns)
Guanosine monophosphate	1.98	2.20	49.64 (*)	4.64 (ns)	1.46 (ns)
Cytidine	1.81	No change	9.56 (ns)	3.43 (ns)	4.12 (ns)
Thyptophan	1.72	No change	38.75 (*)	1.80 (ns)	3.14 (ns)
Choline	1.55	No change	34.87 (*)	0.7(ns)	2.59 (ns)
Tyrosine	1.48	1.77	39.81 (*)	12.61 (*)	3.76 (ns)
Methionine	1.25	No change	4.03 (ns)	49.28 (*)	11.93 (*)
Creatine	1.24	1.24	52.34 (*)	0.86 (*)	0.004 (ns)
Adenosine monophosphate	No change	1.77	34.02 (*)	10.58 (ns)	4.18 (ns)
Serine	No change	1.56	43.77 (*)	2.01 (ns)	19.56 (*)
Proline	No change	1.56	26.80 (*)	0.53 (ns)	0.001 (ns)
Malonyl-Coa	No change	1.52	27.11 (*)	22.26 (*)	0.2403 (ns)
Succinyl-CoA	0.30	0.24	26.15 (*)	26.15 (*)	13.44 (*)
Cytidine triphosphate	0.34	0.34	71.25 (*)	0.69 (ns)	0.13(ns)
Phosphocreatine	0.41	0.42	65.44 (*)	1.89 (ns)	0.50 (ns)
Uridine triphosphate	0.50	0.35	80.87 (*)	0.47 (ns)	1.92 (ns)
Cytidine diphosphate	0.53	0.56	51.16 (*)	0.90 (ns)	0.43 (ns)
Glutamate	0.53	0.67	57.88 (*)	5.53 (ns)	1.38 (ns)
Aconitase	0.56	0.37	51.86 (*)	1.9 (ns)	1.38 (ns)
Glutamine	0.58	0.78	55.67 (*)	8.55 (*)	4.59 (ns)
Citrate	0.58	0.41	59.45 (*)	6.60 (ns)	0.80 (ns)
Adenosine triphosphate	0.61	0.46	67.69 (*)	0.02 (ns)	3.05 (ns)
Histidylmethionine	0.64	No change	25.54 (*)	7.80 (ns)	6.19 (ns)
Glucose-1-phosphate	0.68	No change	22.70 (*)	26.30 (*)	2.51 (ns)
Aspartate	0.77	No change	6.40 (ns)	36.89 (*)	0.03 (ns)
Guanosine triphosphate	No change	0.42	51.71 (*)	0.13 (ns)	10.75 (*)
Acetyl-CoA	No change	0.44	28.25 (*)	32.06 (*)	8.42 (ns)
Uridine diphosphate	No change	0.49	47.04 (*)	0.07 (ns)	1.89 (ns)
Isocitrate	No change	0.60	43.90 (*)	8.45 (ns)	5.80 (ns)
Glucose-6-phosphate	No change	0.61	33.75 (*)	15.72 (*)	0.27 (ns)

Increased metabolites are represented in red whereas reduced metabolites in blue.